High Pressure Chemistry Of Phenyl Radical Reactions With Acetylene

BY

ANDREA COMANDINI
M.S., Politecnico di Milano, 2005
M.S., University of Illinois at Chicago, 2005

THESIS

Submitted as partial fulfillment of the requirements
for the degree of Doctor of Philosophy in Mechanical Engineering
in the Graduate College of the
University of Illinois at Chicago, 2012

Chicago, Illinois

Defense Committee:

Kenneth Brezinsky, Chair and Advisor
Suresh K. Aggarwal
Christos G. Takoudis, Chemical Engineering and Bioengineering
Randall J. Meyer, Chemical Engineering
Robert S. Tranter, Argonne National Laboratory

To Maria

ACKNOWLEDGMENT

I would like to take this opportunity to thank Prof. Kenneth Brezinsky, my graduate advisor for his continuous supervision and encouragement throughout the entire four (and three quarter) years leading to the submission of this work and for providing me all the necessary resources. It was a pleasure to work under him.

I am also thankful to Prof. Suresh K. Aggarwal, Prof. Randall J. Meyer, Prof. Christos G. Takoudis, and Dr. Robert S. Tranter (Argonne National Laboratory) for agreeing to serve on my thesis defense committee and for the useful advice which helped improving this dissertation.

I would like to express my gratitude to several colleagues for very interesting and friendly discussions on the different aspects of my research: Dr. Robert S. Tranter (Argonne National Laboratory) for discussions on every aspect related to the experimental study, Dr. Raghu Sivaramakrishnan (Argonne National Laboratory) for the help on modeling and calculations, and Dr. Stephen J. Klippenstein (Argonne National Laboratory) for a number of very interesting discussions on computational chemistry.

I thank my friends and members of the high pressure shock tube group, especially Tom Malewicki for the help in the development of the experimental set-up.

My last but most grateful thanks to my wonderful partner, Maria, and to my family in Italy for the continuous support and love.

TABLE OF CONTENTS

TABLE OF CONTENTS (continued)

CHAPTER PAGE

LIST OF TABLES

TABLE PAGE

LIST OF FIGURES

FIGURE PAGE

TABLE OF FIGURES (continued)

FIGURE PAGE

TABLE OF FIGURES (continued)

FIGURE PAGE

TABLE OF FIGURES (continued)

FIGURE PAGE

FIGURE PAGE

TABLE OF FIGURES (continued)

FIGURE PAGE

TABLE OF FIGURES (continued)

FIGURE PAGE

SUMMARY

The formation of polycyclic aromatic hydrocarbons (PAHs), especially fused-ring compounds, represents an essential step in the mechanisms of formation of soot. In particular the second-ring species, naphthalene, plays a key role as a building block for the subsequent growth to larger PAHs. Nevertheless the pathways leading to naphthalene are still uncertain requiring further experimental and theoretical investigations. In the present work the pyrolytic reactions of the phenyl radical in the presence of acetylene have been studied as a possible pathway to the formation of the second-ring species.

The experimental work has been conducted using the single-pulse high-pressure shock tube (HPST) present at the University of Illinois at Chicago. A new experimental set-up was studied and developed for accurate measurement of large compounds. The major stable species, including the heavy polycyclic aromatic hydrocarbons, were identified and measured using gas chromatography/mass spectrometry techniques. The experiments were performed over a wide range of high-pressures (25 – 50 atm) and temperatures (900 – 1800 K) which encompass typical conditions in modern combustion chambers.

First phenyl iodide decomposition was studied as a source of phenyl radicals for the subsequent experiments with acetylene. Along with the expected major PAH products, which include biphenyl, terphenyls, and biphenylene, significant amounts of acenaphthylene and four-ring condensed species (chrysene, benzo[a]anthracene, benzo[g,h,i]fluoranthene, and benzo[c]phenanthrene) were measured. Small amounts of other PAH compounds, including naphthalene, were detected in the analyzed mixtures. In particular, the formation of the fused-ring species from the phenyl radical pyrolysis highlights the relevance of unconventional reaction pathways leading to condensed structures.

In order to explore new possible pathways for the formation of such condensed structures, a theoretical study of the radical/π-bond addition reactions between single-ring aromatic hydrocarbons

was performed using ab-initio quantum mechanics calculations. Several pathways leading to the formation of PAH compounds have been addressed as potentially relevant for typical combustion environments. In particular, the potential energy surfaces for the addition between o-benzyne and benzene and between phenyl radicals contain low-energy channels leading to the formation of naphthalene. The proposed pathways complement the conventional growth mechanisms involving the reaction of a single aromatic hydrocarbon with small aliphatic compounds.

The theoretical study was extended to the potential energy surface for the radical/π-bond addition reactions between o-benzyne and the cyclic C5 hydrocarbons. The latter compounds are common intermediates which derive from the oxidation of the phenyl radical in typical combustion systems. The results indicate novel pathways, alternative to the conventional ones, which lead to the formation of indene, an important building block for soot formation.

Once the analysis of the phenyl radical pyrolysis was completed, the phenyl + acetylene reactions were studied. The experiments showed a different distribution of PAH products compared to the experiments conducted in the absence of acetylene. Biphenyl and acenaphthylene were still among the major species, together with phenanthrene (phenylacetylene + phenyl and biphenyl radical + acetylene) and diphenylethyne (phenylacetylene + phenyl). Only small amounts of biphenylene, naphthalene, terphenyls, and four-ring compounds were measured. In this case, the reactions with acetylene play a dominant role compared to the addition reactions between single-ring compounds. On the other hand, the phenyl + acetylene reaction does not lead to the formation of significant amounts of naphthalene possibly due to the relatively low initial concentrations of acetylene in the system.

The experimental results on both the phenyl pyrolysis and the phenyl + acetylene reactions provide unique data on the systems in consideration. In fact, for the first time, it has been possible to detect and accurately measure a variety of PAH compounds, including the fused-ring species, for which mole fraction profiles have been obtained. Such species profiles were utilized to develop and validate a comprehensive chemical kinetic model which helped clarify some of the aspects related to the mechanisms involved in the formation of large polycyclic aromatic hydrocarbons at high pressures.

1. INTRODUCTION

1.1. Background

The era known as the Industrial Revolution was a period in which innovative ideas and discoveries brought about the most fundamental changes to human society since the development of agriculture thousands of years earlier. The transition from a worker-based cottage industry to a machine-based economy, with the growth of factories and mass production, deeply altered not only human but also environmental history. The Industrial Revolution marked the beginning of the period during which mankind began substantially exploiting natural nonrenewable resources and polluting the atmosphere.

Evidence of pollution during the early Industrial Revolution in England and the European continent is widespread, but the public awareness of the relationship between air quality and health built up only later, mainly after the Great Smoke of 1952[1]. In early December of that year a cold fog descended upon London. Because of the cold, Londoners began to burn more coal than usual. In addition there was pollution and smoke from vehicle exhausts, particularly from diesel-fuelled buses which had recently replaced the electric tram system, from the numerous coal-fired power stations within the London area and from other industrial and commercial sources. The resulting air pollution was trapped by the heavy layer of cold air, and the concentration of pollutants built up dramatically. The smog was so dense that in some areas visibility was reduced to a few yards; Figure 1 shows a view of the Nelson's Column in Trafalgar Square during the Great Smog.

Although the Great Smoke lasted only for few days and then quickly dispersed after a change in the weather, medical reports estimated that 4000 had died prematurely and 100000 more were made ill due to the smog effects on the human respiratory tract. More recent research suggests that the number of fatalities was considerably higher at around 12000[2]. The Great Smoke is considered the worst air pollution event in the history of the United Kingdom, but also the most significant in terms of its impact on public awareness, environmental research and government regulation.

Figure 1. Nelson's Column in Trafalgar Square during the Great Smog (source: Wikimedia Commons).

Since the Great Smoke, several environmental disasters related to the usage of nonrenewable natural resources have occured, until the recent BP oil spill in the Gulf of Mexico. Nevertheless, the modern industrial economies, no matter how high-tech, are still carbon-based economies; many of the human activities, from electricity generation to manufacturing, from residential and commercial heating/air conditioning to transportation, are mainly based on fossil fuel combustion. The combustion processes provide the energy necessary for the specific activity, but they also release numerous pollutants into the atmosphere. Particulate matter (soot), ozone, carbon monoxide, sulfur oxides, nitrogen oxides, and lead are representative harmful combustion products chosen by the US Environmental Protection Agency (EPA) as "criteria pollutants" for the definition of the National Ambient Air Quality Standards.

Among these pollutants, soot has recently received a lot of interest within the scientific community, especially after the discovery of the link between exposure to fine particles (<2.5 μm, referred to as $PM_{2.5}$) and adverse health effects. Epidemiological studies show that increased incidence of asthma and asthmatic symptoms is associated with increasing concentrations of $PM_{2.5}$ in the atmosphere[3]. In addition to acute respiratory problems, long-term effects include lung cancer and cardiopulmonary diseases, as studied by Pope at al. in collaboration with the American Cancer Society[4,5]. These studies show that every 10 $\mu g/m^3$ increase in the $PM_{2.5}$ concentration was linked to approximately a 6% and 8% increase in cardiopulmonary and lung cancer mortality respectively. Fine particles inhalation may also worsen underlying health problems such as ischemic heart disease, fatal arrhythmia, and congestive heart failure[6,7].

Strategies to reduce fine particulate matter (PM) formation include optimization of the design of the combustion systems, variation of the fuel composition or usage of appropriate fuel additives. These strategies have shown promise in reducing PM emissions significantly. However, in order to implement such PM mitigation strategies effectively, an accurate description of the fuel burning process is essential. It is clear that soot is a product of incomplete hydrocarbon combustion generated in regions of the flame where there is not enough oxygen to convert the fuel into carbon dioxide and water. In these regions the chemistry is driven by unburned or partially-burned hydrocarbons. Large polycyclic aromatic hydrocarbons (PAHs) are formed from primary aromatic species (first and second ring)[9-11]; PAHs dimerization, coagulation and chemical growth processes lead to the formation of soot precursor particles, characterized by a size of 5-10 nm[9,12-14]. These precursors undergo simultaneous coagulation, coalescence and surface growth to form the final aggregates[9,14]. The physico-chemical description of PM formation is reported schematically in Figure 2.

Within the complexity of the processes leading to soot, the limiting step of the overall chain is the formation of the primary aromatic species. Sometimes, these first and second ring compounds already present in large amounts in raw fuels are also formed during the combustion processes. Many theoretical and experimental studies have been performed on the formation of the first aromatic ring, as described in recent critical reviews[9-11]. On the other hand, the pathways leading to subsequent multi-ring compounds have not been so well studied and understood.

In particular, the recombination reactions between the phenyl radical (C_6H_5) with acetylene (C_2H_2) have not been well studied despite being hypothesized as important pathways to the formation of relevant multi-ring compounds as naphthalene ($C_{10}H_8$, second ring aromatic).

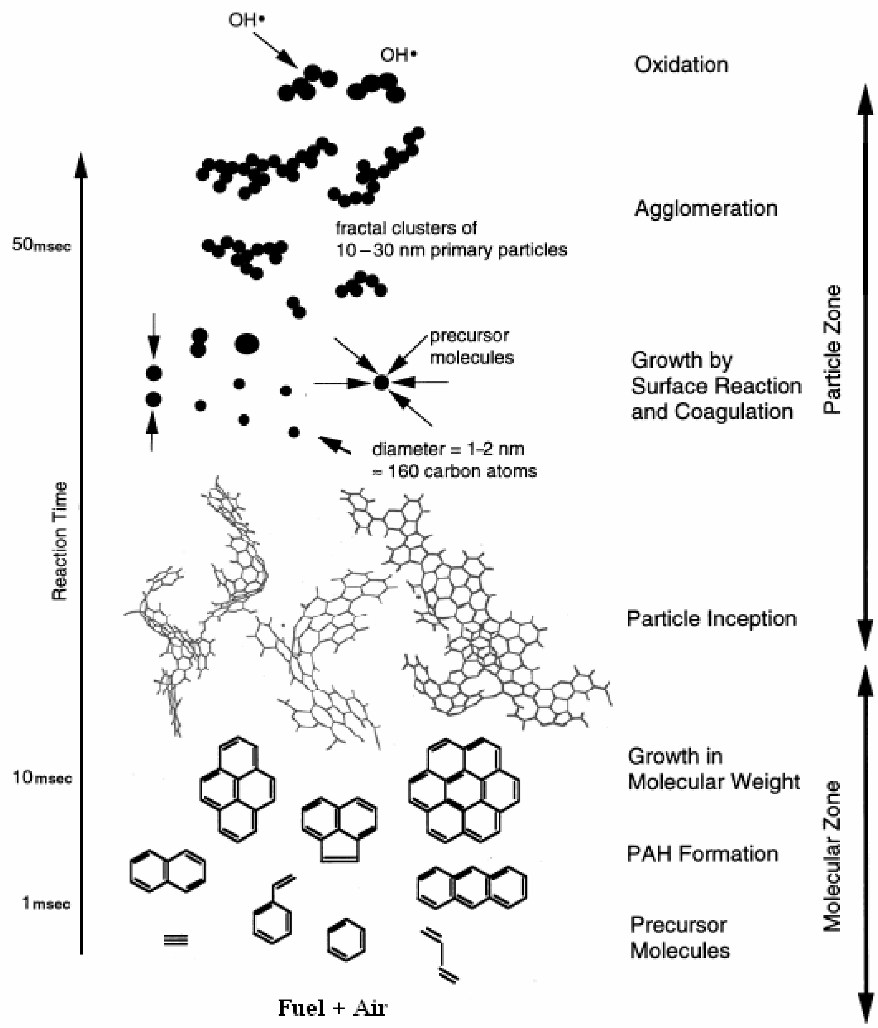

Figure 2. Physico-Chemical Description of PM formation (based on Bockhorn[8]).

1.2. Phenyl + Acetylene

The reaction between phenyl and acetylene has been postulated to be the first major step in the formation of the second ring, naphthalene. This reaction could lead to the formation of an energized 2-phenylvinyl adduct (depicted with a dagger symbol in Figure 3) which can subsequently stabilize to either the 2-phenylvinyl radical (C_6H_5CHCH, compound "b") or decompose to phenylacetylene ($C_6H_5C_2H$, species "a") depending on the pressure and temperature conditions. Both species can lead to the formation of naphthalene, through addition of an additional acetylene to the radical site of the 2-phenylvinyl radical (forming first phenylbutadienyl radical, compound "c") or through the HACA (hydrogen abstraction C_2H_2 addition) mechanism[15,16] starting from phenylacetylene. Moreover 2-phenylvinyl radical could undergo an internal hydrogen abstraction from the ring forming 1-vinyl-2-phenyl radical (species "d"). Subsequent addition of acetylene to the radical site would lead to the second ring aromatic.

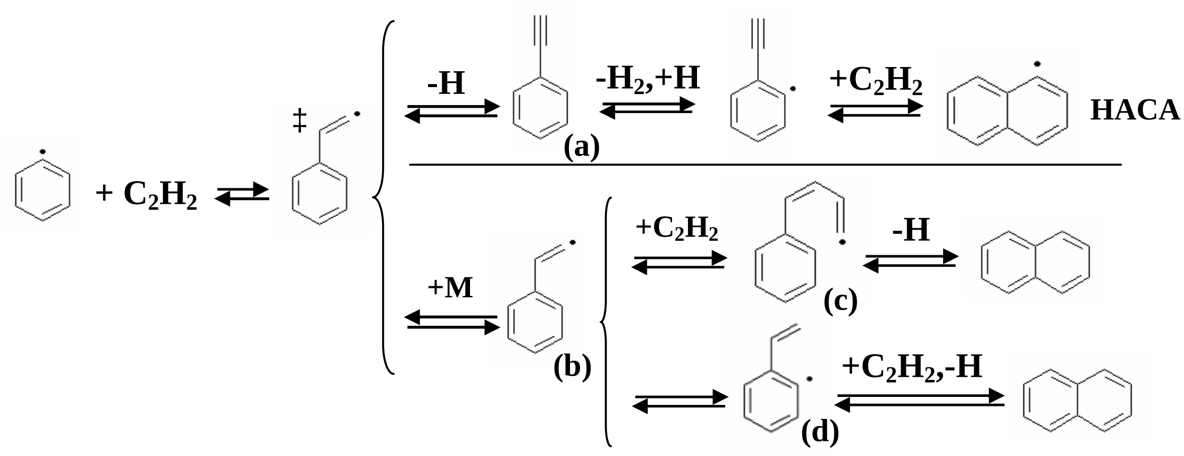

Figure 3. Formation of naphthalene from phenyl + acetylene reaction.

Prior experimental measurements on the total rate constant for the phenyl + acetylene reaction have been made by Fahr and Stein[17], who deduced an Arrhenius expression in a temperature range between 1000 and 1330 K in experiments conducted in a Knudsen cell flow reactor operating at very low pressures (1-10 Torr). In a subsequent study Yu et al.[18] used cavity ring down spectrometry (CRDS) to obtain an estimate of the total addition rate constant at temperatures between 297 and 523 K. Yu et al.[18] performed an RRKM analysis of the reactions and were able to explain their data as well as prior high temperature experiments by Fahr and Stein[17]. At almost the same time Wang and Frenklach[19] studied the reaction as part of an attempt to characterize PAH growth up to the formation of pyrene (four fused rings species, $C_{16}H_{10}$, Figure 21) using semiempirical quantum-mechanical calculations and transition state theory and assessed pressure dependence by means of RRKM approach. Subsequent to these studies, Heckmann et al.[20] performed high temperature studies in their shock tube at pressure ~3 bars and reported the rate constant for $C_6H_5 + C_2H_2 \rightarrow C_6H_5C_2H + H$. In more recent works, Richter et al.[21] and Tokmakov and Lin[22] have performed additional theoretical studies in the attempt to improve the accuracy of the calculated rate constants based on the available experimental data[17,18,20]. Among the experimental measurements, only the Heckmann et al.[20] data were obtained at pressures above atmospheric, i.e. 3 bars. These data are clearly not sufficient to validate the theoretical models, especially in relation to pressure dependence effects and calculations of high-pressure limit rate constants. In addition, to the best of our knowledge there are no experimental investigations which provide a comprehensive speciation analysis of the products of the reaction between phenyl radical and acetylene, including measurement of the large PAH compounds which serve as soot precursors.

Among the competing pathways to the HACA mechanism, which is generally considered the principal pathway for the formation of large PAH compounds, the so-called PAC mechanism (phenyl-addition/cyclization) has been proposed by Shukla and Koshi[23,24] as an efficient pathway for PAHs growth in benzene pyrolysis. In this mechanism, the phenyl radical adds directly to an aromatic molecule leading to subsequent cyclization forming larger compounds. The study of the decomposition of the phenyl radical precursor, such as phenyl iodide, would be important not only to determine from an experimental point of view the products of the PAC mechanism but also as a preliminary study for the subsequent experiments with added acetylene. In particular, the analysis of the products of the self-reaction between phenyl radicals would constitute a reference for the subsequent study on the phenyl + acetylene reaction.

The radical-radical recombination between phenyl radicals has previously been studied as main source of biphenyl[20,25], one of the most important intermediates for PAHs growth. In a recent paper, Tranter et al.[26] revisited the self-reaction of phenyl radicals based on low-pressure shock tube experiments and high-level theoretical calculations. The authors developed a chemical kinetic model which accurately simulates their laser schlieren experimental results. Nevertheless, the model did not include a complete mechanistic description of the PAHs formation which is expected to be relevant at the high pressure conditions present in typical modern combustion devices.

A comprehensive study of the phenyl + acetylene reaction and of phenyl radical pyrolysis would clearly lead to a better understanding of the two mechanisms, HACA and PAC, in relation to the formation of the primary PAH compounds which serve as building blocks for soot.

1.3. Goal and Technical Approach

The present research is focused on the experimental and theoretical examination of the phenyl + acetylene reaction. The decomposition of the phenyl radical precursor was also studied as relevant for the subsequent experiments with acetylene. The experimental investigation has been conducted using the high pressure shock tube present at the University of Illinois at Chicago; experiments has been performed at pressures relevant to typical combustion chambers (25 - 50 atm) for a wide range of temperatures (900 - 1800 K) and for reaction times between 1.2 and 2 ms. Stable species profiles have been obtained by means of GC and GC-MS techniques. Theoretical studies have been performed to estimate thermodynamic properties of the molecules involved in the reaction as well as estimate rate constants parameters for key reactions from analysis of potential energy surfaces. Finally chemical reaction mechanisms have been developed to simulate the experimental data.

The aim of the present work is to provide valuable experimental data on key reactions for the formation of PAH species relevant to soot formation chemistry. The experimental data have been used to validate a comprehensive chemical kinetic model which helped clarifying some of the aspects related to soot formation. The model provides the framework of a detailed comprehensive model for the prediction of the morphology, size, and concentration of soot emission during combustion processes in modern high-pressure combustion chambers. Accurate predictions will lead to a better characterization of the optimal solutions to improve combustion performances and reduce soot emission.

2. THEORY OF THE SHOCK TUBE

Shock tubes are devices where the removal or the bursting of an element separating two gases at different pressures generates a shock wave propagating through the low pressure gas. A shock wave is a disturbance which travels at a velocity higher than the characteristic speed of sound through the medium (in our case, gas). Unlike the sound waves which do not generate a substantial change in the properties of the gas, the shock waves cause an abrupt increase in temperature, pressure, and density of the gas inside the wave. The generation of shock waves inside a controlled volume, the shock tube, coupled with a variety of measurement and analytical instrumentation is a valuable tool for the study of physical and chemical processes where the experimental gases are instantaneously brought to a defined temperature and pressure.

Unless specified, the following paragraphs are based on the book "The Shock Tube in High-Temperature Chemical Physics" by A. G. Gaydon and I. R. Hurle[27]. In order to facilitate the discussion, a schematic of the regions associated with a shock wave is reported in Figure 4.

The simplest shock tube configuration is characterized by a uniform cross section tube where a diaphragm divides the high pressure gas (driver gas) from the low pressure gas (driven gas) which is subjected to the shock wave conditions. The two shock tube sections delimited by the diaphragm are called accordingly driver and driven section. When the diaphragm bursts, a series of subsequent compression waves are generated and propagates through the driven section. Each wave is stronger and possesses a higher velocity compared to the previous waves since it travels through a gas which has already been heated and compressed. As a consequence, the waves will finally coalesce to form a single shock front (Figure 4) across which abrupt pressure, temperature, and density gradients exist. The shock front moves with velocity W_S.

The bursting of the diaphragm will also generate a sequence of rarefaction waves propagating through the driver gas. Since the rarefaction waves travel in a gas of decreasing pressure, density, and temperature, the distance between subsequent waves spreads with time. The region affected by the rarefaction waves is called expansion fan and is limited by the rarefaction head and the rarefaction tail (Figure 4). Rarefaction waves are usually utilized in shock tube experiments to quench the reaction. In fact, these waves are reflected by the end-wall of the shock tube, propagate towards the reaction zone (zone 5 in Figure 4) and finally enter the reaction zone decreasing rapidly the temperature and pressure. We will discuss later in section 2.2 the role played in the quenching process by the contact surface which is defined as the location where the driver and the driven gases are in contact and which travels behind the shock front at a decreased velocity (Figure 4).

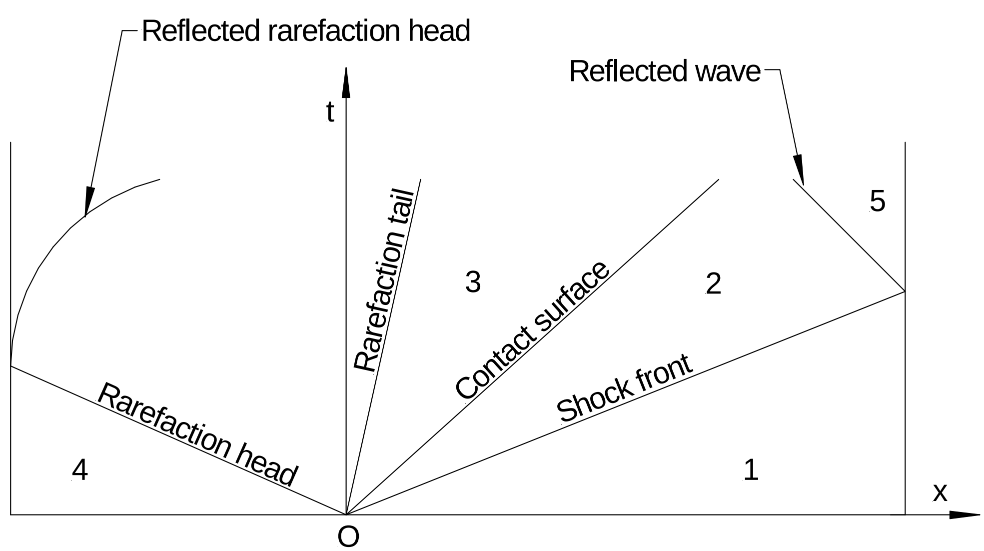

Figure 4. (x,t) diagram showing the various region associated with a shock wave at a time t after the bursting of the diaphragm at the origin O (based on Ref. [27]).

In the following section a simple but useful theory is developed that is able to describe the properties of the shock waves. In order to simplify the analysis, ideal non-reactive gases and inviscid flows are considered. In addition, since the reaction times are usually short (1-3 milliseconds) and since the gases have usually very low emittivity, heat losses by conduction through the walls of the shock tube and by radiation can be excluded.

2.1. Theory of shock waves

Once the compression waves generated after the rupture of the diaphragm coalescence, the shock front propagates as a single entity through the driven section increasing the pressure, temperature, and density of the gas initially at conditions 1 (Figure 4). The final conditions after the passage of the wave front (2 in Figure 4) can be determined by solving the equations for the conservation of mass, momentum and energy. The relations below can be derived[27].

$$\frac{P_2}{P_1} = \frac{2 \cdot \gamma \cdot M_1^2 - (\gamma - 1)}{\gamma + 1} \qquad \textbf{(1)}$$

$$\frac{T_2}{T_1} = \frac{\left(\gamma \cdot M_1^2 - \dfrac{\gamma - 1}{2}\right) \cdot \left(\dfrac{\gamma - 1}{2} \cdot M_1^2 + 1\right)}{\left(\dfrac{\gamma + 1}{2}\right)^2 \cdot M_1^2} \qquad \textbf{(2)}$$

where γ is the specific heat ratio, $M_1 = \frac{W_S}{a_1}$. The speed of sound *a* for a perfect gas of density *ρ*, specific heat *γ*, and pressure *P* can be obtained with the following equation:

$$a = \sqrt{\frac{\gamma \cdot P}{\rho}}$$

Equations 1, and 2 provide the pressure and the temperature of the gas behind incident shock knowing the initial conditions and the Mach number for region 1 in Figure 4. The Mach number can usually be measured experimentally. On the other hand, it would be useful from a practical point of view to obtain a relation between the strength of the shock (and consequently the final conditions behind the shock wave) and only the initial conditions 1 and 4. Applying the assumptions mentioned above, we can obtain equation 3 which relates the initial pressures in the driver and driven sections with M_1[27]. Thus, we can obtain the theoretical Mach number of the shock front using equation 3, and subsequently the final conditions T_2 and P_2 using equations 1 and 2. Based on these considerations, we could theoretically obtain any desired final conditions T_2 and P_2 by just adjusting the ratio between the initial driver and driver section pressures.

$$\frac{P_4}{P_1} = \frac{2\cdot\gamma_1\cdot M_1^2 - (\gamma_1 - 1)}{\gamma_1 + 1}\cdot\left\{1 - \frac{\gamma_4 - 1}{\gamma_1 + 1}\cdot\frac{a_1}{a_4}\cdot\left(M_1^2 - \frac{1}{M_1^2}\right)\right\}^{-\left(\frac{2\cdot\gamma_4}{\gamma_4 - 1}\right)} \qquad \textbf{(3)}$$

Once the incident shock wave arrives at the end-wall it is reflected back and propagates in opposite direction through the gas at conditions T_2, P_2, and ρ_2. The reflected shock wave further increases the temperature and pressure of the gas. In order to determine the conditions behind the reflected shock wave (annotated as 5 in Figure 4), we can utilize the following equations[27].

$$\frac{P_5}{P_1} = \left\{\frac{2\cdot\gamma\cdot M_1^2 - (\gamma - 1)}{\gamma + 1}\right\}\cdot\left\{\frac{(3\cdot\gamma - 1)\cdot M_1^2 - 2\cdot(\gamma - 1)}{(\gamma - 1)\cdot M_1^2 + 2}\right\} \qquad \textbf{(4)}$$

$$\frac{T_5}{T_1} = \frac{\left\{2\cdot(\gamma - 1)\cdot M_1^2 + (3 - \gamma)\right\}\cdot\left\{(3\cdot\gamma - 1)\cdot M_1^2 - 2\cdot(\gamma - 1)\right\}}{(\gamma + 1)^2\cdot M_1^2} \qquad \textbf{(5)}$$

Once again, we can utilize equation 3 to predict M_1 and subsequently the theoretical final conditions P_5 and T_5 by just knowing the initial loading pressures into the shock tube. Before concluding this section on the theory of the shock waves, it is worth mention the fact that behind the reflected shock wave the gas is stationary and characterized by uniform conditions. This property is very important for the definition of the exact conditions during shock tube experiments.

2.2. Experimental observation time

The observation time for a shock tube experiment can be defined as the time during which the conditions of the experimental gas are relatively constant behind the incident or the reflected shock wave, depending on the type of study. The high pressure shock tube present at UIC is a device for the study of chemical processes behind reflected shock wave as described in detail in the next chapter. For the purpose of the present work which utilizes this particular shock tube, we will discuss how to estimate the observation time in a reflected shock wave.

Two events could be responsible for the perturbation of the uniform conditions behind the reflected shock wave which leads to an interruption of the observation time. The first is the arrival of the reflected rarefaction head at the location where the observation occurs. This event which abruptly decreases the pressure and the temperature of the experimental gas can be controlled by increasing the driver section length or adding a portion of heavy gases into the usually light driver gases (helium or hydrogen)[28]. If the driver length is sufficiently long, the observation time is then limited by the interaction between the reflected shock wave and the contact surface. In the usual situation when $\gamma_2 = \gamma_3$, the interaction between the reflected shock wave and the contact surface leads to varying results depending on the relative velocities of the gases in region 2 and 3 (Figure 4). If $a_2 > a_3$ or $a_2 < a_3$ the reflected shock wave is reflected back by the contact surface in form of a shock wave or rarefaction wave respectively. In both cases, the conditions in 5 are altered, and the observation time can be obtained using the expression derived in Ref. [27]:

$$\Delta\tau = \frac{\chi_1}{M_1 \cdot a_1} \cdot \left(\frac{\gamma - 1}{2 \cdot \gamma}\right) \qquad \textbf{(6)}$$

where χ_1 is the length of the driven section.

Only in the case when $a_2 = a_3$ no wave is reflected by the contact surface. In this case the uniform conditions would in theory persist until the arrival of the reflected rarefaction head.

Based on the discussion presented in this section, it is clear how the modification of the driver section length is a crucial element for obtaining the desired observation time as well as uniform conditions in the experimental zone. In addition, the quenching rate should be as fast as possible in order to avoid secondary processes occurring during the quenching process. The maximum quenching efficiency is obtained when the arrival of the rarefaction wave at the contact surface coincides with the reflection of the reflected shock wave from the contact surface for $a_2 < a_3$. Typical quenching rates during the shock tube experiments are between 7 x 10^4 and 1.5 x 10^5 K/s.

2.3. Experimental techniques for shock wave enhancement

Several techniques can be implemented to improve the strength of the generated shock for a given initial pressure ratio between the driver and the driven gases. A widely used technique is the double diaphragm technique. In this case two diaphragms are located in series along the shock tube. The first diaphragm bursts by increasing the pressure in the driver section or by dropping the pressure of the gas located between the two diaphragms. The bursting of the first diaphragm generates a shock wave which increases the pressure of the intermediate gas. At this point, the intermediate gas becomes the new driver gas for the second diaphragm. The double diaphragm technique leads to an improvement of the performances of the shock tube up to around 30%. In addition, the double diaphragm technique allows control with accuracy of the initial experimental conditions and consequently allows easy attainment of the desired final experimental conditions as described in the previous section.

A different technique which is often utilized involves the design of an area reduction between driver and driven section. The area reduction has been shown to lead to an enhancement of the shock wave strength[29]. Detailed studies have been conducted by Alpher and White[29] for several area ratios combined with different driver and driven gases.

The UIC high pressure shock tube discussed in greater detail in the subsequent chapter is also a convergent area shock tube and thereby offers the required increased shock strength. In addition, the shock tube is equipped with a diaphragm section which allows the use of the double diaphragm technique for further improvement of the performances if necessary.

3. EXPERIMENTAL APPARATUS: TRADITIONAL SET-UP

The aim of the present section is to provide a brief overview on the traditional design of the high-pressure shock tube in Prof. Brezinsky's laboratory at the University of Illinois at Chicago. The material discussed in the section is based on Reference 30 which contains a detailed description of the experimental apparatus. The analytical instrumentation used in the laboratory is also described.

3.1. Shock tube

The single-pulse high-pressure shock tube in Prof. Brezinsky's laboratory at the University of Illinois at Chicago[30,31] has unique capabilities to operate at post-shock pressures from 20 to 1000 atmospheres and temperatures up to 2500 K. Reaction times in the range of 0.5 milliseconds to 4 milliseconds can be obtained in the reflected shock wave by changing the lengths of the driver and driven sections. The entire shock tube is heated to 100 ˚C to avoid condensation of the species on the walls; the temperature is controlled with an error of ±1 ˚C throughout the entire length. Gas samples can be withdrawn through an automated sampling apparatus for subsequent species analysis with gas chromatography and mass spectrometry.

The high pressure shock tube has been used in previous studies of hydrocarbon pyrolysis and oxidation as well as heterogeneous reactions. Chemical kinetic models have been developed and validated against the experimental data obtained over a wide range of temperatures and pressures. Selected publications are reported in the reference section[33-36].

The shock tube is composed of a number of sections that are designed to facilitate easy assembly and disassembly; these parts are mounted on wheeled frames that can be moved easily. The various parts composing the shock tube are made from 17-4 PH stainless steel. This material was chosen because of its high yield strength and corrosion resistance.

The driven section is constituted by the transducer section, three different extension pieces, and the dump tank. The transducer section possesses eight ports for PCB model 113A21 and 113A23 piezoelectric transducers positioned perpendicularly to the flow. The transducers have a response time of around 1 microsecond and can be used to monitor pressures from 10 psi to 20000 psi. The pressure traces are utilized to estimate the velocity of the shock wave extrapolated to the end-wall with an uncertainty ≤1% by measuring the time taken for the wave to pass between two transducers and knowing the relative distances between the various ports. The extrapolated velocity is experimentally related to the temperatures in the post-shock reaction by means of chemical thermometers as described later in section 3.2. An additional transducer is located in the end-wall plug parallel to the flow. This transducer provides directly the pressure as well as the reaction time which is considered as the time between the arrival of the incident wave at the end-wall and the time when the pressure reaches the 80% of its maximum value[32]. Uncertainty in the time measurement is no more than 10%.

The total length of the driven section can be varied between 37 and 177 inches in steps of 20 inches by combining the different extension pieces available. As a consequence, the reaction time can be varied between 1 and 4 milliseconds depending on the necessity. The dump tank is located just ahead of the diaphragm section and attached to the driven section by an angled channel pointing towards the end wall of the driven section. Since the volume of the dump tank is much larger than the volume of the shock tube, the dump tank functions as a reservoir which avoids multiple shock waves from occuring. Thus, the high pressure shock tube at UIC is a single-pulse shock tube.

As mentioned in Chapter 2, it is important that the reacting mixture is rapidly quenched; in fact, if the reflected shock wave reenters the reaction zone, it will increase the temperature, modifying the well defined reaction conditions. The shock tube is designed such that the quenching is obtained when the reflected shock front meets the rarefaction wave reflected from the end wall of the driver section as described in the previous chapter. In order to obtain constant reaction conditions as well as fast cooling of the reaction by the rarefaction wave, the length of the driver section is varied by inserting metallic plugs into the driver section end wall. The typical driver section length varies between 40 inches and 60 inches.

The driver and driven sections are separated by the diaphragm section. The diaphragm section has two main functions, one is to separate the driver and driven gases by means of a metallic diaphragm, the second function is to provide a transition between the cross section of the 1 inch diameter driven section and the cross section of the 2 inches diameter driver section. The ratio between the two cross-sectional areas increases by a factor of 2 the shock strength as calculated by Alpher and White[29] for ideal conditions. The transition is created by a conical sealing insert. The insert possesses a hard shaped edge which also provides the sealing on the metallic diaphragm surface when the diaphragm cover is tightened. Similar sealing is provided on the driven section side.

While the ratio between the driven gas loading pressure and the driver gas pressure determines the final experimental temperature (section 2.1), the final pressure P_5 behind the reflected shock wave is almost entirely a function of the bursting pressure P_4. The bursting pressure can be varied by modifying the material and the thickness of the diaphragm, as well as the depth of the scores on the diaphragm surface. These scores allow the diaphragms to open into four triangular pieces which do not interfere with the gas flow. For example, aluminum diaphragms of 0.025 inches thickness and with a score depth of 0.010 and 0.005 inches can be used to achieve a final nominal pressure of 25 and 50 atm respectively. Soft brass diaphragms of 0.032 inches thickness and with a score depth of 0.010 generate a pressure P_5 of about 300 atm, while if the thickness is 0.050 inches and the score depth is 0.016 inches, the final nominal reaction pressure will be 600 atm.

For each experiment, especially for the ones conducted at very high pressure, the rupture of the diaphragm requires a large amount of driver gas (usually helium) which is provided in standard cylinders pressurized to 2600-3000 psi. A gas booster available in the laboratory is routinely used to increase the pressure of the helium driver gas to the desired pressure. The pressurized helium is stored in 5 large high-pressure tanks each of about 6.5 liters in volume.

In the traditional set-up, the single pulse high pressure shock tube has the capability to have reactant and product gases sampled and subsequently analyzed offline using gas chromatographic (GC) and mass spectrometric (MS) techniques. After the reaction in the shock tube has been quenched, a sample of the gas is withdrawn by an angled port drilled into the end wall plug. The sample is stored in stainless steel electropolished vessels which has been previously flushed and evacuated. All the valves in the sample rig are air-actuated high pressure valves (HIPCO model 20-11LF4) and are opened and closed automatically by in-house written control software. In particular, the optimum sampling time was experimentally determined to be 0.3 seconds.

Another section which is connected to the dump tank by a manual ball valve (Butech model K108) is the mixing rig. The mixing rig is utilized to prepare the experimental mixtures in two 40 liters high-pressure cylinders. The mixing rig is divided into two sections, a low-pressure manifold (utilized for the reactant species) and a high-pressure manifold (for high pressure argon bath gas). In addition to the reactant species and the bath gas, neon is added to the mixture as an internal standard in order to account for possible dilution by the driver gas helium. The entire mixing system is heated to 100˚C and well insulated and it is controlled by manual valves. A rotary vane pump (BOC-Edwards RV8) is connected to the system, and it is able to pump the mixing ring down to 10^{-3} Torr.

Several additional auxiliary pumps are present in the laboratory. In particular, the driver section is evacuated using a BOC-Edwards RV 8 rotary vane pump to a few Torr. The driven section is connected to two pumps in series, the first being a rotary vane pump (Leybold-TRIVAC D2-5E) which pumps the section down to values of pressure of about 10-20 mTorr; only when the pressure has reached these values, a turbomolecular pump (BOC-Edwards EXT 70) is activated to reach pressures down to around 1 mTorr. A turbomolecular pump/rotary pump combination (respectively BOC-Edwards EXT 70 and BOC-Edwards E2M1.5) is also connected to the sample rig in order to evacuate the sample vessels.

3.2. Temperature measurement

In the majority of the shock tubes the reaction temperature T_5 is estimated using equations which assume ideal conditions, i.e. equation 5. However these equations are based on several assumptions that are valid only up to modest pressures. In the high-pressure shock tube the gases cannot be described as ideal and the use of ideal shock wave equations lead to inaccurate results.

A solution suitable for the measurement of T_5 in real gases is the use of internal chemical thermometers. Two compounds, the one used as chemical thermometer and the second the species of interest, are shocked simultaneously and thus subjected to the same temperature and pressure conditions. In particular, the temperature can be estimated by monitoring the decay of the chemical thermometer compound, as demonstrated by W. Tsang in his early studies[37,38,39]. An important precondition is that no cross-reaction between the reagent and the chemical thermometer must occur; however this is difficult to achieve when high pressure conditions are implemented. Consequently a modification to this technique was found to be necessary for implementation in the HPST.

An external chemical thermometer is a suitable solution to the problem. In this case the species used as a chemical thermometer is shocked independently of the reagent mixture of interest. The experimental results of the decomposition of the chemical thermometer are used to generate a calibration curve relating temperature to the shock velocity extrapolated to the end-wall. In subsequent experiments with the reagent of interest, the extrapolated velocity is once again measured and the temperature backed out using the calibration curve.

A large number of experiments have been conducted in the high-pressure shock tube using 1,1,1-trifluoroethane, TFE, and cyclohexene as external chemical thermometers[31]. 1,1,1-Trifluoroethane decomposes via the reaction

$$C_2H_3F_3 \rightarrow C_2H_2F_2 + HF$$

This reaction has a well known unimolecular decomposition rate. The standard Arrhenius expression is used to back out the temperature from the extent of decomposition of TFE using the two equations below[31]

$$T = \frac{(-E/R)}{\ln\{\ln(1-x)/At\}} \qquad \textbf{(7)}$$

$$x = \frac{[TFE]_0 - [TFE]_f}{[TFE]_0} \qquad \textbf{(8)}$$

In the expressions *t* is the reaction time, *x* is the extent of the reaction ($[TFE]_0$ and $[TFE]_f$ are obtained from the analysis of the pre-shock and post-shock vessels respectively), *E* and *A* are respectively the activation energy and the pre-exponential factor for the decomposition of TFE[40]. The temperature derived from the rate of formation of 1,1-difluoroethane (DFE) in the post-shock samples is usually similar to that obtained from TFE decomposition thereby giving additional support for the use of this molecule as a chemical thermometer for a temperature range between 1200 K and 1350 K.

Another species suitable to be used as external chemical thermometer is cyclohexene[41]; the decomposition reaction is

$$c-C_6H_{10} \rightarrow C_4H_6 + C_2H_4$$

The procedure to obtain the calibration curve is similar to the one described for the decomposition of TFE. Experiments showed a good agreement between the values of the temperatures obtained from these two different chemical thermometers, with the cyclohexene decomposition used for calibrating at lower temperature ranges (900 - 1100 K).

In addition to cyclohexene, cyclopropanecarbonitrile decomposition can be used to derive the calibration curve for the low temperature experiments (900 - 1100 K)[42,43]. In this case, cyclopropanecarbonitrile (c-C_3H_5CN) isomerizes to form cis-crotonitrile, trans-crotonitrile (cis- and trans-$CH_3CHCHCN$), and vinyl-acetonitrile (CH_2CHCH_2CN). Once again, good agreement between the calibration curves from the different chemical thermometers was obtained.

While several chemical thermometers are available in the low temperature range, at temperatures above 1350 K the secondary reactions are usually relevant and no species will undergo simple unimolecular decomposition for reaction times between 1.2 and 2.5 milliseconds which are the typical times for experiments conducted with the high pressure shock tube. In order to obtain a calibration curve for high temperatures, carbon disulfide (CS_2) decomposition was investigated. As mentioned, the CS_2 decomposition can not be modeled using a single reaction rate constant value. Saito et al.[44] studied CS_2 decomposition and proposed a chemical kinetic model that was used unaltered to determine the calibration curve. The calibration curve obtained using carbon disulfide as chemical thermometer extends between 1700 and 2000 K[45]. An interpolated calibration curve can be used between 1350 K and 1700 K where no experimental data are present[45].

The estimated error in the post-shock temperature is around 1% for temperatures up to 1350 K, and 2% for temperatures higher than 1350 K.

3.3. Analytical instrumentation

The pre-shock and the post-shock samples collected from the driven section are analyzed using gas chromatography and mass spectrometry. There are two Hewlett-Packard 6890 series gas chromatographs (GCs) and a Hewlett-Packard 5973 series mass spectrometer (MS); the latter is connected to one of the two gas chromatographs. When necessary, the samples can be analyzed using both techniques. The gas chromatographs are able to detect mole fractions down to sub-parts per million levels of stable products of the reaction, depending on the detector used for the specific analysis. A variety of detectors can be mounted on the GCs, the Thermal Conductivity Detector (TCD), the Flame Ionization Detector (FID), the Electron Capture Detector (ECD), the Nitrogen Phosphorus Detector (NPD), or the Pulsed Discharge Detector (PDD). Each detector can be calibrated for quantification of specific compounds present in the samples. On the other hand, the MS is used for identification of unknown species. The result of an analysis provides the composition of the pre-shock or post-shock mixtures in terms of mole fractions of the products.

Before a species can be quantified, a relationship between peak area and mole fraction must be determined. This process of detector calibration for its response to individual gas components is done using mixtures of known composition (standard calibrated mixtures and make-up mixtures) and relating, for each species, the specific peak area with the corresponding mole fraction. The specific peak area is obtained dividing the peak area from the GC by the injection pressure measured by a standard Setra pressure gauge. The typical error in the measurement of light hydrocarbons is around 5-10% depending on the accuracy of the calibration as well as the type of detector.

4. MODELING

The high-pressure shock tube present at UIC is a well characterized apparatus used to perform experiments on key reactions over a wide range of high pressures (10 - 100 atm) and temperatures (800 - 2000 K) that encompass typical conditions existent in modern combustion devices. The experimental data includes species profiles for both reactants and stable products. These species profiles are compared to the results from theoretical chemical kinetic models developed to simulate the chemical behavior of the specific reactions. Accurate chemical kinetic models provide an essential component in the design of engines, turbines, and combustors. This chapter provides an overview of modeling techniques.

4.1. Chemical kinetic models

A chemical kinetic model is composed of two main parts, the gas-phase kinetics and the thermodynamic data.

The gas phase kinetics file contains a list of the relevant reactions and their parameters. The main literature databases containing reaction parameters include the NIST online database[46] and the compilations by Tsang and Hampson[47] and by Baulch et al.[48]. When the parameters of a specific reaction are not available in literature, they can be estimated by comparison with the parameters of similar reactions, if any. On the other hand, elementary reactions can be studied theoretically through ab-initio calculations and transition state theory, as it will be described in paragraph 5.3.

Thermodynamic data provide the thermochemical properties (enthalpy, entropy, and specific heat capacity) for the species of interest. The thermochemical properties are used to derive the value of the rate constant parameters of the reverse reaction starting from the parameters of the forward reaction. In fact, from thermodynamic considerations, the rate constant of the general reaction

$A+B \xrightarrow{k_{forward}} C+D$ is related to the rate constant of its reverse $A+B \xleftarrow{k_{reverse}} C+D$ by the following equation

$$k_{reverse} = \frac{k_{forward}}{K_{eq}}$$

where the K_{eq} is the equilibrium constant of the reaction defined as

$$K_{eq} = (RT)^{-\Delta \upsilon} e^{\Delta S^0 / R} e^{\Delta H^0 / RT}$$

ΔS^0 and ΔH^0 are the standard entropy and enthalpy changes at temperature T and $\Delta \upsilon$ the change in number of moles in the reaction. ΔS^0 and ΔH^0 are the parameters derived from the thermodynamic data through approximated expressions. For example, the widely used NASA polynomials[49] approximate the thermodynamic properties as follows

$$S/T = a_1 \ln T + a_2 T + a_3 T^2/2 + a_4 T^3/3 + a_5 T^4/4 + a_7$$

$$H/RT = a_1 + a_2 T/2 + a_3 T^2/3 + a_4 T^3/4 + a_5 T^4/5 + a_6/T$$

$$c_p/R = a_1 + a_2 T + a_3 T^2 + a_4 T^3 + a_5 T^4$$

where a_1-a_7 are numerical coefficients. Two sets of coefficients are usually provided, covering two different temperature ranges (usually 200 – 1000 K and 1000 – 6000 K).

Extensive databases of thermochemical data are available in literature, including the online NIST database[50] and Prof. Burcat's database[51]. When the thermodynamic data are not available in literature, the NASA polynomial can be obtained using FITDAT, a Fortran program part of the

CHEMKIN 3.7.1 package[52,53]. Inputs to FITDAT include the molecular heat of formation and entropy at 298 K ($\Delta H^{0}_{f,298K}$ and S_{298K}) and the vibrational frequencies of the molecule. Such properties can be calculated by means of ab-initio calculations as shown in paragraph 5.2.

Optional input files for specific reactor models include surface kinetics file and gas transport data file. The present work does not make use of these optional data.

4.2. CHEMKIN

The experimental data obtained using the HPST are simulated using CHEMKIN[54,55]. CHEMKIN is a software package that incorporates several modules to facilitate the representation of chemical systems and their solution in terms of chemical kinetic processes.

The shock tube studies performed in the present work involve chemical processes occurring behind reflected shock waves. The gases are subjected to a rapid increase in temperature and pressure which persist for a defined time (usually small, 1-3 milliseconds) before the arrival of the rarefaction wave quenching the reaction. The very brief time scale of the experiments makes the heat losses by conduction and radiation negligible (adiabatic system) and the variations in the pressure minor (isobaric system). An additional feature of gases behind reflected shock waves is the absence of net flow along the direction of propagation. No flow in and/or out the system exists.

Considering the characteristics of the gases behind reflected shock wave, the simulations were performed assuming an adiabatic constant pressure process[32] occurring inside an homogeneous closed batch reactor as implemented in CHEMKIN 3.7[55]. While CHEMKIN 3.7 was utilized to simulate the chemical processes, CHEMKIN 3.6[54] served as a tool for analyzing the chemical kinetic model. In particular, the SENKIN subroutine has been used in this work to simulate the experimental results obtained using the HPST. SENKIN computes the time evolution of a homogeneous reacting gas mixture in a closed system. In addition, the software solves the set of linear differential equations that describe the first-order sensitivity coefficients with respect to the individual reaction rates.

The simulations were performed for the exact conditions observed in the experiments. The raw data are available in the attached Appendix A. In particular the actual pressure for each set differs from the nominal quoted pressures but is close to it. The reaction temperature is the temperature estimated using the chemical thermometer calibration curves. The mixture composition is the actual composition determined by GC analysis.

4.3. Sensitivity analysis and rate of production analysis

Sensitivity analysis is a procedure to determine quantitatively how the solution to a model depends on certain parameters in the model. For the case considered in the present work, the parameters are the elementary reaction rate constants. Thus, the sensitivity analysis shows how the model will respond to changes in the rate parameters in terms of predicted concentrations of the product species. It also provides insight about how important certain reaction pathways are to the model predictions; thus, it is an important tool for the development of chemical kinetics mechanisms.

While the sensitivity analyses show how the model will respond to changes in the rate parameters, the reaction pathway analysis (or rate of production analysis) provides information about how each reaction contributes to the production/consumption of one particular species. The rate of production analysis is particularly useful to construct schemes which clarify how the various compounds are chemically related and what is the relevance of a reaction pathway to the formation/consumption of a specific species. In order to obtain reliable results, the rate of production analysis needs to be performed on chemical kinetic models already validated against the experimental data.

.

5. QUANTUM CHEMISTRY CALCULATIONS

The goal of the present chapter is to provide a brief overview of the computational techniques utilized for estimating both the molecular thermodynamic values and the reaction rate constants when needed for modeling purposes. Detailed discussions of the electronic structure theories and methods that are the bases for these techniques are presented in References 56 and 57.

5.1. Computational chemistry calculations and methods

Computational chemistry provides models which can be used in specific cases for calculating the structures and properties of molecules. The geometry of a nonlinear molecule with *N* nuclei depends on 3*N*-6 independent nuclear coordinates and its energy *U* is a function of these coordinates as well. Quantum chemistry calculations implement theoretical models to determine the configurations of the molecule that minimize *U*. These configurations are the equilibrium geometries of the molecule. Once the geometry has been optimized, vibrational frequency analyses are often performed to determine how the nuclei in the molecule vibrate about the equilibrium position. Each vibrational mode contributes to the energy of the molecule, so it is important to include in the energy expression what is called the molecular vibrational zero-point energy E_{ZPE} (or ZPVE). For the ground vibrational state, the zero-point energy is defined as

$$E_{ZPE} \approx \frac{1}{2}\sum_{k=1}^{3N-6} h\upsilon_k$$

The accuracy of the results of a quantum chemistry calculation depends on the basis set and the computational methods implemented in the specific calculation. The basis set can be defined as a set of functions which can be combined to create the approximate molecular orbitals of the molecule.

Widely used basis sets include those introduced by Pople et al. (3-21G[58,59], 6-21G[58,59], 6-31G[60,61], and 6-311G[62]) and the basis sets by Dunning et al.[63,64] (cc-pVDZ, cc-pVTZ, etc.). As a general rule, the accuracy of the results improves if larger basis sets are utilized. On the other hand, the computational costs can increase significantly too, thus it is often necessary to find a compromise between accuracy and computational costs.

The second factor which influences the results of a calculation is the computational method. The choice of a quantum mechanical method determines the mathematical approximations applied to the solution of the Schrödinger equation. Among the various methods, the density functional theory (DFT)[65,66] methods are often utilized for the optimization of large molecular systems due to their efficiency. The efficiency derives from the fact that the DFT methods do not solve for the wavefunction of the system but for the electron density function. The various properties of the molecule, such as the energy, can be derived from the electron density function. The popular Becke's three-parameter formulation (B3LYP)[67,68] hybrid functional is an example of DFT methods.

Differently from the DFT methods, the ab-initio methods calculate an approximated wavefunction of the system by solving the Schrödinger equation. Although this implies high computational costs, the ab-initio calculations potentially produce very accurate results. The coupled-cluster methods, such as the widely used CCSD(T) method[69], are examples of ab-initio methods.

5.2. Thermodynamic properties

The results obtained implementing the above mentioned methods can be utilized to derive the thermodynamic properties of the molecule. Among the thermodynamic properties the enthalpies of formation are widely used in many applications. When reliable experimental data are not available in literature, the enthalpies of formation have to be estimated.

The simplest way to estimate the enthalpy of formation is through the calculation of the atomization energy[70]. Nevertheless, the heats of formation calculated by means of the atomization scheme are in general not very accurate (compared with the experimental ones) unless very accurate methods and large basis sets are used in the calculations. This is not feasible when large molecular systems are considered.

A more accurate method is the so-called bond separation isodesmic scheme[71,72]. In such a method the atomization reaction is substituted with a reaction with equal number of bonds on both sides. Instead of the atoms, simple species like C_2H_2, C_2H_4, and C_2H_6, are used to balance the reaction. Results obtained using the bond separation isodesmic scheme are in general quite accurate as the errors related to the calculated bond energies cancel out as similar on both sides of the reaction.

Derived from the bond separation isodesmic scheme, the ring conserved isodesmic reaction scheme proposed by Sivaramakrishnan et al.[73] requires the conservation of both the number of bonds and the aromaticity. Thus a similar number of aromatic rings appear on both sides of the reaction. This additional requirement allows the cancellation of the errors associated to the specific nature of the aromatic species.

Other estimation methods have been proposed, including among the others the Benson's group additivity method[74], the bond-additivity method[75], the ring-additivity method[76], and the more recent bond-centered group additivity method[77].

Another thermodynamic property which is often required is the entropy. Entropy can be calculated by summing the translational, rotational, vibrational, and electronic contributions. These contributions do not depend only on the vibrational frequencies, but also on the symmetry number of the molecule as well as on the degeneracy of the various electronic states. More information about each single contribution are contained in the referenced works[56,72].

5.3. Transition state theory

Transition state theory is a statistical theory used for predicting unknown reaction rate constants[78-80] from the quantum chemical calculations. The expression for the high-pressure limit reaction rate constant can be written as[81]

$$k_\infty(T) = \kappa(T)\cdot\frac{k_B T}{h}\cdot\frac{Q^{\ddagger}(T)}{\prod_{i=1}^{n} Q^{R_i}(T)}\cdot e^{-E_0/k_B T} \qquad \textbf{(9)}$$

where k_B is the Boltzmann's constant, h the Planck's constant, $Q^{\ddagger}$ and Q^{R_i} the partition functions of the activated complex and of the reactants respectively, n the number of reactants, and E_0 the difference between the energies of the transition state and of the reactants, including the zero-point vibrational energies (ZPVE).

The transmission coefficient $\kappa(T)$ accounting for tunneling effects can be estimated as[82]

$$\kappa(T) = 1 - \frac{1}{24}\cdot\left(\frac{h\upsilon^{\ddagger}}{k_B T}\right)^2\cdot\left(1+\frac{RT}{E_0}\right)$$

where R is the universal gas constant and $\upsilon^{\ddagger}$ the imaginary frequency associated to the motion along the reaction coordinate.

In order to derive the expression for the reaction rate constant, we need to know the partition functions for the reactants and for the activated complex, as well as their energies. Quantum chemistry computations can provide this information.

The first step is the optimization of the chemical structures for the species involved in the reaction, including the activated complex. Then a vibrational analysis is performed on the optimized structures. The activated complex will have one and only one negative vibrational frequency associated with the motion along the reaction coordinate. In order to test if the complex connects the reactants with the desired products, a reaction path calculation (IRC)[83] can be conducted. The IRC calculation examines a reaction path starting from the transition state and moving in both directions along the reaction coordinate. At each step, an optimized structure is determined, so that the final result is able to clarify which molecular structures that specific activated complex connects. Finally high-level, large basis set calculations are performed on the optimized structures. These calculations provide accurate estimates for the molecular energies; the accuracy of the energy levels is very important as it significantly influences the accuracy of the reaction rate constant value (exponential dependence).

Returning to equation 9, E_0 can be estimated as the difference between the energy of the activated complex and the energy of the reactants. These energies include the corrected zero-point energies. On the other hand, the molecular partition functions can be written as products of the translational, rotational, vibrational, and electronic partition functions. The expressions for the separate partition functions can be found in Reference 72. Thus, the quantum chemistry calculations provide all the information required for solving equation 9 (E_0 and *Q's*). The only unknown parameter in the expression is the temperature. The temperature can be varied over the range required for the specific study and the resulting data can be plotted in the Arrhenius form (logarithm versus 1000/T). If the data can be accurately fitted by linear interpolation, the parameters of the interpolation line can be used to derive the pre-exponential factor and the activation energy in the Arrhenius expression of the rate constant. Otherwise, a three-parameters modified Arrhenius expression can be utilized to fit the calculated rate constant values.

5.4. Ab-initio quantum chemistry programs: Gaussian

Gaussian can be considered the most widely used computational chemistry software. It exists in various editions, starting from the so-called *Gaussian 70* released in 1970 by Pople and co-workers. Subsequent updated versions were released, up to the most recent *Gaussian 09* version. The name *Gaussian* originates from the use of Gaussian orbitals instead of the Slater-type orbitals, a choice made to improve performances on the limited computing capacities.

The University of Illinois at Chicago makes available *Gaussian 03* on a 32-bit cluster for high performance computing. The *Gaussian 03* package[84] includes all common ab-initio and DFT methods as well as many semiempirical methods. Thus *Gaussian 03* can be used to optimize geometries, calculate vibrational frequencies, and search for transition state structures.

Although suitable for supporting optimization and vibrational frequency analyses of PAH species, the high performance computing system at UIC is not efficient for performing the high-level single-point energy calculations (CCSD(T) method). In order to be able to carry on such calculations in a reasonable time frame, part of the work was supported by the National Center for Supercomputing Applications (NCSA) at the University of Illinois at Urbana Champaign.

6. PHENYL PYROLYSIS AND PHENYL + ACETYLENE REACTION

The present chapter contains a detailed analysis of the experimental and modeling investigations of both the phenyl radical pyrolysis (preliminary to the subsequent experiments with acetylene) and the phenyl + acetylene reaction.

First, experiments were conducted utilizing the traditional offline set-up described in Chapter 3. Despite the measurement of the light hydrocarbon products, heavy hydrocarbon compounds could not be detected and quantified with accuracy by the offline traditional procedure. Thus, a new experimental technique was developed and implemented to address the problems related to condensation and adsorption of heavy PAHs. The results of the purely experimental investigation are under review for publication in the journal Review of Scientific Instruments.

Once implemented, the new set-up was utilized to perform new experiments on the reactions of interest. The experimental profiles, which include measurement of both light species and heavy, large molecular weight, multi-ring components, were subsequently used as targets to develop and validate a comprehensive chemical kinetic model for the phenyl pyrolysis and the phenyl + acetylene reaction. The model helped clarifying several aspects related to the growth mechanisms involved in the formation of large PAH compounds which serve as building blocks for soot formation. The work perfomed utilizing the new experimental set-up has been submitted to the Journal of Physical Chemistry A and is under consideration for publication.

As described later in the text (section 6.3.1.5), the experiments obtained with the new technique also inspired an additional purely-theoretical investigation of the mechanisms of formation of fused-ring compounds, namely naphthalene, from the radical/π-bond addition between single-ring aromatic hydrocarbons. Such theoretical investigation will be discussed in a separate chapter (Chapter 7).

6.1. Traditional technique: preliminary experimental results

The initial experiments have examined nitrosobenzene (C_6H_5NO) and phenyl iodide (C_6H_5I) as phenyl radical sources for subsequent reactions with added acetylene.

Nitrosobenzene started decomposing around 950 K, while above approximately 1050 K it is completely gone, Figure 5A, presumably forming phenyl radical and NO. In order to determine if nitrosobenzene is a clean source of phenyl radicals, the GC apparatus was equipped with a pulsed discharge detector (PDD) for NO measurement. The measured mole fraction of nitric oxide was found to be more than ten times the amount expected from a simple NO balance, suggesting that the quantification scheme for NO was not accurate. Moreover the nitric oxide profile showed a drop at high temperatures, indicating possible reactions of NO with the hydrocarbon products from the phenyl decomposition. Nitrosobenzene was abandoned as phenyl radical source.

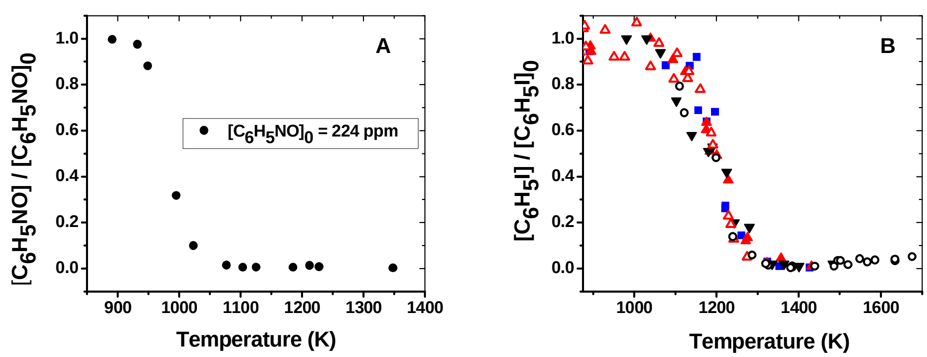

Figure 5. Phenyl pyrolysis, traditional technique. A) Nitrosobenzene decomposition, 100 atm. B) Phenyl iodide decomposition; ■ $[C_6H_5I]_0 \approx 50$ ppm, 50 bar; ▲ $[C_6H_5I]_0 \approx 300$ ppm, 50 bar; ▼ $[C_6H_5I]_0 \approx 850$ ppm, 50 bar; △ $[C_6H_5I]_0 \approx 200$ ppm, 25 bar; ○ $[C_6H_5I]_0 \approx 60$ ppm, 25 bar.

Phenyl iodide showed, Figure 5B, a similar behavior to that for nitrosobenzene in that above a certain temperature, in this case approximately 1350K, all the phenyl iodide had disappeared presumably to phenyl radical and iodine. Figure 5 also indicates that the decomposition of phenyl iodide is pressure insensitive indicating that the decay is in the first order high pressure limit.

The main products of the phenyl iodide decomposition were acetylene, diacetylene, benzene, and phenylacetylene, measured using the FID detector coupled to the PLOT-Q column suitable for separation of light species. The additional FID coupled to the HP1-MS column was used for the quantification of phenyl iodide and the heavy species, i.e. naphthalene. Trace amounts of biphenyl were also observed, but could not be quantified. Subsequent studies showed that the quantitative measurement of heavy species using the traditional set-up was not accurate, due to inaccuracy of the calibration curves as well as condensation and adsorption of the heavy compounds onto the metallic vessel walls.

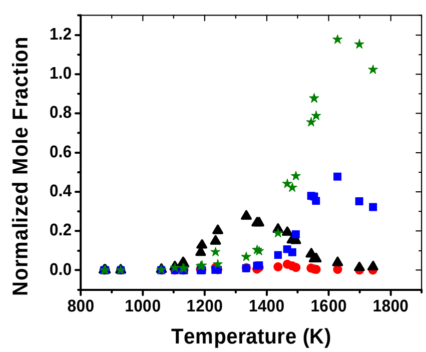

Figure 6. Phenyl pyrolysis, traditional technique, main products. $[C_6H_5I]_0$ = 61 ppm, 25 bar. Black triangles: benzene; red circles: phenylacetylene; green stars: acetylene; blue squares: diacetylene.

Figure 6 shows typical profiles for the main products of the phenyl iodide decomposition. Although acetylene and diacetylene start forming at around 1100K and 1300K respectively, the profiles show a steep increase only above 1400 K presumably in correspondence with the rupture of the aromatic ring. Benzene represents the major product of the reaction at intermediate temperatures. Small amounts of phenylacetylene were also measured.

Phenyl iodide was subsequently used as a phenyl radical source for examination of reactions with acetylene. Different amounts of acetylene (50 and 240 ppm) were added to the initial mixture composed of around 100 ppm of phenyl iodide in argon. Experiments were conducted at nominal pressures of 25 and 50 atm over a range of temperatures between 1000 K and 1650 K. The phenyl iodide decomposition is shown in Figure 7. It is worth mention that neither the pressure nor the phenyl iodide/acetylene mixing ratio seem to have a noticeable effect on phenyl iodide consumption.

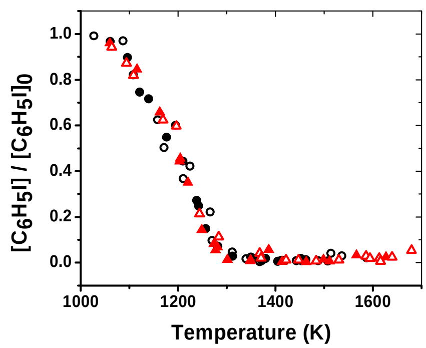

Figure 7. Phenyl + acetylene, traditional technique, phenyl iodide decomposition. Solid symbols: nominal pressure = 25 atm; open symbols: nominal pressure = 50 atm. Circles: $[C_6H_5I]_0$ = 104 ppm, $[C_2H_2]_0$ = 50 ppm; triangles: $[C_6H_5I]_0$ = 118 ppm, $[C_2H_2]_0$ = 240 ppm.

Besides the reactant molecule, several product species could be identified and measured. The corresponding mole fraction profiles for the experiments conducted with 50 ppm of acetylene are presented in Figure 8A. As for the phenyl radical pyrolysis, benzene is the major product at intermediate temperatures. Phenylacetylene is also produced in substantial amounts by the reactions between phenyl radicals and acetylene. Both benzene and phenylacetylene profiles peak at around 1300 K. At temperatures above 1400 K obviously decomposition reactions are dominating as indicated by the steep rise in acetylene and diacetylene concentrations. It is important to notice that both acetylene and diacetylene concentrations increase monotonically up to the temperature limit of the present experimental work (around 1600 K). There is a slight temperature shift in the profiles of these two species at the two different pressures which is not observed for benzene and phenylacetylene. Such a shift was not confirmed in the experimental work conducted with an excess of acetylene in the initial mixture. Thus no definitive conclusions can be drawn on possible pressure-dependent mechanistic pathways which influence the formation of acetylene and diacetylene.

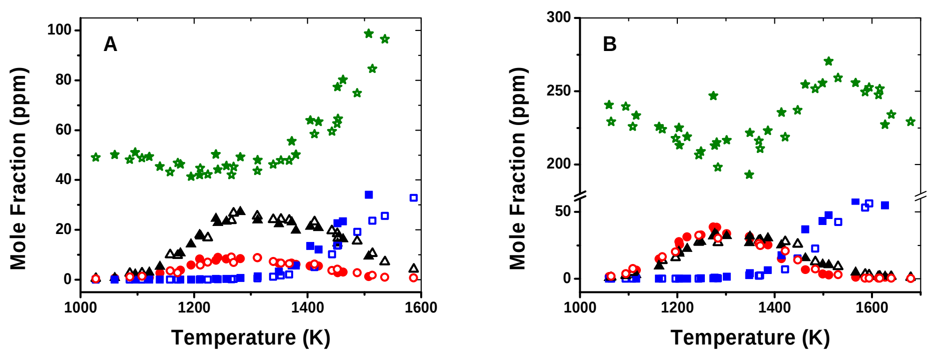

Figure 8. Phenyl + acetylene, traditional technique, major products. A) [C_6H_5I]$_0$ = 104 ppm, [C_2H_2]$_0$ = 50 ppm. B) [C_6H_5I]$_0$ = 118 ppm, [C_2H_2]$_0$ = 240 ppm. Solid symbols: nominal pressure = 25 atm; open symbols: nominal pressure = 50 atm. Triangles: benzene; circles: phenylacetylene; stars: acetylene; squares: diacetylene.

Figure 8B shows the results obtained with excess acetylene (240 ppm). The only substantial difference with the previous case is the increased formation of phenylacetylene. This result is in agreement with chemical intuition since at higher concentrations of acetylene more phenyl radicals are stabilized as phenylacetylene. Correspondingly, the phenylacetylene/benzene branching ratio increases from approximately ⅓ to 1 which corresponds as roughly to the variation in the phenyl iodide/acetylene ratio. Furthermore an interesting difference between the two sets of experiments is that, in case of the higher initial acetylene concentration, at high temperatures no further increase in the acetylene concentration could be detected but in contrast acetylene seems to be consumed. This might be due to the higher tendency for polymerization which leads to formation of larger polyacetylenes.

Although the experimental data presented in this section provide important information on the chemistry involved in the phenyl pyrolysis and in the phenyl + acetylene reactions, the preliminary results are incomplete. In fact the experimental data show a drop in the carbon balance especially at high temperatures in correspondence with the formation of heavy semi- and non-volatile polycyclic hydrocarbons (i.e. naphthalene, biphenyl, phenanthrene, and so on) which are not analyzed (Figure 9). The profiles for the latter species are essential for the understanding of the reactions of the phenyl radical with acetylene as well as for the characterization of the pathways leading to naphthalene and other PAHs. The work reported in the following sections will describe the efforts done for defining an experimental procedure able to provide an accurate and reliable measurement of heavy semi- and non-volatile polycyclic hydrocarbons.

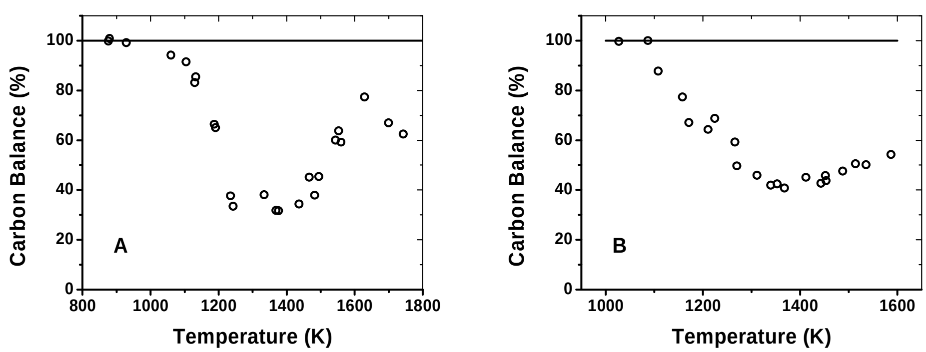

Figure 9. Percentage of carbon recovery, traditional technique. A) $[C_6H_5I]_0$ = 61 ppm, 25 bar. B) $[C_6H_5I]_0$ = 104 ppm, $[C_2H_2]_0$ = 50 ppm, 50 atm.

6.2. Online and offline experimental techniques for PAHs recovery and measurement

The condensation and/or adsorption of heavy semi-volatile and non-volatile compounds are common problems in many analytical systems, including among others, exhaust gas analysis apparatuses[85,86] and ambient air sampling analysis systems[87,88]. Alternatively, specific resins, such as Amberlite XAD-2 polymeric adsorbent have proven to be successful in many practical applications. The resins trap the gas-phase polycyclic aromatics (naphthalene and heavier compounds) present in the gas sample, for subsequent extraction with an appropriate solvent. However, the resin trapping technique is not suitable for systems where the sampling process involves high-speed or very fast (sometimes supersonic) flows, as in the case of high-pressure experimental apparatuses, since the resin can not guarantee the recovery of 100% of the PAH products. The resin trapping method thus can only provide a qualitative but not quantitative measure of the distribution of heavy compounds in the analyzed sample. Sometimes too, when the concentration of the PAHs in the sample is small, a rotary evaporator technique must be used to concentrate the solution obtained from the resin method to permit detection of the absorbed species. However, the experimental investigation by Cheng[89] has shown that the rotary evaporator technique leads to losses in the target species measurement which are molecular weight dependent as well as dependent on the required volumetric reduction in the sample size. Thus the sample concentration step of the resin trapping method not only greatly increases the time required to complete the experimental measurement but also provides an additional source of uncertainty to the possible losses during the sampling as well as during the procedure aimed at extracting the heavy compounds from the resin.

This section presents the experimental investigation on alternative online and offline techniques for the recovery and measurement of the typical PAH compounds which constitute the building blocks for PM formation. In particular, the present techniques apply to all the experimental apparatuses where the conventional techniques which use resins and rotary evaporators fail to provide a complete recovery of the gas-phase semi-volatile and non-volatile components. Among such experimental apparatuses are shock tubes, such as the high-pressure shock tube present at the University of Illinois at Chicago[30], flow reactors, and furnace reactors, designed for the study of chemical reacting flows.

Online vs. offline. The traditional online techniques, which include well established method of time-of-flight (TOF) mass spectrometry, take advantage of the direct connection between the analytical apparatus and the instrumentation used to generate the gas sample which needs to be measured. This allows quick analysis of the sample, which results into the ability to detect short-lived species, such as radicals, and measure compounds which oxidize when stored or tend to condense/adsorb, such as large molecular weight species. Nevertheless, online techniques can not be implemented in those applications where the sample has a large volume or a very high pressure which can not be sustained by the specific analytical apparatus. For example, the gas chromatographic valves for gas injection are rated to a maximum pressure of 300 psi, which is a relatively low pressure compared to the typical conditions implemented in the high pressure shock tube at UIC. In addition, the presence of solid particles (soot) in the sample could interfere with the analysis or even damage the analytical system. Another factor which plays a relevant role in the ability to implement the online techniques is the necessity to have the analytical apparatus available in-situ where the sample is generated. These limitations can be overcome by the use of offline techniques which allow the analysis of samples, such as the air samples[87,88], which are collected over relatively long times and in different geographical locations. Nevertheless, the use of offline techniques is limited to the measurement of stable compounds which can be easily stored. In particular, the measurement of heavy multi-ring species is possible only after the implementation of supplemental procedures such as the resin trap/rotary evaporator technique described above.

6.2.1. Offline technique

The GC/GC-MS offline measurement of light hydrocarbon compounds has been extensively used in our laboratory to measure stable products from high-pressure shock tube oxidative and pyrolytic experiments of PAH formation. Due to the high pressure reached during the experiments (up to 1000 atm, Ref. 30), instead of glass vessels, 150 cc stainless steel electropolished vessels are used to collect the gas sample withdrawn from behind the reflected shock wave during a 0.3 second time window. A portion of the stored sampled gas is subsequently injected into the gas chromatographic system for measurement of the stable species. Despite the success of this sampling procedure in our previous work[35,90], the experimental procedure had not been extended to the sampling of heavy multi-ring compounds. In order to establish a new experimental procedure aimed at extending the analytical capability to large molecules, a series of experiments were initiated using the traditional stainless steel electropolished vessels and naphthalene as representative test compound. The basic idea behind the new technique, which assumes that heavy multi-ring compounds will condense, is to analyze both the non-condensed gas phase species and the condensed components by a combination of gas phase and liquid injection GC analyses.

6.2.1.1. Offline technique: preliminary experiments

Before performing the experiments relevant to the determination of the optimal offline technique, several preliminary experiments were executed to test the uncertainties related to the various auxiliary experimental components.

The first important element to be evaluated when quantitative studies are performed is the uncertainty in the instrument calibrations as well as the linearity of the response. Several liquid solutions with different concentrations of naphthalene in methylene chloride were prepared and analyzed with both the mass spectrometer and the FID detector. The results, reported in Figure 10, clearly indicate that although the MS response is linear on a macroscopic scale, the detector loses sensitivity when the concentration drops below 1 μg/ml (Figure 10b). The difference between the calibration curves obtained fitting the data over the entire range (Figure 10a) or using only the data with concentrations below 1 μg/ml is around 12%. On the other hand, if we repeat the same test using the FID detector (Figure 10c and Figure 10d), the corresponding difference between the calibrations is only 3% which is within the experimental uncertainty of the measurements. Due to the improved linearity, the FID detector was utilized for analysis of liquid samples. Calibrations for other PAH components were obtained with a similar procedure used for Figure 10c and Figure 10d.

A second linear FID detector was used to measure the gas phase components. In this case the calibration was performed using a 250 cc glass vessel equipped with a septum. The vessel was heated to 150°C. Different solutions of naphthalene in methylene chloride were prepared and small amounts injected into the glass vessel, previously evacuated, using a syringe. The solution vaporizes immediately due to the high temperature and high vacuum. Using a mixing rig, the vessel is subsequently filled with argon to a determined pressure. Pressure and temperature are recorded and used subsequently to calculate the actual mole fraction of naphthalene in the gas phase mixture. The gas mixture is allowed to stand for around 10-15 minutes before injection into the GC (to guarantee homogeneity).

Figure 11a contains the experimental results obtained using a 10 μl syringe and different injection volumes. Although for each injection volume the response is linear, the calibration curve for naphthalene varies if obtained by injecting 1, 2, or 3 μl of solution into the glass vessel. In particular, the response becomes lower with increasing injection volume which suggests the presence of trapped sample in the syringe needle. In fact, from a logical point of view, the trapped sample is more relevant when low volumes are injected since the percentage of extra solution is greater. As shown in Figure 11b the use of a 5 μl syringe with plunger in the needle solves the dead volume problem. The experimental points lie on the same curve independently of the injection volume and the calibration curve is now self consistent. All the following experiments were performed using the 5 μl syringe with plunger in the needle. The gas phase calibrations for other species were obtained similarly to the case reported in Figure 11b.

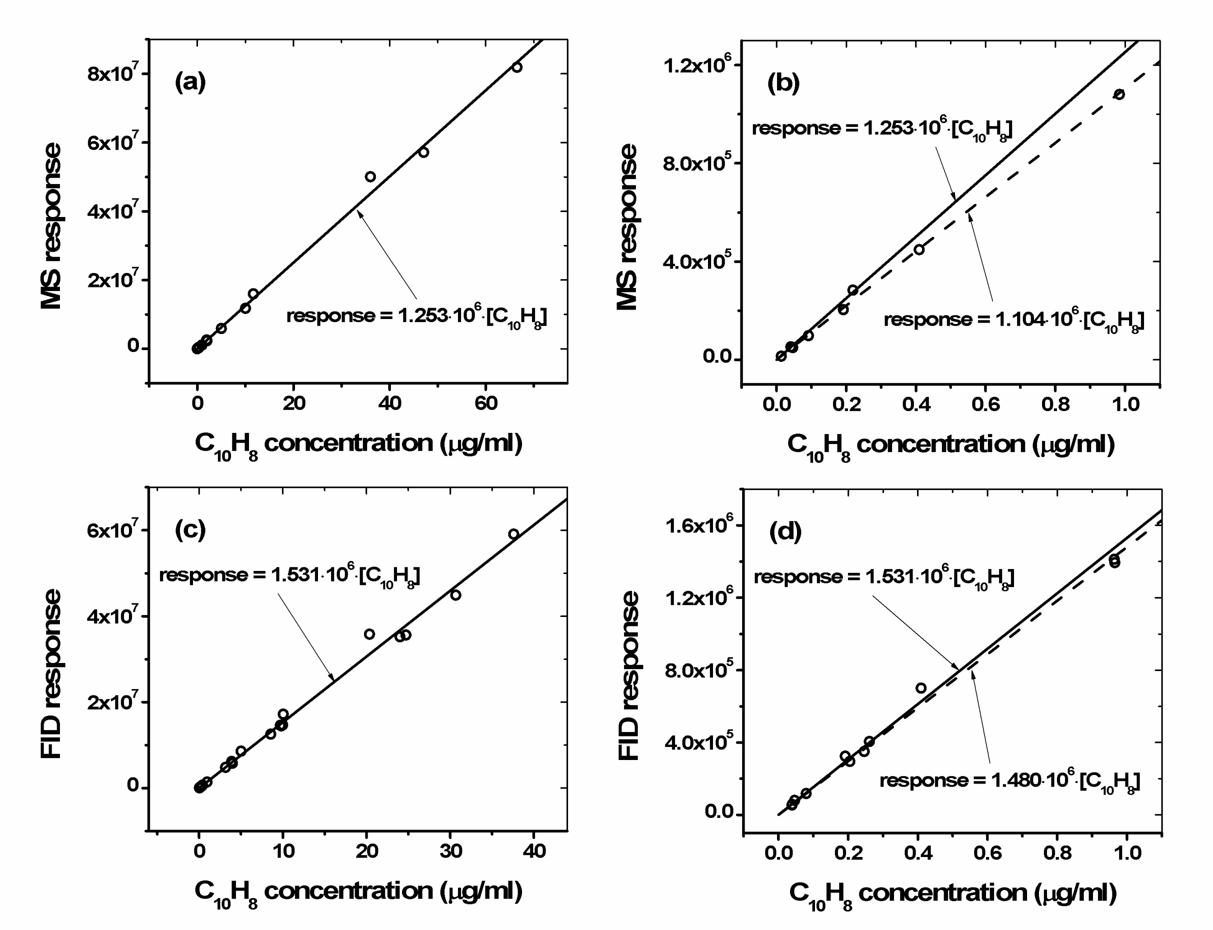

Figure 10. MS [(a) and (b)] and FID [(c) and (d)] naphthalene calibrations using liquid injection port. (b) and (d) represent a zoom-in of the data in A and C respectively. ○ experiment; —— calibration curve; – – calibration curve considering only data with concentrations below 1 μg/ml.

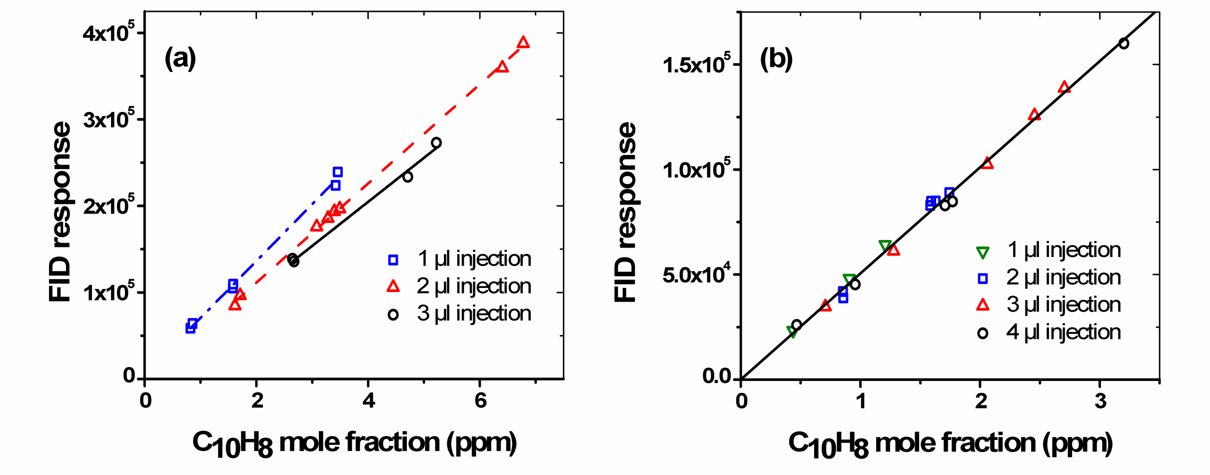

Figure 11. FID gas calibrations. A) 10 µl syringe; B) 5 µl syringe with plunger in the needle.

An additional possible source of uncertainty is related to the syringe calibration. Tests were performed to determine the magnitude of such uncertainty. Solutions of naphthalene in methylene chloride were prepared and the 5 µl syringe used to inject 5 µl of the solution into a measured volume of methylene chloride (dilution step). The diluted mixture is then analyzed and compared with the calculated value (from the measured masses of naphthalene and methylene chloride). The comparison provides a good estimate of the error associated with the use of the syringe. The results, reported in Table 1, indicate that the maximum uncertainty is around 2%, which can be considered almost negligible compared to the uncertainty related to the preparation of the naphthalene and methylene chloride solution and to the GC calibrations.

	measured [$C_{10}H_8$] (µg/mol)	calculated [$C_{10}H_8$] (µg/mol)	error (%)
S1	1.43	1.42	+0.7%
S2	2.58	2.69	-4.1%
S3	1.26	1.29	-2.3%
S4	1.39	1.42	-2.1%
S5	1.43	1.45	-1.4%

Table 1. Tests to evaluate the uncertainty in the syringe calibration.

6.2.1.2. Offline technique: primary experiments

The purpose of the present section is to provide a brief overview of the experimental work performed to determine an optimized procedure for the recovery of PAH compounds using gas phase and liquid injection GC techniques. The experimental set-up consists of a 150 cc stainless steel electropolished vessel connected one side to a septum and on the other to a stainless steel high-pressure valve (Figure 12). The connection section for the septum can be heated to 200-220 °C independently from the vessel body. The test mixture is prepared injecting into the heated connection section a specific volume of solution of naphthalene in methylene chloride. The flash vaporization of the injected solution is guaranteed by the high temperature of the connection section and by previous evacuation of the vessel. The injection volumes vary from 1 μl to 5 μl while the concentrations of the solutions from around 450 μg/ml to 2000 μg/ml. These values give a final naphthalene gas phase mole fraction between 1 and 10 ppm after dilution with argon (17 to 19 psi). The gas phase mixture simulates a gas sample withdrawn from an experimental apparatus or from the atmosphere containing a low concentration of target contaminant (1-10 ppm). This is definitely the most challenging situation especially if quantitative measurements are required but experiments similar to the ones presented here can be easily repeated using higher concentrations of naphthalene if necessary for the specific application.

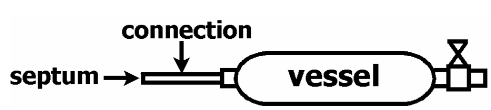

Figure 12. Assembly for PAH recovery experiments.

The first set of experiments has been conducted maintaining the vessel at room temperature during the entire analytical process. This technique represents the simplest solution since it does not require any additional instrumentation. After standing for at least 15 minutes to homogenize, the gas mixture is analyzed through the HP-1ms column. The mole fraction of naphthalene obtained from the analysis can be converted into actual μg of naphthalene using the ideal gas law (gas phase component). In the meantime, the vessel is flushed with methylene chloride. The volume of solvent used during the flushing procedure varied between 30 and 100 ml with no difference in the results. The resulting solution of naphthalene dissolved in methylene chloride is subsequently injected into the DB-17ms column. Multiplied by the measured volume of methylene chloride used in the flushing procedure, the concentration obtained from the analysis provides the condensed component of naphthalene in the sample. The sum of the gas phase and condensed components can be compared with the injected mass of naphthalene to obtain the percentage recovery for the specific experiment.

The results, presented in Table 2, are divided into two groups. The flushing procedure for the experiments from N1 to N4 was conducted introducing the methylene chloride into the vessel, closing the vessels, and shaking for 10 minutes. Within a 10% of discrepancy, the measured mass of naphthalene is higher than the actual mass introduced into the vessel. The reason for this unexpected result, confirmed also by tests conducted with lighter compounds as described later in the manuscript, is associated with the relatively high mole fractions of naphthalene in gas phase. Part of this gas phase component is clearly dissolved into the methylene chloride during the flushing procedure and thus it is counted twice both in gas and in liquid phase.

Improvement in the accuracy of the procedure was obtained by modifying the flushing technique (N5 to N8 in Table 2). The new flushing technique consists in introducing the solvent into the vessel and continuously rotating the open vessel for approximately 2 minutes. In this case the major part of the gas phase naphthalene is allowed to exit the vessel together with the methylene chloride vapor. After two minutes of rotation, the vessel is closed and subjected to the usual shaking for around 8 minutes. With the implementation of the new procedure the percentage of naphthalene recovered is closer to the desired 100% and only a couple of percentage points higher. Tests were also conducted to remove the gas component of the mixture using a gentle flow of argon through the vessel just before the flushing but the attempts resulted in lower recovery rates.

	gas (µg)	condensed (µg)	total (µg)	injected (µg)	recovery (%)
N1	2.70	2.69	5.39	5.06	106.5%
N2	2.63	2.73	5.36	5.01	107.0%
N3	5.56	4.95	10.51	10.00	105.1%
N4	2.68	2.89	5.57	5.00	111.4%
N5	2.71	2.43	5.16	5.00	103.2%
N6	1.60	1.52	3.12	2.99	104.3%
N7	0.82	1.15	1.97	1.92	102.6%
N8	2.58	2.46	5.04	4.90	102.9%

Table 2. Experiments with vessel at room temperature.

In order to further improve the recovery results eliminating the excess naphthalene, we started a series of experiments performing the entire analytical procedure with the vessel cooled to a temperature between -10 and -15 °C. Table 3 contains the related results. The recovery is accurate with an uncertainty of around 7% which is totally within the uncertainties associated with the preparation of the mixture and with the GC measurements. Since the gas phase component is small, no substantial differences were observed between the results obtained with the two flushing methods described above, i.e. the shaking (N9-N14) and the rolling techniques (N15-N17).

	gas (µg)	condensed (µg)	total (µg)	injected (µg)	recovery (%)
N9	0.46	4.47	4.93	5.06	97.4%
N10	2.23	8.19	10.42	10.13	102.9%
N11	0.27	4.40	4.67	5.01	93.4%
N12	0.62	4.33	4.95	5.01	98.8%
N13	0.74	4.00	4.74	4.90	96.7%
N14	0.60	4.68	5.28	4.90	107.8%
N15	0.35	4.41	4.76	4.90	97.1%
N16	0.03	1.90	1.93	1.96	98.5%
N17	1.63	3.50	5.13	4.90	104.7%

Table 3. Experiments with cooled vessel.

Additional experiments were performed using a 500 cc stainless steel electropolished vessel to test possible dependence of the recovery results on the shape of the vessel, in particular on the ratio between surface area and volume. All the experiments were conducted cooling the vessel since this procedure showed slightly better recovery results compared to the procedure at room temperature. In this case solutions with naphthalene concentrations between 1800 and 9000 μg/ml and injection volumes between 1.5 and 8 μl were used to obtain a final argon-naphthalene mixture with a naphthalene mole fraction between 1 and 17 ppm. Similarly to the experiments reported in Table 3, the maximum error is around 7% (Table 4), becoming even smaller when relatively large masses of naphthalene are injected into the vessel (N26-N28). No difference between the shaking (N18-N24) and the rolling (N25-N28) flushing techniques is once again observable. The results confirm the excellent recovery rates obtained with the proposed analytical methodology and indicate that the specific shape of the vessel does not affect the accuracy of the procedure.

	gas (μg)	**condensed (μg)**	**total (μg)**	**injected (μg)**	**recovery (%)**
N18	4.19	5.56	9.75	9.67	100.8%
N19	1.89	2.53	4.42	4.57	96.7%
N20	1.53	2.68	4.21	4.57	92.1%
N21	1.25	1.60	2.85	2.74	104.0%
N22	2.09	2.59	4.68	4.57	102.4%
N23	1.71	2.80	4.51	4.57	98.7%
N24	1.59	10.08	11.67	10.91	107.0%
N25	1.06	9.87	10.93	10.91	100.2%
N26	1.48	26.78	28.26	27.42	103.1%
N27	0.99	35.66	36.65	36.55	100.3%
N28	2.01	52.94	54.95	54.83	100.2%

Table 4. Experiments with cooled 500 cc vessel.

Before proceeding with the analysis of the recovery of compounds with different molecular weights and specific properties compared to naphthalene, the effect of the variation in the mixture pressure was also evaluated. As mentioned before, the results presented are referred to gas mixtures prepared at a total pressure between 17 and 19 psi, slightly above atmospheric pressure. Experiments were repeated using the 150 cc vessel and around 39 psi mixtures with the vessel at room temperature. Thus we would expect a recovery percentage between 102 and 110% as in the case of the experiments in Table 2. Surprisingly the results did not confirm the expectations. As shown in

Table 5, although the experiments were conducted at room temperature, the recovery rate is low indicating a loss of naphthalene for both flushing procedures (N29-N31 shaking, N32-N33 rolling). This unexpected behavior could be a consequence of the quick release of the gas mixture, which largely exceeds atmospheric pressure for these experiments, when the vessel is opened to allow the introduction of the methylene chloride used for the flushing procedure. Part of the naphthalene condensed on the walls of the vessel could vaporize at the new low pressure conditions and not get dissolved in the methylene chloride. This is a very important point to consider when designing an experiment. In fact if the pressure of the gas withdrawn for analysis is too high, a low recovery rate as the one reported in Table 5 could be obtained. A solution to the problem could be an increased volume of the vessel so that the pressure is decreased to the atmospheric value in the vessel. The shape of the vessel does not influence accuracy of the recovery technique as discussed previously in the text.

	gas (µg)	**condensed (µg)**	**total (µg)**	**injected (µg)**	**recovery (%)**
N29	2.58	2.00	4.58	4.98	92.0%
N30	2.37	1.85	4.22	4.90	86.1%
N31	2.38	1.61	3.99	4.90	81.4%
N32	2.27	1.89	4.16	4.98	83.5%
N33	0.51	0.60	1.11	1.20	92.5%

Table 5. Experiments at higher pressures and vessel at room temperature.

	gas (µg)	**condensed (µg)**	**total (µg)**	**injected (µg)**	**recovery (%)**
B1	0.00	38.34	38.34	37.93	101.1%
B2	0.15	21.66	21.81	21.07	103.5%
B3	0.03	4.81	4.84	4.98	97.2%
B4	0.01	114.64	114.65	115.81	99.0%
B5	0.02	88.48	88.50	90.08	98.2%
B6	0.02	65.01	65.03	64.34	101.1%

Table 6. Experiments for biphenyl recovery with cooled 500 cc vessel.

All the experiments reported in the previous paragraphs use naphthalene, the simplest among the multi-ring hydrocarbons, as reference compound. Species with larger molecular weights are expected to have lower vapor pressure than naphthalene, thus the recovery would be similar with the only difference being less of gas phase component compared to the solid condensed component. In order to test the recovery rates of the proposed technique for heavier species, the experiments with the 500 cc cooled vessel were repeated for biphenyl as a test compound using the rolling technique as the flushing procedure. The prepared gas mixtures in this case simulate a gas sample containing a mole fraction from 1 to 30 ppm of biphenyl. The results are reported in Table 6 and indicate an excellent recovery rate over the entire mass range. The excellent accuracy of the proposed method is again demonstrated for species like biphenyl which are practically non-volatile and have a very small vapor component.

Very different considerations apply for compounds having a smaller molecular weight than naphthalene but still sufficiently high to partially condense on the surface of the vessel. These compounds include for example small halogenated hydrocarbons and other semi-volatile compounds. Experiments have been conducted using iodobenzene as test species in order to determine if the procedure for the recovery of large PAH hydrocarbons is suitable also for lighter species. Of course the completely volatile compound can be easily measured with a simple gas analysis before the flushing procedure.

The preliminary experiments conducted using the procedures described above showed a percentage of recovery for iodobenzene much higher than 100% (around 130 to 140%). This is mainly due to the gas phase component which is predominant with respect to the condensed phase even when the 500 cc vessel is cooled to -15 °C. As, to a minor extent, for the naphthalene experiments at room temperature, part of the iodobenzene in gas phase is dissolved into the flushing solution, and thus measured twice in the total iodobenzene mass balance. This hypothesis was confirmed by blowing nitrogen through the vessel for 3-5 seconds right before the methylene chloride flushing. The results were accurate (error in the range between -9% to +2%) which indicate that the gas phase is responsible for the extra iodobenzene. On the other hand, as previously emphasized in the manuscript, this method of storing samples in a vessel is not suitable for the measurement of PAH compounds such as naphthalene.

Although the experiments for iodobenzene are clearly not satisfactory, a careful analysis of the results suggests a different approach to the problem. At a defined temperature the ratio between the amount of iodobenzene in gas phase and in condensed phase is almost constant. Experiments at room temperature were conducted to verify this hypothesis over a wide range of mole fractions (5 to 200 ppm) using both the 500 cc vessel and a new stainless steel electropolished 300 cc vessel. The results shown in Figure 13 indicate that the percentage of iodobenzene in gas phase is around 80% for the 500cc vessel and around 89% for the 300cc vessel. Excluding a few experiments, marked with a cross, which are clearly wrong possibly due to an error in the experimental procedure, all the condensed phase percentages lie close to the two fitting values within a 5-7% uncertainty. This uncertainty is similar to the one obtained for the recovery of naphthalene. Very interesting from an experimental point of view is the difference in average condensed phase percentages between the two vessels. The surface area to volume ratio clearly has a significant effect on the proportions between gas phase and condensed phase components. This suggests that new tests need to be repeated in case of the use of a different vessel. Once the average condensed phase percentage is obtained similarly to the case in Figure 13, this value can be used to scale the gas phase mole fraction. For example, if for a specific gas sample the gas phase mole fraction of iodobenzene is 100 ppm, the total iodobenzene mole fraction would be 125 ppm (100 divided by 0.8) and 112 ppm (100 divided by 0.89) in the case we used the 500 cc or the 300 cc vessel, respectively.

Finally, in order to evaluate the effect of the temperature on the percentage of iodobenzene in gas phase, a few experiments were also conducted with the 500cc vessel cooled to -12°C. The percentage dropped from an average value of 80% to values between 63% and 70% (mole fractions between 80 and 180 ppm, data not shown).

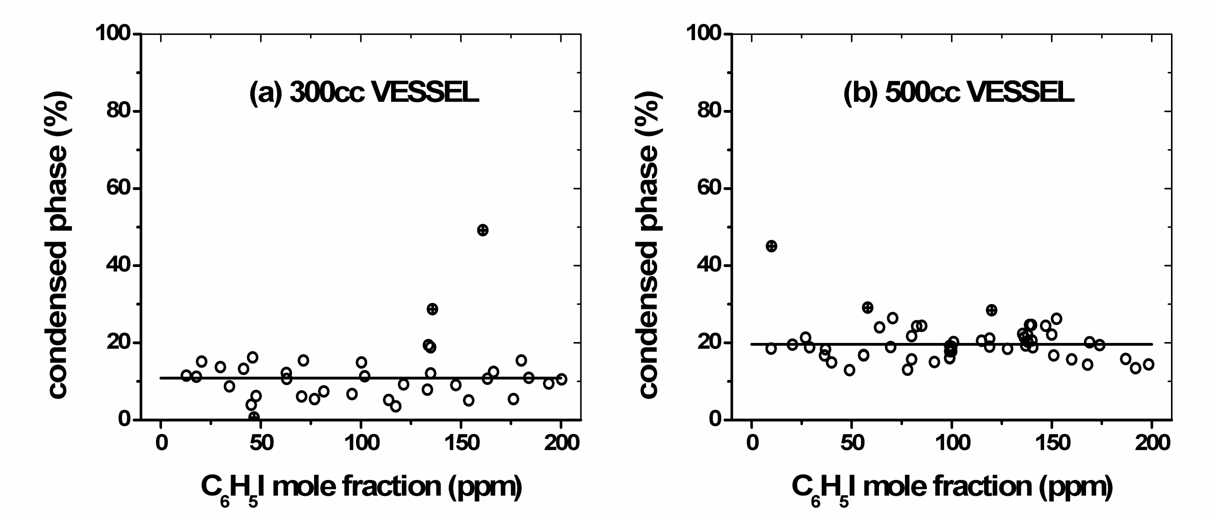

Figure 13. Percentage of iodobenzene (C_6H_5I) in condensed phase. Vessel at room temperature.

6.2.1.3. Optimal offline recovery technique

Now that we have presented all the experimental results related to the recovery of semi- and non-volatile compounds, including PAH intermediates, a short paragraph which summarizes the main findings and suggests the optimal offline technique is provided. For the experimental results, the sample vessel can be maintained at room temperature during the collection of the gas sample from a specific experimental apparatus, from automotive exhaust systems, or from the atmosphere. Once the sample is collected, gas injection into a GC column specifically suitable for the separation of light hydrocarbons, such as the HP-PLOT Q column, is required for the measurement of the gas phase volatile components of the mixture. The mole fraction of the semi-volatile species, such as iodobenzene, can be corrected by a factor that takes into account the component in condensed phase. After the injection for light species measurement, the vessel is cooled to ≈-15 °C and a new gas injection performed to measure the residual gas phase fraction of multi-ring compounds. The GC column in this case needs to be suitable for separation of heavy hydrocarbons (DB-17ms or HP-1ms).

The sample vessel is subsequently flushed with methylene chloride and the solution injected into the GC for further analysis. The gas phase and liquid phase analyses done with the vessel cooled provide accurate quantitative measurements of heavy semi-volatile and non-volatile species (i.e. naphthalene, biphenyl, and so on). The expected error in the final recovery of the heavy components is around ±7%.

Before concluding it is worth mention that if a cooling apparatus is not available or if it is necessary to reduce the time of the experiment, the analyses of the PAH semi- and non-volatile components can be performed at room temperature. In this case the flushing technique should be modified to the rolling + shaking technique as described in the text. The performance of the technique is similar in terms of recovery of heavy non-volatile components, although for semi-volatile species such as naphthalene a small overestimation of the total mole fraction is expected.

6.2.2. Offline technique: experimental results

Experiments on the phenyl iodide pyrolysis as well as on the reactions between the phenyl radical and acetylene have been performed using the new offline experimental procedure. Similar conditions to the preliminary data reported in section 6.1 were used, with nominal pressure of 50 atm, temperature range between 900 K and 1850 K, and reaction times of 1.5-2 ms. The phenyl iodide in the initial mixture was around 45 ppm, with or without addition of 180 ppm of acetylene. The species profiles were consistent with the preliminary results obtained with the traditional technique for the lighter compounds (phenyl iodide, acetylene, diacetylene, benzene, phenylacetylene). The profiles are reported in Figure 14A and Figure 15A.

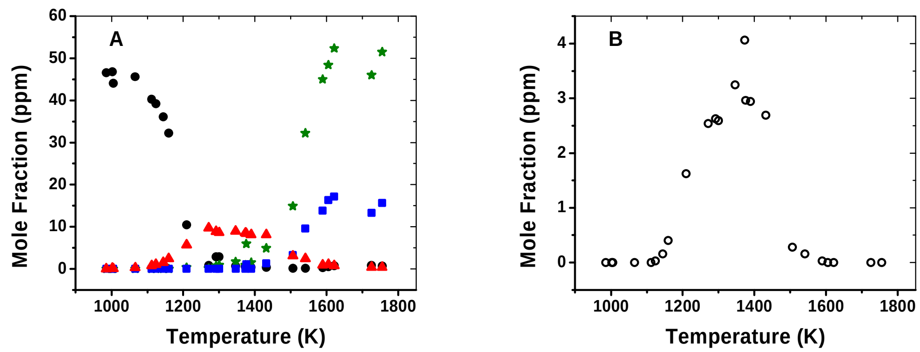

Figure 14. Phenyl pyrolysis, flushing technique, $[C_6H_5I]_0$ = 46 ppm, 50 bar. A) Light hydrocarbons. Circles: phenyl iodide; triangles: benzene; stars: acetylene; squares: diacetylene. B) Biphenyl.

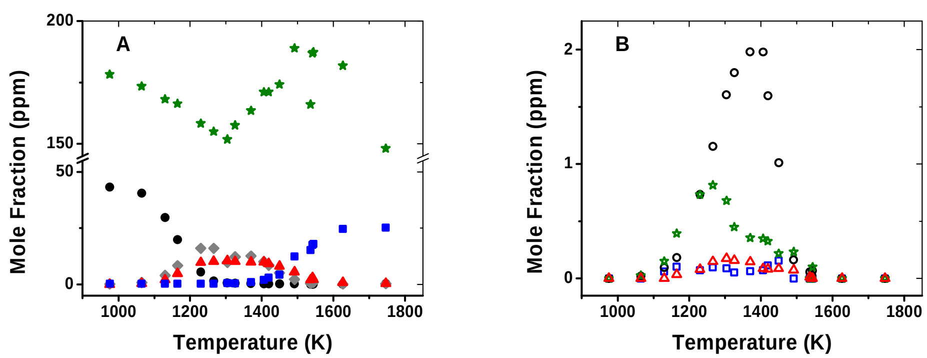

Figure 15. Phenyl + acetylene, flushing technique, $[C_6H_5I]_0$ = 43 ppm, $[C_2H_2]_0$ = 178 ppm, 50 atm. A) Light hydrocarbons. Circles: phenyl iodide; triangles: benzene; rhombuses: phenylacetylene; stars: acetylene; squares: diacetylene. B) PAHs. Circles: biphenyl; stars: diphenylethyne; triangles: phenanthrene; squares: naphthalene.

In addition to the compounds that could be measured with the traditional technique, profiles were obtained for naphthalene, biphenyl, phenanthrene, and diphenylethyne (chemical structures reported in Figure 21). In particular, Figure 14B shows the results for biphenyl which is the only PAH compound produced in substantial amounts from the phenyl radical self-reactions. On the other hand, several multi-ring compounds, including the major ones biphenyl and diphenylethyne, were identified in the study of the phenyl + acetylene reaction (Figure 15B). Small amounts of naphthalene and phenanthrene were also measured.

Although improvements were observed in the ability to collect and measure heavy polycyclic hydrocarbons, the carbon balance analyses still showed a drop at high temperatures (Figure 16). Although analyses were conducted to understand the causes of the drops, no plausible explanation could be found. Nevertheless, subsequent experimental tests on a different set-up showed that one of the seals of the automated valve had been destroyed, releasing pieces of graphite and powder in the vessels. The solid particles are chemically active and can easily adsorb PAH compounds from the gas phase. The recovery through the offline flushing technique was certainly influenced by the presence of particles in the system.

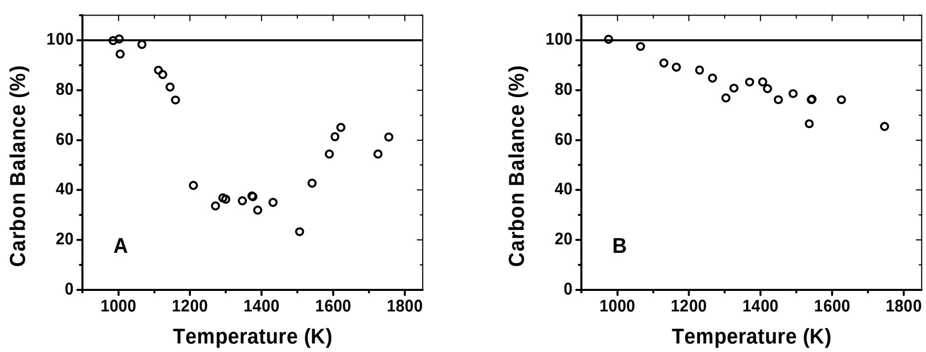

Figure 16. Percentage of carbon recovery, flushing technique. A) $[C_6H_5I]_0$ = 46 ppm, 50 bar. B) $[C_6H_5I]_0$ = 43 ppm, $[C_2H_2]_0$ = 178 ppm, 50 atm.

6.2.3. Online technique

The purpose of the present section is to provide an overview on the implementation of an online experimental set-up and methodology for measurement of heavy PAH gas phase compounds by conventional GC technique. The proposed technique combines the advantages of the conventional gas chromatography (sensitivity and ability to separate complex mixtures) with the simplicity in design and experimental procedure typical of the online techniques.

The GC apparatus described in section 3.3 was connected directly to the high-pressure shock tube present at the University of Illinois at Chicago[30] (Figure 17). A three-foot long, 1/4” OD tube connects the automated valve positioned at the end of the shock tube to the first GC. The gas is transferred to the GC injection valve through a 1/16” tube, fills the sample loop and flows to the second GC through a 1/8” tube. In this second GC, the gas fills in series two sample loops, before entering a sampling rig. The sampling rig is connected to an Edwards E2M1.5 rotary pump, a heated MKS capacitance manometer (type 631B, 1000 Torr full scale), a 150 cc reservoir, and a line for helium gas. Two additional lines are present, one connected to an exhaust line for safety purposes, the other available for connection of gas mixture bottles or vessels for calibration procedures. All the lines and connections present in the sampling section were built with treated stainless steel tubing, including the GC sample loops which were in-house cut using 1/16” tube. In addition, the lines are evenly wrapped with heavy insulated heating tapes of different width and watt density based on the thickness of the specific tube to be wrapped. Seven different heating zones are present, each associated with one type-J thermocouple. The temperature is set at 150 °C to avoid condensation of large molecules and is controlled by means of a multi-zone temperature controller by Omega (model CN1507-TC).

Particular attention was addressed to the choice of the optimal type of tubes used to build the entire sampling section. In order to avoid adsorption of species, first glass-lined tubes were considered. These tubes can be bent only at 800 °C. They are fragile and must be deactivated (if necessary). Thus they don’t represent an easy solution to be implemented especially considering that in a complex sampling system the lines must usually be curvilinear. Excluding the glass-lined tubes if possible, other solutions include deactivated fused silica-lined tubing provided by Sigma-Aldrich. The internal wall of these tubes is covered by a thin layer of fused silica which is well known for its extremely low absorption characteristics and inertness to chemicals. Moreover this kind of tube can be easily bent although, due to the specific manufacturing technique, only 1/16" and 1/8" OD tubes are commercially available. The size of these tubes would clearly constrain the gas flow downstream to the shock tube sampling valve (Figure 17) and would cause a withdrawal of too small of a gas sample for subsequent GC analyses, especially when low pressure experiments are conducted (low pressure in this case means 25 atm or less nominal pressure).

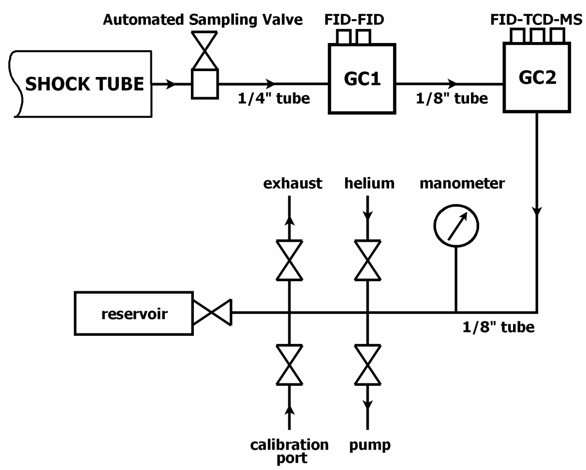

Figure 17. Schematic of the online set-up.

On the other hand, Restek provides treated stainless steel tubing specifically designated as inert with performances claimed to be as good as the ones from deactivated fused silica-lined tubing. Their 1/4" and 1/8" OD tubes are also electropolished for extreme inertness. In addition, Restek provides treated 1/16" tubes as well as tube connections and unions. The Restek solution was adopted to build the entire experimental sampling set-up.

The experimental procedure implemented for the collection and measurement of gas samples from the shock tube is relatively simple. After evacuation of the lines, the pump line is closed just before firing a shock. By controlling the exhaust line as well as the reservoir valve, it is possible to decrease/increase the pressure in the lines once the sample is collected from the tube (automatic valve opened for around 2 ms). In particular, it is important that the pressure does not reach very high values since the standard GC gas valves can only sustain pressures up to 300 psi, a relatively low value in relation to the shock tube experimental conditions. Once the pressure in the line is stabilized (usually in few seconds), gas injections into the two GCs are performed almost simultaneously. The lines are then flushed several times with helium to remove all the sample gas.

The separation of the gas sample is performed through a combination of columns/detectors specifically studied to identify and quantify all the components present even in the most complex mixtures. The first GC, utilized to measure heavy compounds, uses an FID coupled with a DB-17ms column while the second GC is used for measurement of light hydrocarbons (FID and HP-PLOT Q column) and inert species (TCD and HP-PLOT MoleSieve). The mass spectrometer present in the second GC can be connected for identification of unknown species if necessary. The GC calibration for the relatively light hydrocarbons can be performed using certified gas mixtures as well as in-house prepared calibration mixtures. Typical errors in the measurement of such species are around 5-10%. On the other hand, the calibration of large PAH compounds can not be performed in gas phase due to the difficulties associated with the preparation of appropriate gas phase calibration mixtures. The best solution to derive estimated calibration curves for heavy species is to use a combination of gas and liquid phase analyses as described next. In particular, the calibration curves can be deduced from the gas phase calibration curve for naphthalene based on the relative ratio between the corresponding liquid phase calibration curves. The gas phase calibration of naphthalene was obtained with accuracy using the experimental procedure described in section 6.2.1.1, related to the offline technique, while the liquid phase calibration curves can be obtained using certified solutions of PAHs in appropriate solvents (Sigma-Aldrich). The uncertainty in the calibration curves can be roughly estimated as proportional to the percentage difference between the molecular weights of the specific compound and the one of the reference species, naphthalene. Thus, the maximum uncertainty in the measurement of C12 hydrocarbons is estimated as 15-20%, of C14 compounds as 20-25%, and so on.

The online recovery technique has been tested on a relatively simple system, the decomposition of phenyl iodide (C_6H_5I). The results, in terms of carbon recovery, were compared with similar experiments conducted using the traditional technique which consisted of collecting the gas sample in electropolished stainless steel heated vessels for subsequent offline injection into the GC system (Figure 18). The experiments conducted with the traditional set-up show a substantial drop (down to 40%) in the carbon balance in correspondence with the formation of large PAH compounds which could not be measured. On the other hand, the results obtained with the online technique indicate an excellent performance of the new method, with an accuracy of ±10% in terms of carbon recovery.

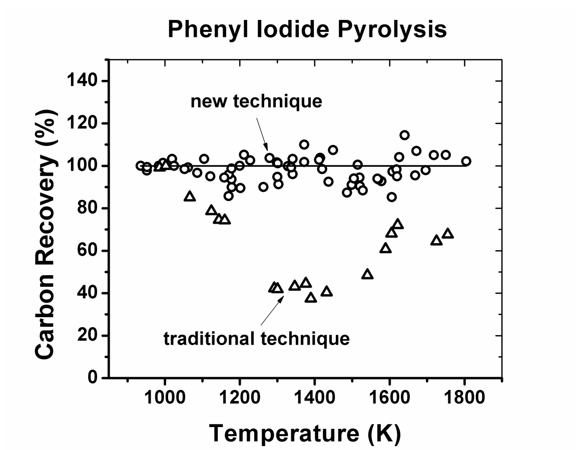

Figure 18. Carbon recovery from phenyl iodide experiments; ○ online technique; Δ traditional technique. Adapted from Ref. 91.

The difference observed in Figure 18 between the results of the two techniques is mainly due to the ability to measure PAH compounds by the online technique. In fact, the species profiles for the light components are very similar in the two cases. A typical online gas chromatogram obtained with the FID detector coupled to the DB-17ms column is shown in Figure 19 where elution times for the major PAH groups (C12, C14, and so on) are indicated. Species profiles can be obtained for components with mole fractions down to sub-ppm levels, although products present in even smaller trace amounts can also be easily detected. Similar excellent recovery results were obtained for the pyrolytic and oxidative reactions of m-xylene[92] and n-propylbenzene[93].

The online technique described in detail in the previous paragraphs represents an excellent solution for identification and measurement of all components, including large PAH compounds, present in complex hydrocarbon gas mixtures. When possible from a logistical and experimental point of view, the implementation of this technique could lead to a substantial improvement in the experimental results extending the analytical capability to compounds which are usually barely detectable due to condensation and adsorption. However, in cases where soot is present in large amount in the sample, the direct transfer lines could become dirty (lose inertness) or get obstructed. This poses limitations in the possibility of using the online technique for some applications. A practical solution to the problem could be the use of particulate traps just at the entrance of the sampling system. New tests should be repeated to confirm that no losses of PAH compounds are present across the particulate trap, as well as to determine an optimal technique to recover all the heavy species contained on the particles surface.

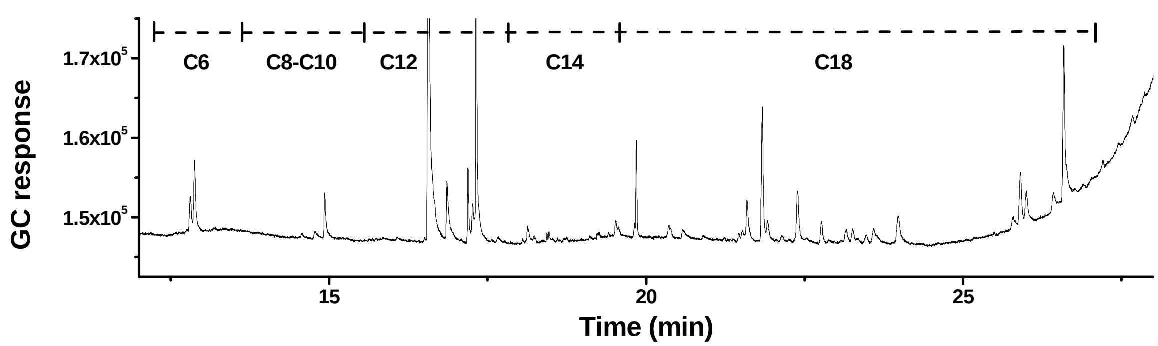

Figure 19. Typical gas chromatogram (FID detector, DB-17ms column), online technique. Adapted from Ref. 91.

6.3. Online technique: primary results

In order to fully analyze the reaction systems in consideration, several experimental sets were obtained by varying both the initial concentrations of the reactants and the nominal pressure. First the phenyl iodide decomposition has been investigated as a source of phenyl radicals for the subsequent experiments on the phenyl + acetylene reaction. Three experimental sets were conducted at a nominal pressure of 50 atm and initial phenyl iodide mole fraction of approximately 25, 50, and 100 ppm. One additional data set at 25 atm with approximately 50 ppm of reactant in the initial mixture was carried out to test possible pressure effects. The carbon balance for most of the experimental sets presents a maximum error of ~10% as shown in

Figure 20a which indicates efficient recovery of all the reaction products as well as reliability of the GC calibration curves. The only exception is constituted by the data set obtained using an initial phenyl iodide mole fraction of 100 ppm for which the carbon balance drops to 75% in the high temperature range. In this case the relatively large C_6H_5I concentration leads to the formation of significant quantities of PAH intermediates. These intermediates could subsequently undergo processes such as aggregation or dimerization which lead to the formation of heavier PAHs and soot that can not be measured through gas phase GC technique.

Subsequent experimental work has been conducted in order to study the phenyl + acetylene reaction. In this case three experimental sets were obtained varying the initial acetylene mole fraction approximately from 250 ppm to 500 ppm with an initial phenyl iodide concentration of approximately 50 ppm. The carbon balance, as for the case of phenyl pyrolysis, indicates good recovery of the product species for all the data sets (Figure 20b).

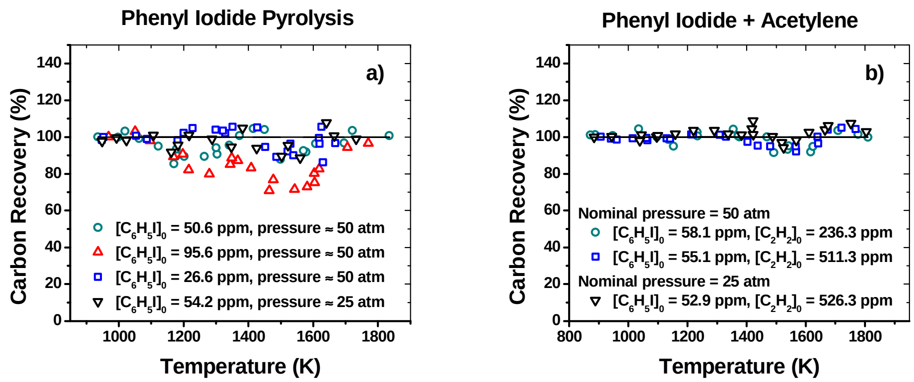

Figure 20. Experimental carbon balance. a) Phenyl iodide decomposition; b) phenyl + acetylene reaction.

A chemical kinetic model was developed to simulate the high-pressure experimental data on both the phenyl pyrolysis and the phenyl + acetylene reaction (Appendices B and C). Both the CHEMKIN 3.6.2[54] and the CHEMKIN 4.1.1[55] suite of programs were used to implement the model. For the modeling calculations, the exact reaction time, temperature and pressure were specified for each shock along with the initial mole fractions of the reactants. The simulations were performed assuming an adiabatic constant pressure process. As discussed in our previous publication addressing this issue[35], the adiabatic constant pressure process assumption leads to reasonable accuracy in predicting the stable species profiles.

The main reactions relevant to the formation and consumption of PAH compounds with associated reaction rate parameters are reported in Table 7. The thermochemical parameters for the species in the model were mainly taken from Burcat and Ruscic[51] and from chemical kinetic models available in literature[94,95]. The data not available in literature were estimated using the FITDAT data-fitting utility from the CHEMKIN 3.7.1 collection[52]. The enthalpies of the compounds, if not available on the NIST database, were calculated using the ring-conserved isodesmic reaction scheme[73]. The relative geometry optimizations and vibrational analyses were performed using the uB3LYP hybrid functional[67,68] with the Pople's valence triple-ζ basis set 6-311+G(d,p)[96]. For species containing iodine atoms, i.e. the iodobiphenyls, the DGDZVP basis set[97] was used. All of the calculations were carried out with the Gaussian 03 program package[84].

Denomination	Reaction	A	n	Ea	Reference
	Halogenated compounds				
R1	$C_6H_5I \rightarrow C_6H_5+I$	1.374E+15	0.00	64406	[99]
R2	$C_6H_5+I \rightarrow C_6H_5I$	1.00E+13	0.00	0	est., see text
R3	$C_6H_5I \leftrightarrow o\text{-}C_6H_4+HI$	8.24E+13	0.00	64406	see text
R4	$C_6H_5I+H \leftrightarrow C_6H_5+HI$	8.73E+05	2.35	-37.3	[128][a]
R5	$C_6H_5+HI \leftrightarrow C_6H_6+I$	3.00E+12	0.00	0	est., see text
R6	$C_6H_5I+C_6H_5 \leftrightarrow C_{12}H_{10}+I$	2.00E+12	0.00	11000	[103]
R7	$C_6H_5I+C_6H_5 \leftrightarrow o\text{-}C_{12}H_9I+H$	3.183E+11	0.00	4305	see text
R8	$C_6H_5I+C_6H_5 \leftrightarrow m\text{-}C_{12}H_9I+H$	3.183E+11	0.00	4305	see text
R9	$C_6H_5I+C_6H_5 \leftrightarrow p\text{-}C_{12}H_9I+H$	1.592E+11	0.00	4305	see text
R10	$o\text{-}C_{12}H_9+I \rightarrow o\text{-}C_{12}H_9I$	1.00E+13	0.00	0	est.
R11	$m\text{-}C_{12}H_9+I \rightarrow m\text{-}C_{12}H_9I$	1.00E+13	0.00	0	est.
R12	$p\text{-}C_{12}H_9+I \rightarrow p\text{-}C_{12}H_9I$	1.00E+13	0.00	0	est.
R13	$o\text{-}C_{12}H_9I \rightarrow o\text{-}C_{12}H_9+I$	1.374E+15	0.00	64406	see text
R14	$m\text{-}C_{12}H_9I \rightarrow m\text{-}C_{12}H_9+I$	1.374E+15	0.00	64406	see text
R15	$p\text{-}C_{12}H_9I \rightarrow p\text{-}C_{12}H_9+I$	1.374E+15	0.00	64406	see text
R19	$H+HI \leftrightarrow H_2+I$	3.98E+13	0.00	0	[103]
	Biphenyl and Benzene				
R20	$C_6H_5+ C_6H_5 \leftrightarrow C_{12}H_{10}$	3.09E+12	0.036	-1702	[26] see text
R21	$C_6H_5+ C_6H_5 \leftrightarrow o\text{-}C_6H_4+ C_6H_6$	8.52E-04	4.57	-5735	[26] see text
R22	$C_6H_5+ C_6H_5 \leftrightarrow m\text{-}C_6H_4+ C_6H_6$	8.52E-04	4.57	-5735	[26] see text
R23	$C_6H_5+ C_6H_5 \leftrightarrow p\text{-}C_6H_4+ C_6H_6$	4.26E-04	4.57	-5735	[26] see text
R24	$o\text{-}C_6H_4 \leftrightarrow m\text{-}C_6H_4$	2.12E+14	0.00	73489.5	[102]
R25	$m\text{-}C_6H_4 \leftrightarrow p\text{-}C_6H_4$	2.83E+14	0.00	63045.7	[102]
R26	$p\text{-}C_6H_4 \leftrightarrow z\text{-}C_6H_4$	1.00E+13	0.00	17800	see text
R27	$o\text{-}C_6H_4+C_6H_5 \leftrightarrow o\text{-}C_{12}H_9$	1.00E+13	0.00	3720	see text
R28	$m\text{-}C_6H_4+C_6H_5 \rightarrow m\text{-}C_{12}H_9$	1.00E+13	0.00	3720	see text
R29	$p\text{-}C_6H_4+C_6H_5 \rightarrow p\text{-}C_{12}H_9$	1.00E+13	0.00	3720	see text
R30	$m\text{-}C_{12}H_9 \rightarrow m\text{-}C_6H_4+C_6H_5$	2.223E+15	0.00	87232	see text
R31	$p\text{-}C_{12}H_9 \rightarrow p\text{-}C_6H_4+C_6H_5$	2.223E+15	0.00	87232	see text
R35	$o\text{-}C_{12}H_9+H \leftrightarrow C_{12}H_{10}$	4.27E+13	0.338	-158	[26]
R36	$m\text{-}C_{12}H_9+H \leftrightarrow C_{12}H_{10}$	1.25E+13	0.284	-155	[26]
R37	$p\text{-}C_{12}H_9+H \leftrightarrow C_{12}H_{10}$	2.78E+13	0.185	15.3	[26]
R38	$C_6H_5+ C_6H_6 \leftrightarrow C_{12}H_{10}+H$	9.55E+11	0.00	4305	[106]
R44	$C_6H_5+H(+M) \leftrightarrow C_6H_6(+M)$	1.00E+14	0.00	0	[105][b]
	Terphenyls and Triphenylene				
R46	$C_{12}H_{10}+C_6H_5 \leftrightarrow$ o-TERPH+H	6.367E+11	0.00	4305	see text
R47	$C_{12}H_{10}+C_6H_5 \leftrightarrow$ m-TERPH+H	6.367E+11	0.00	4305	see text
R48	$C_{12}H_{10}+C_6H_5 \leftrightarrow$ p-TERPH+H	3.183E+11	0.00	4305	see text
R49	$o\text{-}C_{12}H_9+C_6H_5 \rightarrow$ o-TERPH	1.00E+13	0.00	0	est.
R50	$m\text{-}C_{12}H_9+C_6H_5 \rightarrow$ m-TERPH	1.00E+13	0.00	0	est.
R51	$p\text{-}C_{12}H_9+C_6H_5 \rightarrow$ p-TERPH	1.00E+13	0.00	0	est.
R52	o-TERPH $\rightarrow o\text{-}C_{12}H_9+C_6H_5$	2.92E+15	0.00	109812	see text
R53	m-TERPH $\rightarrow m\text{-}C_{12}H_9+C_6H_5$	2.92E+15	0.00	109812	see text

R54	p-TERPH → p-$C_{12}H_9$+C_6H_5	2.92E+15	0.00	109812	see text
R55	o-TERPH ↔ TRIPH+H_2	1.50E+15	0.00	84700	see text
R56	o-$C_{12}H_9$+o-C_6H_4 ↔ TRIPH+H	1.00E+14	0.00	38000	see text
R57	$C_{12}H_8$+o-C_6H_4 ↔ TRIPH	4.96E+09	0.827	-1370	see text
	Biphenylene and Acenaphthylene				
R58	o-C_6H_4+o-C_6H_4 ↔ $C_{12}H_8$	4.96E+09	0.827	-1370	[26]
R59	o-$C_{12}H_9$ → BIPHENH	5.00E+12	0.00	31056	[112][c]
R60	BIPHENH → o-$C_{12}H_9$	3.00E+13	0.00	19350	[112][c]
R61	BIPHENH → $C_{12}H_8$+H	5.00E+13	0.00	38223	[112][c]
R62	$C_{12}H_8$+H → BIPHENH	4.00E+13	0.00	5972	[112][c]
R63	BIPHENH → BENZOH	1.00E+13	0.00	31056	[112][c]
R64	BENZOH → BIPHENH	1.00E+13	0.00	46345	[112][c]
R65	BENZOH → BENZO+H	5.00E+13	0.00	41567	[112][c]
R66	BENZO+H → BENZOH	1.00E+14	0.00	1911	[112][c]
R67	BENZOH → A2R5+H	1.00E+13	0.00	44673	[112][c]
R68	$C_{12}H_{10}$ → $C_6H_5CHC_5H_4$	1.00E+14	0.00	109412	[112][c]
R69	$C_6H_5CHC_5H_4$ → $C_{12}H_{10}$	1.00E+13	0.00	76445	[112][c]
R70	$C_6H_5CHC_5H_4$ → BENZO+H_2	5.00E+13	0.00	56617	[112][c]
R71	$C_6H_5CHC_5H_4$ → A2R5+H_2	5.00E+13	0.00	60917	[112][c]
R72	$C_{12}H_8$ → C_6H_4oct	6.152E+14	0.00	77387.6	p.w.
R73	C_6H_4oct → $C_{12}H_8$	7.482E+12	0.00	4059.6	p.w.
R74	C_6H_4oct → BENZOHyl	1.205E+13	0.00	13712.9	p.w.
R75	BENZOHyl → C_6H_4oct	5.321E+13	0.00	31139.8	p.w.
R76	BENZOHyl → BENZO	1.941E+13	0.00	10615.0	p.w.
R77	BENZO → BENZOHyl	4.188E+13	0.00	75265.9	p.w.
R80	BENZO → A2R5	4.699E+14	0.00	77831.2	p.w.
R81	$C_{10}H_7$-1+C_2H_2 ↔ A2R5+H	1.87E+07	1.787	3262	[22]
	Phenylacetylene				
R90	C_6H_5+C_2H_2 ↔ C_8H_6+H	1.00E+13	0.00	7648	[20]
R92	C_8H_6+H ↔ $C_6H_4C_2H$+H_2	3.23E+07	2.095	15842	[111] *1.5
R95	o-C_6H_4+C_2H_2 ↔ C_8H_6	2.00E+13	0.00	20000	[126]
	Diphenylethyne and Phenanthrene				
R96	C_8H_6+C_6H_5 → DPE+H	1.00E+13	0.00	7648	see text
R97	DPE+H → C_8H_6+C_6H_5	4.00E+14	0.00	9691	see text
R98	o-$C_{12}H_9$+C_2H_2 ↔ PHEN+H	1.87E+07	1.787	3262	[95]
R99	C_8H_6+C_6H_5 ↔ PHEN+H	9.55E+11	0.00	4305	[95]
R110	$C_{12}H_{10}$+C_2H_2 → PHENH	16.92	2.60	42193	[131]
R111	PHENH→ PHEN+H_2	4.73E+09	0.797	17176	[131]
	Naphthalene				
R146	o-C_6H_4+C_6H_6 → BICYCLO	1.1618E+04	2.526	5915.9	[118] see text
R147	BICYCLO → o-C_6H_4+C_6H_6	4.910E+16	0.00	66811	[118] see text
R148	BICYCLO ↔ $C_{10}H_8$+C_2H_2	7.458E+14	0.0956	54780.1	[118]
R149	$C_6H_4C_2H$+C_2H_2 ↔ $C_{12}H_7$-1	1.87E+07	1.787	3262	est.[d]
R151	$C_{12}H_7$-1+H(+M) ↔ $C_{12}H_8$(+M)	1.00E+14	0.00	0	est.[b]
	Phenyl Decomposition				
R157	C_6H_5(+AR) ↔ o-C_6H_4+H(+AR)	4.30E+12	0.62	77300	[126][b]
R159	o-C_6H_4 ↔ C_4H_2+C_2H_2	1.20E+18	-0.34	87776	[126]
R162	C_6H_2+H ↔ C_6H_3	1.10E+30	-4.92	10800	[105]
R164	C_4H_2+ C_2H ↔ C_6H_2+H	3.00E+13	0.00	0	[126]
R167	z-C_6H_4+H ↔ C_6H_3+H_2	1.33E+06	2.53	9240	[94]
R191	C_2H+H_2 ↔ C_2H_2+H	4.90E+05	2.50	560	[94]

R193	$C_2H+C_2H_2 \leftrightarrow C_4H_2+H$	9.60E+13	0.00	0	[105]

Table 7. Chemical kinetic model, relevant reactions and associated reaction rate parameters. [a] modified within the uncertainty provided in ref. [128]; [b] reaction with fall-off parameters; [c] Ea from [112], A value estimated; [d] high-pressure limit for $C_{10}H_7$+C_2H_2 [21].

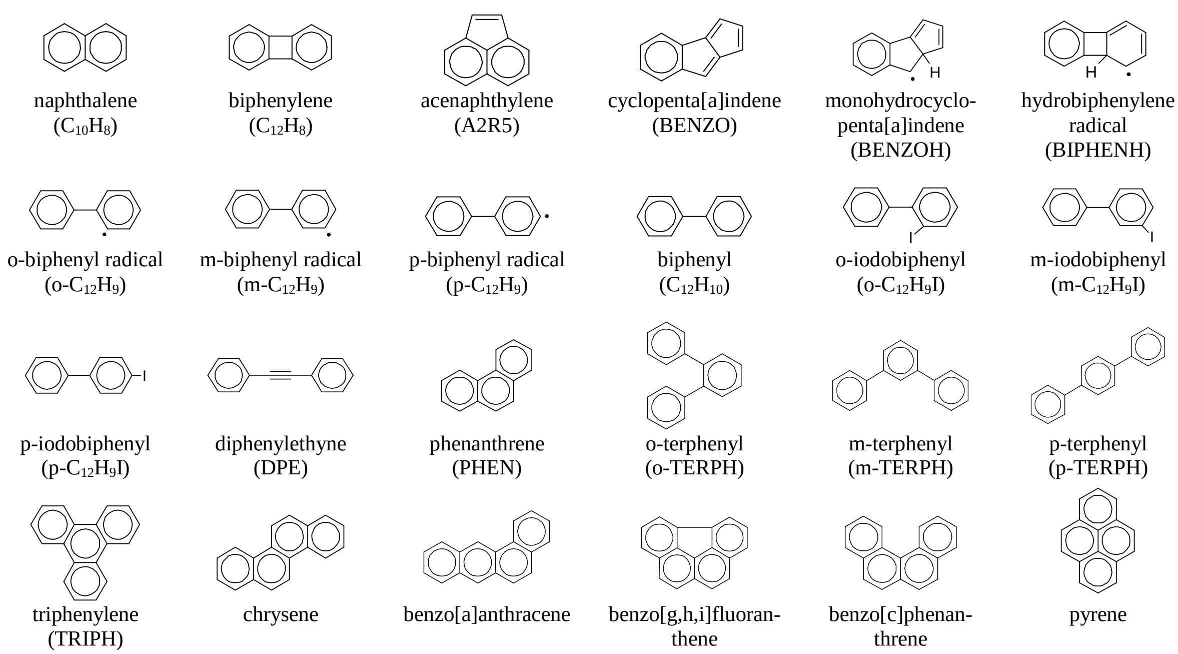

Figure 21. Molecular structures of the major polycyclic aromatic hydrocarbons discussed in the text.

In the following paragraphs the relevant results from the experimental work and from the modeling simulations will be discussed for both the phenyl pyrolysis and the phenyl + acetylene reaction. In order to facilitate the discussion, the molecular structures of the major polycyclic aromatic hydrocarbon products analyzed in this work are reported in Figure 21. Before proceeding with the discussion it is worth mentioning the fact that the model was optimized mainly based on the experimental sets having accurate carbon recovery (initial concentration of phenyl iodide around 50 ppm or lower). All the experimental results are reported in the supplemental material (Appendix A) including for each experiment the actual conditions (pressure, temperature, and reaction time) as well as the mole fractions of the major products.

6.3.1. Phenyl Pyrolysis

A typical chromatogram obtained from the pyrolysis of phenyl iodide at a nominal pressure of 50 atm and initial mole fraction of 50.6 ppm is reported in Figure 22. The chromatogram clearly shows the complexity of the reaction system in consideration. Although only the major products are annotated, several additional peaks were detected. Such peaks correspond to compounds produced in trace amounts during the reaction, including among the others indene, di-iodobenzenes, fluorene, 1-iodonaphthalene, anthracene, phenanthrene, iodobiphenyls, 2-phenylindene, 1-phenylnaphthalene, 2-phenylnaphthalene, pyrene, and other unidentified C18 species. Although the formation of such compounds suggests the presence of several minor mechanistic pathways, from a practical point of view only the major products and the associated reactions were considered for the development of the chemical kinetic model. The main results are reported below.

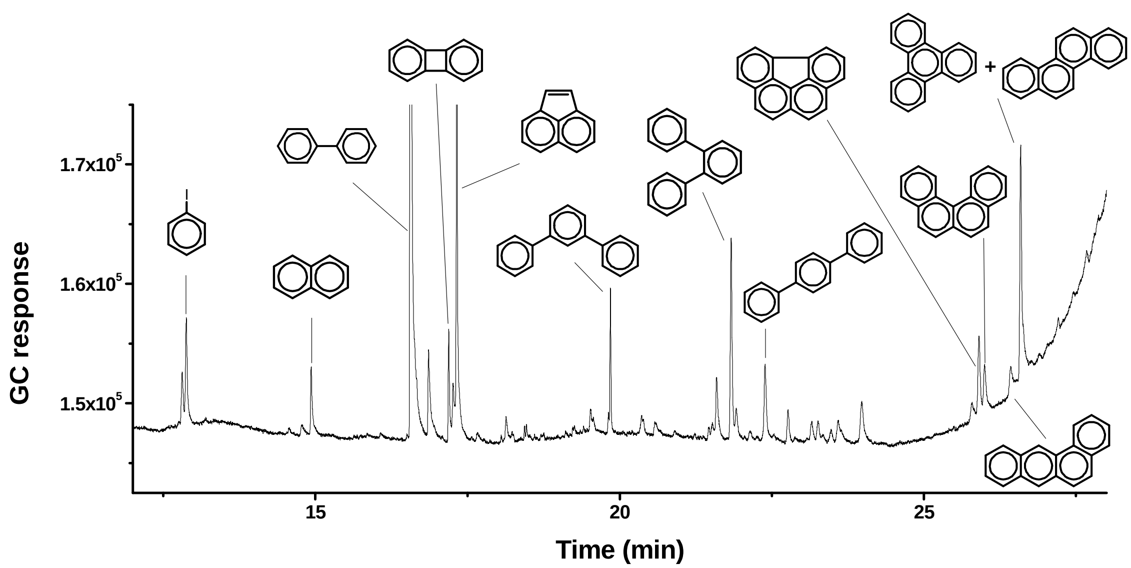

Figure 22. Typical chromatographic signal for phenyl radical pyrolysis. FID detector, DB-17ms column.

6.3.1.1. Phenyl Iodide Decomposition

A comprehensive analysis of the C-I fission in phenyl iodide decomposition has been performed by Tranter et al.[26] in their recent investigation of the self-reaction between phenyl radicals. The authors compared the experimental data present in literature[98–101] with their experimental results as well as the reaction rate constants obtained with a Gorin model RRKM calculation. It is not the purpose of the present work to repeat a detailed analysis of the thermal decomposition of phenyl iodide. Thus, only a brief discussion of the main results obtained using the HPST is presented below.

The normalized profiles for the decomposition of phenyl iodide are reported in Figure 23a. The experiments do not indicate any significant dependence on the initial mole fraction of the reactant or on the reaction pressure. At the conditions of the present study the experimental decay of phenyl iodide is not only due to the C-I bond fission leading to the formation of phenyl radicals and iodine atoms, but it is also influenced by the secondary reactions of the phenyl iodide with different product species including phenyl radicals and hydrogen atoms when present in the system. Moreover the recombination reaction between phenyl radicals and iodine atoms to form C_6H_5I will play a relevant role lowering the apparent decomposition rate. Thus the high-pressure conditions implemented in the present investigation do not allow the determination of the absolute rate constant for the phenyl iodide decomposition, although an apparent overall reaction rate constant can be derived from the Arrhenius plot presented in Figure 23b. The Arrhenius expression of the apparent reaction rate constant is $k \cong 3.24 \cdot 10^{10} \exp(-21797/T)$ (s^{-1}).

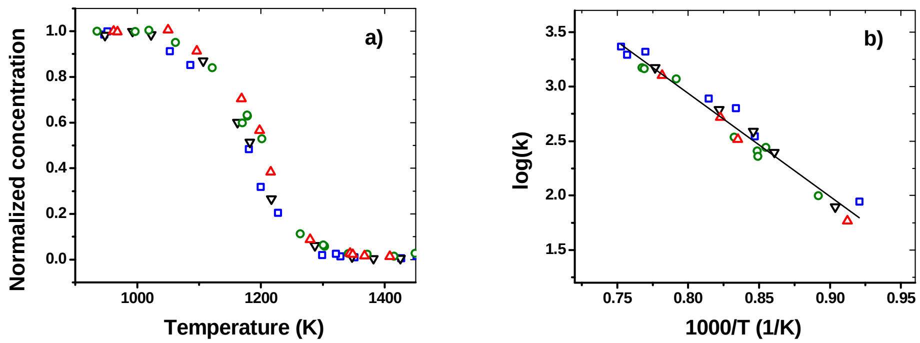

Figure 23. a) Normalized phenyl iodide decomposition; b) Arrhenius plot of the measured apparent reaction rate constant for phenyl iodide decomposition between 1086 and 1328 K, k in s^{-1}. ○ $[C_6H_5I]_0$ = 50.6 ppm, p ~ 50 atm; Δ $[C_6H_5I]_0$ = 95.6 ppm, p ~ 50 atm; □ $[C_6H_5I]_0$ = 26.6 ppm, p ~ 50 atm; ∇ $[C_6H_5I]_0$ = 54.2 ppm, p ~ 25 atm; —— linear interpolation.

The high-pressure limit reaction rate constant for the C-I fission derived by Kumaran et al.[99] based on their low-pressure experiments best fits our experimental data although the phenyl iodide concentrations are slightly overpredicted by the model when the reverse reaction rate constant is calculated using the equilibrium constant. Better agreement between experiments and simulations was obtained assuming a temperature independent reaction rate constant k_2 for the recombination between phenyl radicals and iodine atoms (Table 7). In addition, as suggested by Tranter et al.[26], the branching ratio between the two main unimolecular decomposition channels forming respectively C_6H_5 + I and o-C_6H_4 + HI was assumed to be approximately 6%. The rate parameters for the two unimolecular decomposition reactions are reported in Table 7 (R1, R2, and R3).

Figure 24 shows the excellent agreement between the phenyl iodide experimental profiles and the modeling results for the experiments conducted at nominal pressures of 25 and 50 atm and initial phenyl iodide mole fractions of around 25 and 50 ppm. Similar agreement was obtained for the data set at 50 atm and higher initial phenyl iodide mole fraction (95.6 ppm).

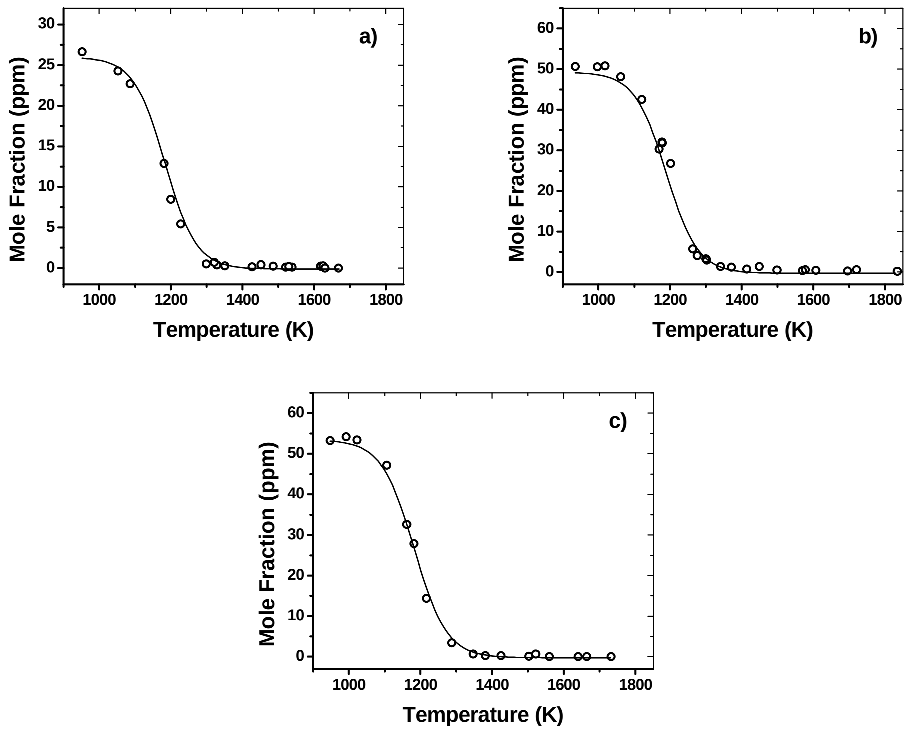

Figure 24. Phenyl iodide decomposition. ○ experiments; —— simulations. a) $[C_6H_5I]_0$ = 26.6 ppm, p ~ 50 atm; b) $[C_6H_5I]_0$ = 50.6 ppm, p ~ 50 atm; c) $[C_6H_5I]_0$ = 54.2 ppm, p ~ 25 atm.

6.3.1.2. Formation of Benzene, Biphenyl, and Substituted Biphenyls

Biphenyl is one of the most important building blocks for the formation of large PAH compounds and it constitutes the primary product of the radical-radical recombination between phenyl radicals[20,25]. If the only reaction channel available for the self-reaction between phenyl radicals was the radical-radical recombination, biphenyl would be the major product of the phenyl iodide decomposition. Only small amounts of other stable compounds would be measured, including for example benzene from the recombination of the phenyl radicals with hydrogen atoms. Surprisingly the experiments indicated that a large amount of benzene is produced even at low temperatures where the hydrogen atoms are present in the system only in small concentrations. As shown in Figure 25a at temperatures between 1250 K and 1400 K around 25% of the phenyl radicals produced from the phenyl iodide decomposition is converted into benzene. The results presented in Figure 25a also indicate that the chemical mechanisms which lead to the formation/consumption of benzene are not dependent on either the initial phenyl iodide mole fraction or reaction pressure. Moreover the peculiar shape of the profiles, characterized by a rapid increase up to 1250 K in correspondence with the end of the phenyl iodide decay followed by a slight decrease up to 1450 K and a more rapid decrease at higher temperatures, suggests that at least two reaction mechanisms are responsible for the formation of benzene. The main mechanism was proposed and studied in detail by Tranter et al.[26] who highlighted for the first time the complexity of the self-reaction between phenyl radicals. The authors examined the different reaction channels by high-level computational methods and concluded that the reaction between phenyl radicals does not proceed only through recombination to form biphenyl, but also through hydrogen abstraction to form benzene and ortho-, meta-, and para-benzynes. The key role of the benzynes, in particular of o-benzyne, will be discussed later in the text in relation to the formation of terphenyls, biphenylene, acenaphthylene, naphthalene, and the four-ring compounds.

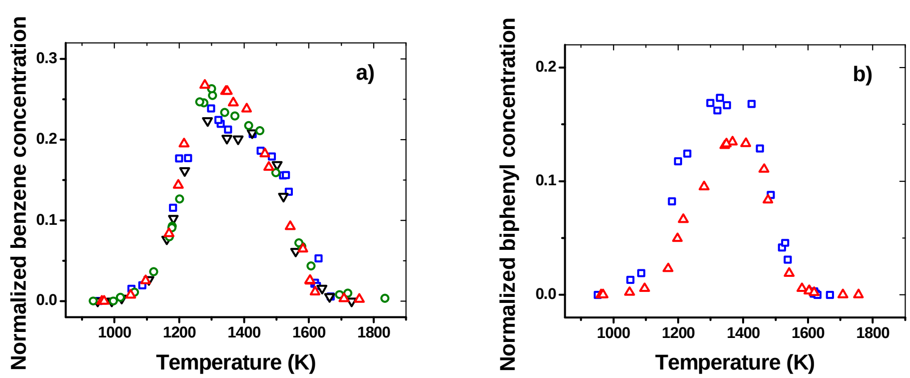

Figure 25. a) Normalized benzene decomposition; b) normalized biphenyl decomposition. ○ ***[C6H5I]0 = 50.6 ppm, p ~ 50 atm;*** Δ ***[C6H5I]0 = 95.6 ppm, p ~ 50 atm;*** □ ***[C6H5I]0 = 26.6 ppm, p ~ 50 atm;*** ∇ ***[C6H5I]0 = 54.2 ppm, p ~ 25 atm.***

The reaction rate constants associated with the two competing channels for the self-reaction between phenyl radicals, i.e. the recombination channel and the hydrogen-abstraction channel, were calculated by Tranter et al.[26] using high-level theoretical calculations and transition state theory. As suggested by the authors, the branching ratio for the three hydrogen abstraction channels leading to o-benzyne + benzene, m-benzyne + benzene, and p-benzyne + benzene was estimated as 0.40-0.40-0.20 and the corresponding reaction rate constants taken as the high-pressure limit expressions calculated in [26] reduced, within the stated error limits, by a factor of two (reactions R21–R23, Table 7). A similar reduction, within the error limits, in the corresponding low-pressure expressions was applied by Tranter et al. in order to improve the agreement between the simulations and the low-pressure experiments suggesting that the rate constant may be off by a factor of two across the entire pressure range. The isomerization between the three benzyne isomers has been studied theoretically by Moskaleva et al.[102] who derived reaction rate constant expressions utilized in the present work (R24 and R25). The p-benzyne can also easily undergo a Bergman decyclization to form 1,5-hexadiyn-3-ene. The corresponding reaction rate constant was estimated based on a reaction barrier of 17.8 kcal/mol as calculated in Ref. [102] (R26). Finally the reaction rate constant for the recombination reaction was reduced by a factor of two compared to the expression derived by Tranter et al.[26] for a pressure of 100 atm (R20). This modification, within the estimated uncertainty provided by the authors, lead to the improvement of the modeling results not only for biphenyl but also for other intermediates such as the terphenyls.

We mentioned earlier the fact that the benzene profiles in Figure 25a suggest the relevance of a second reaction mechanism which lead to the formation of benzene. Such a mechanism involves the reaction between phenyl radical and hydrogen iodide to form benzene and iodine atoms. Hydrogen iodide derives mainly from the direct decomposition of C_6H_5I into o-C_6H_4 + HI as described in section 6.3.1.1 and at later times in the reaction by the abstraction reaction between phenyl iodide and hydrogen atoms (R4 in Table 7). Thus although the phenyl iodide is usually considered as a clean source of phenyl radicals its chemical properties lead to the formation of halogenated species, in this case HI, which can subsequently influence the formation of the intermediates of interest, in this case benzene, derived from the reaction of the phenyl radicals.

An estimated temperature-independent rate constant for the reaction between C_6H_4 and HI has been used in the present model (reaction R5, Table 7). In view of the decreased reactivity of the phenyl radical compared to the hydrogen atom, k_5 is an order of magnitude lower than the reaction rate constant for reaction R19, H + HI → H_2 + I (Ref. [103]), although nearly twice the value extrapolated from the expression derived by Rodgers et al.[104] who experimentally investigated the title reaction at relatively low temperatures (648–773 K).

The model simulates with good accuracy the profiles of biphenyl for the experiments conducted at 50 atm with initial C_6H_5I mole fraction of 26.6 ppm and at 25 atm with 54.2 ppm of reactant (Figure 26a and c). Above 1450 K the biphenyl concentrations are overpredicted by the model, but as discussed later in the text this discrepancy is mainly due to the fact that the model is not able to correctly predict the chemistry relevant to high-temperature conditions. The remaining $C_{12}H_{10}$ profiles (Figure 26b and d) are overestimated by the model even at low temperatures, in particular in the case presented in Figure 26d (initial mole fraction of 95.6 ppm). The drop in the relative carbon balance described above in relation to Figure 20a suggests the presence of pathways for the formation of larger compounds which are not measured in the present study. Such pathways could be responsible for the consumption of biphenyl at relatively high phenyl radical concentrations. Such hypothesis is supported by the comparison between the normalized experimental profiles for biphenyl in the case of initial phenyl iodide mole fraction of 26.6 and 95.6 ppm at a nominal pressure of 50 atm (Figure 25b). In contrast with the case of benzene where no dependence on the pressure and the initial C_6H_5I mole fraction was observed (Figure 25a), the normalized profiles show a significant drop in the biphenyl concentrations at higher phenyl iodide mole fractions.

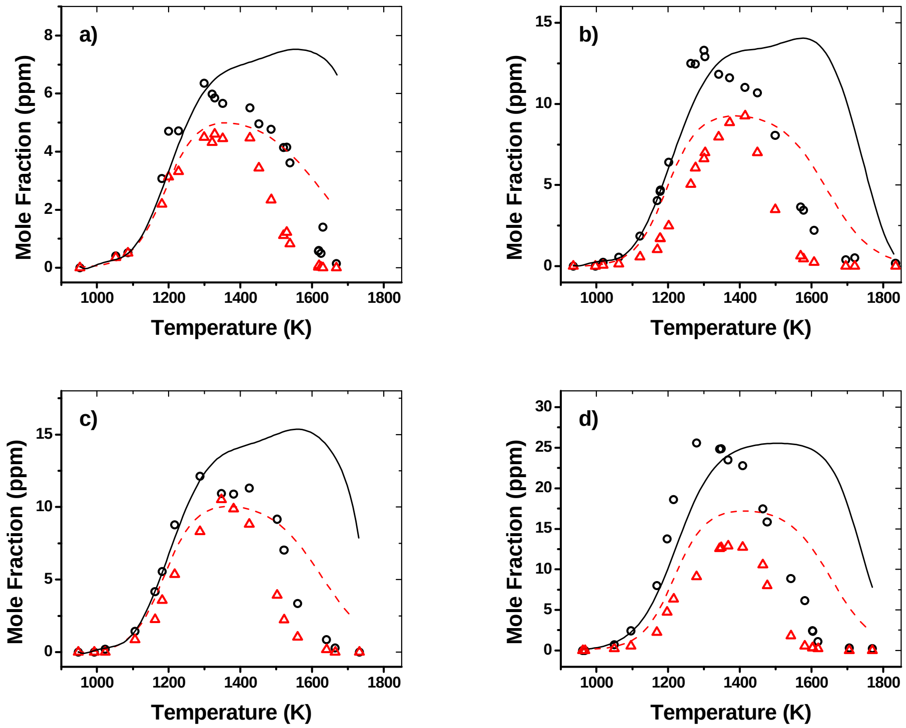

Figure 26. **○ *Benzene experiments; —— benzene simulations; △ biphenyl experiments, – – biphenyl simulations; a) [C6H5I]0 = 26.6 ppm, p ~ 50 atm; b) [C6H5I]0 = 50.6 ppm, p ~ 50 atm; c) [C6H5I]0 = 54.2 ppm, p ~ 25 atm; d) [C6H5I]0 = 95.6 ppm, p ~ 50 atm.***

Different considerations apply for the simulation of the benzene profiles. As shown in Figure 26 the initial slope of formation is well reproduced by the model for most of the experimental sets with the exception of the set conducted with initial phenyl iodide mole fraction of 95.6 ppm for which the initial slope is underpredicted. The rate of production analysis performed at 1217 K and 29.1 atm with initial mole fraction of 54.2 ppm shows that at the beginning the formation of benzene is mainly influenced by the abstraction channel between phenyl radicals with smaller contributions from the reaction between phenyl and hydrogen iodide and from the recombination between phenyl and hydrogen[105] (Figure 27a). In Figure 27a the lines for the ortho- and meta-benzyne channels are superimposed. As the reaction progresses, the reaction C_6H_5 + HI becomes the predominant pathway for the formation of benzene. Its contribution is essential for the accurate description of the benzene profiles in the low-temperature range of the present study as shown in Figure 28 where the modeling results from the complete model are compared to the results obtained when the reaction $C_6H_5 + HI \leftrightarrow C_6H_6 + I$ is removed (experimental set with initial concentration of 54.2 ppm and nominal pressure of 25 atm). Similar reactions between C_6H_5 and HX could also be relevant when a generic C_6H_5X precursor is utilized, i.e. C_6H_5Cl or C_6H_5Br. In these cases the reaction rate constants are expected to be lower than k_5 since in general the H-X bond would be stronger than the H-I bond.

While the benzene profiles are well reproduced for temperatures below 1350 K, at higher temperatures the model fails to simulate accurately the decay observed in the experimental data. In particular, above 1450 K where the experimental concentrations drop rapidly the model predicts an increase in the benzene mole fraction up to around 1600 K. As indicated in Figure 27b which shows the rate of production analysis performed at 1502 K the formation of benzene is still mainly due to the hydrogen-abstraction channel. In comparison to the low temperature case, the contributions provided by the reaction R5 and R44 are only minor. In order to understand if other reaction rate parameters could be responsible for the overestimation observed at high temperatures, the sensitivity analysis was also performed at the same conditions which confirmed the importance of the above mentioned reactions (Figure 29). The sensitivity analysis also indicates a strong dependence on the rate parameters of reaction R20, the recombination between phenyl radicals to form biphenyl. The modification of the related reaction rate parameters within the corresponding uncertainties does not lead to a substantial improvement of the benzene profile at high temperatures without affecting the accuracy of the predictions for other compounds, i.e. biphenyl and benzene at low temperatures. This is clearly an indication that the model is not complete and requires the addition of reaction pathways which reduce the predicted formation of benzene at high temperatures. We will analyze this issue in more details later in the manuscript in correspondence with the discussion about the formation of the light hydrocarbons (section 6.3.1.7).

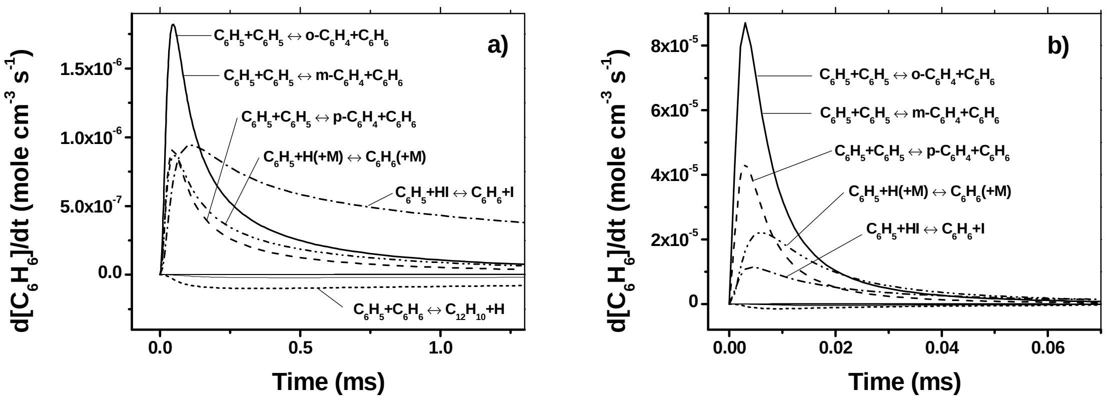

Figure 27. Benzene, rate of production analysis, $[C_6H_5I]_0$ = 54.2 ppm. a) T = 1217 K, p = 29.1 atm; b) T = 1502 K, p = 25.3 atm.

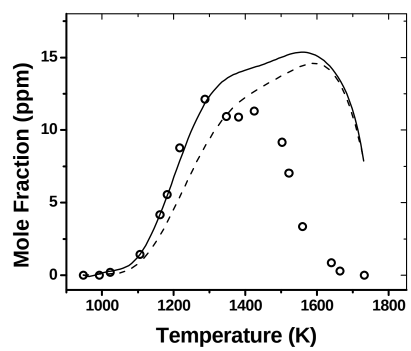

Figure 28. Benzene, $[C_6H_5I]_0$ = 54.2 ppm, p ~ 25 atm. ○ experiments; —— model in Table 7; – – model in Table 7 omitting C_6H_5 + HI ↔ C_6H_6 + I.

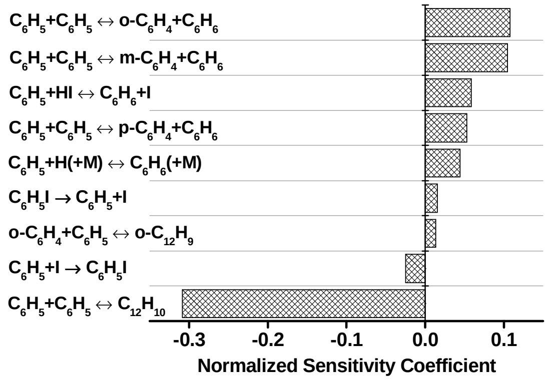

Figure 29. Sensitivity analysis for benzene. $[C_6H_5I]_0$ = 54.2 ppm, T = 1502 K, p = 25.3 atm, t = 1.68 ms.

In addition to benzene and biphenyl, iodobiphenyls have been measured in the low temperature range of our experiments. Once again the measurement of halogenated species indicates that the phenyl iodide is not an ideal source of phenyl radicals. Although the study of the iodobiphenyls chemistry is not the focus of the present work, it is essential to include the corresponding reactions in the chemical kinetic model in order to obtain a better agreement between simulations and experimental results for the low temperature profiles of several species, including benzene, biphenyl, and the terphenyls. The experimental measurement of the three iodobiphenyl isomers is also important to define the primary products of the addition between the phenyl radical produced by decomposition of the phenyl iodide precursor and the precursor itself. Such addition process becomes relevant at the high pressures implemented in the present study or at low pressures when large concentrations of the precursor are utilized. A brief analysis of the main experimental and modeling results regarding the iodobiphenyls is provided below which can serve as reference for future investigations on the decomposition of phenyl radical precursors and the related chemistry.

As soon as the phenyl iodide starts decomposing, iodobiphenyls are produced indicating a strong correlation between the two processes. In fact the three isomeric forms are mainly generated from the reaction between C_6H_5I and C_6H_5 in a similar fashion as the reaction between phenyl radical and benzene leads to the formation of biphenyl and hydrogen[106]. The pre-exponential factors of the corresponding reaction rate constants have been adjusted based on the multiplicity of the specific reaction pathway (R7–R9, Table 7). Once produced, the iodobiphenyls can dissociate to form biphenyl radicals and iodine atoms (R10–R15). The dissociation and recombination reaction rate constants have been assumed similar to the ones relative to the phenyl iodide decomposition, i.e. R1 and R2.

The experimental profiles are well reproduced by the model as shown in Figure 30. In particular, for the sets in Figure 30a and Figure 30c both the shapes of the profiles and the maximum mole fractions are accurately predicted. The m-iodobiphenyl is the isomer present in larger amounts in these experiments, while the p-iodobiphenyl shows the lowest concentrations. It is important to notice how the model correctly replicates such hierarchy. When we analyze the experimental results obtained with higher concentrations of phenyl iodide (Figure 30b and d), we notice that the o-iodobiphenyl is the most abundant among the three isomers. This indicates the presence of alternative pathways for the formation or consumption of the iodobiphenyls compared to the cases shown in Figure 30a and b. Although the shapes of the profiles are well reproduced by the model, the calculated mole fractions are overestimated compared to the experiments, especially when 95.6 ppm of phenyl iodide are pyrolyzed (Figure 30d), thus we can hypothesize that additional consumption reactions should be added to the model. Such reactions include for example the reactions between the iodobiphenyls and C_6H_5 or H.

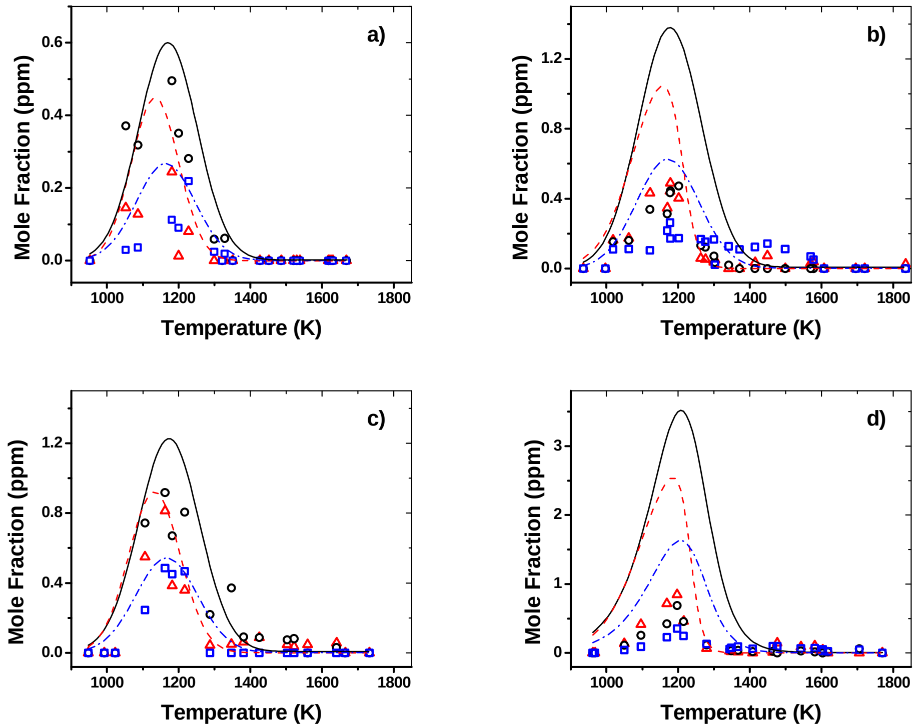

Figure 30. **△** *o-Iodobiphenyl exp., – – o-iodobiphenyl sim.; ○ m-iodobiphenyl exp., —— m-iodobiphenyl sim.; □ p-iodobiphenyl exp., – · – p-iodobiphenyl sim. a) $[C_6H_5I]_0$ = 26.6 ppm, p ~ 50 atm; b) $[C_6H_5I]_0$ = 50.6 ppm, p ~ 50 atm; c) $[C_6H_5I]_0$ = 54.2 ppm, p ~ 25 atm; d) $[C_6H_5I]_0$ = 95.6 ppm, p ~ 50 atm.*

6.3.1.3. Terphenyls

The obvious step in the growth towards larger PAH compounds which follows the formation of biphenyl is the subsequent addition of a phenyl radical to form the terphenyls. The mechanism of phenylation of biphenyl to form o-, m-, and p-terphenyls was proposed by Brooks et al.[107] who measured trace amounts of these polyphenyls in their study on benzene pyrolysis at relatively low temperatures (873–1036 K). The o-, m-, and p-terphenyls are well separated by the GC method implemented in the present study as shown in Figure 22 and mole fraction profiles could be obtained for all three isomers (Figure 31). The experimental profiles reach a maximum around 1275–1300 K with the m-terphenyl being the most abundant among the isomers. The mole fraction of o-terphenyl is lower not only compared to the mole fraction of m-terphenyl but also compared to the mole fraction of p-terphenyl. This experimental finding is surprising since from a simple analysis of the multiplicity of the specific reaction pathways for the addition between biphenyl and phenyl we would expect similar yields of the o- and m-terphenyls, in proportion twice the yield of p-terphenyl. The experimental results clearly suggest that o-terphenyl is consumed by reactions which does not involve the other isomers or that additional reaction pathways are involved in the formation of the three terphenyls. Both hypotheses are in principle correct, although only one has a substantial impact in the modeling results as discussed below.

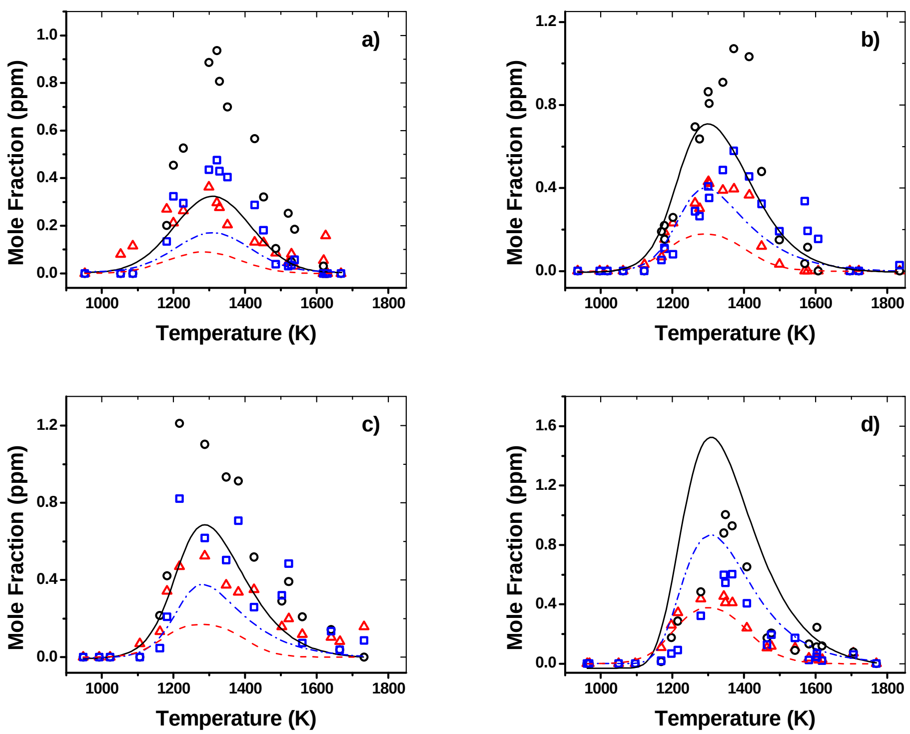

Figure 31. *△ o-Terphenyl exp., – – o-terphenyl sim.; ○ m-terphenyl exp., —— m-terphenyl sim.; □ p-terphenyl exp., – · – p-terphenyl sim. a) $[C_6H_5I]_0$ = 26.6 ppm, p ~ 50 atm; b) $[C_6H_5I]_0$ = 50.6 ppm, p ~ 50 atm; c) $[C_6H_5I]_0$ = 54.2 ppm, p ~ 25 atm; d) $[C_6H_5I]_0$ = 95.6 ppm, p ~ 50 atm.*

o-Terphenyl can undergo a cyclodehydrogenization process to form triphenylene (R55 in Table 7). The corresponding reaction rate constant has been estimated based on the rate constant proposed by Zhang et al.[108] for the cyclodehydrogenization of cis-1,2-diphenylethene to form phenanthrene. Due to the high activation energy involved in the process (84.7 kcal/mol) its contribution is not sufficient to justify the significant difference between the experimental o- and m-terphenyls mole fractions especially in consideration of the temperature range of the present study.

We can now consider alternative pathways for the formation of the terphenyls which could explain the discrepancy between the expected concentrations and the experimentally observed ones. As discussed in the previous section, the decomposition of the iodobiphenyls leads to the formation of biphenyl radicals and iodine atoms. Even more significant for the formation of the o- and m-biphenyl radicals are the reactions of phenyl radical with o-benzyne and m-benzyne, respectively (R27 and R28). The corresponding reaction for the formation of the p-$C_{12}H_9$ radical (R29) does not play an important role in the modeling results since the p-benzyne radical quickly isomerizes to form 1,5-hexadiyn-3-ene (R26) and is not available for reaction with phenyl. Once produced the three biphenyl radicals can recombine with an additional phenyl radical to form directly the terphenyls (R49–R51).

We discussed in generic terms about additional pathways to the terphenyls, but we did not explain how these pathways could address our initial question about the unexpected relatively low o-terphenyl concentrations. The explanation is found in the fact that the pathway for the formation of o-terphenyl from o-$C_{12}H_9$ (Figure 21) + C_6H_5 is not as effective as the corresponding ones for m- and p-terphenyls even though o-C_6H_4 is the most abundant among the benzyne isomers which implies an relatively high concentration of o-biphenyl radicals compared to the m- and p- ones. In fact the o-biphenyl radical can isomerize and form the hydrobiphenylene radical (R59, see Figure 21 for chemical structure) reducing the concentration of o-$C_{12}H_9$ available for recombination with phenyl. We will discuss this reaction in the section relative to acenaphthylene formation (section 6.3.1.4). On the other hand, the m-$C_{12}H_9$ and the p-$C_{12}H_9$ are mainly consumed by reaction with C_6H_5 to form m-and p-terphenyls. In addition we need to consider that o-benzyne not only reacts with phenyl to form the o-biphneyl radical but is also consumed by other reactions involved in the formation of different PAH compounds, i.e. biphenylene, naphthalene, and the four-ring species. Such reactions will be discussed later in the corresponding sections.

To the best of our knowledge, no previous investigation has studied or proposed reaction rate constants for the steps involved in the formation of the terphenyls. Consequently, the corresponding parameters have been estimated as reported in Table 7. In particular, the activation energy for the recombination reactions between the benzynes and the phenyl radical (R27–R29) has been estimated as similar to the barrier calculated by Tokmakov and Lin[22] for the reaction between phenyl radical and acetylene forming the 2-phenylvinyl radical. The approximated reaction rate parameters for the dissociation reactions R30 and R31 respectively for m-$C_{12}H_9$ and p-$C_{12}H_9$ are analogous to the parameters for the reverse of reaction R27 for which the thermochemical parameters are well established. Likewise the reactions for the decomposition of the terphenyls into biphenyl radicals + phenyl radicals (R52–R54) are analogous to the reverse of $C_6H_5 + C_6H_5 \leftrightarrow C_{12}H_{10}$. Finally the reaction rate constants for $C_6H_5 + C_{12}H_{10}$ forming terphenyls and H atoms (R46–R48) have been estimated based on the reaction rate constant for $C_6H_5 + C_6H_6$ forming biphenyl + H[106]. The corresponding pre-exponential factors were adjusted based on the multiplicity of the specific pathway.

As shown in Figure 31 the simulation results reproduce the shape of the terphenyl profiles with very good accuracy in particular in relation to the estimated temperature range where the profiles reach the maximum value. It is also noticeable how the relative concentrations between the three isomers are in good agreement with the experiments, with m-terphenyl produced in larger amounts compared to p-terphenyl and o-terphenyl.

The results presented in the current section indicate that in order to have an accurate representation of the phenyl radical chemistry it is necessary to consider the detailed pathways involved in the formation of the terphenyls. A particularly important role is played by the presence of the o- and m-benzynes as primary reactants involved in the formation of the biphenyl radicals which serve as building blocks for the terphenyls. We will discuss in the next sections how the benzyne chemistry influences the formation of other PAH compounds relevant for the formation of soot.

6.3.1.4. Biphenylene and Acenaphthylene

In view of the formation of substantial amounts of o-benzyne radicals by the decomposition of the phenyl iodide (R3), by the H-abstraction between phenyl radicals (R21), and by the isomerization of m-benzyne (R24), we would expect biphenylene to be among the major stable products of the decomposition of phenyl iodide. Once again the experimental results do not reflect the expectations. As shown in Figure 32 less than 1 ppm of biphenylene is produced even with initial phenyl iodide mole fraction equal to 95.6 ppm.

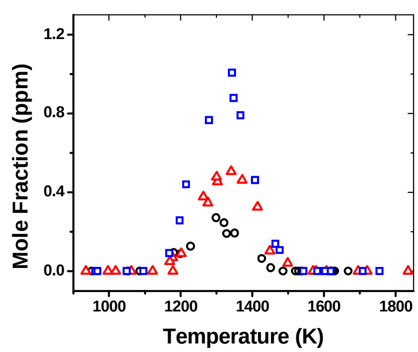

Figure 32. Biphenylene experimental concentrations at p ~ 50 atm. ○ $[C_6H_5I]_0$ = 26.6 ppm; △ $[C_6H_5I]_0$ = 50.6 ppm; □ $[C_6H_5I]_0$ = 95.6 ppm.

The production of small amounts of biphenylene is a confirmation of the fact that o-benzynes are consumed by other reactions, i.e. the reaction with phenyl radical to form o-$C_{12}H_9$ described in the previous section. Figure 32 also indicates that the production of biphenylene is proportional to the initial concentration of the fuel, in agreement with the fact that biphenylene derives from the recombination between o-benzyne radicals whose formation is directly linked to the fuel or its primary products as described above. The high-pressure limit reaction rate constant for the recombination between the benzyne radicals has been recently calculated by Tranter et al.[26] and utilized in the present model without any adjustment (R58).

While the formation of biphenylene is at least from a descriptive point of view simple, the mechanisms involved in the formation of acenaphthylene are more complex and still not well clarified. Our discussion starts with the simple experimental observation of the fact that acenaphthylene is produced in considerable amounts during the pyrolysis of the phenyl radical. The experimental profiles are reported in Figure 33 and indicate as expected that acenaphthylene is not a primary product of the recombination between phenyl radicals. In fact its formation does not occur in the low temperature range of our experiments. As shown in Figure 33 acenaphthylene profiles are characterized by a rapid increase starting at around 1250 K which is typical of an isomerization process with relatively high pre-exponential and activation energy or of a process involving secondary products. The profiles reach the maximum at around 1500 K before dropping rapidly at higher temperatures.

The conventional formation pathway for acenaphthylene involves the well studied reaction between naphthyl radical and acetylene[21,109] Naphthyl radicals are generally formed through the HACA mechanism[15,110] starting from phenyl and acetylene through the phenylacetylene intermediate. Thus the whole process requires the addition of three acetylene molecules to a phenyl radical with an intermediate H-abstraction from the phenylacetylene. The present experiments are performed without acetylene in the initial mixture, and although acetylene is produced at high temperatures we can exclude the naphthyl + acetylene reaction as relevant to the formation of acenaphthylene. A good proof for this hypothesis is provided by the measurement of the intermediate phenylacetylene. As shown in Figure 34 phenylacetylene is produced in trace amounts even when large concentrations of phenyl iodide are pyrolyzed. In addition as discussed in the second part of the paper the presence of much larger concentrations of acetylene would not be sufficient to justify the high mole fractions of acenaphthylene reported in Figure 33.

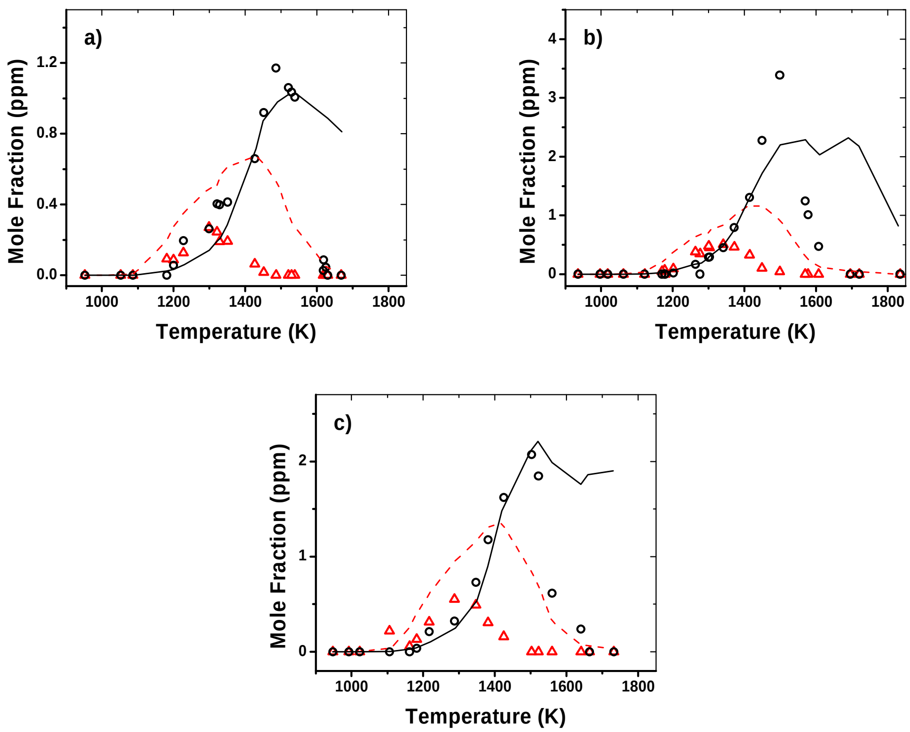

Figure 33.* Δ *Biphenylene exp., – – biphenylene sim.; ○ acenaphthylene exp., —— acenaphthylene sim. a) [C_6H_5I]$_0$ = 26.6 ppm, p ~ 50 atm; b) [C_6H_5I]$_0$ = 50.6 ppm, p ~ 50 atm; c) [C_6H_5I]$_0$ = 54.2 ppm, p ~ 25 atm.

Richter et al.[111] reported the presence of large amounts of acenaphthylene in their benzene flame experiments. The authors hypothesized that acenaphthylene is produced through the formation of the hydrobiphenylene radical (Figure 21 for chemical structure) from the addition between biphenylene and hydrogen, followed by isomerization to acenaphthylene. The proposed pathway is part of a more complex potential energy surface which has been recently studied in details by Shukla et al.[112] using ab-initio calculations. The authors explored the possible pathways involved in the isomerization of biphenyl and o-biphenyl radical in relation to the formation of several stable compounds including among the others acenaphthylene.

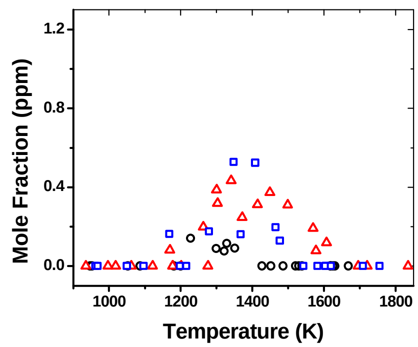

Figure 34. Phenylacetylene experimental concentrations at p ~ 50 atm. ○ [C_6H_5I]$_0$ = 26.6 ppm; Δ [C_6H_5I]$_0$ = 50.6 ppm; □ [C_6H_5I]$_0$ = 95.6 ppm.

The theoretical results presented in Ref. [112] have been included in the model (R59–R71). Due to the complexity of the problem in consideration few assumptions were made. First of all only the more stable compounds were considered as possible final products of the isomerization processes. These compounds include biphenylene, acenaphthylene, and cyclopenta[a]indene (benzopentalene, BENZO in Figure 21 and Table 7). The activation energies of the elementary reactions are assumed as equal to the relative theoretical barriers. The corresponding pre-exponential factors are estimated based on the values for similar reactions. When a global step is considered, a similar approach was used considering the barrier between the reactants and the maximum energy of the specific path as the activation energy. The pre-exponential was estimated based on the reaction constituting the limiting step in the global process.

The reaction pathway which involves the isomerization of biphenyl (R68–R71) does not play a significant role at the temperature conditions implemented in the present study although biphenyl is formed in large amounts. In fact the entrance barrier of almost 110 kcal/mol is too high to allow a significant flux to enter the potential energy surface. Even a ten-fold increase in the estimated pre-exponential factor does not lead to a significant change in the modeling results. On the other hand, the energy required for the isomerization of the o-biphenyl radical is much lower as the corresponding barrier is equal to around 31 kcal/mol (R59). Considering the fact that o-biphenyl radicals are formed in considerable amounts by the recombination between phenyl and o-benzyne radicals (R27) as discussed in the previous section, we expect the corresponding isomerization (R59) to occur even in the temperature range of our experiments. Thus we have to discuss in more details the reaction scheme utilized in the present model which is based on the potential energy surface investigated by Shukla et al.[112]

The entrance reaction step involves the isomerization of o-biphenyl radical into hydrobiphenylene radical (R59 and R60). Hydrobiphenylene radical can isomerize to form monohydrocyclopenta[a]indene (BENZOH in Figure 21 and in Table 7) or undergo a hydrogen-loss process to biphenylene + H. Although the latter pathway (R61 and R62) is favorable from an entropic point of view, the corresponding barrier is around 7 kcal/mol higher than the barrier for the isomerization to monohydrocyclopenta[a]indene (R63 and R64). As also suggested by Shukla et al.[112] the isomerization pathway is favorable at relatively low temperatures as also confirmed by the low concentrations of biphenylene observed in the experiments (Figure 32). Once formed, the monohydrocyclopenta[a]indene intermediate can undergo a hydrogen-loss process to form cyclopenta[a]indene + H (R65 and R66) or proceed through a series of isomerization reactions followed by a hydrogen-loss to form acenaphthylene + H (R67). Clearly the former pathway is favorable due to the entropy contribution and due to the fact that it is constituted by a single elementary step.

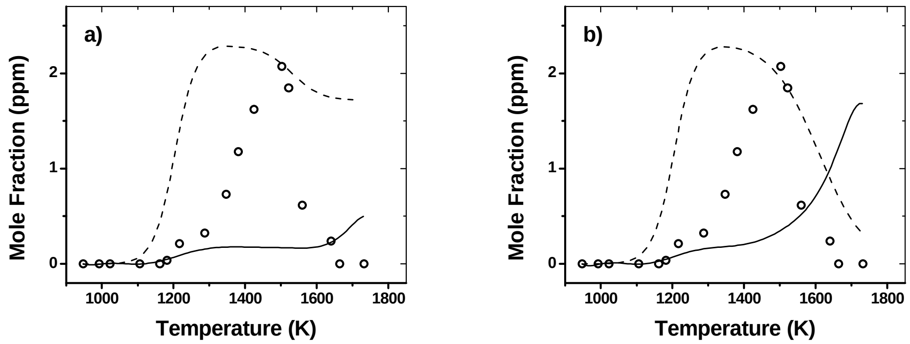

Figure 35. ***○ Acenaphthylene exp.; —— acenaphthylene sim.; – – cyclopenta[a]indene sim. a) model in Table 7 omitting reaction R80; b) model in Table 7 with*** **k**$_{80}$ ***calculated from [116].*** $[C_6H_5I]_0$ ***= 54.2 ppm, p ~ 25 atm.***

Figure 35a shows the modeling results for acenaphthylene and cyclopenta[a]indene from the scheme described in the previous paragraph. The pathway leading to cyclopenta[a]indene is clearly predominant and the experimental profile for acenaphthylene is substantially underestimated. At this point it is important to underline the fact that although cyclopenta[a]indene was not measured in the experiments we cannot exclude its formation just on the basis of the experimental observations as cyclopenta[a]indene dimerizes quickly even at room temperature. Previous studies indicate that in order to obtain n.m.r. spectra for this species the analyses had to be run at -70 ºC[113,114]. Thus we have to base our considerations about cyclopenta[a]indene formation exclusively on the theoretical study by Shukla et al.[112]

The results presented in Figure 35a suggest the possibility of an isomerization pathway between cyclopenta[a]indene and the more stable acenaphthylene. Such pathway has experimental evidence in the work performed by Brown et al.[113,114] and by Wiersum and Jenneskens[115] on the formation of ring-contracted aromatic hydrocarbons, including acenaphthylene, starting from diradical compounds. Blake et al.[116] used ab-initio calculations to investigate the potential energy surface for the isomerization of the biphenyl diradical into acenaphthylene through the formation of the stable cyclopenta[a]indene.

The results in Ref. [116] were used to calculate the reaction rate constants for relevant isomerization reactions. Conventional transition state theory (TST) with rigid rotor harmonic oscillator assumptions and estimated tunneling effects[82] was used to evaluate the high-pressure limit reaction rate constants from the quantum chemical calculations. Only the contributions from the low frequency torsional modes, if any, were calculated using free rotor approximation. In particular, the isomerization between cyclopenta[a]indene and acenaphthylene was treated as a single step reaction (R80) with rate constant equal to the one for the limiting step in the global process which in reality is composed by several isomerization steps. The Arrhenius expression of the reaction rate constant calculated based on the molecular properties from [116] is $k_{80} \cong 2.704 \cdot 10^{14} \exp(-43866.5/T)$ (s^{-1}). The modeling results obtained using such expression are reported in Figure 35b. The acenaphthylene profile is still underestimated by the model. Clearly the activation energy is too high to allow the isomerization process to occur in the temperatures range where the experimental acenaphthylene concentration starts increasing (1300–1500 K).

In order to improve the agreement between experimental and modeling profiles for acenaphthylene we derived an expression for the isomerization between cyclopenta[a]indene and acenaphthylene based on the experimental profiles for acenaphthylene. Such estimate is based on the assumption that acenaphthylene is mainly produced through the above mentioned isomerization process. This assumption should be sufficiently accurate since the conventional formation pathway for acenaphthylene can not play a significant role as discussed earlier in the text. The expression used to evaluate the reaction rate constant is the following:

$$k = \frac{-\ln\left(\frac{[BENZO]_0 - \Delta[BENZO]}{[BENZO]_0}\right)}{t}$$

where $[BENZO]_0$ is the initial concentration of cyclopenta[a]indene as estimated by the model ignoring reaction R80, $\Delta[BENZO] = [BENZO]_0 - [BENZO]_t \cong [A2R5]_t$, and t is the reaction time. $[A2R5]_t$ is the experimental concentration of acenaphthylene at the reaction time t.

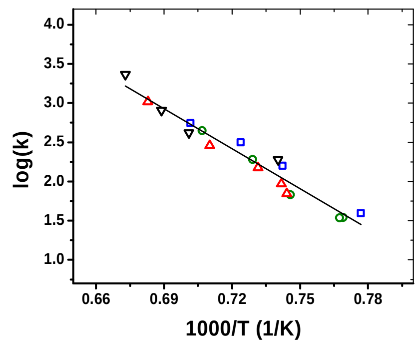

Figure 36. Arrhenius plot of the measured reaction rate constant for isomerization of cyclopenta[a]indene into acenaphthylene between 1287 and 1486 K, k in s^{-1}. ○ $[C_6H_5I]_0$ = 50.6 ppm, p ~ 50 atm; △ $[C_6H_5I]_0$ = 95.6 ppm, p ~ 50 atm; □ $[C_6H_5I]_0$ = 26.6 ppm, p ~ 50 atm; ∇ $[C_6H_5I]_0$ = 54.2 ppm, p ~ 25 atm; —— linear interpolation.

The Arrhenius plot of the reaction rate constant for R80 is reported in Figure 36. The linear interpolation of the experimental results provides the expression for the reaction rate constant for the isomerization of cyclopenta[a]indene into acenaphthylene, which is equal to $k_{80} \cong 4.699 \cdot 10^{14} \exp(-39192.3/T)$. The pre-exponential factor is slightly higher than the one obtained above from the calculations based on the results from Ref [116] but within a two-fold factor. On the other hand, the activation energy is around 9 kcal/mol lower than the theoretical one. Further theoretical calculations performed with multireference methods will clarify if the discrepancy between the theoretical and the experimental activation energies is due to inaccuracy in the theoretical methods implemented in [116] or to the presence of additional lower energy isomerization pathways.

It is important to mention that the experimentally derived rate expression is function of the parameters of a complex model which includes among the others the estimated reaction rate parameters for the formation of cyclopenta[a]indene (R59–R67) as well as the reaction rate parameters for the formation of o-biphenyl radical, R27. Thus its accuracy depends also on the accuracy of such relevant parameters in the model.

The results obtained including the experimental k_{80} expression into the model are shown in Figure 33. The formation of acenaphthylene is well reproduced by the model in terms of shape of the curve as well as mole fraction levels. In the high temperature range of our study, above 1500 K where the experimental profiles drop, the concentrations are overestimated by the model. We can attribute this discrepancy to the absence of reaction pathways forming lighter compounds as we will discuss later in the appropriate section. Similar results were obtained for the experimental set conducted at nominal pressure equal to 50 atm with 95.6 ppm initial C_6H_5I mole fraction.

In Figure 33 the profiles of biphenylene are also reported. The simulations predict the experimental profiles accurately in the low temperature range up to 1300 K where the formation of biphenylene is mainly driven by the recombination reaction between o-benzyne radicals (R58). At higher temperatures where the experimental profiles decay the modeling results do not follow the experimental trends so accurately. Above 1300 K the contribution from the isomerization reaction from hydrobiphenylene radical to biphenylene + H (R61 and R62) becomes relevant and causes the mentioned discrepancy. Thus the experimental profiles indicate that such reaction pathway could be even less relevant than estimated. On the other hand, additional channels which consume biphenylene could be important especially in the high temperature range of our study.

In order to test this hypothesis, a series of theoretical calculations were initiated. The model includes the results of such theoretical study performed to analyze possible biphenylene isomerization pathways (R72–R77). In particular, the study was inspired by the experimental investigations by Wiersum and Jenneskens[115] and by Brown et al.[113,114] as well as by the study by Scott[117] which indicate that biphenylene is a precursor of cyclopenta[a]indene and consequently of acenaphthylene.

This possibility was investigated. The geometry optimizations and vibrational analyses were performed using the uB3LYP hybrid functional[67,68] with the Pople's valence triple-ζ basis set 6-311+G(d,p)[96]. The energetics of the optimized structures were refined by single point energy calculations performed with coupled-cluster method using both single and double substitutions and including triple excitations (CCSD(T))[69] with Dunning's correlation consistent polarized double-ζ basis set (cc-pVDZ)[63]. Frozen-core (FC) assumption was also used. All of the calculations were carried out with the Gaussian 03 program package[84]. The results of the calculations are reported in Appendix A (Cartesian Coordinates, electronic energies, zero-point vibrational energies, and imaginary vibrational frequencies).

The results of the theoretical investigation are shown in Figure 37. The pathway identified in the present study involves the formation of a benzocyclooctatetraene-like structure (C_6H_4oct) (see Figure 37 for chemical structure) and subsequent reorganization to form a cyclopenta[a]indene-like radical (BENZOHyl) (Figure 37). Since the calculations were performed on spin-singlet structures, hydrogen-transfer processes are favorable compared to hydrogen-loss processes. As expected the BENZOHyl radical isomerizes to form cyclopenta[a]indene. Among the species in Figure 37 the only one which showed diradical character is BENZOHyl. The relative energy was estimated as

$$E = E(CCSD(T)) + E(uB3LYP) - E(rB3LYP)$$

where *E(uB3LYP)* and *E(rB3LYP)* are the energies of the diradical and closed-shell compounds estimated respectively by uB3LYP/6-311+G(d,p) and rB3LYP/6-311+G(d,p) methods.

Reaction rate constants for the elementary steps involved in the isomerization process were calculated using conventional TST and rigid rotor harmonic oscillator assumptions. The rate parameters are reported in Table 7 (R72–R77). No adjustments to the reaction rate constants were made. Clearly biphenylene is a very stable compound and its dearomatization can occur only at relatively high temperatures. Only above 1500 K the contribution of the proposed pathway becomes relevant for both the consumption of biphenylene and the formation of acenaphthylene through the cyclopenta[a]indene intermediate. Further considerations on the necessity of further studies on the biphenylene isomerization are dependent on the accuracy of the rate parameters of the reactions involved in the formation of biphenylene as well as on the understanding of the mechanisms which leads to the formation of the light hydrocarbons discussed later in the manuscript.

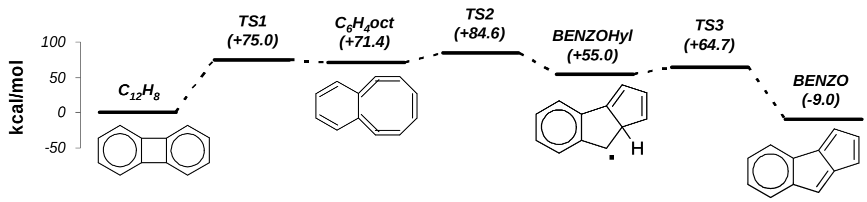

Figure 37. Potential energy surface for the isomerization of biphenylene into cyclopenta[a]indene. uB3LYP/6-311+G(d,p) optimized structures. CCSD(T)/cc-pVDZ energies in kcal/mol, including ZPVE.

6.3.1.5. Naphthalene

The presence of fused-ring structures formed during the pyrolysis of the phenyl radical is definitely the most surprising and challenging experimental finding in the present investigation. We already discussed about the formation of acenaphthylene and its modeling. Naphthalene, the simplest among the condensed compounds, was also measured although in lower concentrations compared to acenaphthylene. The experimental profiles are shown in Figure 38. In particular, it is interesting to notice how naphthalene is produced as soon as the phenyl iodide starts decaying suggesting a link between the formation of the second-ring species and the primary products of the phenyl iodide decomposition.

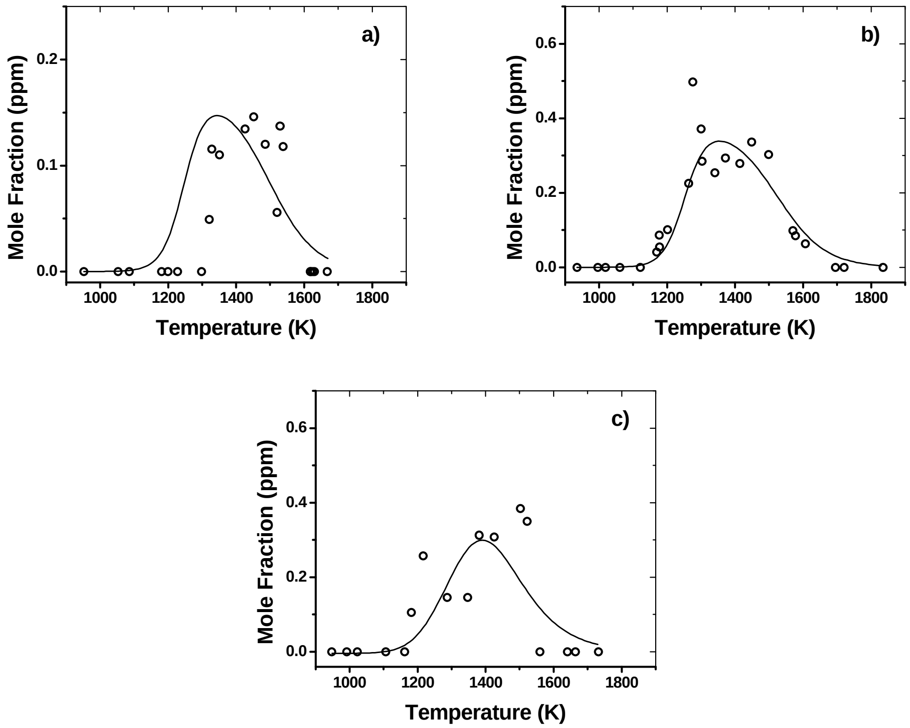

Figure 38. ***○ Naphthalene exp., —— naphthalene sim. a) $[C_6H_5I]_0$ = 26.6 ppm, p ~ 50 atm; b) $[C_6H_5I]_0$ = 50.6 ppm, p ~ 50 atm; c) $[C_6H_5I]_0$ = 54.2 ppm, p ~ 25 atm.***

Clearly the HACA mechanism[15,110] can not be responsible for the experimental formation of naphthalene since acetylene is not present in the reactant mixture or produced in large amounts at low temperatures. Based on the experimental results, we started a series of theoretical calculations on the radical/π-bond addition between single-ring aromatics and we concluded that the reaction between o-benzyne and benzene leads mainly to the formation of naphthalene and acetylene through a two-step process involving the 1,4-cycloaddition between o-benzyne and benzene and the subsequent fragmentation of the intermediate[118]. The details of the study are reported in Chapter 7. Similar results were reported by Shukla et al.[112] Both benzene and o-benzyne are formed as primary products of the decomposition of the phenyl iodide and reaction between phenyl radicals, thus the proposed pathway was included in the model (R146–R148). The reaction rate constant k_{147} was calculated based on the structures and energetics provided in Appendix D using conventional TST. In addition the reaction rate constant for the entrance reaction, the 1,4-cycloaddition, was multiplied by a factor of two within the uncertainty provided in section 7.2. For consistency k_{147} was also multiplied by a two-fold factor.

The results of the simulations are reported in Figure 38 and show an excellent agreement with the experiments not only in terms of profile shape but also in terms of concentrations. The experimental results confirm the relevance of the radical/π-bond addition between o-benzyne and benzene as source of the second-ring species in this kind of pyrolytic systems.

6.3.1.6. Four-Ring Compounds

Even more surprising than the formation of acenaphthylene and naphthalene was the identification and measurement of a variety of four-ring fused compounds including chrysene, triphenylene, benzo[a]anthracene, benzo[g,h,i]fluoranthene, and benzo[c]phenanthrene. An example of the profiles for these species is shown in Figure 39 for the experimental set conducted at a nominal pressure of 50 atm with an initial phenyl iodide mole fraction equal to 95.6 ppm for which the mole fractions of the four-ring compounds are maximum. The experimental profiles provide critical information on how these large compounds could be formed.

First of all it is important to notice that chrysene and triphenylene coelute in the present analytical set-up. In fact it is not possible to separate these two compounds using a (50%-Phenyl)-methylpolysiloxane phase column as the DB-17ms[119]. The LC-50 column, dimethyl-(50% Liquid Crystal), is not suitable for measuring the lighter PAH species, but it provides a good separation of heavy isomers, as for example triphenylene and chrysene. A series of relevant experiments were conducted with a LC-50 column attached to the second FID detector in parallel with the DB-17ms column, so that heavy species could be separated through the two different columns for better resolution. The results indicated that the peak area measured with the DB-17ms is constituted by 90%

of chrysene and 10% of triphenylene. With this in mind, we can clearly state that the major four-ring compound produced in the pyrolysis of phenyl radical is chrysene. Only small amounts of the other isomers are produced.

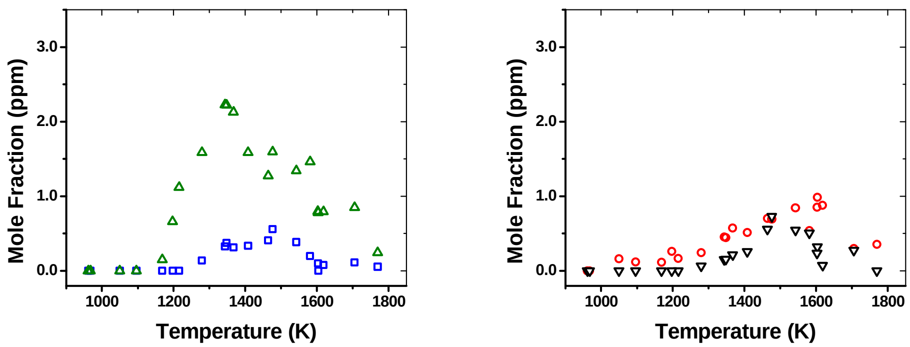

Figure 39. Experimental mole fraction, $[C_6H_5I]_0$ = 95.6 ppm, p ~ 50 atm. △ chrysene (~90%) + triphenylene (~10%); □ benzo[a]anthracene; ○ benzo[g,h,i]fluoranthene; ∇ benzo[c]phenanthrene.

Even more important from a mechanistic point of view is the fact that the chrysene is formed as soon as phenyl iodide starts decomposing. Conventional pathways for the formation of this compound include the HACA mechanism starting from phenanthrene. Since phenanthrene is only measured in trace amounts in the experiments and acetylene is not produced at low temperatures, the HACA mechanism can not be responsible for the formation of chrysene. Thus, such species must be produced by some sort of recombination between three single-ring aromatic compounds. On the other hand, benzo[a]anthracene, benzo[g,h,i]fluoranthene, and benzo[c]phenanthrene are formed at higher temperatures, indicating that these isomers could derive from the isomerization of chrysene.

In order to understand the mechanisms of formation of chrysene we deconstructed its molecular structure into simpler components. The only reasonable pathway we were able to identify is the one reported in Figure 40. The primary reactants on the right of the figure are naphthyl vinyl radical and phenyl radical which can recombine to form an intermediate compound which undergoes ring closure and dehydrogenization to chrysene. This process is a sort of PAC mechanism of the naphthyl vinyl radical. The main problem with the proposed pathway is the fact that the naphthyl vinyl radical once formed would isomerize quickly to form acenaphthylene[109] and would not be available for the recombination reaction with the phenyl radical. A different mechanism must be responsible for the formation of chrysene.

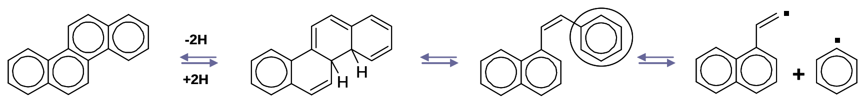

Figure 40. Deconstruction of the molecular structure of chrysene.

Shukla and Koshi[23,24] identified the presence of triphenylene in their experimental work on benzene pyrolysis. Thus, we can hypothesize that triphenylene is produced as the primary four-ring compound in our experiments too and that it subsequently undergoes isomerization to form chrysene. Since such an isomerization process is unknown, from a modeling point of view we will consider only the formation of triphenylene and compare the modeling results with the sum of the experimental mole fractions of all the four-ring species (Figure 41). The correspondence between the calculated triphenylene concentrations and the measured concentrations provides an estimate of the accuracy of the reaction pathways in the model keeping in mind the fact that triphenylene subsequently undergoes isomerization into chrysene and at higher temperatures into benzo[a]anthracene, benzo[g,h,i]fluoranthene, and benzo[c]phenanthrene too.

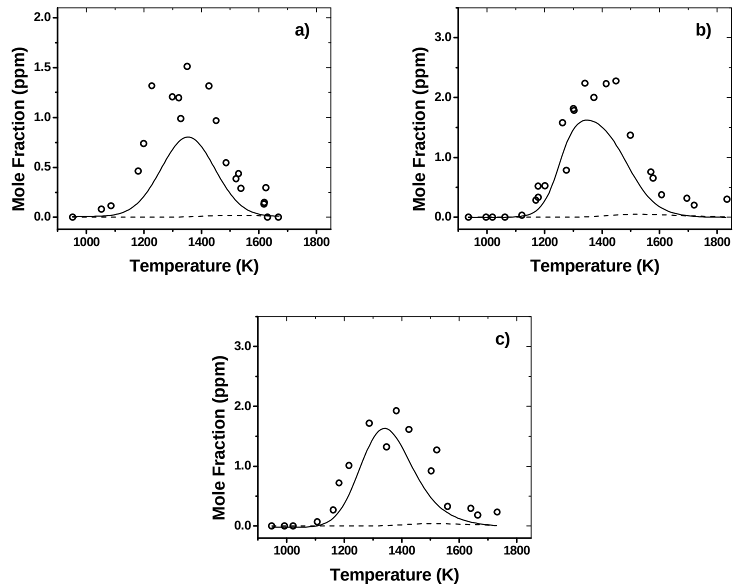

Figure 41. ***○ Sum four-ring compounds exp., —— triphenylene, model in Table 7; – – triphenylene, model in Table 7 omitting R57. a) $[C_6H_5I]_0$ = 26.6 ppm, p ~ 50 atm; b) $[C_6H_5I]_0$ = 50.6 ppm, p ~ 50 atm; c) $[C_6H_5I]_0$ = 54.2 ppm, p ~ 25 atm.***

The formation of triphenylene is the prototype of the PAC mechanism[23,24]. Shukla and Koshi hypothesized that phenyl adds to biphenyl to form o-terphenyl which subsequently undergoes cyclodehydrogenization process to triphenylene. The latter step has always been controversial. Experimental studies on benzene pyrolysis[120] and on biphenylene pyrolysis[121] indicate that the cyclodehydrogenization process does not occur, although studies supporting the contrary are present in literature[107,122]. We will try to use our experimental results to clarify the point.

We have already discussed the formation of o-terphenyl in a previous section (section 6.3.1.3) and mentioned that from a modeling point of view its cyclodehydrogenization is energetically unfavorable due to its high activation energy (84.7 kcal/mol, R55). This consideration is based on estimated parameters which may not be very accurate, so we need to find a more convincing justification to rule out the cyclodehydrogenization process. Such justification derives from a simple empirical observation. The amount of o-terphenyl produced in the system (Figure 31) is not sufficient to justify the high mole fractions of four-ring compounds observed in the experiments even if o-terphenyl were entirely converted into triphenylene. Thus a different mechanism must be involved in the formation of the four-ring compounds.

Fields and Meyerson[123,124] reported the measurement of triphenylene in their pyrolytic studies on the reaction between o-benzyne and benzene. The authors hypothesized that the formation of triphenylene is mainly due to trimerization of o-benzyne radicals. Lindow and Friedman[121,125] investigated the liquid and vapor-phase pyrolysis of biphenylene and based on the distribution of the product species concluded that a relatively high concentration of the diradical species in Figure 42 is present especially in the high temperature range of their experiments (730 °C). Such diradical can react with o-benzyne and form triphenylene as shown in Figure 42. An important consideration reported by Lindow and Friedman is that naphthalene is not produced even when the experiments are conducted in benzene for which the estimated barrier is less than 7 kcal/mol[118]. This indicates that the reaction between the diradical intermediate and the o-benzyne radical must be very fast in order to justify the fact that all the o-benzyne radicals are consumed by the pathway in Figure 42 even when large concentrations of benzene are present. In order to account for such favorable trimerization process, we assumed that o-benzyne reacts directly with biphenylene with a reaction rate constant similar to the one used for the dimerization of o-benzyne radicals (R58).

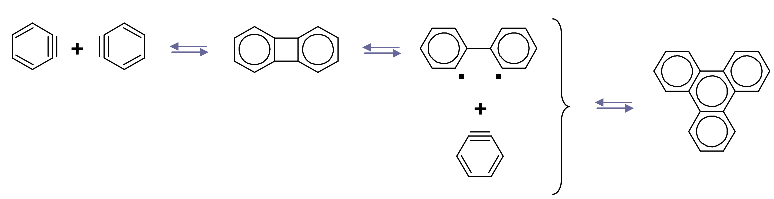

Figure 42. o-Benzyne trimerization pathway.

The results of the simulations are reported in Figure 41. The modeling profiles are in excellent agreement with the experiments not only for the general shape but also in terms of maximum mole fractions of the product species. This indicates that the proposed pathway is most likely correct although we need also to take into account the large uncertainty in the quantification of the four-ring species before drawing a conclusion on the accuracy of the estimated reaction constant k_{57}. For comparison the modeling results using only the PAC mechanism are also shown in Figure 41 (dashed lines). The results confirm the hypothesis that the PAC mechanism is not adequate to explain the formation of the four-ring compounds in the system in consideration.

Before concluding this section, we would like to mention that the diradical intermediate in Figure 42 can dimerize as shown in the previous studies on the biphenylene pyrolysis[121,125]. This process could be responsible for the discrepancy between experimental and modeling profiles for biphenylene reported in the corresponding section and in Figure 33. Such hypothesis requires additional theoretical validations.

6.3.1.7. Light Hydrocarbons

Although the main focus of the present investigation is to study the formation of polycyclic aromatic hydrocarbons and the relevance of the chemical mechanisms involved, several light hydrocarbons were measured including the major products benzene, acetylene, diacetylene, and triacetylene. Benzene formation has been already discussed earlier in the text in the corresponding section and no additional analyses are necessary for the purpose of the present investigation. The main consideration we need to keep in mind about the discussion on benzene is the fact that although the low temperature profiles are well reproduced by the model the benzene concentrations in the high temperature range of our study are overestimated by the model (Figure 26). Overestimation of the experimental profiles at high temperatures has been also observed for other product species, i.e.

biphenyl (Figure 26), biphenylene and acenaphthylene (Figure 33). Of course this means that the formation of other experimental compounds is underestimated. However before considering the modeling results we start as usual with the analysis of the experimental profiles of the remaining major compounds, i.e. acetylene, diacetylene, and triacetylene.

As expected, the formation of acetylene and polyacetylenes occurs in the high temperature range of our study mainly above 1400 K. Wang et al.[126] investigated the decomposition of the phenyl radical using ab-initio calculations and concluded that it proceeds through C-H fission to form o-benzyne (R157) which subsequently undergoes fragmentation into acetylene and diacetylene (R159). The derived reaction rate constants were included in the model used by the authors to accurately simulate the decomposition of benzene in shock-tube experiments where the polyacetylenes were measured[127]. Based on the mechanism proposed by Wang et al.[126], the formation of acetylene and diacetylene are strictly coupled and the corresponding concentrations should be very similar at least at low temperatures. As shown in Figure 43 the experimental profiles from the present study do not follow the expected behavior.

The first obvious discrepancy between the experimental and the expected trends consists in the fact that acetylene is produced in much larger concentrations compared to diacetylene even at the relatively low temperatures when the profiles starts to increase rapidly (1400 K). The second less evident difference between the acetylene and the diacetylene profiles is that acetylene is produced also below 1400 K although in small amounts (few ppm). These evidences suggest that there could be an additional low-energy reaction pathway which favors the formation of acetylene. The comparison between the experimental profiles for acetylene and diacetylene and the modeling results confirm such hypothesis (Figure 43). In fact, although the modeling profiles start increasing around 1400 K as the experiments indicate, the o-benzyne fragmentation pathway is not sufficient to justify the steep increase in the experimental mole fractions especially of acetylene. In addition the experimental profiles reach a sort of equilibrium at relatively low temperatures, around 1700 K for acetylene and 1600 K for diacetylene, while the modeling profiles do not reproduce such behavior. Finally no formation of acetylene is predicted at temperatures below 1400 K indicating that the model is not complete.

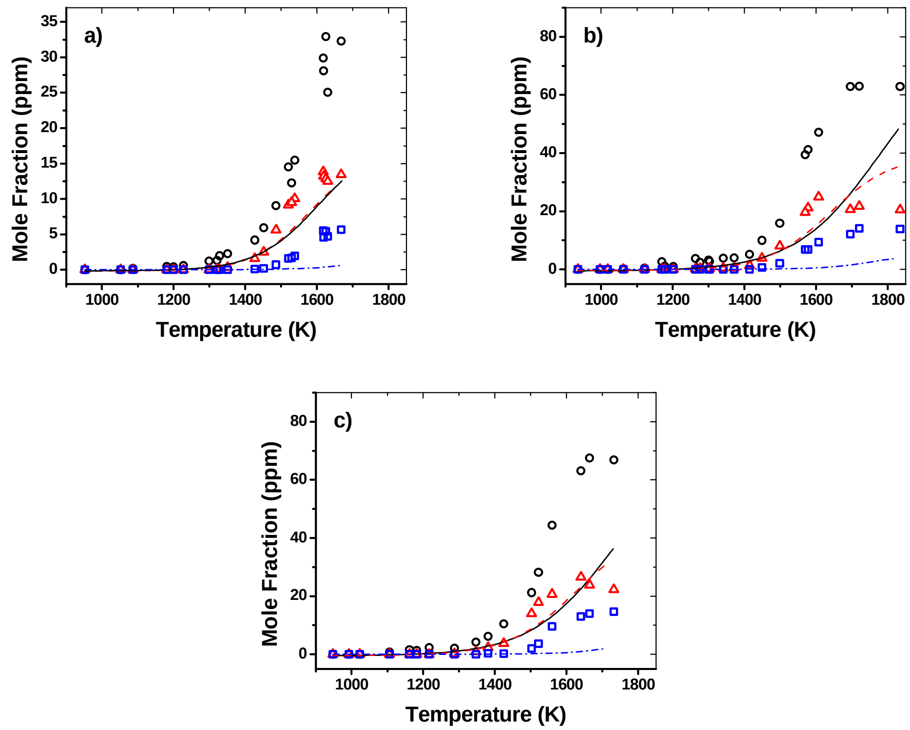

Figure 43. ***○ Acetylene exp., —— acetylene sim.; △ diacetylene exp., – – diacetylene sim.; □ triacetylene exp., – · – tracetylene sim. a) [$C_6H_5I]_0$ = 26.6 ppm, p ~ 50 atm; b) [$C_6H_5I]_0$ = 50.6 ppm, p ~ 50 atm; c) [$C_6H_5I]_0$ = 54.2 ppm, p ~ 25 atm.***

Different considerations apply for triacetylene. The corresponding experimental profiles have a similar trend to the profiles of acetylene and diacetylene with a relatively steep increase starting around 1450 K before reaching the equilibrium value around 1700 K. Of course the mole fractions of triacetylene are lower than the ones of acetylene and diacetylene. This is in agreement with the hypothesis that triacetylene could be mainly formed through polymerization.

The polymerization steps are included into the model but constitute only a minor pathway for the formation of triacetylene. Reaction pathway analysis indicates that triacetylene is mainly produced through decomposition of the C_6H_3 radical (reverse of R162, Ref. [105]) which is formed principally by reaction R167, z-C_6H_4+H $\leftrightarrow$ C_6H_3+H_2 (Ref. [94]). As already discussed, z-C_6H_4 is the product of the Bergman decyclization of p-benzyne (R26). As shown in Figure 43 the model significantly underestimates the concentrations of triacetylene. In particular, the polymerization mechanism should play a more relevant role for the formation of such polyacetylene as we will also discuss in the second part of the manuscript in relation to the phenyl + acetylene reaction.

The results reported in the present section indicate that although the formation of the PAH products is well simulated by the model, additional work is required in order to reach a similar accuracy with respect to the profiles of the light hydrocarbon compounds. On the other hand, the experimental results provide a very important benchmark for further development of the chemical kinetic model and for testing novel reaction pathways in particular in relation to the formation of acetylene. Possible pathways could involve the direct fragmentation of the large PAH compounds into small aliphatic hydrocarbons. A key role could be played by the presence of hydrogen atoms which could quite easily add to the various sites available in PAH compounds and allow the access into alternative potential surfaces at the high pressure conditions implemented in the present study. These hypotheses clearly require further theoretical validations.

6.3.1.8. PAC, Benzyne Chemistry, and Polymerization

Now that we presented a complete analysis of the experimental and modeling results on the pyrolytic reactions of the phenyl radical, we summarize the main findings in view of the initial purpose of the investigation, i.e. clarifying the role of the relevant reaction mechanisms. The considerations reported in this section apply specifically to the primary growth reaction steps up to the formation of the four-ring compounds. However, much of the present discussion can be extended to systems which involve reactions between even larger compounds.

First of all the experimental and modeling results indicate that for the system under consideration the PAC mechanism is not enough. In particular, the cyclization of o-terphenyl is energetically unfavorable in the temperature range of this study, and the PAC mechanism alone is not sufficient to account for the formation of the large four-ring PAH compounds.

On the other hand, it is clear from the entire prior discussion that the presence of the benzynes enhances the formation of almost all the PAH compounds measured in the present investigation. While the p-benzyne undergoes rapid isomerization into 1,5-hexadiyn-3-ene (Bergman decyclization R26) and does not contribute to the growth process, the m-benzyne is the primary factor in the formation of the m-terphenyl. In fact it recombines with phenyl radicals to form m-$C_{12}H_9$ radicals (R28) which constitute the primary building block for the formation of the m-terphenyl through reaction R50. Nevertheless we focus our attention on the chemistry associated with the o-benzyne radical, the most abundant among the benzyne isomers and definitely the most influential intermediate in relation to PAHs formation.

o-Benzyne is mainly produced by three reaction pathways as shown in Figure 44a, i.e. the decomposition of phenyl iodide into o-benzyne and HI (R3), the H-abstraction between phenyl radicals (R21), and the isomerization of m-benzyne (R24). Once formed o-benzyne reacts with the most abundant radical intermediates present in the system, i.e. o-benzyne to form biphenylene (R58) and phenyl to form o-$C_{12}H_9$ (R27). In particular, o-biphenyl radical is a very important intermediate for the formation of PAH compounds as indicated in Figure 44b. In fact in addition to constituting the primary building block for the formation of o-terphenyl (R49) it can easily isomerize into the hydrobiphenylene radical (R59) which is the precursor for the formation of cyclopenta[a]indene, acenaphthylene, and biphenylene - to a minor extent. The reaction rate analysis in Figure 44b confirms that o-$C_{12}H_9$ is mainly formed by reaction between o-benzyne and phenyl radical. Moreover o-benzyne is also responsible for the formation of naphthalene through cycloaddition with benzene and subsequent fragmentation of the intermediate (R146–R148) and possibly for the formation of triphenylene through trimerization (R57).

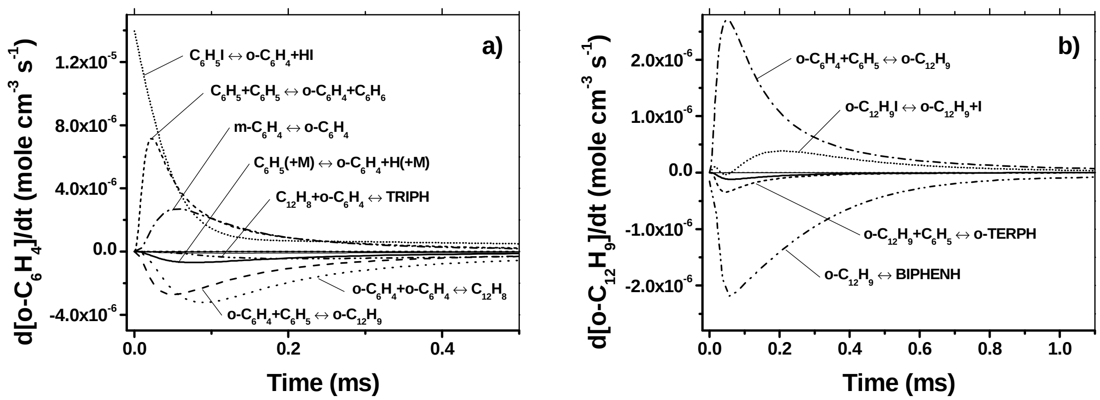

Figure 44. Rate of production analysis, $[C_6H_5I]_0$ = 54.2 ppm, T = 1287 K, p = 28.3 atm. a) o-benzyne radical; b) o-biphenyl radical.

The results summarized above not only highlight the importance of the o-benzyne chemistry for the formation of a variety of PAH components relevant to the formation of soot, but also draw attention to a wider category of compounds, the diradicals. In particular, at high-temperatures where the dehydrogenization or H-abstraction processes play a significant role the presence of relatively high concentrations of diradical species could drive the growth to larger PAH compounds by cycloaddition or even more rapidly by diradical-diradical recombination. Clearly these processes would be in competition with the conventional growth mechanisms, i.e. the HACA mechanism or the PAC mechanism.

A final note regarding the formation of acetylene at relatively high temperatures and the consequent polymerization process: the experimental profiles indicate that below 1300–1400 K the formation of PAH compounds is the predominant pattern. All the polycyclic aromatic hydrocarbons but acenaphthylene have the highest concentrations in this temperature range after which the profiles drop. Above 1400 K the formation of acetylene becomes predominant together with the polymerization process to form the polyacetylenes. Further investigations are required in order to clarify the high-temperature mechanisms responsible from a theoretical point of view.

6.3.2. Phenyl + Acetylene Reaction

Now that the mechanisms which lead to the formation of PAH compounds from the pyrolysis of the phenyl radical have been studied in details both experimentally and theoretically we can move to the second part of our investigation which regards the reaction between the phenyl radical and acetylene. Just as for the phenyl pyrolysis study, we will present the major experimental and modeling results with particular attention to the specific mechanisms involved in the formation of the PAH products. The experimental and modeling results at 25 atm are very similar to the results obtained at 50 atm with higher acetylene concentrations and thus are not shown. It is worth mentioning that although not discussed in details trace amounts of several other PAH compounds were detected including most of the compounds shown in Figure 22. However, the pathways characteristic of the phenyl pyrolysis now play only a minor role.

6.3.2.1. Phenyl Iodide Decomposition and Acetylene Profiles

The mechanisms of decomposition of the phenyl radical precursor phenyl iodide are of course similar to the ones described for the phenyl pyrolysis study. The only major difference is the presence of hydrogen atoms in the system from the reaction between phenyl radical and acetylene to form phenylacetylene and H. The free hydrogen atoms can react with the phenyl iodide and abstract the iodine atom (reaction R4 in Table 7). This reaction was studied both experimentally and theoretically by Gao et al.[128] and the reaction rate constant derived by the authors was used in the present model within the given uncertainty limits. The experimental and modeling profiles for phenyl iodide are reported in Figure 45. Good agreement between experiments and simulations was obtained.

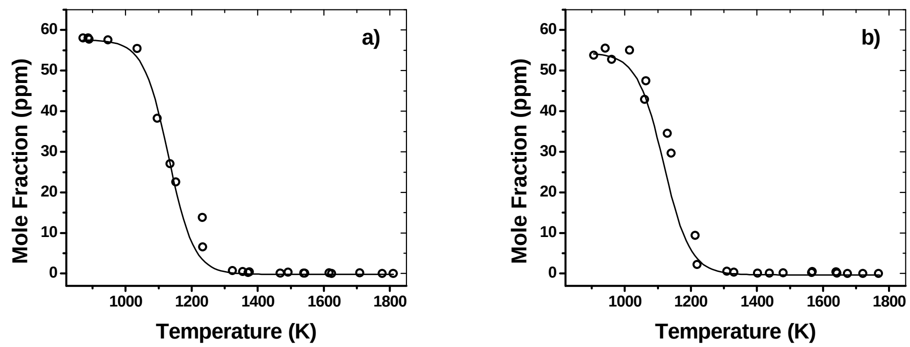

Figure 45. Phenyl iodide decomposition. ○ exp.; —— sim. a) [C_6H_5I]$_0$ = 58.1 ppm, [C_2H_2]$_0$ = 236.3 ppm, p ~ 50 atm; b) [C_6H_5I]$_0$ = 55.1 ppm, [C_2H_2]$_0$ = 511.3 ppm, p ~ 50 atm.

In these experimental sets, acetylene is also added as a reactant to the initial mixture. As we can observe in Figure 46 the acetylene profiles show similar trends for all sets. The trends are characterized by a drop in correspondence with the decay of the phenyl iodide, a recovery above 1300 K before a more consistent drop at higher temperatures (above around 1600 K). The model accurately predicts the experimental behavior of the acetylene profiles with regards to both the shape of the profiles and the concentrations. Clearly this indicates that the chemistry involved in the formation and consumption of acetylene is well represented by the model. Only at high temperatures does the model overestimate the experimental mole fractions. We will discuss the reason for such a discrepancy in the section related to the polyacetylenes (section 6.3.2.6).

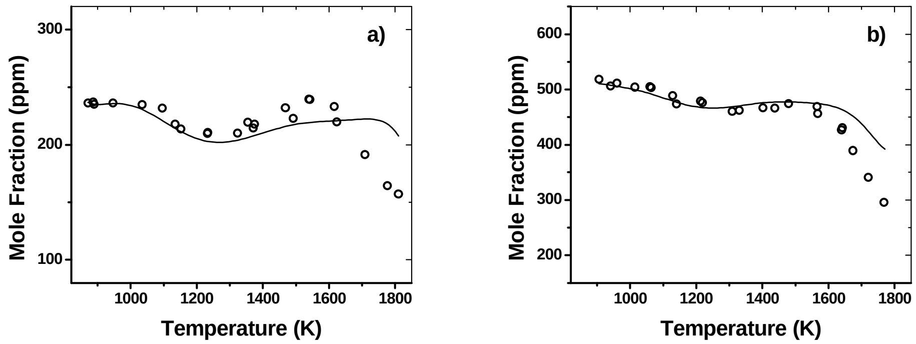

Figure 46. Acetylene decomposition. ○ ***exp.; —— sim. a) [C_6H_5I]$_0$ = 58.1 ppm, [C_2H_2]$_0$ = 236.3 ppm, p ~ 50 atm; b) [C_6H_5I]$_0$ = 55.1 ppm, [C_2H_2]$_0$ = 511.3 ppm, p ~ 50 atm.***

6.3.2.2. Phenylacetylene and Benzene

Phenylacetylene is obviously the major product from the reaction between the phenyl radical and acetylene (R90). At low temperatures the process is mainly limited by the concentration of phenyl radicals in the system as indicated in Figure 47 where the experimental profiles for phenylacetylene are reported for the two sets conducted at a nominal pressure of 50 atm and with different initial amounts of acetylene (236.3 ppm and 511.3 ppm). In fact the initial slope for the formation of phenylacetylene is similar in both cases independently of the C_2H_2 mole fraction. Above 1175 K the experimental profiles start diverging and in the temperature range where the phenylacetylene profiles reach the maximum value (around 1275 K) the ratio between the phenylacetylene mole fractions is around 0.69, higher compared to the ratio between the acetylene concentrations (around 0.46). Thus, although the initial acetylene mole fraction does have an influence on the formation of phenylacetylene, the initial mole fraction of phenyl iodide is a limiting factor even at intermediate temperatures.

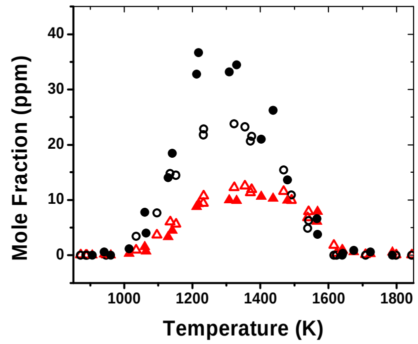

Figure 47. Experiments, p ~ 50 atm. ○ phenylacetylene, $[C_6H_5I]_0$ = 58.1 ppm, $[C_2H_2]_0$ = 236.3 ppm; Δ benzene, $[C_6H_5I]_0$ = 58.1 ppm, $[C_2H_2]_0$ = 236.3 ppm; ● phenylacetylene, $[C_6H_5I]_0$ = 55.1 ppm, $[C_2H_2]_0$ = 511.3 ppm; ▲ benzene, $[C_6H_5I]_0$ = 55.1 ppm, $[C_2H_2]_0$ = 511.3 ppm.

On the other hand, the experimental profiles for benzene indicate that the formation of this product is almost entirely dependent on the initial phenyl iodide concentration. In fact, as shown in Figure 47, the initial acetylene mole fraction does not have an influence on the concentration of benzene produced along the entire temperature range of our study. This is a clear indication that the pathways for the formation of benzene are very efficient and involve reactions with very reactive compounds. This is indeed the case. As shown in Figure 48 the reactions responsible for the formation of benzene are the recombination between phenyl and H (R44) and the reaction between phenyl and HI (R5). The main difference with the experiments conducted without acetylene is the relevance of reaction R44 even at low temperatures due to the presence of large concentrations of H atoms from reaction R90. Reaction R5 still has a major influence on the ability to model the benzene formation. On the other hand, the hydrogen-abstraction channel between phenyl radicals (R21–R23) has a minor role due to the fact that the phenyl radicals are removed by the efficient reaction with acetylene and not available for self-reaction.

The results of the simulations are reported in Figure 49. The model reproduces correctly the formation of both species for temperatures up to 1300 K. At higher temperatures, especially above

1400 K, the concentrations of benzene and phenylacetylene are overestimated. This behavior is similar to what we observed in the modeling results of the major species of the study on the phenyl pyrolysis. We can attribute this discrepancy to the same reason hypothesized in the first part of the manuscript - that the model does not include relevant pathways which consume the intermediates forming smaller compounds, i.e. the polyacetylenes.

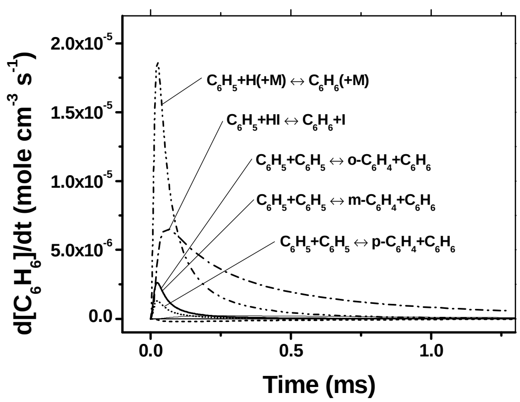

Figure 48. Benzene, rate of production analysis. $[C_6H_5I]_0$ = 58.1 ppm, $[C_2H_2]_0$ = 236.3 ppm, T = 1233 K, p = 47.1 atm.

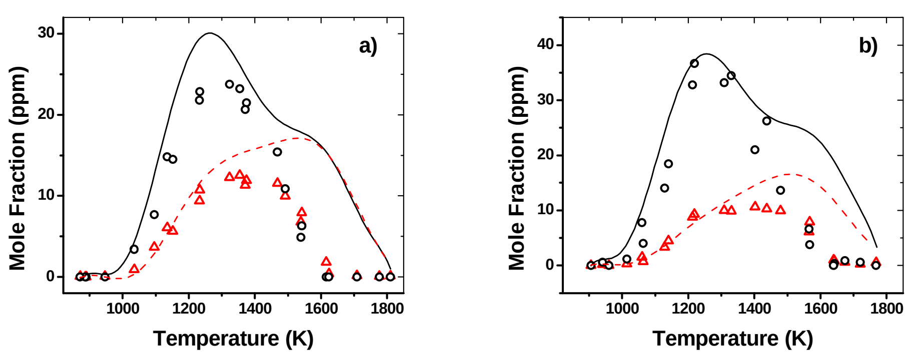

Figure 49. ○ Phenylacetylene exp., —— phenylacetylene sim.; Δ benzene exp., – – benzene sim. a) $[C_6H_5I]_0$ = 58.1 ppm, $[C_2H_2]_0$ = 236.3 ppm, p ~ 50 atm; b) $[C_6H_5I]_0$ = 55.1 ppm, $[C_2H_2]_0$ = 511.3 ppm, p ~ 50 atm.

6.3.2.3. Diphenylethyne and Phenanthrene

If we compare the distribution of PAH products in the phenyl + acetylene system with the one observed for the phenyl pyrolysis study we would be surprised that not many additional product peaks were measured. The major difference in adding acetylene as an initial reactant consists in the presence of the C14 compounds, i.e. diphenylethyne and phenanthrene. The experimental profiles of these compounds are reported in Figure 50. The experiments indicate that the formation of diphenylethyne is slightly faster than the one of phenanthrene in the low temperature range of our study. In addition diphenylethyne concentrations reach slightly higher values compared to phenanthrene before decaying above 1250–1300 K.

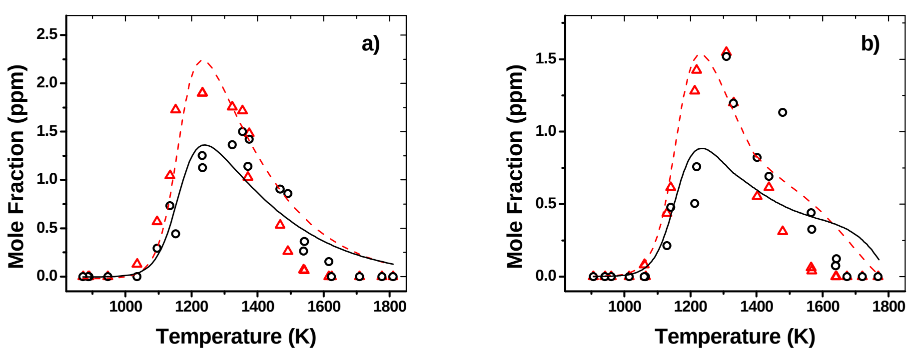

Figure 50. ***○ Phenanthrene exp., —— phenanthrene sim.; Δ diphenylethyne exp., – – diphenylethyne sim. a) [$C_6H_5I]_0$ = 58.1 ppm, [$C_2H_2]_0$ = 236.3 ppm, p ~ 50 atm; b) [$C_6H_5I]_0$ = 55.1 ppm, [$C_2H_2]_0$ = 511.3 ppm, p ~ 50 atm.***

The mechanisms of formation for phenanthrene are quite well known. The first relevant mechanism involves the reaction between o-biphenyl radical and acetylene forming phenanthrene + H (R98). At low temperature such reaction provides only a minor contribution to the formation of phenanthrene for the case in consideration. In fact the major contribution derives from the reaction between phenyl radical and phenylacetylene. Such reaction has been investigated by Iparraguirre and Klopper[129] using ab-initio calculations but due to the complexity of the study we preferred to use for modeling purposes an estimated global reaction rate constant (R99) based on the model presented in Ref. [95].

On the other hand, to the best of our knowledge no previous studies have considered the formation of diphenylethyne although the potential energy surface proposed in Ref. [129] contains intermediate structures which could be precursors for diphenylethyne. In view of the structure of diphenylethyne and the system in consideration, finding the pathway for its formation becomes trivial. Clearly diphenylethyne is formed through addition between phenyl radical and phenylacetylene with subsequent hydrogen loss in a similar fashion as the reaction between C_6H_5 and C_2H_2 forming phenylacetylene + H. This is the reason why we considered the same reaction rate constant for both processes ($k_{96} = k_{90}$). The reaction rate constant for the reverse reaction (R97) was estimated based on the results by Hertzler and Frank[130] on the reaction between phenylacetylene and H. In particular, the pre-exponential factor was multiplied by a factor of two due to the multiplicity of the reaction pathway.

The results of the simulations show excellent agreement with the experiments especially for the profiles of diphenylethyne (Figure 50). The formation of phenanthrene at low temperatures is also well simulated by the model indicating that the corresponding reaction rate parameters in the model are appropriate. In particular, it is worth highlighting that the relative formation slopes are well reproduced. The major discrepancy between experiments and simulations consists in the fact that the phenanthrene experimental profiles obtained with higher C_2H_2 mole fractions reach higher concentrations than the modeling profiles. This is a consequence of the fact that the modeling profiles reach the maximum at around 1250 K in correspondence with the maximum $C_6H_5C_2H$ values while the maximum experimental value is obtained at higher temperatures (around 1350 K). Different alternative pathways for the formation of phenanthrene were considered including the Diels-Alder mechanism between biphenyl and acetylene studied by Kislov et al. (R110 and R111, Ref. [131]). No improvement in the modeling results could be obtained.

6.3.2.4. Biphenyl and Acenaphthylene

The mechanisms of formation of biphenyl and acenaphthylene have been described in detail in the sections 6.3.1.2 and 6.3.1.4 since both are produced in large concentrations by the pyrolytic reactions of the phenyl radical. The two C12 compounds are present also when acetylene is added in the initial mixture although in lower amounts as shown in Figure 51. In particular, biphenyl formation is significantly reduced due to the fact that phenyl radicals are removed by the reaction with acetylene and thus are not available for self-recombination.

A similar consideration applies for acenaphthylene although in this case the reduction is not as substantial as expected due to the fact that the HACA mechanism provides a significant contribution to the production of the species (R92 + R149 + R81). The relevance of the HACA mechanism of course depends on the initial concentration of acetylene. Figure 52 shows the results of the rate of production analyses for acenaphthylene conducted at similar temperature and pressure conditions but for different initial acetylene mole fractions. While the results in Figure 52a indicate that in the system with an initial acetylene concentration of 236.3 ppm the HACA mechanism competes with the alternative formation pathways which were found to be significant in the study conducted without acetylene, an increase in the acetylene concentration enhances the relevance of the hydrogen-abstraction acetylene-addition pathway (Figure 52b). In the latter case the HACA mechanism clearly dominates the acenaphthylene formation processes.

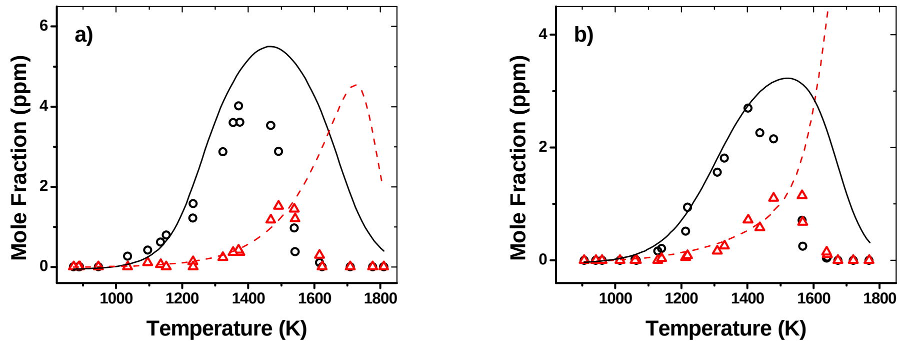

Figure 51. *○ Biphenyl exp., —— biphenyl sim.; △ acenaphthylene exp., – – acenaphthylene sim. a) [C_6H_5I]$_0$ = 58.1 ppm, [C_2H_2]$_0$ = 236.3 ppm, p ~ 50 atm; b) [C_6H_5I]$_0$ = 55.1 ppm, [C_2H_2]$_0$ = 511.3 ppm, p ~ 50 atm.*

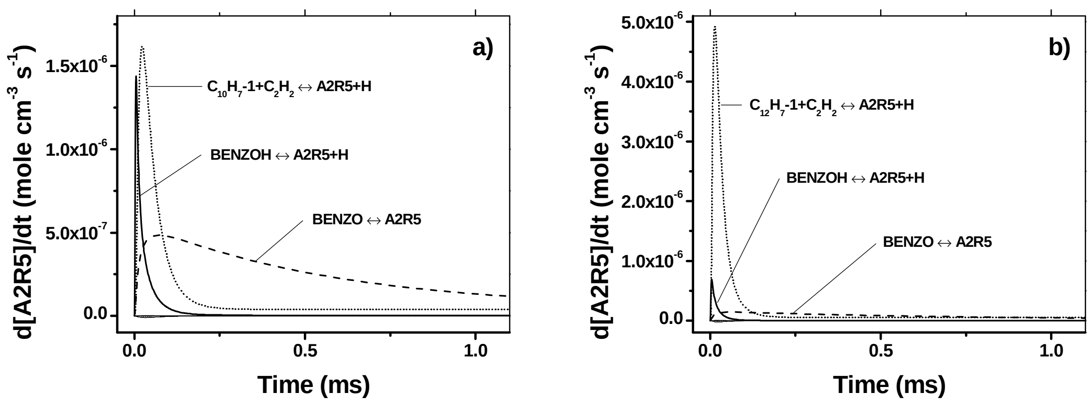

Figure 52. *Acenaphthylene, rate of production analysis. a) [C_6H_5I]$_0$ = 58.1 ppm, [C_2H_2]$_0$ = 236.3 ppm, T = 1491 K, p = 50.3 atm; b) [C_6H_5I]$_0$ = 55.1 ppm, [C_2H_2]$_0$ = 511.3 ppm, T = 1479, p = 51.1 atm.*

The modeling profiles are reported in Figure 51. The experimental profiles of biphenyl are well simulated by the model although overestimated at temperatures higher than 1400 K. The formation of acenaphthylene is also accurately predicted up to around 1500 K which confirms the accuracy of the reaction pathways considered in the present work. At higher temperatures the experimental profiles drop rapidly while the simulated mole fractions increase up to 1725 K before decaying. This is another confirmation of the fact that the model is not complete but should include additional pathways which lead for example to the formation of light compounds.

6.3.2.5. Naphthalene

The analysis performed on acenaphthylene indicates that the HACA mechanism has a major role in the formation of such a compound. As is well known, one of the elementary steps of the HACA mechanism involves the formation of the naphthyl radical through reaction R149. Naphthyl radical could react with hydrogen atoms and lead to the formation of the second-ring species (R151). Thus it is interesting to understand if for the system under consideration naphthalene is produced in substantial amounts and how the formation of naphthalene compares with the results of the phenyl pyrolysis study (Figure 38).

The experimental results clearly show that the pathways previously identified as leading to naphthalene do not play a significant role at the conditions implemented in the present investigation (Figure 53). The amounts of naphthalene produced are indeed comparable with the ones observed in Figure 38. On the other hand, the profiles in Figure 53 have a very peculiar trend typical of a bimodal formation process. While the second rise starting at around 1300 K is at least from a qualitative point of view captured by the model, the first increase which seems instantaneous with respect to the phenyl iodide decomposition can not be explained by the model which includes the previously identified formation steps. The most reasonable explanation for such instantaneous formation of naphthalene is related to the possible stabilization of the phenylvinyl radical from the reaction between phenyl and acetylene and the subsequent addition of a second acetylene molecule to form the second-ring species (Figure 3). Although this pathway is not expected to be very favorable it could account for the small naphthalene production observed at low temperatures. However, it is not currently included in the model since the reaction between phenyl radical and acetylene to form phenylacetylene and atomic hydrogen treated as a single-step process has a reaction rate constant experimentally determined in Ref. [20] and which was sufficient for modeling our phenylacetylene results.

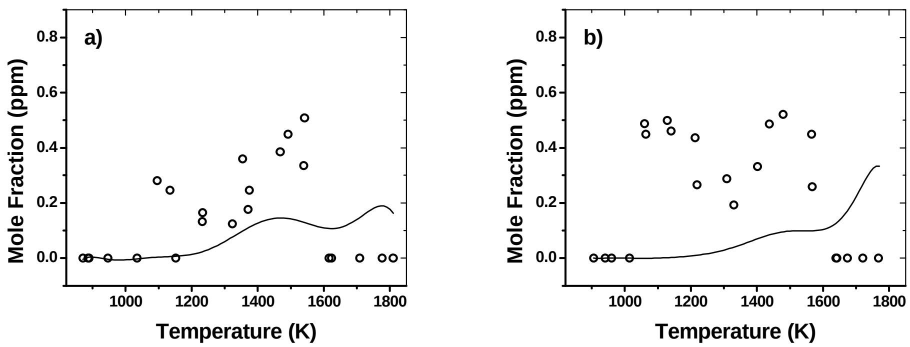

Figure 53. ***○ Naphthalene exp., —— naphthalene sim. a) [C_6H_5I]$_0$ = 58.1 ppm, [C_2H_2]$_0$ = 236.3 ppm, p ~ 50 atm; b) [C_6H_5I]$_0$ = 55.1 ppm, [C_2H_2]$_0$ = 511.3 ppm, p ~ 50 atm.***

Before concluding the analysis on naphthalene, it is worth mentioning that the predicted formation of the second-ring compound around 1400 K is mainly due to the mechanism proposed in Ref. [118] involving the reaction between o-benzyne and benzene. The HACA mechanism constitutes only a minor pathway since the naphthyl radicals produced are consumed quickly by reaction with acetylene to form acenaphthylene and thus are not available for recombination with H atoms to form naphthalene.

6.3.2.6. Polyacetylenes

Similarly to what we observed in the study on the phenyl pyrolysis, in the high temperature range of the present investigation the polyacetylenes become the main products while the PAH compounds are consumed. Figure 54 shows the comparison between the diacetylene and the triacetylene profiles for experiments conducted at nominal pressure of 25 atm with and without acetylene in the initial mixture. Clearly the presence of acetylene enhances the formation of the polyacetylenes supporting the hypothesis that the polymerization process plays a key role at high temperatures. In addition we can also notice that the profiles in Figure 54 start increasing all in the same temperature range (around 1400–1450 K) which suggests that the mechanistic pathways are common for the two cases presented.

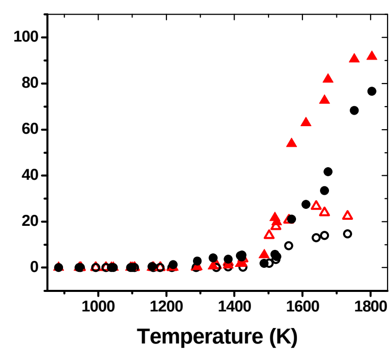

Figure 54. Experiments, p ~ 25 atm.* ○ *triacetylene, [C_6H_5I]$_0$ = 54.2 ppm;* △ *diacetylene, [C_6H_5I]$_0$ = 54.2 ppm;* ● *triacetylene, [C_6H_5I]$_0$ = 52.9 ppm, [C_2H_2]$_0$ = 526.3 ppm;* ▲ *diacetylene, [C_6H_5I]$_0$ = 52.9 ppm, [C_2H_2]$_0$ = 526.3 ppm.

The experimental results as well as the modeling profiles for both diacetylene and triacetylene are shown in Figure 55. The most evident discrepancy consists in the substantial underestimation of the profiles for triacetylene. As also pointed out in relation to the results presented in Figure 43, the polymerization process responsible for the formation of triacetylene is clearly not described accurately by the model. On the other hand, we can notice that the triacetylene profiles show an early small increase between 1200 and 1400 K where the concentration of diacetylene is nearly zero. This could suggest that other pathways to the formation of triacetylene exist which do not involve the intermediate formation of diacetylene. Further studies are required to improve the accuracy of the mechanisms involved in the formation of diacetylene and triacetylene at high temperatures.

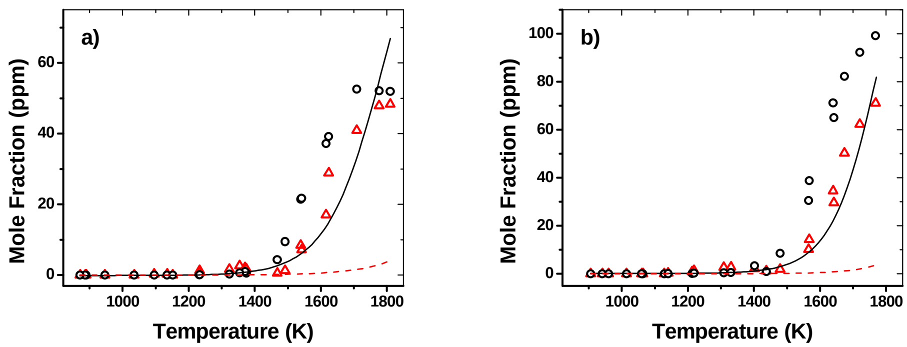

Figure 55. *○ Diacetylene exp., —— diacetylene sim.; Δ triacetylene exp., – – triacetylene sim. a)* $[C_6H_5I]_0$ *= 58.1 ppm,* $[C_2H_2]_0$ *= 236.3 ppm, p ~ 50 atm; b)* $[C_6H_5I]_0$ *= 55.1 ppm,* $[C_2H_2]_0$ *= 511.3 ppm, p ~ 50 atm.*

6.3.2.7. Effects of Acetone Impurity

Although the purity of the acetylene as stated by the supplier companies is 99.6% the relative level of acetone, used as a stabilizer for acetylene, can vary typically in the range between 1% and 2% when acetylene is withdrawn from the tank. Several studies have indicated that the acetone impurity does not affect significantly the experimental results on acetylene pyrolysis and oxidation[132] especially when small concentrations of acetylene are utilized. When acetylene is part of a multi-component reactant mixture for studies on acetylene-addition reactions such as in the present investigation the consequences of the acetone impurity are expected to be even less relevant since the chemistry is driven by the reactions with the most abundance among the components, i.e. acetylene. For this reason, in this kind of studies acetylene is usually not purified. However with the use of a Balston filter, small mole fractions of acetone were detected in the reactant mixtures and analyzed together with the relative products to estimate the actual magnitude of the uncertainty caused by the presence of such impurity.

First, a sub-mechanism for acetone chemistry was added to the chemical kinetic model. The sub-mechanism is based on the chemical kinetic mechanism used by Colket et al.[133] to accurately simulate experiments on acetylene pyrolysis in the presence of trace amounts of acetone. The reaction rate constants for the decomposition of acetone were updated based on the mechanism proposed by Dooley et al.[134] for the simulation of n-decane/iso-octane/toluene surrogate mixtures. The only modification in the rate constants is related to the H-abstraction reaction between acetone and H for which the estimated pre-exponential factor was multiplied by a factor of two in order to obtain a better agreement between experiments and simulations. Additional reactions relevant for the acetone chemistry include the reaction between acetone and phenyl radical studied by Choi et al.[135] and the reaction between CH_3 and HI to form CH_4 and I. The rate constant for the latter reaction was estimated based on the low-temperature work by Seetula et al.[136]

The experimental and modeling results for acetone and the major related products, i.e. methane and toluene, are presented in Figure 56 for the sets conducted at 50 atm. The decay of acetone and the formation of the intermediates are quite well reproduced by the model although at high temperatures methane mole fractions are overestimated. For the purpose of the present study no additional improvements are necessary since the model can already provide a good estimate of how the major stable products of the phenyl + acetylene reaction are affected by the acetone impurity. The comparison between the simulations conducted without and with acetone in the initial reactant mixture is shown in Figure 57 for the compounds which are mostly affected by the impurity. Figure 57a, b, and c contain the profiles respectively for single-ring, C12, and C14 compounds for the experimental set conducted with an initial acetylene mole fraction equal to 236.3 ppm. The results clearly indicate that in this case the acetone impurity, around 1.5 ppm, does not significantly influence the formation of the intermediate compounds. The maximum error is around 2–4%. The error in the profiles of the species not shown which include phenyl iodide, acetylene, and the polyacetylenes is even smaller.

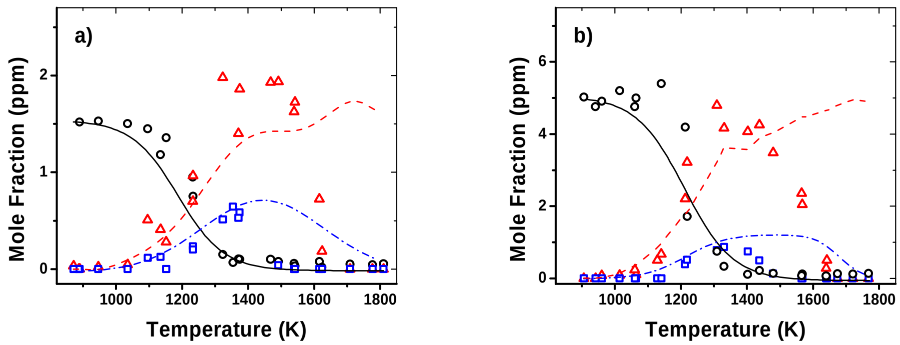

Figure 56. *○ Acetone exp., —— acetone sim.; △ methane exp., – – methane sim.; □ toluene exp., – · – toluene sim. a) [C_6H_5I]$_0$ = 58.1 ppm, [C_2H_2]$_0$ = 236.3 ppm, p ~ 50 atm; b) [C_6H_5I]$_0$ = 55.1 ppm, [C_2H_2]$_0$ = 511.3 ppm, p ~ 50 atm.*

The analyses performed on the experimental sets conducted with around 500 ppm initial acetylene mole fraction indicate the presence of larger relative amounts of acetone, around 1% of the acetylene in the mixture. As shown in Figure 57d, e, and f the effects of the acetone impurity in the profiles are larger than in the previous case but still below the uncertainty in the experimental measurements. The profiles for phenyl iodide, acetylene, and the polyacetylenes are almost unaltered by the presence of acetone. Thus we can conclude that the acetone impurity does not influence significantly the experimental profiles for the intermediate measured in the present work especially in relation to the experiments conducted with smaller amounts of initial acetylene in the reactant mixture.

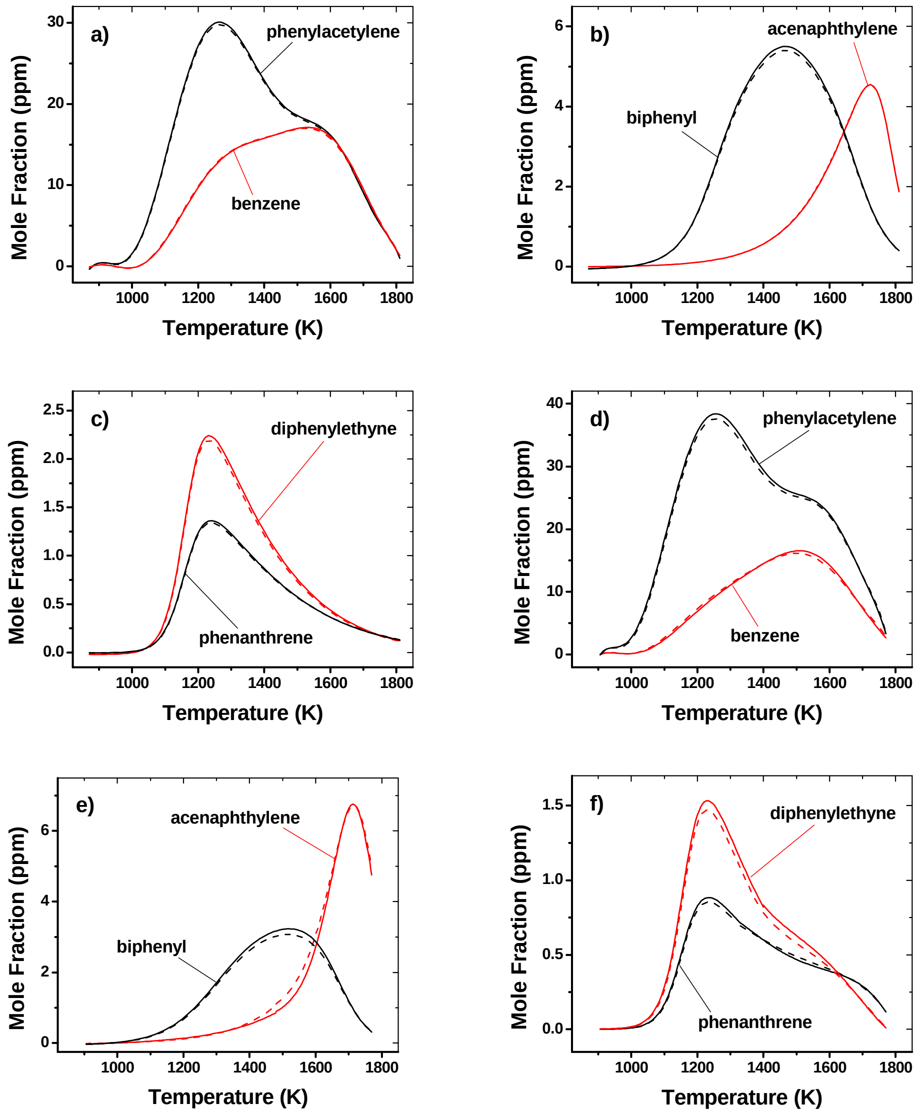

Figure 57. Numerical simulations. a), b), and c) solid lines: $[C_6H_5I]_0$ = 58.1 ppm, $[C_2H_2]_0$ = 236.3 ppm, p ~ 50 atm; dashed lines: $[C_6H_5I]_0$ = 58.1 ppm, $[C_2H_2]_0$ = 236.3 ppm, $[CH_3COCH_3]_0$ = 1.5 ppm, p ~ 50 atm. d), e), and f) solid lines: $[C_6H_5I]_0$ = 55.1 ppm, $[C_2H_2]_0$ = 511.3 ppm, p ~ 50 atm; dashed lines: $[C_6H_5I]_0$ = 55.1 ppm, $[C_2H_2]_0$ = 511.3 ppm, $[CH_3COCH_3]_0$ = 5.0 ppm, p ~ 50 atm.

6.3.2.8. HACA, Addition between Single-Ring Aromatics, Benzyne Chemistry, and Polymerization

Summarizing the main results on the experimental and modeling study of the phenyl + acetylene reaction we can state that the formation of multi-ring compounds is influenced by two main mechanisms, the HACA mechanism and the reaction between single-ring aromatics. In particular, the C14 compounds, i.e. phenanthrene and diphenylethyne, derive mainly from the reaction between phenyl radical and phenylacetylene, although especially at higher temperatures the contribution of the o-$C_{12}H_9$ + C_2H_2 for the formation of phenanthrene becomes important. Once again we need to remember that the o-benzyne radical plays a key role in the formation of o-$C_{12}H_9$ as discussed in the first part of the paper.

With regard to the formation of acenaphthylene the discussion is slightly more complex since the mechanisms involved differ based on the relative concentrations of the phenyl radicals and the acetylene in the system. For low acetylene mole fractions the HACA mechanism is one of the relevant pathways to acenaphthylene although not the dominant. In this case the isomerization of the o-biphenyl radical is still the most important pathway as in the study on the phenyl pyrolysis. Consequently o-benzyne becomes a key intermediate in the acenaphthylene formation. When acetylene concentration is increased the HACA mechanism is definitely the main source for acenaphthylene.

As in the phenyl pyrolysis study, above a certain temperature the polymerization process becomes dominant and the PAHs concentrations drop. The temperature range of maximum PAHs production is around 1300–1400 K after which the experimental profiles for diacetylene and triacetylene rapidly rise. The model does not accurately simulate the chemistry for the polymerization mechanism relevant to high temperature conditions indicating that additional studies are required to clarify this aspect of the problem. In this case the experimental results suggest that new pathways for the formation of triacetylene could be possible.

7. FORMATION OF NAPHTHALENE FROM THE RADICAL/π-BOND ADDITION BETWEEN SINGLE-RING AROMATIC HYDROCARBONS

The material presented in this chapter is reprinted with permission from Comandini, A.; Brezinsky, K. *Journal of Physical Chemistry A* 115, 5547–5559, 2011. Copyright 2011 American Chemical Society. It was felt by the author of this thesis (A.C.) that the way this material was presented in the journal article could not be improved by simple revision of the manuscript. Thus, the following sections mostly reproduce the material already discussed in the article.

The experimental results on the phenyl pyrolysis reported in section 6.3.1.5 confirm that the conventional mechanisms for the formation of large polycyclic aromatic hydrocarbons[9,10,11] are not sufficient to explain the experimentally observed formation of the multi-ring fused compounds such as naphthalene. We can clearly state that although formation of benzene is fairly well characterized[9,10,11], the pathways leading to the second-ring species are still not well understood.

The literature studies on naphthalene formation mainly focus on the addition of single-ring aromatics with small aliphatics. Examples of such addition pathways include the HACA mechanism (hydrogen abstraction acetylene addition)[15,110], the addition of vinylacetylene and 1,3-butadiene to phenyl radical[129,137,138], the reaction of 1,3-butadien-1-yl with benzene[138,139], and the addition of propargyl radical to phenyl and methylphenyl radicals[11]. Alternative mechanisms include the reaction between cyclopentadienyl radicals[140-142] and the addition between o-benzyne and benzene.

Benzyne radicals are members of a group of very reactive compounds known as arynes. In particular o-benzyne can undergo a variety of reactions involving the addition of linear or cyclic compounds to the triple bond of its structure. The review on the addition reactions of o-benzyne with heterocyclic compounds provided by Bryce and Vernon[143] contains an entire section focused on the reactions between o-benzyne and the six-membered ring azines, a class of organic compounds characterized by a ring structure like that of benzene but with one or more carbon atoms replaced by nitrogen atoms. Of even greater relevance for soot formation are the experimental studies of the benzene (deuterated and not) + o-benzyne reaction. This reaction was investigated for the first time by Miller and Stiles[144] which studied the pyrolysis of $C6H4Na^{+}COO^{-}$ in benzene at 45 ºC using gas chromatographic techniques as part of their pioneering experimental work on arynes compounds. In subsequent experimental investigations Fields and Meyerson[123,124,145] pyrolyzed phthalic anhydride ($C_6H_4(CO)_2O$) in benzene at 690 ºC and identified three main products of the reaction, i.e. biphenyl, naphthalene, and acetylene, along with small amounts of biphenylene and triphenylene. Friedman and Lindow[121] reexamined at similar conditions the reaction between o-benzyne (from phthalic anhydride precursor) and benzene (deuterated and not) and experimentally identified the additional products acenaphthylene and acenaphthene. The PAH compounds formed during the reaction consisted of naphthalene (80%), biphenyl (9%), acenaphthylene (6%) and acenaphthene (5%) using infrared, ultraviolet, and mass spectra. Based on the relative abundance of the deuterated isomers, Friedman and Lindow hypothesized mechanistic pathways for the formation of each species (Figure 58). In particular naphthalene, by far the most abundant among the products, is expected to derive mainly from the insertion reaction of o-benzyne with benzene (1,4 cycloaddition) followed by thermal fragmentation of the intermediate compound benzobicyclo[2,2,2]octatriene. If we define the radical/π-bond addition as the addition of a radical site of a reactant species to any of the CC π-bonds of the other reactant, the experimental study from Friedman and Lindow clearly addressed the importance of such radical/π-bond addition (insertion reaction) in the formation of PAH compounds relevant to soot formation.

A different but related reaction system which proceeds through radical/π-bond addition is the benzene + phenyl reaction. This reaction was studied in the past both theoretically and experimentally as an important pathway for the formation of biphenyl, an intermediate species for PAH growth. The rate constants for both the forward and the reverse processes were measured using a combination of experimental techniques including the flash photolysis technique[146], the low-pressure Knudsen cell flow reactor-mass spectrometric technique[18], the single-pulse shock tube technique[147], and the cavity ringdown kinetic spectrometry (CRDS) technique[106]. In addition to the CRDS experiments, Park et al.[106] carried out a theoretical study on the radical/π-bond C_6H_5 + C_6H_6 addition reaction using DFT methods and RRKM calculations aimed to model the available experimental data on biphenyl formation. No alternative reaction pathways were investigated.

Besides the reactions between benzene and single-ring phenyl and o-benzyne radicals, the recent theoretical results by Tranter et al.[26] indicate that the self-reaction between phenyl radicals can proceed through radical/π-bond addition. Phenyl radicals play a relevant role in combustion processes because of their ability to recombine with small aliphatic species to form naphthalene. Furthermore the radical-radical recombination between phenyl radicals leads to the formation of biphenyl as experimentally studied by Park and Lin[25] using the laser photolysis/mass spectrometry technique and by Heckmann et al.[20] in shock-tube experiments. Both studies focused on the direct radical-radical recombination of the reactant species to form biphenyl.

As also mentioned in section 1.2, Tranter et al.[26] revisited the self-reaction of phenyl radicals based on low-pressure shock-tube experiments and high-level theoretical calculations. The study addressed for the first time the relevance of the abstraction channel leading to the formation of benzene and benzyne radicals. Above 1400 K the abstraction channel becomes dominant, while at low temperatures the radical-radical σ-recombination pathway to biphenyl prevailed. Besides the recombination and abstraction channels, the radical/π-bond addition reaction between phenyl radicals was partially investigated from a theoretical point of view as a minor path compared to two dominant channels described above. Due to the low stability of the complexes involved as well as the low-pressure conditions of the study, the authors hypothesized that most of the flux entering the radical/π-bond addition energy surface redissociates back to the reactants, while the remaining part yields biphenyl or biphenyl radical + H. Nevertheless the authors did not conduct a detailed theoretical study on the potential energy surface to confirm such hypothesis or define different pathways, relevant to higher pressures, for the radical/π-bond addition reaction.

The idea of a pivotal role of the π-bonds in combustion processes acquires even more relevance in consideration of the recent developments in the pioneering research on particle nucleation and growth. In his review paper presented at the 33rd International Symposium on Combustion[148], Wang proposed an innovative explanation for the unexpected experimentally observed features of nascent soot particles in premixed flames. These features include the presence of an aromatic core composed of stacked PAH compounds surrounded by an aliphatic shell[149]. Wang proposed that such a core-shell structure derives from π-electron interactions between aromatic π radicals and closed-shell aromatic compounds. Although the π-π bonding concept proposed by Wang certainly requires further validations, it confirms the scientific interest in the characterization of the effective role of the π-bonds in relation to unexplored chemical mechanisms relevant to soot formation.

Inspired by the numerous theoretical and experimental works described above, the present investigation focuses on the *theoretical* examination of radical/π-bond addition reactions between aromatic compounds relevant to the formation of two-ring fused species. In particular, the addition between o-benzyne and benzene has been fully investigated for the first time from a theoretical point of view in order to test the pathways that Friedman and Lindow inferred from their experimental work. The theoretical study has been extended to the systems involving the radical/π-bond addition between benzene and phenyl radical and between phenyl radicals. Although these reactions are expected to lead mainly to the formation of biphenyl and biphenyl radical as described in the theoretical works by Park et al.[106] and by Tranter et al.[26], the unexplored possibility of additional pathways leading to the formation of fused PAH compounds, never before addressed, have been tested in the present investigation.

7.1. Computational methodology

All geometry optimizations and vibrational analyses were performed using the B3LYP method[67,68] with unrestricted open shell wave functions and Pople's valence triple-ζ basis set including diffuse and polarization functions (6-311+G(d,p))[96]. Structure optimizations of the local minima and saddle points were obtained using respectively the Berny geometry optimization algorithm[150] and the combined synchronous transit-guided quasi-Newton (STQN) method[151] as implemented by Gaussian 03 program package[84].

The energetics of the optimized structures were refined by single point energy calculations performed with coupled-cluster method (uCCSD(T))[62] with Dunning's correlation consistent polarized double-ζ basis set (cc-pVDZ)[63]. Frozen-core (FC) assumption was also used. All of the calculations were carried out with the Gaussian 03 program package[84].

The results of the calculations are reported in Appendix D (Cartesian Coordinates, electronic energies, zero-point vibrational energies, and imaginary vibrational frequencies).

Conventional transition state theory (TST) was used to evaluate the high-pressure limit reaction rate constants from the quantum chemical calculations. The transmission coefficient $\kappa(T)$ accounting for tunneling effects was estimated as[82]

$$\kappa(T) = 1 - \frac{1}{24} \cdot \left(\frac{h\upsilon^{\ddagger}}{k_B T} \right)^2 \cdot \left(1 + \frac{RT}{E_0} \right)$$

where R is the universal gas constant and $\upsilon^{\ddagger}$ the imaginary frequency associated to the motion along the reaction coordinate.

7.2. Benzene + o-benzyne

The experimental work performed by Friedman and Lindow[121] on the relatively low-temperature pyrolysis of o-benzyne in benzene and benzene-d6 indicates that the products of the addition reaction consist mainly of naphthalene-d4 (80%). Considering the distribution of the remaining product species as well as the products of the pyrolysis of benzobicyclo[2,2,2]octatriene and benzocyclooctatetraene[121] (shown in Figure 58), we hypothesize that at least 70-75% of the C_6H_6 + o-C_6H_4 reaction proceeds through the benzobicyclo[2,2,2]octatriene intermediate (radical/π-bond insertion) to finally form naphthalene through fragmentation of the intermediate. On the other hand we can also hypothesize that the reaction will mainly occur on the singlet potential energy surface since the singlet spin-state o-benzyne molecule is more stable than the corresponding triplet configuration. Thus the radical/π-bond addition reaction between benzene and singlet o-benzyne could be the dominant pathway with naphthalene as major product. In order to test these hypotheses for the formation of the experimentally observed naphthalene, a series of theoretical calculations were initiated.

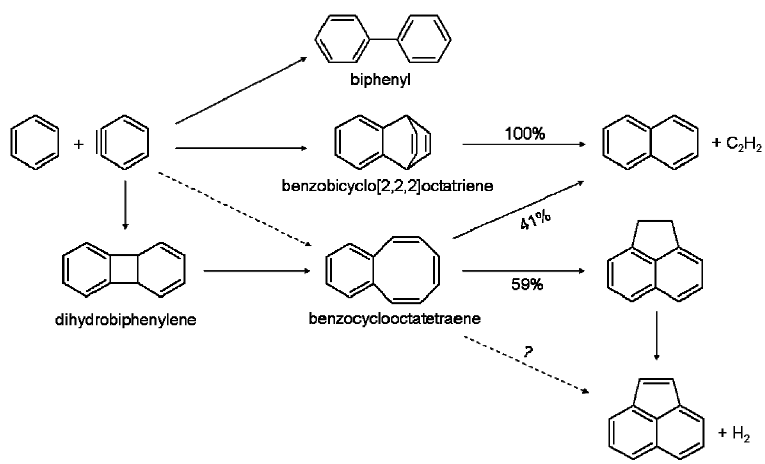

Figure 58. Benzene + o-benzyne reaction, based on Friedman and Lindow[121].

Figure 59 shows the results of the calculations performed on the potential energy surface for the singlet radical/π-bond addition reaction. The system proceeds along an unique channel leading to the formation of benzobicyclo[2,2,2]octatriene ($S1^s$) through an energy barrier of 6.8 kcal/mol (1,4 cycloaddition). Benzobicyclo[2,2,2]octatriene can easily dissociate into naphthalene and acetylene through TS2. The barrier for such dissociation process is 13.6 kcal/mol lower than the barrier for redissociation of $S1^s$ back to the reactants.

As already mentioned above, the experimental work on the reaction between benzene and o-benzyne indicates that the reaction leads not only to the formation of naphthalene but possibly also to the formation of other different PAH compounds including biphenyl, acenaphthylene and acenaphthene (Figure 58). Beno et al.[152] studied the initial step of the o-benzyne + benzene reaction in relation to the interaction between an o-benzyne molecule located inside a large host molecular structure and the host molecule. The authors performed calculations at the B3LYP/6-31G(d) level of theory and reported the presence of two transition states, the one corresponding to TS1 (Figure 59) and an additional transition state TS** as reported in Figure 60. TS** leads to the formation of a stable biphenyl-like compound (S** in Figure 60), which could isomerize to form biphenyl and/or benzocyclooctatetraene.

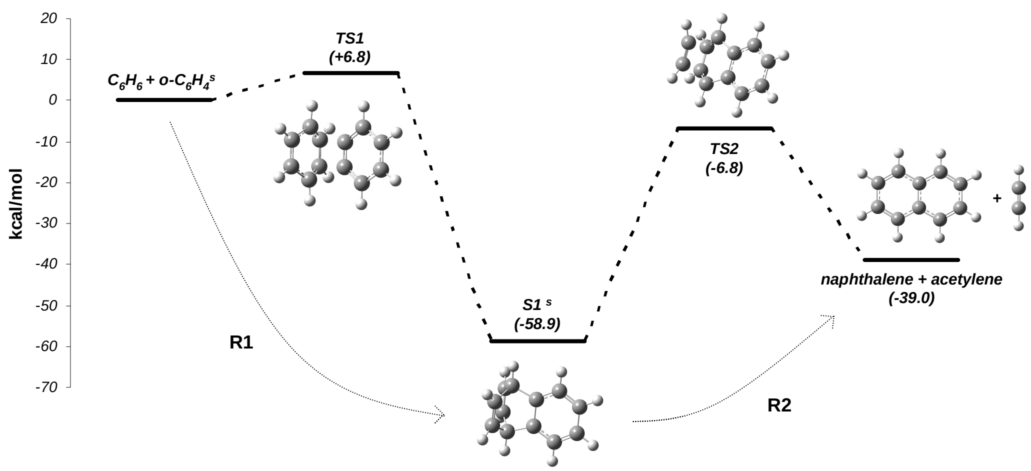

Figure 59. Potential energy surface for benzene + singlet o-benzyne radical/π-bond 1,4 cycloaddition. uB3LYP/6-311+G(d,p) optimized structures. uCCSD(T)/cc-pVDZ relative energies in kcal/mol, including ZPVE.

We were able to reproduce the results by Beno et al.[152] using the same basis set they used. The results are reported in Figure 60. As discussed by the authors, the calculated energy difference between the two transition states is small, around 2 kcal/mol. Nevertheless the biphenyl-like complex S** is bound by only 10.9 kcal/mol with respect to TS** and a consistent part of the flux entering the channel will redissociate back to the reactants. Surprisingly we could not confirm the presence of TS** using our 6-311+G(d,p) basis set. Any attempt to identify such saddle point did not converge or converged but to a transition state structure similar to TS6 in Figure 63 not relevant to the specific case. At this point we can not draw a definitive conclusion on the presence and the relevance of the stepwise o-benzyne + benzene channel shown in Figure 60. If the stepwise channel exists as indicated by Beno et al.[152], we expect this channel to account for maximum 25-30% of the total reaction between o-benzyne and benzene.

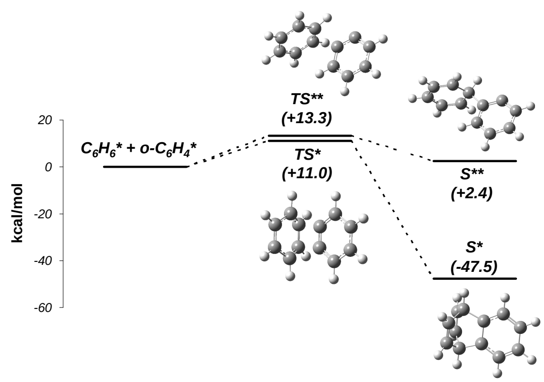

Figure 60. Benzene + singlet o-benzyne radical/π-bond addition. uB3LYP/6-31G(d) optimized structures and energies, including ZPVE.

Another important element that we need to take into consideration is the fact that the experimental work by Friedman and Lindow[121] is subject to uncertainties due to the nature of the pyrolytic study performed. As hypothesized by the authors, the observed C12 compounds could not be the result of chemical processes but they could possibly derive from catalytic mechanisms occurring on the surface of the fused quartz chips used in the experiments. This hypothesis is supported by a study conducted by Friedman[153] on the pyrolysis of o-benzyne (from benzenediazonium-2-carboxylate, $C_6H_4N_2^+COO^-$) in benzene at 45 ºC in the presence of silver ions. The PAH products formed in the experiments conducted without silver ions in solution were composed almost entirely of naphthalene (88%) and biphenylene (11%). Increasing amounts of silver ions concentration were related to increased yields of biphenyl and benzocyclooctatetraene. A similar catalytic mechanism could be responsible for the formation of these products even at the higher temperatures of the study by Friedman and Lindow[121]. This means that the relative importance of the stepwise o-benzyne + benzene channel shown in Figure 60 which through isomerization of S** leads to biphenyl and benzocyclooctatetraene could be even lower than hypothesized at the beginning of the paragraph.

Calculations were also performed to try to identify a possible concerted 1,2 cycloaddition pathway in alternative to the 1,4 cycloaddition shown in Figure 59. No corresponding transition state could be identified. Depending on the initial guess for the transition state structure, the calculations either could not converge or converged to the 1,4 cycloaddition TS1 transition state presented in Figure 59.

At this point it is clear that both the experimental results by Friedman and Lindow[121] and the theoretical calculations indicate the presence of a reaction channel which leads to the formation of naphthalene and acetylene as shown in Figure 59. Due to the possibly important role of such route, the corresponding reaction rate constants have been estimated.

Species	T1 Diagnostic
C_6H_6	0.010
$C_6H_4^S$	0.012
TS1	0.011
$S1^S$	0.011
TS2	0.011
naphthalene	0.010
acetylene	0.012

Table 8. T_1 diagnostic for the calculations in Figure 59.

First the T_1 diagnostic[154] was implemented to test the level of accuracy of the calculations presented in Figure 59. The results, reported in Table 8, are all below the 0.02 threshold for closed shell species which indicates that the energy calculations do not suffer from a strong multi-reference character and provide reliable energy barriers for the elementary reactions. Thus high-pressure limit rate constants for C_6H_6 + o-$C_6H_4^s \rightarrow S1^s$ (R1) and $S1^s \rightarrow C_{10}H_8 + C_2H_2$ (R2) have been estimated based on the calculated properties of the species involved. The fitted modified Arrhenius expressions for R1 and R2 over a temperature range between 1000 K and 2000 K are

$$k_{R_1}(T) = 5.809\times10^{3}T^{2.526}\exp(-2979.0/T)\ [\mathrm{cm^3\ mol^{-1}\ s^{-1}}]$$

$$k_{R_2}(T) = 7.458\times10^{14}T^{0.0956}\exp(-27584.8/T)\ [\mathrm{s^{-1}}]$$

The reaction rate constants calculated from TST for R1 and R2 are reported in Table 9. The error associated with these calculations is mainly due to the uncertainty in the reaction barriers. In particular the barrier for the entrance reaction R1 is expected to be over-estimated by the theoretical methods implemented in the present work, as also reported for the corresponding reactions for the benzene + phenyl and phenyl + phenyl systems. As described in the corresponding sections, the estimated entrance barrier for $C_6H_6 + C_6H_5$ is 2.4 kcal/mol higher than the optimal experimental value, while for the $C_6H_5 + C_6H_5$ reaction the barrier is around 4 kcal/mol higher than the value obtained from higher-level energy calculations. A 3 kcal/mol decrement in the R1 barrier would cause an increase of the rate constant value of around 2.1 times at 2000 K, 2.7 times at 1500 K, and 4.5 times at 1000 K.

We discussed in sections 6.3.1.5 and 6.3.2.5 how the reaction between benzene and o-benzyne plays an important role in the formation of naphthalene at the high-pressure conditions of the pyrolytic studies performed on the phenyl pyrolysis and the phenyl + acetylene reactions. In practical applications, characterized by high-pressure oxidative environments, the relevance of the singlet channel described in Figure 59 depends mainly on the concentration of o-benzyne in the reacting system, since benzene is usually present in large amounts. o-Benzyne radicals derive mainly from the dehydrogenization of phenyl radicals. The process involves an energy barrier of around 78 kcal/mol[155] , considerably lower than the overall energy necessary for the fragmentation of C_6H_5 into n-C_4H_3 + C_2H_2[126,156]. Thus o-benzyne is the main product of the thermal decomposition of the phenyl radical. At relatively high temperatures we expect high concentrations of phenyl radicals produced by dehydrogenization of benzene, thus the concentration of o-benzyne radicals should be substantial and the singlet channel of the radical/π-bond addition reaction with benzene could play a significant role in the formation of naphthalene. On the other hand, the proposed pathway may not play a major role in combustion systems because it will be in competition with different other channels involving the consumption of o-benzyne. In particular the HACA mechanism could represent the main source of o-benzyne consumption through double addition of acetylene leading to the formation of naphthalene. Moreover o-benzyne can dissociate into acetylene and diacetylene as investigated both experimentally and theoretically[102,126,157].

	Temperature (K)					
reaction	1000	1100	1200	1300	1400	1500
R1	1.12×10^{10}	1.86×10^{10}	2.90×10^{10}	4.30×10^{10}	6.10×10^{10}	8.37×10^{10}
R2	$1.54E \times 10^{03}$	1.89×10^{04}	1.53×10^{05}	9.03×10^{05}	4.14×10^{06}	1.55×10^{07}
	Temperature (K)					
reaction	1600	1700	1800	1900	2000	
R1	1.12×10^{11}	1.45×10^{11}	1.85×10^{11}	2.31×10^{11}	2.84×10^{11}	
R2	4.91×10^{07}	1.36×10^{08}	3.37×10^{08}	7.60×10^{08}	1.58×10^{09}	

Table 9. Calculated TST rate constants for R1 in cm^3 mol^{-1} s^{-1} and for R2 in s^{-1}.

The present study could be extended to systems involving different benzyne-like species. For example, in a recent paper García-Cruz et al.[158] performed high-level theoretical calculations

(CASSCF and CASPT2) on the pyrene-like structures and showed that the dehydrogenization of pyrene to form the corresponding diradical species occurs with a lower barrier compared to the dehydrogenization of benzene to o-benzyne. Similarly to the o-benzyne radical, 1,2-didehydropyrene and 4,5-didehydropyrene (Figure 61) could react with benzene to form a 5-ring species through benzene insertion and subsequent fragmentation. Thus the radical/π-bond addition could contribute to the growth in the number of aromatic rings.

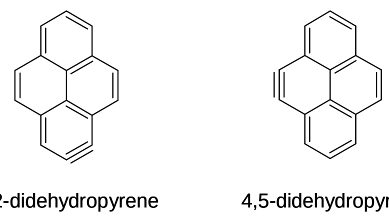

Figure 61. Schematic representation of the molecular structures of 1,2- and 4,5-didehydropyrene.

The results reported in the previous paragraphs indicate that the benzene + singlet o-benzyne proceeds mainly through 1,4 cycloaddition. Although the singlet o-benzyne radical is 31.9 kcal/mol more stable than the corresponding triplet configuration based on the CCSD(T) calculations, the triplet surface could be accessible, especially at high temperatures. Thus the possibility for additional channels through the benzene + triplet o-benzyne reaction was investigated.

The reaction between benzene and triplet o-benzyne proceeds through several channels (Figure 62 and Figure 63). The first channel involves the hydrogen abstraction from the benzene ring to form two phenyl radicals. The calculated barrier through TS3 is 8.2 kcal/mol.

The second channel proceeds through the formation of a biphenyl-like species (S2) with an entrance barrier of 2.9 kcal/mol. The radical site can abstract the H atom from the second ring forming biphenyl. Nevertheless the barrier for such abstraction reaction is 11.6 kcal/mol higher than the barrier for redissociation back to the reactants, thus this channel is energetically unfavorable. On the other hand S2 can easily isomerize and form S3 through torsional motion around the C-C bond between the two rings. S3 is a biphenyl-like species characterized by several low frequency vibrational modes including the ones corresponding to the relative torsional motion between the two rings and to the bending motion of one ring towards the other. Along the torsional motion, the system can undergo isomerization to form dihydrobiphenylene (S4), reported as the intermediate species between reactants and benzocyclooctatetraene in Figure 58. Once formed, benzocyclooctatetraene can isomerize and lead to the formation of acenaphthylene and acenaphthene as hypothesized by Friedman and Lindow[121] based on their experimental work (Figure 58). Friedman and Lindow also reported the presence of biphenyl-d5 as a product of the reaction between o-benzyne and benzene-d6. The formation of biphenyl-d5 could be explained considering the pathway from S2 and S3 to $C_{12}H_9$ + H. In this case the energy barrier for the dissociation of S2 is 26.9 kcal/mol, while the corresponding barrier for S3 is 26.2 kcal/mol, 5.2 kcal/mol higher than the barrier for the formation of dihydrobiphenylene.

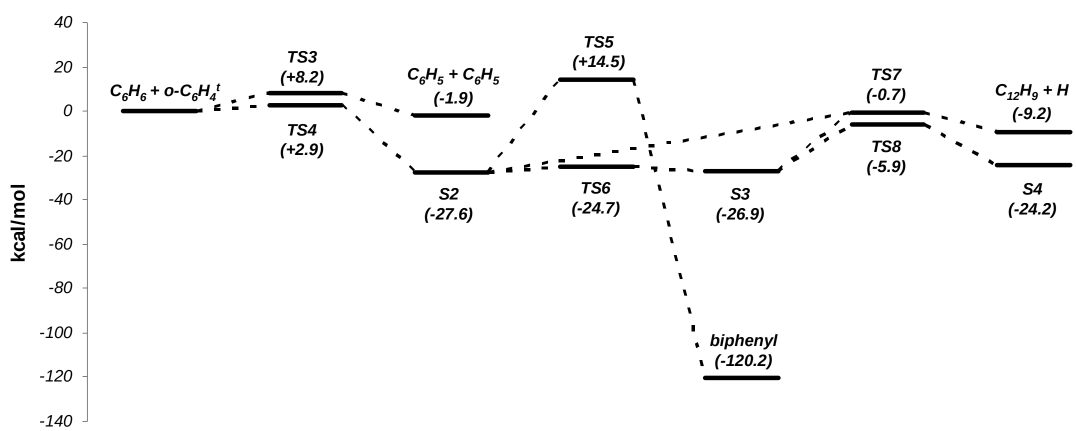

Figure 62. Potential energy surface for benzene + triplet o-benzyne radical/π-bond addition. uCCSD(T)/cc-pVDZ relative energies in kcal/mol, including ZPVE.

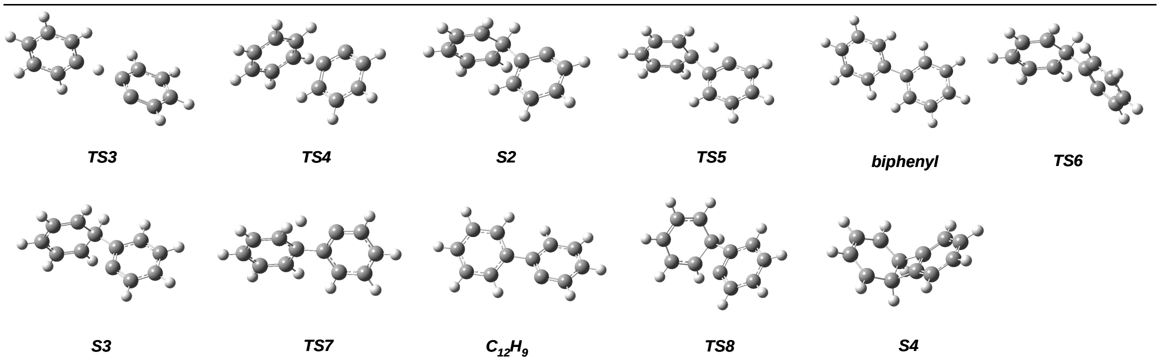

Figure 63. Species on the potential energy surface for benzene + triplet o-benzyne radical/π-bond addition. uB3LYP/6-311+G(d,p) optimized structures.

The present study on the triplet potential energy surface provides plausible pathways for the experimentally observed formation of biphenyl, acenaphthylene, and acenaphthene as products of the o-benzyne + benzene reaction. On the other hand a Boltzmann distribution of triplet states with excitation energy of 31.9 kcal/mol as calculated in the present work would lead to a very small population of triplet o-benzynes especially at the temperatures implemented in the experimental work by Friedman and Lindow[121] (690 ºC). Unless a transient nonequilibrium population of triplet state o-benzynes is present, the channels presented in Figure 62 cannot account for the formation of the C12 compounds observed experimentally.

7.3. Benzene + phenyl

The radical/π-bond addition reaction between benzene and phenyl radical (Figure 64 and Figure 65) involves the doublet electronic state. The entrance barrier has been calculated as 5.1 kcal/mol and the biphenyl-like species S5 is bound by 31.0 kcal/mol. The optimized structures for TS9 and S5 are similar to those obtained by Park et al.[106] since similar optimization methods were used. On the other hand the relative energy levels of both the transition state and the $C_{12}H_{11}$ complex are different due to the CCSD(T) calculations implemented in the present work. In particular, the relative energy of TS9 lies between the value calculated by Park et al.[106] (7.93 kcal/mol) and the optimal value derived from the experimental work (2.70 kcal/mol). Thus the CCSD(T) calculations improve the accuracy of the entrance barrier, although the calculated barrier is still 2.4 kcal/mol higher than the optimal value. The higher-level calculations also provide a better estimate of the relative energy of the $C_{12}H_{11}$ complex.

We will now focus our attention on the possible reaction pathways to fused ring structures. Two possible channels lead to the formation of bicyclo-like species and both are associated with the low-frequency bending vibrational motion of the biphenyl-like complex S5. The first channel involves both a C-H fission and a hydrogen transfer process to form benzobicyclo[2,2,2]octatriene ($S1^s$). Since the relative energy of the corresponding transition state TS10 is 62.7 kcal/mol, such a path is energetically unfavorable. The second pathway proceeds through ring closure to form a bicyclo-like species (S6) which can subsequently undergo a C-H dissociation process to form $S1^s$. Once again the energies of the saddle points TS11 and TS12 are higher than the redissociation barrier by 12.0 kcal/mol and 25.1 kcal/mol respectively. Thus the only channel energetically available to the system is the path leading to the formation of biphenyl through C-H dissociation (TS13).

The relative energy level of the transition state TS13 lies once again between the calculated value from Park et al. and the optimal value. On the other hand the CCSD(T) calculations over-estimate by 8.7 kcal/mol the energy barrier for the addition reaction between biphenyl and H forming the S5 complex in comparison with the experimental value reported by Park et al.[106]. This discrepancy is not relevant for the purpose of the present study, and no additional analyses were performed.

To conclude, the results reported in the present section are in agreement with both the theoretical work from Park et al.[106] and the absence of any experimental evidence of the presence of fused ring species as products of the benzene + phenyl reaction. As expected, the radical/π-bond addition reaction between phenyl radical and benzene leads to the formation of biphenyl only.

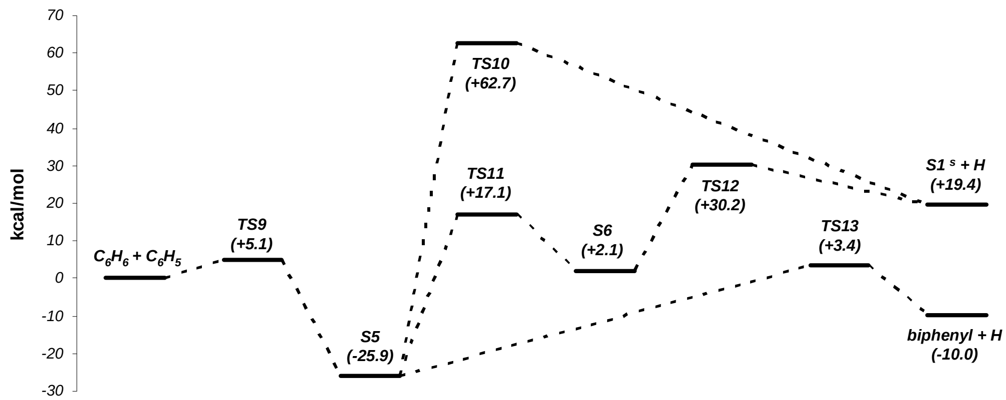

Figure 64. Potential energy surface for benzene + phenyl radical/π-bond addition. uCCSD(T)/cc-pVDZ relative energies in kcal/mol, including ZPVE.

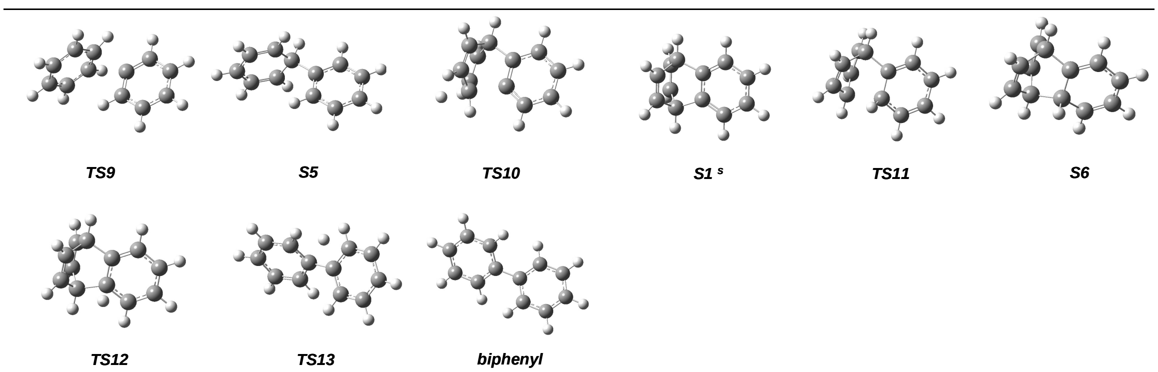

Figure 65. Species on the potential energy surface for benzene + phenyl radical/π-bond addition. uB3LYP/6-311+G(d,p) optimized structures.

7.4. Phenyl + phenyl

The radical/π-bond addition reaction between phenyl radicals proceeds along different pathways depending on the carbon atoms involved in the formation of the initial bond between the two aromatic rings (Figure 66). If the two radical sites are involved in the reaction (case 1), the system undergoes rapid reorganization to form biphenyl. In the other cases, the addition reaction produces a $C_{12}H_{11}$ biphenyl-like complex which can subsequently undergo several isomerization reactions. First consider case 2, where the initial bond involves the radical site of one phenyl and the carbon atom opposite to the radical site of the second phenyl radical.

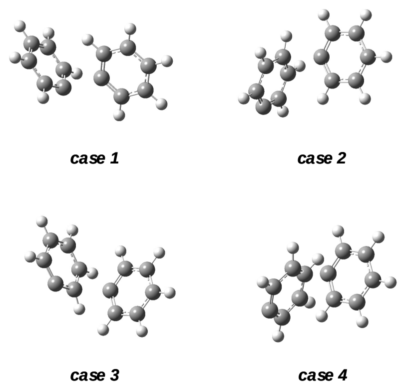

Figure 66. Radical/π-bond addition reaction between phenyl radicals.

In order to have a clear picture of the potential energy surface, the three different possible channels have been analyzed separately. All the channels include an initial common elementary addition step which leads to the formation of the biphenyl-like species. As shown in Figure 67 and Figure 68 (potential energy surface and species for channel 1 of case 2), such an addition step could proceed through either a singlet or a triplet state saddle point ($TS14^s$ and $TS14^t$ respectively). $TS14^t$ is 2.2 kcal/mol more stable than $TS14^s$. Both entrance barriers are higher by around 4 kcal/mol with respect to the corresponding values calculated by Tranter et al.[26]. This discrepancy is mainly due to the different computational methods implemented for the energy calculations. The multi-reference second order perturbation theory (CASPT2) used by Tranter et al.[26] is expected to be more accurate than the single-reference methods such as CCSD(T). On the other hand the computational costs associated with the use of a multi-reference method would not be justified by the scope of the present study.

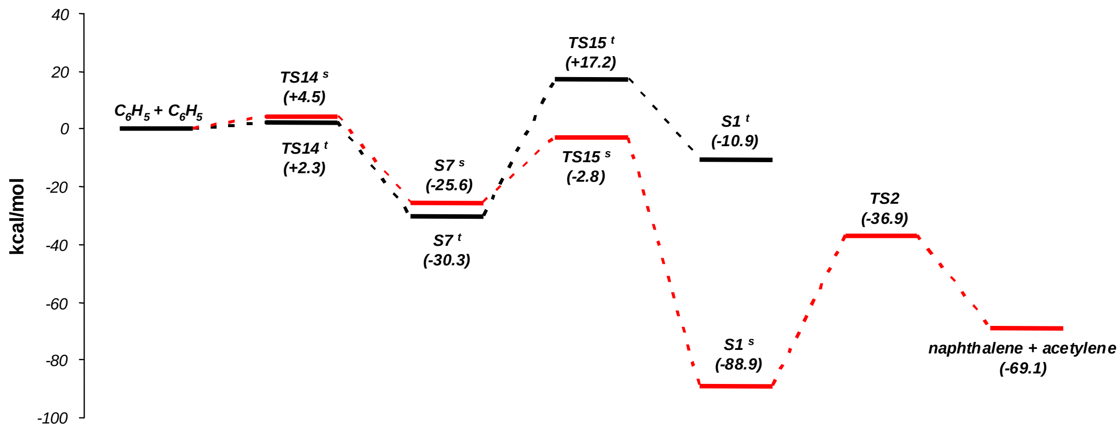

Figure 67. Potential energy surface for phenyl + phenyl radical/π-bond addition, case 2, channel 1. uCCSD(T)/cc-pVDZ relative energies in kcal/mol, including ZPVE.

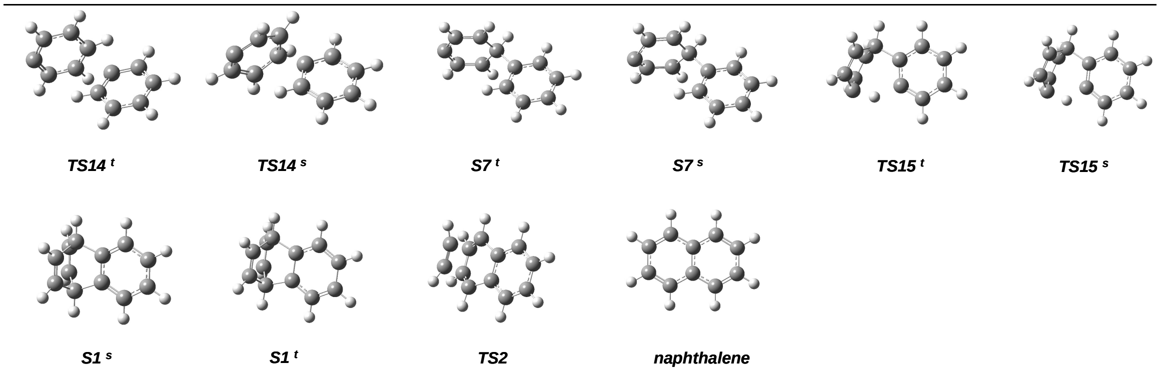

Figure 68. Species on the potential energy surface for phenyl + phenyl radical/π-bond addition, case 2, channel 1. uB3LYP/6-311+G(d,p) optimized structures.

Due to the lower entrance barrier, the addition reaction will mainly proceed on the triplet surface to form the biphenyl-like species $S7^t$. Associated with the low-frequency bending mode, the system can undergo an isomerization process involving an hydrogen transfer to form spin-triplet benzobicyclo[2,2,2]octatriene ($S1^t$). The barrier for such isomerization on the triplet surface is 47.5

kcal/mol, higher than the barrier for the redissociation process back to the reactants (32.6 kcal/mol). Thus this pathway is energetically unfavorable. On the other hand the same isomerization process on the singlet surface would involve a transition state ($TS15^s$) characterized by a much lower energy. In such a case the calculated isomerization barrier is only 22.8 kcal/mol, 7.3 kcal/mol lower than the barrier for redissociation. Therefore the radical/π-bond addition pathway on the singlet surface leads to the formation of spin-singlet benzobicyclo[2,2,2]octatriene ($S1^s$) which can easily dissociate into naphthalene and acetylene (reaction R2 as marked in Figure 59).

Although as mentioned, the singlet pathway is in general energetically unfavorable compared to the triplet one, the accessibility to the singlet pathway is provided by the triplet-to-singlet intersystem crossing, as shown in Figure 67, during the isomerization process from the biphenyl-like species to benzobicyclo[2,2,2]octatriene. Such intersystem crossing forces the system towards the lower energy singlet path to form naphthalene and acetylene. Thus as in the benzene + o-benzyne system, the presence of a bond which involves the π-orbitals allows the system to proceed towards the formation of benzobicyclo[2,2,2]octatriene and the fused-ring naphthalene as a final product.

Other channels for the formation of two-ring fused species have been analyzed for case 2 (Figure 69 and Figure 70, channel 2). In this case $S7^s$ and $S7^t$ undergo ring closure along the low-frequency bending motion without involving the hydrogen transfer process. As for channel 1, the singlet saddle point ($TS16^s$) is more stable than the triplet one ($TS16^t$) and a triplet-to-singlet intersystem crossing, as shown, is possible. The isomerization process leads to the formation of bicyclo-like compounds ($S8^s$ and $S8^t$ for spin-singlet and spin-triplet states respectively). The energy for $S8^s$ has been estimated based on the CCSD(T) energy for $TS16^s$ and the difference between the B3LYP energies for $S8^s$ and $TS16^s$.

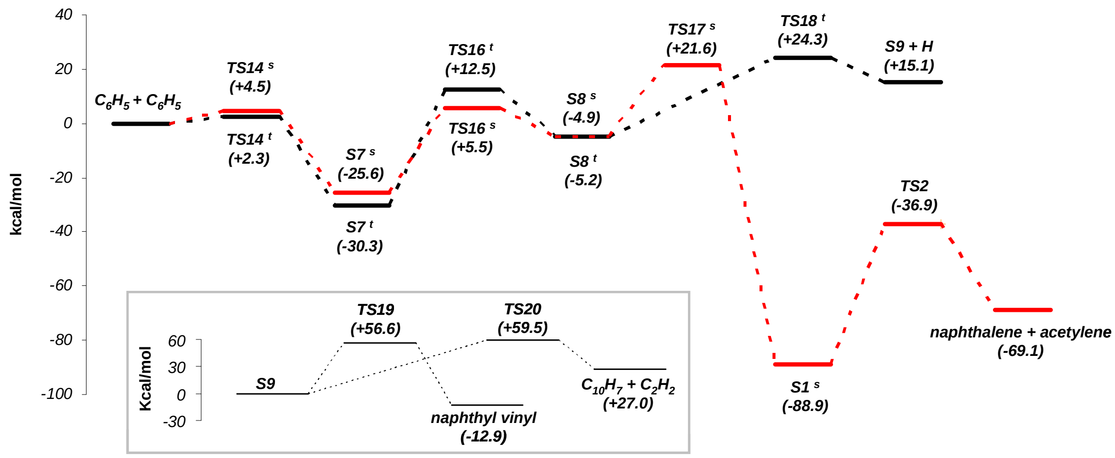

Figure 69. Potential energy surface for phenyl + phenyl radical/π-bond addition, case 2, channel 2. uCCSD(T)/cc-pVDZ relative energies in kcal/mol, including ZPVE.

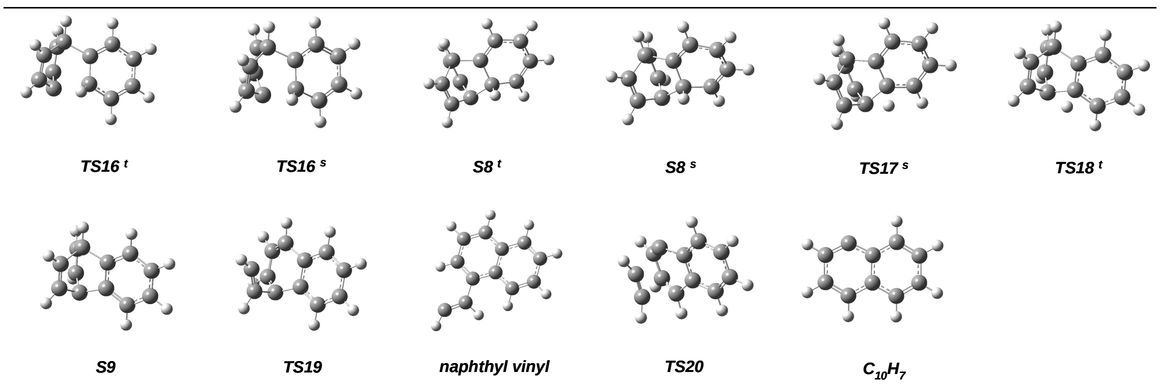

Figure 70. Species on the potential energy surface for phenyl + phenyl radical/π-bond addition, case 2, channel 2. uB3LYP/6-311+G(d,p) optimized structures. Structures for $TS14^s$, $TS14^t$, $S7^s$, $S7^t$, $S1^s$, TS2, and naphthalene reported in Figure 68.

Depending on the spin-state, the bicyclo-like compounds undergo different processes. A hydrogen transfer leads to the formation of benzobicyclo[2,2,2]octatriene ($S1^s$) from $S8^s$ (Figure 69). On the other hand $S8^t$ undergoes a C-H dissociation to form one of the possible isomers of the benzobicyclo[2,2,2]octatrienyl radical (S9). Such isomer is not only a possible source for naphthyl radical through fragmentation, but it can also isomerize to form naphthyl vinyl radical. Naphthyl vinyl radical is an important intermediate for the formation of acenaphthylene, as confirmed in previous theoretical and experimental investigations[19,21,109]. The energy barriers as well as the structures involved in the benzobicyclo[2,2,2]octatrienyl isomerization and fragmentation are shown in Figure 69 and Figure 70.

Although leading to the formation of two-ring fused compounds, the channels described in Figure 69 are energetically unfavorable. The lowest energy barrier for isomerization from biphenyl-like species to $S8^s$ and $S8^t$ is 1.0 kcal/mol higher than the redissociation barrier. Moreover $S8^s$ and $S8^t$ lie around 5 kcal/mol below the reactants energy. As a consequence, $TS17^s$ and $TS18^t$ energies are more than 20 kcal/mol higher than the reference energy of the reactants. The system is forced back towards the reactants.

In competition with the channels leading to the formation of bicyclo-like species and subsequently to the two-ring fused aromatic hydrocarbons, channel 3 of case 2 involves hydrogen transfer and/or C-H fission to form biphenyl and biphenyl radical (Figure 71 and Figure 72). Due to the carbene character of the species involved, the singlet channel proceeds through a series of hydrogen transfers to form biphenyl as hypothesized by Tranter et al.[26] The first transfer occurs with a barrier of only 20.9 kcal/mol, around 9 kcal/mol lower than the redissociation barrier. The following steps involve saddle points characterized by even smaller relative energies ($TS24^s$ and $TS25^s$). Thus the singlet path is forced towards the production of biphenyl. Although no transition state for the C-H dissociation was found on the singlet surface, the corresponding barrier is expected to be higher than the H-atom transfer barrier as for the case of benzene[159].

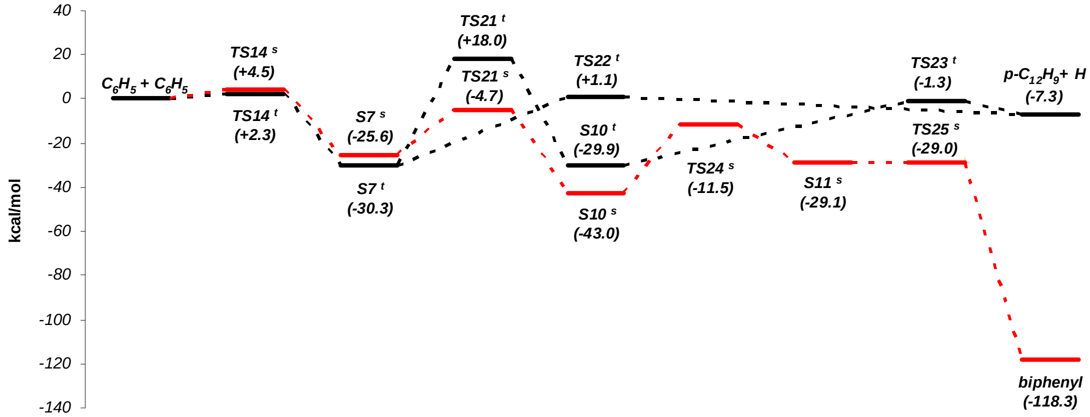

Figure 71. Potential energy surface for phenyl + phenyl radical/π-bond addition, case 2, channel 3. uCCSD(T)/cc-pVDZ relative energies in kcal/mol, including ZPVE.

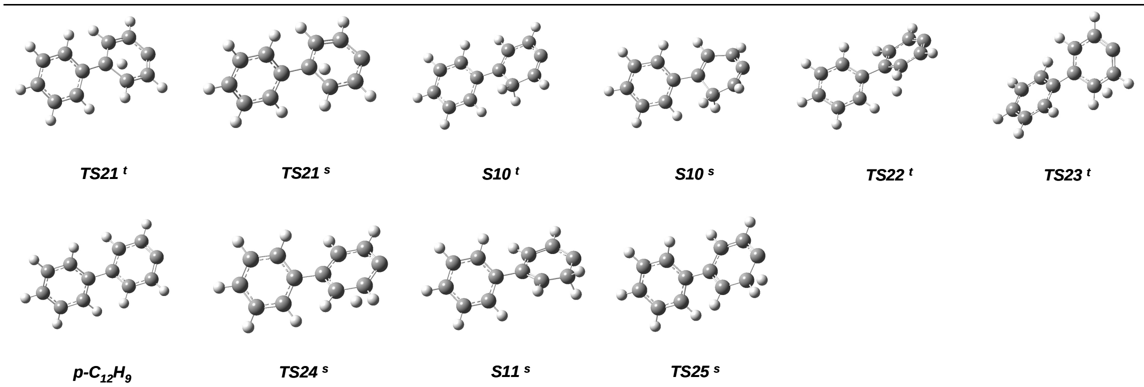

Figure 72. Species on the potential energy surface for phenyl + phenyl radical/π-bond addition, case 2, channel 3. uB3LYP/6-311+G(d,p) optimized structures. Structures for TS14^s, TS14^t, S7^s, and S7^t reported in Figure 68. Structure for biphenyl reported in Figure 65.

For the triplet radical/π-bond addition the lowest energy path involves C-H fission through TS22^t to directly form p-$C_{12}H_9$ radical and hydrogen. The barrier for such process is 31.4 kcal/mol, slightly lower than the redissociation barrier (32.6 kcal/mol). In addition to the dissociation reaction, S7^t can undergo a hydrogen transfer to form S10^t complex. However the barrier for such process is much higher than the dissociation barrier. These results are once again in agreement with the hypothesis by Tranter et al.[26]

Considering the fact that the phenyl + phenyl radical/π-bond addition proceeds mainly through the triplet surface, we would expect that channel 3 leads mainly to the formation of p-$C_{12}H_9$. On the other hand the triplet-to-singlet intersystem crossing could increase the importance of the low-energy singlet path towards biphenyl.

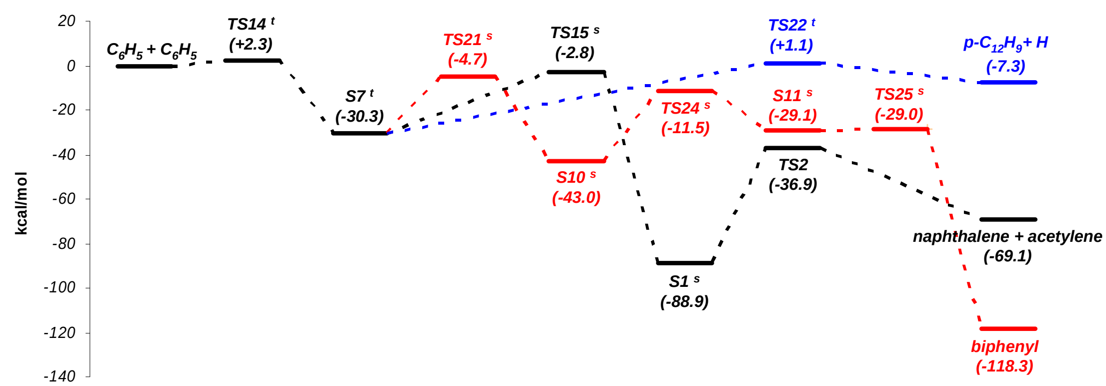

Figure 73. Potential energy surface for phenyl + phenyl radical/π-bond addition, case 2, most favorable reaction channels. uB3LYP/6-311+G(d,p) optimized structures. uCCSD(T)/cc-pVDZ relative energies in kcal/mol, including ZPVE. Structures reported in Figure 68 and Figure 72.

To summarize the results reported in Figure 67, Figure 69, and Figure 71, the phenyl + phenyl radical/π-bond addition in case 2 (Figure 66) proceeds towards two main processes, one leading to the formation of naphthalene + acetylene, the other to the formation of biphenyl and biphenyl radical (Figure 73). The relative importance of such competing channels could be determined by calculating the global reaction rate constants and the consequent branching ratio. However this examination would have only a minor impact on the ability to model actual combustion systems because either path shown in Figure 73 will be less favorable than the radical-radical recombination and the hydrogen abstraction channels shown by Tranter et al.[26] In addition, the results reported in Figure 73 require further validations using a more accurate multi-reference method such as the one implemented by Tranter et al.[26] in their recent investigation on the self-reaction of phenyl radicals. Nevertheless, the ab-initio theoretical results presented in this section address an alternative possible pathway leading to the formation of fused PAH compounds starting from a radical/π-bond addition.

In order to complete the detailed analysis of the potential energy surface of the phenyl + phenyl radical/π-bond addition, the present study has been extended to cases 3 and 4 presented in Figure 66. Since the results are very similar, only the calculations for case 3 are reported (Figure 74). Differently than in case 2, no singlet channels could be found. Thus we can assume that the reaction proceeds only on the triplet surface (similar results were obtained by Tranter et al.[26]).

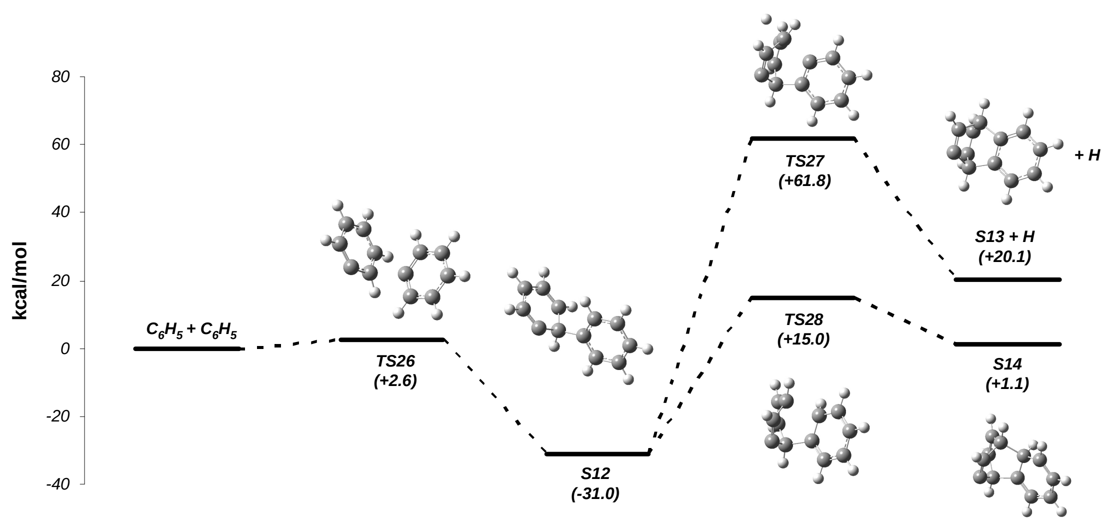

Figure 74. Potential energy surface for phenyl + phenyl radical/π-bond addition, case 3. uB3LYP/6-311+G(d,p) optimized structures. uCCSD(T)/cc-pVDZ relative energies in kcal/mol, including ZPVE.

The reaction proceeds similarly to the benzene + phenyl system. The entrance barrier for the formation of the biphenyl-like species is 2.6 kcal/mol, similar to the corresponding barrier observed in case 2. On the other hand the two pathways leading to the formation of bicyclo-like species are not energetically accessible. In fact the corresponding transition states (TS27 and TS28) lie 61.8 kcal/mol and 15.0 kcal/mol higher than the reactants energy level. Thus part of the entrance flux will redissociate back to the reactants, while part will undergo C-H fission or hydrogen transfer process to form biphenyl radical + hydrogen and biphenyl, respectively (pathways not shown).

8. RADICAL/π-BOND ADDITION BETWEEN o-BENZYNE AND CYCLIC C5 HYDROCARBONS

In Chapter 7 we presented the theoretical investigation on the radical/π-bond addition between single-ring aromatic hydrocarbons as possibly relevant to the formation of fused-ring compounds[118]. In particular, the potential energy surface for the reaction between o-benzyne and benzene contains a low-energy pathway leading to naphthalene and acetylene through the fragmentation of the bicyclo intermediate, which has been proven experimentally to be an effective pathway to the second-ring species (sections 6.3.1.5 and 6.3.2.5). The peculiar chemical structure of the o-benzyne reactant constitutes the key element in the process as it determines its high reactivity through cycloaddition reactions (Diels-Alder additions). The possibility of o-benzyne addition through concerted reactions, such as the Diels-Alder reactions, is of course not limited to the case studied in Chapter 7. For example, the review article by Bryce and Vernon[143] includes a variety of literature studies on the addition reactions of the o-benzyne radical with single and multi-ring heterocyclic compounds. Not all of these reactions are significant for actual combustion systems as the species flow entering the specific potential energy surface depends on the concentrations of the intermediates involved in the reaction. However, among the major intermediate compounds common to most of the combustion applications are the cyclic C5 hydrocarbons.

Cyclopentadienyl radicals (CPDyl, c-C_5H_5) are mainly produced by the rapid decarbonylation of the phenoxy radical (C_6H_5O) into c-C_5H_5 and CO[160]. The phenoxy radical is an abundant intermediate in oxidation environments deriving from the reaction between the phenyl radical and O_2 to form C_6H_5O and atomic oxygen[161]. The pyrolytic reactions involving both the cyclopentadienyl radicals and the corresponding closed-shell cyclopentadiene molecules (CPD, c-C_5H_6) have been extensively studied both experimentally and numerically in relation to the formation of various PAH compounds including naphthalene and indene (Ref. [162], [163], [164], and references therein). The reactions between the cyclic C5 hydrocarbons and other intermediate compounds have never been investigated in such detail although some studies have been conducted. In particular, the reaction between cyclopentadiene and o-benzyne was studied experimentally by Wittig and Knauss[165] in the late 1950s but few other investigations are present in literature[166]. The experimental results of Wittig and Knauss, as summarized by Meinwald and Gruber[167], indicate that the addition between o-C_6H_4 and CPD occurs only through 1,4-cycloaddition to form the bicyclo intermediate benzonorbornadiene[165] (see Figure 75 for chemical structure). No additional information is available. To the best of our knowledge no studies have ever been performed on the reaction between o-benzyne and the cyclopentadienyl radical.

The purpose of the present investigation is to explore the potential energy surface for the radical/π-bond addition between o-benzyne and the cyclic C5 hydrocarbons, i.e. cyclopentadiene and cyclopentadienyl radical, and test the possibility of low-energy pathways to the typical PAH compounds relevant to the formation of soot. The study will help clarify some aspects related to the chemistry of these important intermediates. The results presented in this chapter have been submitted to the Journal of Physical Chemistry A for consideration as material for publication.

8.1. Computational methodology

The methodology implemented to perform the theoretical study is similar to the one described in section 7.1 in relation to the investigation of the radical/π-bond addition between single-ring aromatic hydrocarbons. However, no single-point energy calculations were performed to improve the accuracy of the energetics of the reactions between o-benzyne and cyclic C5 hydrocarbons. Multireference single-point energy calculations with appropriate active spaces would provide more accurate results especially in the case of open-shell singlet or doublet wave functions but this kind of calculations is not easily feasible for the molecules considered here. On the other hand the relative energies obtained with the present method are sufficiently accurate to draw conclusions on the accessibility of the various reaction pathways as well as to provide indications of the relative importance of the different channels.

The results of the calculations are reported in Appendix E (Cartesian Coordinates, electronic energies, zero-point vibrational energies, and imaginary vibrational frequencies).

8.2. o-Benzyne + Cyclopentadiene

The first potential energy surface investigated in the present work is related to the reaction between spin-singlet o-benzyne radical and cyclopentadiene. The results of the calculations are reported in Figure 75 while the corresponding transition state molecular structures are shown in Figure 76. In agreement with the experimental results described in before[167], the lowest-energy entrance channel proceeds through 1,4-cycloaddition to form the bicyclo compound S1 (benzonorbornadiene). The entrance barrier is around 2 kcal/mol through the transition state TS1 (see Figure 76 for chemical structure). TS1 does not possess a structural symmetry which is characteristic of the corresponding transition state on the benzyne + benzene reaction studied in Chapter 7 and the structures of the two reactant molecules are almost unaltered when approaching the transition state configuration. This is due to the transition state been reached quite early in the cycloaddition process with a distance of around 2.53 Å between the two carbon atoms which create the first bond between o-C_6H_4 and c-C_5H_6.

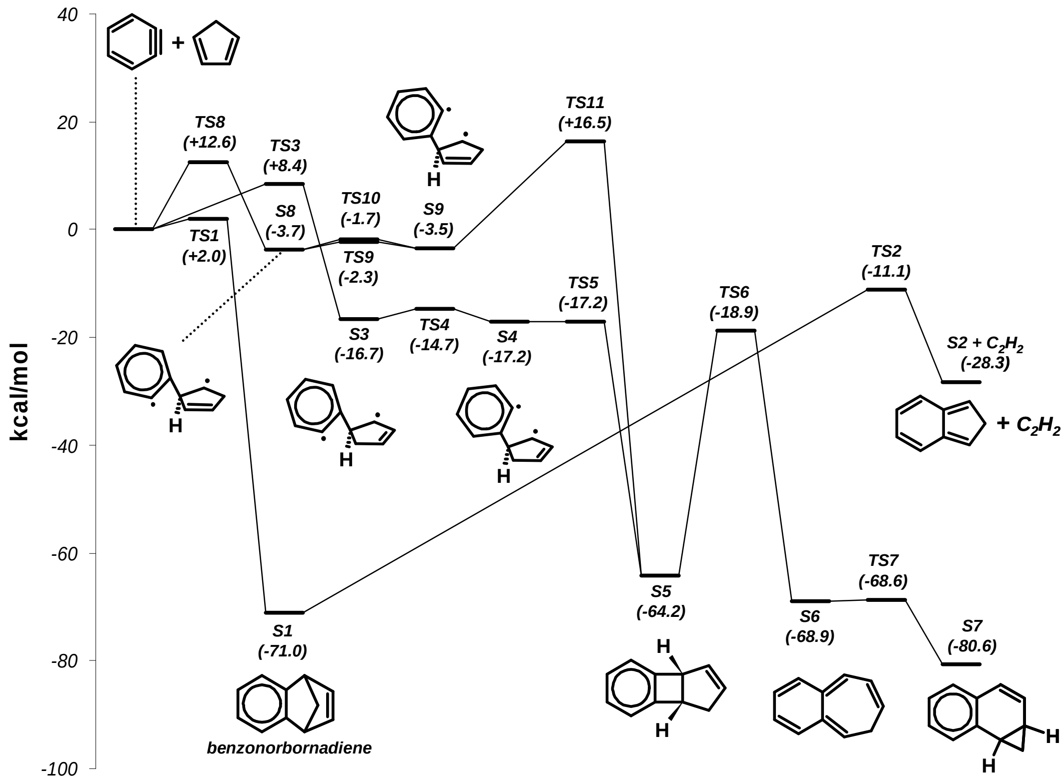

Figure 75. Potential energy surface for the radical/π-bond addition between o-benzyne and cyclopentadiene. uB3LYP/6-311+G(d,p) relative energies in kcal/mol, including ZPVE.

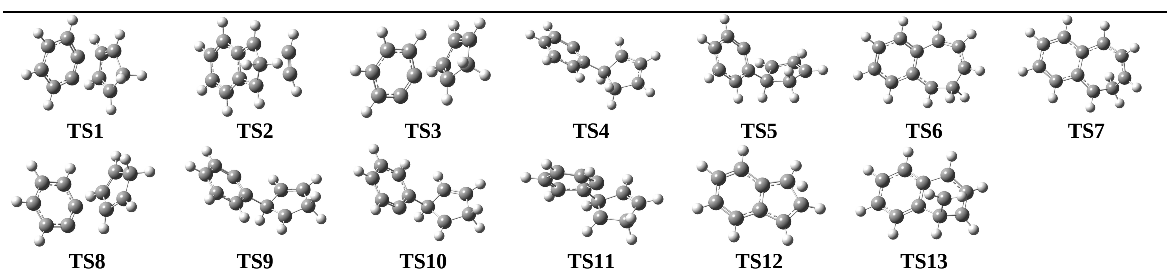

Figure 76. uB3LYP/6-311+G(d,p) transition state structures for potential energy surfaces in Figure 75, Figure 78, and Figure 80.

Based on the present calculations, the reaction rate constants for the entrance step can be calculated using transition state theory. The calculated values are well fitted by the following modified Arrhenius expression (in $cm^3mol^{-1}s^{-1}$).

$$k(o-C_6H_4+c-C_5H_6 \rightarrow S1) = 37.89 \cdot T^{2.996} \exp(-499/T)$$

The uncertainty in the above expression can be estimated as a factor of 3-4 mainly due to the uncertainty in the reaction barrier. The Arrhenius plot of the calculated reaction rate constant is reported in Figure 77 which also contains the *k* values for the similar 1,4-cycloaddition process between o-benzyne and benzene as calculated in section 7.2 (Ref. [118]). The reaction between o-benzyne and cyclopentadiene is clearly faster at low temperatures due to the lower entrance barrier, the difference being around 5 kcal/mol. For temperatures above 1600 K the o-C_6H_4 + C_6H_6 reaction becomes faster due mainly to the higher multiplicity of the corresponding pathway. More generally, it is worth mentioning that the reaction rate constants for the two 1,4-cycloaddition processes reported in Figure 77 differ by less than a two-fold factor over the entire range between 1000 and 2000 K. This observation not only indicates that the two processes are similar but also suggests that the *k* values reported in Figure 77 could define the typical range for the reaction rate constants of most o-benzyne cycloaddition processes.

Similarly to the reaction between o-benzyne and benzene for which the initial 1,4 adduct undergoes fragmentation to form naphthalene and acetylene, benzonorbornadiene can undergo a similar process to form the stable S2 adduct and acetylene. S2 is an isomeric form of the more stable indene. As shown in Figure 78 the isomerization process between S2 and indene is very favorable as it proceeds through a reaction barrier of only 16.6 kcal/mol for the hydrogen-transfer process (see Figure 76 for the structure of the transition state TS12). Thus we can conclude that the 1,4-

cycloaddition between o-benzyne and cyclopentadiene leads finally to the formation of indene and acetylene.

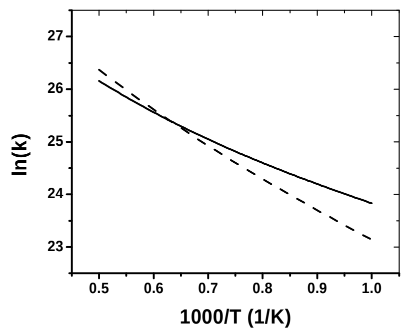

Figure 77. Arrhenius plot of the calculated 1,4-cycloaddition reaction rate constant between o-benzyne and: —– cyclopentadiene (present work); – – benzene (Ref. [118]).

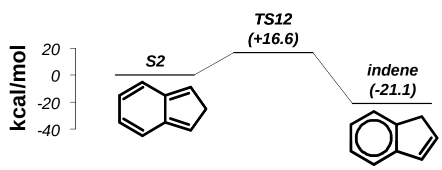

Figure 78. Potential energy surface for the isomerization of indene. uB3LYP/6-311+G(d,p) relative energies in kcal/mol, including ZPVE.

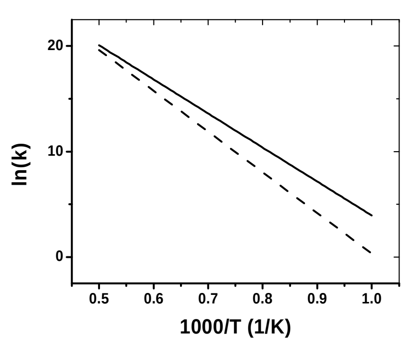

Figure 79. Arrhenius plot of the calculated reaction rate constant for the fragmentation of benzonorbornadiene into: —– S2 + C_2H_2; – – o-C_6H_4 + C_5H_6.

Benzonorbornadiene can also undergo fragmentation into the initial reactants, o-benzyne and cyclopentadiene, but the barrier for this process is around 13 kcal/mol higher compared to the fragmentation into S2 and acetylene described above. This difference in the reaction barriers determines the latter process to be the dominant one over the entire temperature range of the present study as indicated in Figure 79 (reaction rate constants calculated using transition state theory). In the high temperature range the difference between the reaction rate constants become smaller due to the higher entropy contribution in the case of formation of o-benzyne and benzene. The Arrhenius fit of the reaction rate constants in Figure 79 are provided below (in s^{-1}).

$$k\left(S1 \rightarrow o-C_6H_4 + c-C_5H_6\right) = 7.943 \cdot 10^{16} \cdot \exp\left(-38595.3/T\right)$$

$$k\left(S1 \rightarrow S2 + C_2H_2\right) = 5.272 \cdot 10^{15} \cdot \exp\left(-32268.4/T\right)$$

The radical/π-bond addition between spin-singlet o-benzyne and cyclopentadiene not only proceeds through concerted 1,4-cycloaddition but it can undergo a stepwise reaction to form a stable intermediate characterized by the two rings connected through a single C-C bond and the planes containing the rings positioned almost perpendicularly (S3 and S8 in Figure 75). Similar stepwise reactions are also present in the potential energy surface for the radical/π-bond addition between singlet o-benzyne + benzene[112,152], triplet o-benzyne + benzene[118], phenyl radical + benzene[106,118], and between phenyl radicals[26,118]. In the specific case of the reaction studied in the present investigation between o-C_6H_4 and c-C_5H_6 four different carbon atoms are available on the cyclopentadiene molecular structure for the formation of the primary C-C bond with the o-benzyne radical site. Nevertheless the symmetry of the c-C_5H_6 molecule reduces the problem to only two different cases which will be discussed in the following paragraphs.

The lower-energy stepwise channel proceeds through the addition between one of the two radical sites in the o-benzyne molecule and the carbon atoms close to the CH_2 moiety in the cyclopentadiene molecule. The corresponding transition state (TS3 in Figure 76) is characterized by a distance of around 2.00 Å between the two reactant molecules which is relatively small compared to the case of the 1,4-cycloaddition presented above. Due to the smaller distance, the two molecular structures of o-C_6H_4 and c-C_5H_5 are in this case slightly distorted at the saddle point. Since the reaction barrier is around 6.4 kcal/mol higher compared to the concerted cycloaddition, the stepwise channel leading to the formation of the intermediate S3 is clearly less favorable compared to the concerted process to benzonorbornadiene (S1), in agreement with the experimental results available in literature[165-167].

Once formed, S3 can isomerize to form the S4 complex which has similar molecular structure but different torsional angle between the two rings. The torsional barrier is around 2 kcal/mol through the transition state TS4 (Figure 76). Due to the presence of the CH_2 moiety the molecular structure of S4 is characterized by a relatively small distance between the two radical sites present in the molecule. A simple bending motion between the two rings leads to the formation of a second C-C bond between the two radical sites. The bending barrier through TS5 is less than 0.05 kcal/mol thus the process can be considered barrierless based on the uncertainty of the implemented method. The resulting intermediate compound (S5) is bound by around 47 kcal/mol with respect to S4 and can isomerize through a ring expansion process to form S6 (Figure 75). The isomerization barrier through the transition state TS6 to form the ring-expanded intermediate S6 is only 1.7 kcal/mol lower than the barrier for the isomerization of S5 back to S4. On the other hand, once formed, S6 quickly isomerizes to form a new stable intermediate S7 through a barrier of only 0.3 kcal/mol. S7 (1,2-dihydro-1,2-methanonaphthalene) is the most stable compound on the potential energy surface with a relative energy equal to 80.6 kcal/mol thus it is possibly the final product of the stepwise addition process. 1,2-dihydro-1,2-methanonaphthalene is a stable compound which can be easily measured with traditional analytical techniques such as gas chromatography. Experimental studies on the reaction between o-benzyne and cyclopentadiene performed at different pressure and temperature conditions, which complement the results obtained by Wittig and Knauss[165], would clarify the actual role of the stepwise channel by comparing the yield of 1,2-dihydro-1,2-methanonaphthalene (S7) with those of benzonorbornadiene (S1) and indene from the 1,4-cycloaddition process. The latter products can also be measured with traditional analytical techniques.

Before proceedings with the discussion on alternative channels, it is worth mention that no transition state which connects the S4 adduct with benzonorbornadiene could be identified. A similar transition state is part of the potential energy surface for the reaction of the o-benzyne radical with benzene as studied by Shukla et al.[112] On the other hand, due to the CH_2 moiety on the cyclopentadiene molecule, the lower-energy o-C_6H_4 + c-C_5H_6 stepwise channel is forced towards the formation of the stable S5 intermediate as discussed above.

The second stepwise channel on the potential energy surface for the radical/π-bond addition between o-benzyne and cyclopentadiene is the least favorable. In this case the entrance step leads to the formation of a C-C bond between the o-benzyne radical site and one of the two carbon atoms not bonded to the CH_2 moiety in the cyclopentadiene molecule. The relative energy of the corresponding transition state (TS8 in Figure 76) is 12.6 kcal/mol while the resulting adduct (S8 in Figure 75) is only bounded by 16.3 kcal/mol. S8 can isomerize through torsional motion to form the intermediate S9. Depending on the direction of the torsional rotation (clockwise or counterclockwise), two different transition states were identified, TS9 and TS10 (Figure 76). The isomerization will occur almost indifferently through TS9 or TS10 since the two corresponding barriers (respectively 1.4 kcal/mol and 2.0 kcal/mol) are indeed very similar. The resulting S9 adduct can subsequently isomerize into S5 through the formation of a second C-C bond across the C6 and C5 rings. On the other hand, the energy barrier through TS11 (Figure 76) is around 4 kcal/mol higher than the dissociation barrier back to the reactants, thus the specific stepwise channel is not favorable.

Further analyses were performed to identify additional channels in particular for the isomerization of the benzonorbornadiene intermediate. In addition to the fragmentation of this intermediate to form the S2 indene-like compound and acetylene, the rupture of the CH-CH_2 bond in the benzonorbornadiene molecule could proceed through the transition state TS13 (see Figure 76 for molecular structure) to the formation of a possible alternative stable intermediate (at the moment unknown). On the other hand, we could not identify any corresponding stable product and the IRC calculation on TS13 does not support the hypothesis that TS13 is a direct transition state between benzonorbornadiene and the S7 adduct as depicted in Figure 80. At this point it is not clear if the transition state TS13 is relevant for the title reaction and consequently if the dashed pathway shown in Figure 80 is actually present on the potential energy surface.

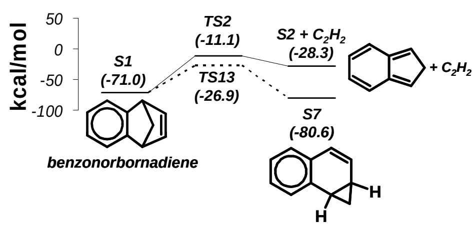

Figure 80. Possible alternative pathway for the isomerization of benzonorbornadiene. uB3LYP/6-311+G(d,p) relative energies in kcal/mol, including ZPVE.

The theoretical results described in present section indicate that the potential energy surface for the radical/π-bond addition between o-benzyne and cyclopentadiene contains a favorable pathway which leads to the formation of indene and acetylene through the fragmentation of the 1,4-cycloadduct benzonorbornadiene. Similarly to the reaction between benzene and o-benzyne (section 7.2), the practical relevance of the proposed pathway depends definitely on the concentrations of o-benzyne and cyclopentadiene in the specific combustion system. Cyclopentadiene is generally an abundant intermediate in oxidative environments since its corresponding radical complex (c-C_5H_5) derives from the fast decarbonylation of the phenoxy radical. On the other hand, o-benzyne is produced mainly by dehydrogenization of the phenyl radical through an energy barrier of around 78 kcal/mol[155]. Abstraction of a hydrogen atom from the phenyl ring could provide additional pathways for the formation of o-benzyne at relatively low-temperatures. For example, the self-reaction between phenyl radicals investigated by Tranter et al.[26] does not proceeds only through recombination but also through hydrogen abstraction to form benzene and benzynes. The typical abundance of the single-ring aromatics could result in relatively high concentrations of the o-benzyne radical and as a consequence in the relevance of the proposed pathway. This hypothesis awaits further modeling and experimental validations.

8.3. o-Benzyne + Cyclopentadienyl Radical

The radical/π-bond addition between the o-benzyne radical and the cyclopentadienyl radical involves the doublet electronic state. Just as for the reaction between benzene and the phenyl radical which occurs on a doublet potential energy surface too[106,118], the o-C_6H_4 + c-C_5H_5 addition proceeds through a stepwise reaction which leads to the formation of a $C_{11}H_9$ intermediate (S10 in Figure 81). No transition state for the the radical/π-bond addition could be identified, thus the process can be considered barrierless No concerted transition state could be identified too as expected based on similarity with other previously studied reaction spin-doublet and triplet systems[26,106,118].

The S10 adduct can undergo a hydrogen transfer process to form the stable intermediate S12 through a barrier of around 30 kcal/mol (see Figure 82 for the molecular structure of the transition state TS16). Although this barrier is relatively small, it is definitely larger than the barrier for the torsional rotation of the C_6H_4 ring forming the complex S11 (Figure 81). More importantly the relative energy of TS16 is higher compared to the barriers for the isomerization of S11, thus the channel leading to the formation of S12 is energetically unfavorable.

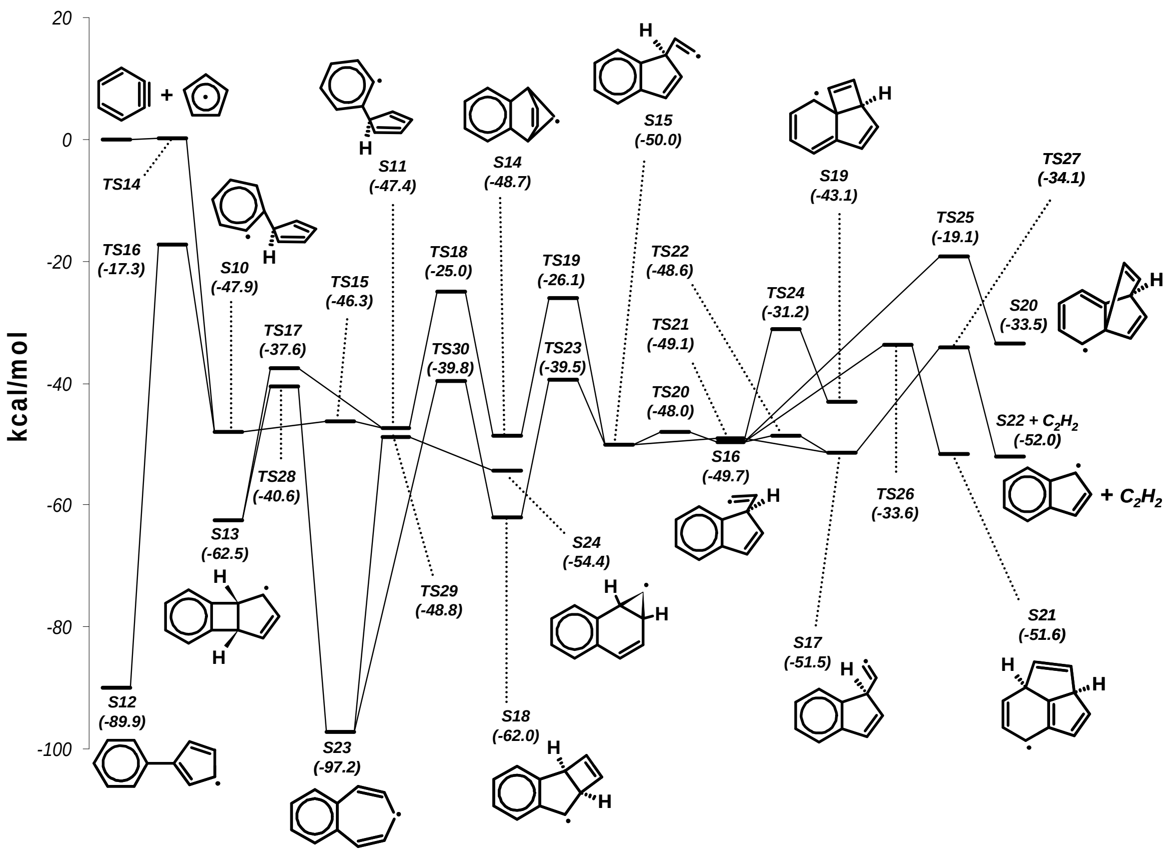

Figure 81. Potential energy surface for the radical/π-bond addition between o-benzyne and cyclopentadienyl radical. uB3LYP/6-311+G(d,p) relative energies in kcal/mol, including ZPVE.

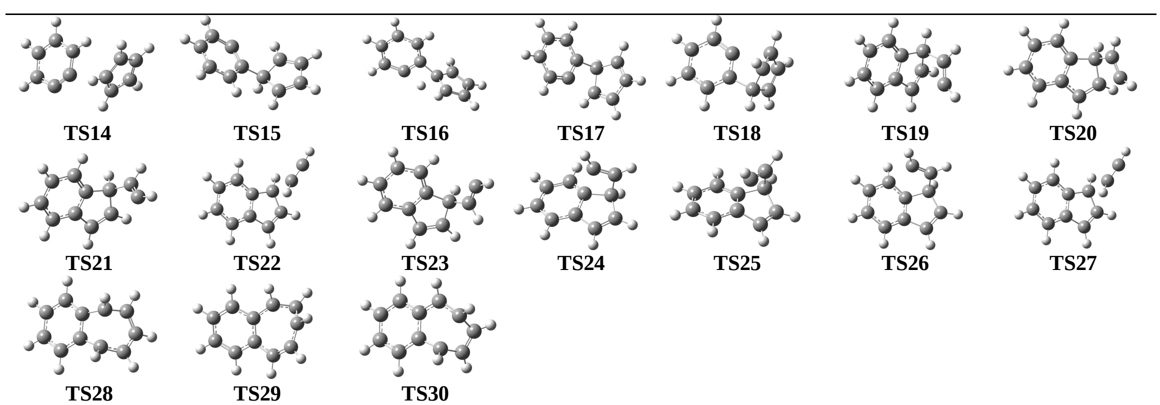

Figure 82. uB3LYP/6-311+G(d,p) transition state structures for potential energy surfaces in Figure 81.

The lowest energy and thus most favorable pathway proceeds indeed through the transition state TS17 starting from S11 with a barrier of around 10 kcal/mol (Figure 81 and Figure 82). In this case the coupled rotation and bending motions of the C_6H_4 ring towards the C5 ring leads to the formation of a second C-C bond between the radical site in S11 and the carbon close to the primary C-C bond between the two rings. The resulting adduct (S13 in Figure 81) is similar to the intermediate S5 described for the potential energy surface of the stepwise addition between o-benzyne and cyclopentadiene (Figure 75) although in this case S13 is a radical intermediate. On the other hand, the corresponding energy barriers through TS5 and TS17, respectively for S5 and S13, are quite different. Two are the possible reasons for such difference. The first obvious reason is that in the o-C_6H_4 + c-C_5H_6 reaction the second C-C bond leading to the formation of S5 occurs between two radical sites (Figure 75) while only one radical site is present in S11 (Figure 81). The second possible reason is due to the actual molecular structures of the species involved. We mentioned in the section 8.2 that the molecular structure of the adduct S4 in Figure 75 is strongly influenced by the presence of the CH_2 moiety in the C5 ring and how this peculiar feature favors the formation of S5. This is clearly demonstrated by the fact that the corresponding formation process through TS5 is barrierless. In the case of S11 the structure is symmetric with respect to the C_6H_4 ring and the step which leads to S13 requires a consistent distortion of the lowest-energy configuration represented by S11.

The symmetry in the molecular structure which is characteristic of the S11 adduct is also responsible for the presence of an additional transition state which leads to the formation of the bicyclo benzonorbornadienyl radical (S14 in Figure 81). The corresponding reaction barrier through the TS18 transition state (Figure 82) is 22.4 kcal/mol which is 12.6 kcal/mol higher than the barrier for the isomerization of S11 into S13 described in the previous paragraph. Due to the spin-doublet character, benzonorbornadienyl radical does not undergo direct fragmentation but isomerizes to form the indenylvinyl radicals (S15, S16, and S17, Figure 81) through the rupture of a C-C bond on the C5 ring. The three isomers differ only by the torsional angle of the C_2H_2 moiety and are connected by low-barrier rotational transition states (TS20, TS21, and TS22 in Figure 82).

Depending on the specific isomer, the indenylvinyl radical undergoes different isomerization processes. As shown in Figure 81, the radical site on the C_2H_2 moiety can form an additional C-C bond starting from S15 and S16 to form a variety of stable adducts (S18, S19, S20, and S21). Among these isomerization steps, the lowest-barrier channel leads to the formation of S18 which is also the most stable among the above mentioned adducts. Differently than the other isomers, the S17 indenylvinyl radical can only fragment to form the indenyl radical + acetylene. The corresponding barrier through the transition state TS27 is relatively low (17.6 kcal/mol) but higher than the barrier for the isomerization of S15 into S18. Thus we can conclude that although the potential energy surface for the radical/π-bond addition between o-C_6H_4 and CPDyl contains a pathway for the formation of indene, such channel is unfavorable from an energetic point of view.

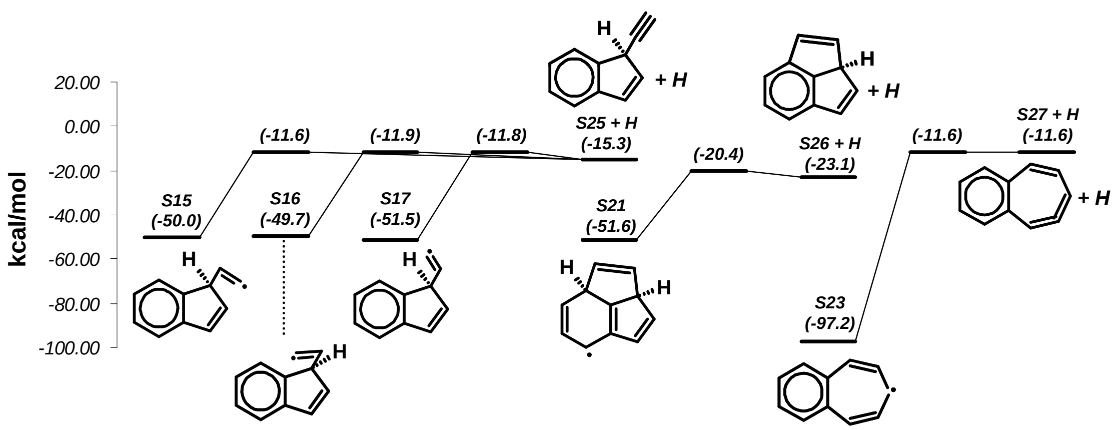

Figure 83. Lower energy H-loss reactions on the potential energy surface for the radical/π-bond addition between o-benzyne and cyclopentadienyl radical. uB3LYP/6-311+G(d,p) relative energies in kcal/mol, including ZPVE.

We previously mentioned that the lowest-energy pathway for the radical/π-bond addition between o-benzyne and cyclopentadienyl radical leads to the formation of the S13 adduct. On the other hand, S13 is definitely not the final product of the title reaction since it can undergo a relatively low-barrier (around 22 kcal/mol) ring expansion isomerization to form S23. The isomerization of the S23 adduct requires higher energies since the corresponding barriers are around 50 kcal/mol or higher.

The last aspect that we need to take into account on a doublet potential energy surface is the competition between the isomerization steps and the hydrogen-elimination processes which are energetically accessible and lead to the formation of spin-singlet adducts and hydrogen atoms. All the possible spin-singlet intermediates were considered although only the lower-energy elementary steps are summarized in Figure 83. The compound which can most favorably undergo the H-loss process is S21, to form the stable and potentially detectable species, S26, while the reaction of S23, the most stable adduct on the potential energy surface, to form S27 + H involves a barrier of around 85.6 kcal/mol. As shown in Figure 83, the reaction between S27 and H can be considered barrierless based on the corresponding uB3LYP/6-311+G(d,p) energies.

The complexity of the potential energy surface for the radical/π-bond addition between o-benzyne and cyclopentadienyl radical does not allow an immediate identification of the final product of the reaction. From a simple analysis of the pathways in Figure 81, we can hypothesize that at relatively low temperature the ring expanded S23 intermediate could be the major product due to its high stability and low-energy formation pathway. S23 is a radical, similarly to all the products and transition states on the potential energy surface of Figure 81. Thus, once formed, it will presumably react with other radicals present in the combustion system, including hydrogen atoms to form a stable ring-expanded intermediate. At higher temperatures, where S23 can isomerize, the system could proceeds through fragmentation to the formation of indenyl radical. Hydrogen-loss reactions (Figure 83) which could compete at high temperatures involve transition states with higher energies compared to the fragmentation pathway, thus are energetically unfavorable. Similarly to S23, indenyl radical will recombine with other radical in the system, including hydrogen atoms to form indene.

Further theoretical and experimental validations are required to verify these hypotheses. In particular, the use of experimental techniques able to detect and measure radicals, such as the time of flight mass spectrometry, would clarify which among the radicals in Figure 81 are produced by the radical/π-bond addition between o-benzyne and cyclopentadienyl radical or possibly identify the presence of additional pathways which have not been considered in the present work.

9. CONCLUSIONS

The present work is composed of various parts, one exclusively experimental that is devoted to the development of a new experimental technique for the measurement of PAH compounds (A), a part focused on the experimental and modeling study of the phenyl pyrolysis and phenyl + acetylene reaction (B), and finally a theoretical part on the computational chemistry investigation of several relevant potential energy surfaces (C).

A. Two different techniques for the recovery and measurement of semi-volatile and non-volatile PAH compounds present in gas samples have been investigated experimentally using GC analytical techniques. The online technique consists in the direct connection between the analytical apparatus and the high-pressure shock tube at the University of Illinois at Chicago. Treated stainless steel lines and connections were used to build the sampling rig. The new experimental technique was tested on different reaction systems and showed excellent recovery results, within 10% error in the total carbon recovery. The technique allows measurement of large multi-ring compounds, including two-, three-, and four-ring species, which could not be detected by the traditional procedure of sampling and storage in a vessel. The experimental online technique represents, in our opinion, the simplest and optimal, although not always practical, solution to the problems of condensation and adsorption of heavy PAH compounds.

The alternative offline technique, which can be easily implemented with any experimental apparatus, has been experimentally investigated using stainless steel electropolished vessels and a variety of target compounds, i.e. naphthalene and biphenyl as representative PAH species and iodobenzene as representative semi-volatile light compound. The experiments simulate the collection and analyses of gas samples containing ppm levels of these representative compounds. A detailed optimal offline technique for the measurement of heavy compounds has been obtained which includes cooling the vessel at -15 °C, injecting a gas sample into the GC, flushing the vessel with methylene chloride, and finally injecting a liquid sample into the GC. For semi-volatile species such as iodobenzene, a different solution has been proposed which involves the determination of the constant percentage in condensed phase and the application of a correction factor to the gas phase measurement. The experiments have indicated excellent recovery for all the target compounds with a maximum uncertainty of ±7%. Although the offline technique constitutes an excellent alternative solution when the online technique can not be implemented, it is not the preferred solution due to its increased procedural complexity compared to the online technique.

B. The pyrolysis of the phenyl radical and the pyrolytic reactions of the phenyl radical with acetylene have been investigated at nominal pressures of 25 and 50 atm and for a temperature range between 900 and 1800 K. The experimental work was performed using GC/GC-MS diagnostic coupled to a high-pressure shock tube apparatus. For the first time it has been possible to detect and accurately measure both small hydrocarbon products including single-ring aromatics and a variety of multi-ring PAH compounds for which mole fraction profiles have been obtained as a function of temperature. A chemical kinetic model has been developed to simulate the experimental results with particular attention to the formation of the PAH products from both reaction systems. The study helped clarify some of the aspects related to the chemistry involved in the formation of large multi-ring compounds.

In particular, the experimental and modeling results on the phenyl radical pyrolysis indicate that the formation of the PAH compounds is strongly influenced by the benzyne chemistry and especially by the reactions involving the o-benzyne radical. Such reactions have been proposed as relevant for the production of several multi-ring compounds including the terphenyls, acenaphthylene, and the four-ring species. With regards to the acenaphthylene formation a new reaction rate constant expression for the isomerization between cyclopenta[a]indene and acenaphthylene was derived from the experimental profiles, while a new reaction pathway for the isomerization of biphenylene was investigated from a theoretical point of view using ab-initio calculations. In addition, based on the experimental results we revealed the importance of several other reactions such as the reaction between phenyl radical and hydrogen iodide and the reaction between phenyl iodide and phenyl radical to form the iodobiphenyls. Similar reactions should be included in future studies on the phenyl radical derived from phenyl iodide.

The investigation on the phenyl + acetylene system revealed that the formation of PAH compounds is driven by the reaction between phenyl radical and phenylacetylene with regard to phenanthrene and diphenylethyne, while the HACA mechanism plays a key role in the formation of acenaphthylene when high concentrations of acetylene are present in the reactant mixture.

Finally both experimental studies suggest that above a certain temperature the polymerization process becomes dominant. Additional theoretical studies are required in order to clarify the relative high-temperature chemistry. The experimental profiles obtained in this work represent a valuable benchmark for the validation of such future studies.

C. A comprehensive study of the potential energy surfaces for the radical/π-bond addition reactions between different single-ring aromatic hydrocarbons has been performed for the first time using theoretical calculation techniques. Several pathways leading to the formation of PAH compounds have been proposed as relevant for typical combustion environments.

The ab-initio calculations on the addition between benzene and singlet o-benzyne radical confirm from a theoretical point of view the possibly significant role of o-benzyne in the formation of naphthalene as observed in the experimental work by Friedman and Lindow[121]. The system proceeds through the formation of a benzobicyclo[2,2,2]octatriene intermediate (reaction R1) which subsequently undergoes fragmentation to form naphthalene and acetylene (reaction R2). The high-pressure limit rate constants for the elementary reactions R1 and R2 were estimated based on the calculated properties of the species involved. On the other hand the calculations on the benzene + triplet o-benzyne system confirm the presence of a pathway leading to the formation of a biphenylene-like compound as hypothesized by Friedman and Lindow[121] in their pyrolytic experimental investigation on the system in consideration (Figure 58). Alternative channels for the addition between benzene and triplet o-benzyne lead to the formation of phenyl radicals (H-abstraction) and biphenyl radical + hydrogen (addition + C-H fission).

Further studies on the potential energy surface for the radical/π-bond addition between benzene and phenyl radical reveal that the only products of the reaction are biphenyl and hydrogen, in agreement with previous experimental and theoretical studies. On the other hand the radical/π-bond addition between phenyl radicals proceeds along a variety of pathways on both a singlet and a triplet energy surface. In competition with the expected channels leading to the formation of biphenyl (addition + H-transfer) or biphenyl radical + hydrogen (addition + C-H fission), a new pathway proceeding through the benzobicyclo[2,2,2]octatriene intermediate and leading to the formation of naphthalene and acetylene has been proposed as potentially relevant for the second-ring species formation. Such a pathway can be considered as a prototype for an aromatic radical adding to the non-radical π-bond site of another aromatic radical leading directly to fused ring structures.

The present investigation supports the idea that the π-bonding could possibly play a significant role in the mechanisms of growth of PAH species and soot. In particular the radical/π-bond addition between aromatic hydrocarbons represents a direct channel for the formation of fused multi-ring compounds as naphthalene. The investigated pathways complement the conventional growth mechanisms involving the reaction of a single aromatic hydrocarbon with small aliphatic compounds as acetylene for the HACA mechanism.

A comprehensive investigation on the potential energy surfaces for the radical/π-bond addition reactions between o-benzyne and the cyclic C5 hydrocarbons has also been performed for the first time using computational chemistry techniques. In particular, new pathways leading to the formation of the typical PAH compounds relevant to soot formation were proposed.

The ab-initio calculations of the reaction between o-benzyne and cyclopentadiene confirm from a theoretical point of view that the reaction proceeds mainly through concerted 1,4-cycloaddition to form the benzonorbornadiene adduct as observed experimentally[165-167]. A novel pathway which involves the fragmentation of benzonorbornadiene has been proposed for the first time as relevant to the formation of indene. The stepwise channels have also been studied and are found to be not favorable from an energetic point of view compared to the concerted pathway to indene.

The additional studies on the potential energy surface of the radical/π-bond addition between o-benzyne and the cyclopentadienyl radical represent to the best of our knowledge the first attempt to investigate this reaction. In competition with the isomerization pathways, a channel which leads to the formation of indenyl radical and acetylene is present on the potential energy surface. At high temperatures this channel could possibly be relevant to the formation of indene-like soot precursors.

The present investigation confirms that the radical/π-bond addition reactions could possibly play a significant role in the mechanisms of growth of PAH species and soot. In this particular case, the reactions between o-benzyne and the cyclic C5 hydrocarbons constitute a direct pathway to the formation of indene which complements the traditional reaction pathways involving the first aromatic ring and small C3 aliphatic hydrocarbons.

10. FUTURE WORK

The study of the phenyl + acetylene reactions provided valuable experimental and theoretical results which clarified some of the mechanisms involved in the formation of the typical PAH compounds observed in sooting combustion environments. These results clearly confirm the necessity of additional studies which could further clarify the pathways which leads to PAHs. In particular, the recombination reactions between the benzyl radical ($C_6H_5CH_2$) with acetylene could be studied both experimentally and theoretically in relation to the formation of indene. Indene, just like naphthalene, constitutes an important intermediate for soot formation processes.

Bittner and Howard[168] postulated benzyl radical reactions as possible important paths to PAH formation. Benzyl radicals are formed from the decomposition of alkylated aromatics such as toluene, ethyl benzene, and the xylenes. The subsequent reaction of benzyl with acetylene was postulated to lead to indene[168]. A recent set of theoretical calculations focusing on the potential energy surface for the reaction of benzyl with acetylene[169,170] have not only confirmed the pathway to indene but also pointed out the significance of pressure dependence of this reaction in combustion systems. Vereecken and Peeters[170] have predicted the reaction to proceed through the formation of a multitude of C_9H_9 isomers (species “a” in Figure 84) that eventually dissociate to indene (species “b”), phenylallene ($C_6H_5CHCCH_2$, species “c”), and 3-phenyl-1-propyne ($C_6H_5CH_2CCH$, species “e”) with indene being the favored product at high pressures and temperatures. In addition phenylallene could possibly isomerize into 1-phenylpropyne ($C_6H_5CCCH_3$, species “d”).

Recent work in the high pressure shock tube laboratory on high pressure pyrolysis of toluene[35] revealed the presence of indene as one of the major products. The benzyl plus acetylene reaction appeared to be the dominant contributor to the majority of the indene produced. The other C_9H_8 isomers were not observed in these experiments. However, since this was an indirect study because toluene was the source for the benzyl radical and because the experiments were performed at $T > 1200$ K, large parts of the Vereecken and Peeters[170] analyses could not be tested.

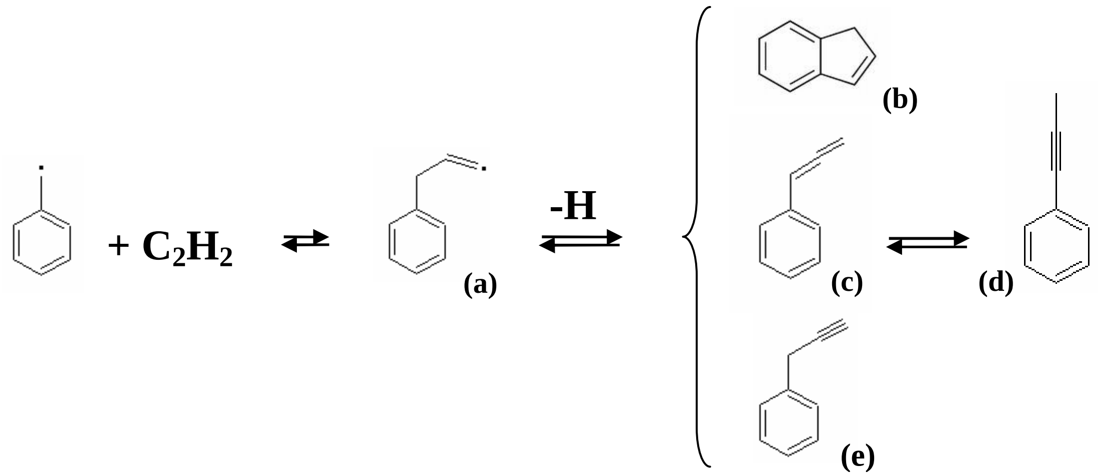

Figure 84. Benzyl + acetylene reaction.

Using the experimental technique developed in the present work, the reactions between the benzyl radical and acetylene could be investigated at the high pressure and high temperature conditions typical of modern combustion devices. The results could clarify the mechanisms proposed by the theoretical study by Vereecken and Peeters[170] and possibly highlight the presence of additional reaction channels not considered in previous investigations.

REFERENCES

1. Davis, D. L.; Bell, M. L.; Fletcher, T. *Environmental Health Perspectives* 110(12), A734-A735, 2002
2. Bell, M. L.; Davis, D. L.; Fletcher, T. *Environmental Health Perspectives* 112(1), 6-8, 2004
3. Von Klot, S.; Woelke, G.; Tuch, T.; Heinrich, J.; Dockery, D. W.; Schwartz, J.; Kreyling, W. G.; Wichmann, H. E.; Peters, A. *European Respiratory Journal* 2002, 20(3), 691-702
4. Pope, III C. A.; Burnett, T. R.; Thurston, D. G.; Thun, J. M.; Calle, E.; Krewski, D.; Ito, K. *Journal of the American Medical Association* 2002, 287, 1132-1141
5. Pope, C. A.; Burnett, R. T.; Thurston, G. D.; Thun, M. J.; Calle, E. E.; Krewski, D.; Godleski, J. J. *Circulation* 109, (2004), 71–77
6. Brook, R. D.; Brook, J.R.; Rajagopalan, S. *Curr. Hypertens. Res.* 5, (2003), 32–39
7. Johnson,R. L. *Circulation* 2004; 109; 5-7
8. Bockhorn, H. Soot Formation in Combustion-Mechanisms and Models, Ed. H. Bockhorn, Springer Series in Chemical Physics, Volume 59, 1994, 3-9
9. Frenklach, M. Phys. *Chem. Chem. Phys.* 2002, 4, 2028-2037
10. Richter H.; Howard, J. B. *Prog. Ener. Comb. Sci.* 2000, 26, 565-608
11. Lindstedt, R. P.; Maurice, L. Q.; Meyer, M. *Faraday Discuss.* 2001, 119, 409-432
12. Lighty, J. S.; Veranth, J. M.; Sarofim, A. F. *J. Air & Waste Manage. Assoc.* 50:1565-1618, 2000
13. Koylu, U . O.; Mcenally, C. S.; Rosner, D. E.; Pfefferle, L. D. *Combustion and Flame*, 110, 494–507, (1997)
14. Di Stasio, S. *Carbon*, 39, 109–118, (2001)
15. Frenklach, M.; Clary, D. W.; Gardiner, W. C.; Stein, S. E. *Proc. Combust. Inst*. 1984, 20, 887
16. Bockhorn, H.; Fetting, F.; Wenz, H. W. *Ber. Bunsen-Ges. Phys. Chem*. 1983, 97, 1067
17. Fahr, A.; Stein S. E. *Proc. Combust. Inst.* 1988, 22, 1023-1029
18. Yu, T.; Lin, M. C.; Melius, C. F. *Int. J. Chem. Kin.* 1994, 26, 1095-1104
19. Wang, H. Frenklach, M. *J. Phys. Chem*. 1994, 98, 11465-11489.
20. Heckmann, E.; Hippler, H. Troe, J. *Proc. Combust. Inst.* 1996, 26, 543-550
21. Richter, H. ; Mazyar, O. A. ; Sumathi, R. ; Green, W. H. ; Howard, J. B. ; Bozzelli, J. W. *J. Phys. Chem. A* 2001, 105, 1561-1573
22. Tokmakov, I. V.; Lin, M. C. *J. Am. Chem. Soc.* 2003, 125, 11397-11408
23. Shukla, B.; Koshi, M. *Phys. Chem. Chem. Phys.* **2010**, 12, 2427–2437.
24. Shukla, B.; Koshi, M. *Combust. Flame* **2011**, 158, 369–375.
25. Park, J.; Lin, M. C. *J. Phys. Chem. A* **1997**, 101, 14–18.
26. Tranter, R. S.; Klippenstein, S. J.; Harding, L. B.; Giri, B. R.; Yang, X.; Kiefer, J. H. *J. Phys. Chem. A* **2010**, 114, 8240–8261
27. A.G. Gaydon, I.R. Hurle, “The Shock Tube in High-Temperature Chemical Physics”, Reinhold Publishing Corporation, New York, 1963
28. A.A. Amadio, J. de Vries, J.M. Hall, E.L. Petersen, and M.W. Crofton, “Driver-Gas Tailoring for Low-Temperature Chemical Kinetics”, Proceedings of the 4th Joint Meeting of the US Sections of The Combustion Institute, 2005
29. R.A. Alpher, D.R. White, “Flow in shock tubes with area change at the diaphragm section”, Journal of Fluid Mechanics, 3, 457, 1958
30. Tranter, R. S.; Fulle, D.; Brezinsky, K. *Rev. Sci. Inst.* 2001, 72, 3046-3054
31. Tranter, R. S.; Sivaramakrishnan, R.; Srinivasan, N.; Brezinsky, K. *Int. J. Chem. Kin.* 2001, 33, 722-731
32. Tang, W.; Brezinsky, K. *Int J Chem Kinet* 38: 75–97, 2006
33. Sivaramakrishnan, R.; Tranter, R. S.; Brezinsky, K. *J. Phys. Chem. A* 2006, 110, 9388-9399

34. Sivaramakrishnan, R.; Brezinsky, K.; Vasudevan, H.; Tranter, R. S. *Combust. Sci. and Tech.*, 178: 285–305, 2006
35. Tang, W.; Tranter, R. S.; Brezinsky, K. *J. Phys. Chem. A* 2005, 109, 6056-6065
36. Sivaramakrishnan, R.; Tranter, R. S.; Brezinsky, K. *J. Phys. Chem. A* 2006, 110, 9400-9404
37. W. Tsang from *Shock Waves in Chemistry*, Assa Lifshitz, Ed. Marcel Decker, 59-129, 1981
38. W. Tsang *J. Chem. Phys.*, 40, 1171-1172, 1963
39. W. Tsang *J. Chem. Phys.*, 41 (8), 2487-2494, 1964
40. Tsang, W.; Lifshitz, A. *Int. J. Chem. Kinet.* **1998**, 30, 621–628
41. Kiefer, J. H.; Shah, J. N. J Phys Chem 1987, 91, 3024
42. Lifshitz, A.; Shweky, I.; Kiefer, J. H.; Sidhu, S. S. Shock Waves; *Proceedings of the 18th International Symposium on Shock Waves*, Sendia, Japan (**1991**); K. Takayama, Ed.; Springer–Verlag: Berlin (**1992**) 825
43. Faina Dubnikova and Assa Lifshitz; J. Phys. Chem. A 1998, 102, 5876-5885.
44. Saito, K.; Toriyama, Y.; Yokubo, T.; Higashihara, T.; Murakami, I. *Bull. Chem. Soc.* **1980**, 53, 1437–1438
45. Culbertson, B. "Homogeneous and Heterogeneous Reaction Rates for the Reactions of Carbon with Carbon Dioxide and Water", PhD dissertation, University of Illinois at Chicago, 2009.
46. NIST Standard Reference Database 17, Version 7.0 (Web Version), Release 1.5
47. Tsang W.; Hampson, R. F. *J. Phys. Chem. Ref. Database*, 15, 1986
48. Baulch, D. L.; Cobos, C. J.; Cox, R. A.; Frank, P.; Hayman, G.; Just, Th.; Kerr, J. A.; Murrels, T.; Pilling, M. J.; Troe, J.; Walker, R. W.; Warnatz, J. *J. Phys. Chem. Ref. Data*, 23, 847-1033, 1994
49. Kee, R. J.; Rupley, F. M.; Miller, J. A. "The Chemkin Thermodynamic Database", Sandia National Laboratories Report SAND87-8215B, 1990
50. NIST JANAF Thermochemical Tables, Fourth Edition, *J. Phys. Chem. Ref. Data*, Monograph No. 9, M. W. Chase Jr., (Ed.), 1998
51. Burcat, A.; Ruscic, B. Ideal Gas Thermochemical Database with updates from Active Thermochemical Tables. ftp://ftp.technion.ac.il/pub/supported/aetdd/thermodynamics.
52. Kee, R. J.; Rupley, F. M.; Miller, J. A.; Coltrin, M. E.; Grcar, J. F.; Meeks, E.; Moffat, H. K.; Lutz, A. E.; Dixon-Lewis, G.; Smooke, M. D.; Warnatz, J.; Evans, G. H.; Larson, R. S.; Mitchell, R. E.; Petzold, L. R.; Reynolds, W. C.; Caracotsios, M.; Stewart, W. E.; Glarborg, P.; Wang, C.; Adigun, O.; Houf, W. G.; Chou, C. P.; Miller, S. F. Chemkin Collection, Release 3.7.1, Reaction Design, Inc., San Diego, CA, 2003.
53. Kee, R. J.; Rupley, F. M.; Miller, J. A. Sandia National Laboratories Report SAND87-8215B
54. Kee, R. J.; Rupley, F. M.; Miller, J. A.; Coltrin, M. E.; Grcar, J. F.; Meeks, E.; Moffat, H. K.; Lutz, A. E.; Dixon-Lewis, G.; Smooke, M. D.; Warnatz, J.; Evans, G. H.; Larson, R. S.; Mitchell, R. E.; Petzold, L. R.; Reynolds, W. C.; Caracotsios, M.; Stewart, W. E.; Glarborg, P.; Wang, C.; Adigun, O. CHEMKIN Collection, 3.6 ed., Reaction Design Inc., San Diego, CA, 2000.
55. Kee, R. J.; Rupley, F. M.; Miller, J. A.; Coltrin, M. E.; Grcar, J. F.; Meeks, E.; Moffat, H. K.; Lutz, A. E.; Dixon-Lewis, G.; Smooke, M. D.; Warnatz, J.; Evans, G. H.; Larson, R. S.; Mitchell, R. E.; Petzold, L. R.; Reynolds, W. C.; Caracotsios, M.; Stewart, W. E.; Glarborg, P.; Wang, C.; McLellan, C. L.; Adigun, O.; Houf, W. G.; Chou, C. P.; Miller, S. F.; Ho, P.; Young, P. D.; Young, D. J.; Hodgson, D. W.; Petrova, M. V.; Puduppakkam, K. V. CHEMKIN Release 4.1, Reaction Design, San Diego, CA, 2006.
56. Levine, I. "Quantum Mechanics", 5th edition, 2000
57. Cramer, C. J. "Essentials of Computational Chemistry – Theories and Models", 2nd edition, 2005
58. Binkley, J. S.; Pople, J. A.; Hehre, W. J. *J. Am. Chem. Soc*., 102, 939-47, 1980

59. Gordon, M. S.; Binkley, J. S.; Pople, J. A.; Pietro, W. J.; Hehre, W. J. *J. Am. Chem. Soc.*, 104, 2797-803, 1982
60. Ditchfield, R.; Hehre, W. J.; Pople, J. A. *J. Chem. Phys*., 54, 724, 1971
61. Hehre, W. J.; Ditchfield, R.; Pople, J. A. *J. Chem. Phys.*, 56, 2257, 1972
62. Raghavachari, K.; Binkley, J. S.; Seeger, R.; Pople, J. A. *J. Chem. Phys.*, 72, 650-54, 1980
63. Dunning, T. H. *J. Chem. Phys*., 90, 1007, 1989
64. Woon, D.; Dunning, T. H. *J. Chem. Phys.*, 98, 1358, 1993
65. Hohenberg, P.; Kohn, W. *Phys. Rev*., 136, B864, 1964
66. Kohn, W.; Sham, L. J. *Phys. Rev*., 140, A1133, 1965
67. Becke, A. D. *J. Chem. Phys.* **1993**, 98, 5648–5652.
68. Lee, C.; Yang, W.; Parr, R. G. *Phys. Rev. B* **1988**, 37, 785–789.
69. Raghavachari, K.; Trucks, G. W.; Pople, J. A.; Head-Gordon, M. *Chem. Phys. Lett*., 157, 479, 1989
70. J. W. Ochterski "Thermochemistry in Gaussian", Gaussian Inc., 2000
71. J. B. Foresman, A. Frisch "Exploring Chemistry with Electronic Structure Methods", Gaussian Inc., 2nd edition, 1996
72. K. K. Irikura, D. J. Frurip "Computational thermochemistry: prediction and estimation of molecular thermodynamics", American Chemical Society, 1998
73. Sivaramakrishnan, R.; Tranter, R. S.; Brezinsky, K. *J. Phys. Chem. A* 2005, 109, 1621-1628
74. Benson, S. W. "Thermochemical Kinetics", 2nd edition, 1976
75. Herndon, W. C.; Nowak, P. C.; Connor, D. A.; Lin, P. J. *J. Am. Chem. Soc*., 114, 41-47, 1992
76. Stein, S. E.; Barton, B. D. *Thermochim. Acta*, 168, 179-186, 1990
77. Yu, J.; Sumathi, R.; Green Jr., W. H. *J. Am. Chem. Soc*., 126, 12685-12700, 2004
78. Eyring, H. *J. Chem. Phys.* 3, 107, 1935
79. Evans, M. G.; Polanyi, M. *Trans. Faraday Soc.*, 31, 875, 1935
80. Wigner, E. *Trans. Faraday Soc.* **1938**, 34, 29–41
81. Fueno, T. "The Transition State: A Theoretical Approach", 1999
82. Shavitt, I. *J. Phys. Chem.* **1959**, 31, 1359–1367.
83. Gonzalez, C.; Schlegel, H. B. *J. Chem. Phys.* **1989**, 90, 2154.
84. Frisch, M. J.; Trucks, G. W.; Schlegel, H. B.; Scuseria, G. E.; Robb, M. A.; Cheeseman, J. R.; Montgomery, J. A., Jr.; Vreven, T.; Kudin, K. N.; Burant, J. C.; Millam, J. M.; Iyengar, S. S.; Tomasi, J.; Barone, V.; Mennucci, B.; Cossi, M.; Scalmani, G.; Rega, N.; Petersson, G. A.; Nakatsuji, H.; Hada, M.; Ehara, M.; Toyota, K.; Fukuda, R.; Hasegawa, J.; Ishida, M.; Nakajima, T.; Honda, Y.; Kitao, O.; Nakai, H.; Klene, M.; Li, X.; Knox, J. E.; Hratchian, H. P.; Cross, J. B.; Bakken, V.; Adamo, C.; Jaramillo, J.; Gomperts, R.; Stratmann, R. E.; Yazyev, O.; Austin, A. J.; Cammi, R.; Pomelli, C.; Ochterski, J. W.; Ayala, P. Y.; Morokuma, K.; Voth, G. A.; Salvador, P.; Dannenberg, J. J.; Zakrzewski, V. G.; Dapprich, S.; Daniels, A. D.; Strain, M. C.; Farkas, O.; Malick, D. K.; Rabuck, A. D.; Raghavachari, K.; Foresman, J. B.; Ortiz, J. V.; Cui, Q.; Baboul, A. G.; Clifford, S.; Cioslowski, J.; Stefanov, B. B.; Liu, G.; Liashenko, A.; Piskorz, P.; Komaromi, I.; Martin, R. L.; Fox, D. J.; Keith, T.; Al-Laham, M. A.; Peng, C. Y.; Nanayakkara, A.; Challacombe, M.; Gill, P. M. W.; Johnson, B.; Chen, W.; Wong, M. W.; Gonzalez, C.; Pople, J. A. *Gaussian 03*, revision D.01; Gaussian, Inc.: Wallingford, CT, 2004.
85. *Method 429 - Determination of Polycyclic Aromatic Hydrocarbon (PAH) Emissions from Stationary Sources* (California Environmental Protection Agency – State of California Air Resources Board, Sacramento, 1997).
86. A. R. Collier, C. A. Jemma, B. Wedekind, D. E. Hall, and P. Heinze, "Sampling and Analysis of Vapor-Phase and Particulate-Bound PAH From Vehicle Exhaust", SAE paper No. 982727, 1998.

87. W. T. Winberry, Jr., and G. Jungclaus, *Compendium Method TO-13A - Determination of Polycyclic Aromatic Hydrocarbons (PAHs) in Ambient Air Using Gas Chromatography/Mass Spectrometry (GC/MS)*, (U.S. Environmental Protection Agency, Cincinnati, 1999).
88. H. N. Berko, *Technical Report No. 2: Polycyclic aromatic hydrocarbons (PAHs) in Australia*, (Environment Australia - Department of the Environment and Heritage, Perth, Western Australia, 1999).
89. C. C. Cheng, Polycyclic Arom. Comp. **23**, 315 (2003).
90. S. Garner, R. Sivaramakrishnan, K. Brezinsky, Proc. Combust. Inst. **32**, 461 (2009)
91. A. Comandini, T. Malewicki, and K. Brezinsky, *Chemistry of PAHs Formation from Phenyl Radical Pyrolysis and Phenyl + Acetylene Reaction*, submitted to J. Phys. Chem. A (2011).
92. S. Gudiyella, T. Malewicki, A. Comandini, and K. Brezinsky, Combust. Flame **158**, 687 (2011).
93. S. Gudiyella, and K. Brezinsky, *High Pressure Study of n-Propylbenzene Oxidation*, submitted to Combust. Flame (2011).
94. Wang, H.; Dames, E.; Sirjean, B.; Sheen, D. A.; Tangko, R.; Violi, A.; Lai, J. Y. W.; Egolfopoulos, F. N.; Davidson, D. F.; Hanson, R. K.; Bowman, C. T.; Law, C. K.; Tsang, W.; Cernansky, N. P.; Miller, D. L.; Lindstedt, R. P. A high-temperature chemical kinetic model of n-alkane (up to n-dodecane), cyclohexane, and methyl-, ethyl-, n-propyl and n-butyl-cyclohexane oxidation at high temperatures, JetSurF version 2.0, September 19, 2010 (http://melchior.usc.edu/JetSurF/JetSurF2.0).
95. Richter, H.; Granata, S.; Green, W. H.; Howard, J. B. *Proc. Comb. Inst.* **2005**, 30, 1397–1405 (http://web.mit.edu/anish/www/MITcomb.html)
96. Krishnan, R.; Binkley, J. S.; Seeger, R.; Pople, J. A. *J. Chem. Phys.* **1980**, 72, 650–654.
97. Godbout, N.; Salahub, D. R.; Andzelm, J.; Wimmer, E. *Can. J. Chem.* **1922**, 70, 560–571.
98. Robaugh, D.; Tsang, W. *J. Phys. Chem.* **1986**, 90, 5363–5367.
99. Kumaran, S. S. ; Su, M. C. ; Michael, J. V. *Chem. Phys. Lett.* **1997**, 269, 99–106.
100. Kominar, R. J.; Krech, M. J.; Price, S. J. W. *Can. J. Chem.* **1976**, 54, 2981–2984.
101. Butler, E. T.; Polanyi, M. *Trans. Faraday Soc.* **1943**, 39, 19–35.
102. Moskaleva, L. V.; Madden, L. K.; Lin, M. C. *Phys. Chem. Chem. Phys.* **1999**, 1, 3967–3972.
103. Giri, B. R.; Bentz, T.; Hippler, H.; Olzmann, M. *Z. Phys. Chem.* **2009**, 223, 539–549.
104. Rodgers, A. S.; Golden, D. M.; Benson, S. W. *J. Am. Chem. Soc.* **1967**, 89, 4578–4583.
105. Wang, H.; Frenklach, M. *Combust. Flame* **1997**, 110, 173–221.
106. Park, J.; Burova, S.; Rodgers, A. S.; Lin, M. C. *J. Phys. Chem. A* **1999**, 103, 9036–9041.
107. Brooks, C. T.; Peacock, S. J.; Reuben, B. G. *J. Chem. Soc. Faraday Trans. I* **1979**, 75, 652–662.
108. Zhang, L.; Cai, J.; Zhang , T.; Qi, F. *Combust. Flame* **2010**, 157, 1686–1697.
109. Lifshitz, A.; Tamburu, C.; Dubnikova, F. *J. Phys. Chem. A* **2009**, 113, 10446–10451.
110. Frenklach, M.; Wang, H. *Proc. Combust. Inst.* **1990**, 23, 1559–1566.
111. Richter, H.; Benish, T. G.; Mazyar, O. A.; Green, W. H.; Howard, J. B. *Proc. Combust. Inst.* **2000**, 28, 2609–2618.
112. Shukla, B.; Tsuchiya, K.; Koshi, M. *J. Phys. Chem. A* **2011**, 115, 5284–5293.
113. Brown, R. F. C.; Choi, N.; Coulston, K. J.; Eastwood, F. W.; Wiersum, U. E.; Jenneskens, L. W. *Tetrahedron Letters* **1994**, 35:25, 4405–4408.
114. Brown, R. F. C.; Eastwood, F. W. *Pure & Appl. Chem.* **1996**, 68:2, 261–166.
115. Wiersum, U. E.; Jenneskens, L. W. *Tetrahedron Letters* **1993**, 34:41, 6615–6618.
116. Blake, M. E.; Bartlett, K. L.; Jones Jr., M. *J. Am. Chem. Soc.* **2003**, 125, 6485–6490.
117. Scott, L. T. *Pure & Appl. Chem.* **1996**, 68:2, 291–300.
118. Comandini, A.; Brezinsky, K. *J. Phys. Chem. A* **2011**, 115, 5547–5559.

119. Poster, D. L.; Schantz, M. M.; Sander, L. C.; Wise, S. A. *Anal. Bioanal. Chem.* **2006**, 386, 859–881.
120. Jacobelli, C.; Perez, G.; Polcaro, C.; Possagno, E.; Bassanelli, R.; Lilla, E. *J. Anal. Appl. Pyrol.* **1983**, 5, 237–243.
121. Friedman, L.; Lindow, D. F. *J. Am. Chem. Soc.* **1968**, 90:9, 2324–2328.
122. Copeland, P. G.; Dean, R. E.; McNeil, D. *J. Chem. Soc.* **1960**, 1687–1689.
123. Fields, E. K.; Meyerson, S. *Chem. Commun.* **1965**, 20, 474–476.
124. Fields, E. K.; Meyerson, S. *J. Org. Chem.* **1966**, 31, 3307–3309.
125. Lindow, D. F.; Friedman, L. *J. Am. Chem. Soc.* **1967**, 89:5, 1271–1272.
126. Wang, H.; Laskin, A.; Moriarty, N. W.; Frenklach, M. *Proc. Combust. Inst.* **2000**, 28, 1545–1555.
127. Laskin, A.; Lifshitz, A. *Proc. Combust. Inst.* **1996**, 26, 669–675.
128. Gao, Y.; Fessel, K.; McLeod, C.; Marshall, P. *Chem. Phys. Lett.* **2008**, 451, 8–13.
129. Aguilera-Iparraguirre, J.; Klopper, W. *J. Chem. Theory Comput.* **2007**, 3, 139–145.
130. Hertzler, J.; Frank, P. *Ber. Bunsenges. Phys. Chem.* **1992**, 96, 1333–1338.
131. Kislov, V. V.; Islamova, N. I.; Kolker, A. M.; Lin, S. H.; Mebel, A. M. *J. Chem. Theory Comput.* **2005**, 1, 908–924.
132. a) Kruse, T.; Roth, P. *J. Phys. Chem. A* **1997**, 101, 2138–2146; b) Kern, R. D.; Xie, K.; Chen, H.; Kiefer, J. H. *23th International Symposium on Combustion*, The Combustion Institute (**1990**) 69–75; c) Frank, P.; Just, T. *Combust. Flame* **1980**, 38, 231–248.
133. Colket III, M. B.; Seery, D. J.; Palmer, H. B. *Combust. Flame* **1989**, 75, 343–366.
134. Dooley, S.; Won, S. H.; Chaos, M.; Heyne, J.; Ju, Y.; Dryer, F. L.; Kumar, K.; Sung, C. J.; Wang, H.; Oehlschlaeger, M. A.; Santoro, R. J.; Litzinger, T. A. *Combust. Flame* **2010**, 157, 2333–2339.
135. Choi, Y. M.; Park, J.; Lin, M. C. *J. Phys. Chem. A* **2003**, 107, 7755–7761.
136. Seetula, J. A.; Russell, J. J.; Gutman, D. *J. Am. Chem. Soc.* **1990**, 112, 1347–1353.
137. Appel, J.; Bockhorn, H.; Frenklach, M. *Combust. Flame* **2000**, 121, 122.
138. Fascella, S.; Cavallotti, C.; Rota, R.; Carrà, S. *J. Phys. Chem. A* **2004**, 108, 3829.
139. Goldaniga, A.; Faravelli, T.; Ranzi, E. *Combust. Flame* **2000**, 122, 350.
140. Dean, A. M. *J. Phys. Chem.* **1990**, 94, 1432.
141. Marinov, N. M.; Pitz, W. J.; Westbrook, C. K.; Castaldi, M. J.; Senkan, S. M. *Combust. Sci. Technol.* **1996**, 116, 211.
142. Marinov, N. M.; Pitz, W. J.; Westbrook, C. K.; Vincitore, A. M.; Castaldi, M. J.; Senkan, S. M.; Melius, C. F. *Combust. Flame* **1998**, 114, 192.
143. Bryce, M. R.; Vernon, J. M. *Advances in Heterogeneous Chemistry* **1981**, 28, 183.
144. Miller, R. G.; Stiles, M. *J. Amer. Chem. Soc.* **1963**, 85, 1798.
145. Fields, E. K.; Meyerson, S. *J. Amer. Chem. Soc.* **1966**, 88, 21.
146. Scaiano, J. C.; Stewart, L. C. *J. Amer. Chem. Soc.* **1983**, 105, 3609.
147. Manion, J. A.; Tsang, W. *Proceedings of Chemical and Physical Processes in Combustion*, **1996** Fall Technical Meeting, 527.
148. Wang, H. *Proc. Combust. Inst.* **2010**, 33, 41.
149. Cain, J. P.; Gassman, P. L.; Wang, H.; Laskin, A. *Phys. Chem. Chem. Phys.* **2010**, 12, 5206.
150. Schlegel, H. B. *J. Comp. Chem.* **1982**, 3, 214.
151. Peng, C.; Schlegel, H. B. *Isr. J. Chem.* **1993**, 33, 449.
152. Beno, B. R.; Sheu, C.; Houk, K. N.; Warmuth, R.; Cram, D. J. *Chem. Commun.* **1998**, 301.
153. Friedman L. *J. Amer. Chem. Soc.* **1967**, 89, 3071.
154. Lee, T. J.; Taylor, P. R. *Int. J. Quantum Chem.* **1989**, S23, 199.
155. Davico, G. E.; Bierbaum, V. M.; DePuy, C. H.; Ellison, G. B.; Squires, R. R. *J. Am. Chem. Soc.* **1995**, 117, 2590.

156. Madden, L. K.; Moskaleva, L. V.; Kristyan, S.; Lin, M. C. *J. Phys. Chem. A* **1997**, 101, 6790.
157. Xu, C.; Braun-Unkhoff, M.; Naumann, C.; Frank, P. *Proc. Combust. Inst.* **2007**, 31, 231.
158. García-Cruz, I.; Martínez-Magadán, J. M.; Bofill; J. M.; Illas, F. *J. Phys. Chem. A* **2004**, 108, 5111.
159. Miller, J. A.; Klippenstein, S. J. *J. Phys. Chem. A* **2003**, 107, 7783.
160. Harrison, A. G.; Honnen, L. R.; Dauben, H. J.; Lossing, F. P. *J. Am. Chem. Soc.* **1960**, 82, 5593–5598.
161. Lovell, A. B.; Brezinsky, K.; Glassman, I. *Proc. Combust. Inst.* **1988**, 22, 1063–1074.
162. Kislov, V. V.; Mebel, A. M. *J. Phys. Chem. A* **2008**, 112, 700–716.
163. Butler, R. G.; Glassman, I. *Proc. Combust. Inst.* **2009**, 32, 395–402.
164. Kim, D. H.; Mulholland, J. A.; Wang, D.; Violi, A. *J. Phys. Chem. A* **2010**, 114, 12411–12416.
165. Wittig, G.; Knauss, E. *Chem. Ber.* **1958**, 91, 895–907.
166. Mich, T. F.; Nienhouse, E. J.; Farina, T. E.; Tufariello, J. J. *J. Chem. Educ.* **1968**, 45, 272.
167. Meinwald, J.; Gruber, G. W. *J. Am. Chem. Soc.* **1971**, 93, 3802–3803.
168. Bittner, J. D.; Howard, J. B. *Proc. Combust. Inst*. 1981, 18, 1105
169. Vereecken, L.; Peeters, J.; Bettinger, H. F.; Kaiser, R. I.; Schleyer, P. V. R.; Schaefer, H. F. *J. Am. Chem. Soc.* 2002, 124, 2781-2789
170. Vereecken, L.; Peeters, J. *Phys. Chem. Chem. Phys.* 2003, 5, 2807-2817

APPENDICES

APPENDIX A

Included for each experimental set presented in section 6.3:

- experimental conditions (temperatures - K, pressures - atm, and reaction times - ms);
- mole fractions of the major products (ppm).

Included for each optimized stationary structures reported in section 6.3.1.4:

- Cartesian Coordinates (Ångströms);
- uB3LYP/6-311+G(d,p) electronic energies (hartrees);
- CCSD(T)/cc-pVDZ electronic energies (hartrees);
- zero-point vibrational energies ZPVE (hartrees);
- imaginary vibrational frequencies (cm^{-1}) (only for saddle points).

Experimental data set I: $[C_6H_5I]_0$ = 26.6 ppm, p ~ 50 atm.

temperature	pressure	time	acetylene	diacetylene	benzene	phenylacetylene	phenyl iodide	triacetylene	naphthalene	biphenyl	biphenylene
1052.5	68.5	1.79	0.00	0.00	0.40	0.00	24.28	0.00	0.00	0.35	0.00
1086.2	53.7	1.82	0.17	0.00	0.52	0.00	22.69	0.00	0.00	0.51	0.00
1180.6	53.7	2.08	0.45	0.00	3.08	0.00	12.89	0.00	0.00	2.19	0.09
1298.9	55.9	1.89	1.22	0.00	6.35	0.09	0.51	0.00	0.00	4.50	0.27
1199.5	48.7	1.81	0.40	0.00	4.70	0.00	8.46	0.00	0.00	3.13	0.09
1328.5	51.1	1.85	1.96	0.00	5.85	0.12	0.36	0.00	0.12	4.61	0.19
1451.6	54.1	1.69	5.91	2.48	4.96	0.00	0.40	0.16	0.15	3.43	0.02
1350.8	50.1	1.84	2.25	0.32	5.66	0.09	0.24	0.00	0.11	4.45	0.19
1426.6	55.1	1.71	4.20	1.56	5.51	0.00	0.13	0.11	0.13	4.47	0.06
1520.5	53.2	1.49	14.53	9.14	4.14	0.00	0.09	1.57	0.06	1.11	0.00
1538.2	58.7	1.47	15.46	10.03	3.61	0.00	0.08	1.95	0.12	0.82	0.00
1618.0	53.7	1.42	29.88	13.82	0.57	0.00	0.21	5.51	0.00	0.03	0.00
952.0	57.9	1.77	0.00	0.00	0.00	0.00	26.64	0.00	0.00	0.00	0.00
1321.2	63.8	1.88	1.31	0.09	5.98	0.08	0.68	0.00	0.05	4.32	0.25
1227.6	53.9	2.05	0.58	0.00	4.72	0.14	5.43	0.00	0.00	3.31	0.13
1619.2	56.3	1.42	28.10	13.23	0.59	0.00	0.21	4.57	0.00	0.08	0.00
1624.8	57.7	1.39	32.94	12.86	0.50	0.00	0.24	5.46	0.00	0.02	0.00
1486.0	52.3	1.55	9.04	5.61	4.77	0.00	0.23	0.70	0.12	2.34	0.00
1529.5	51.5	1.51	12.29	9.50	4.16	0.00	0.16	1.68	0.14	1.22	0.00
1630.1	55.1	1.50	25.04	12.47	1.40	0.00	0.00	4.72	0.00	0.00	0.00
1667.8	45.4	1.33	32.28	13.45	0.14	0.00	0.00	5.66	0.00	0.00	0.00

acenaphthylene	o-iodobiphenyl	m-iodobiphenyl	p-iodobiphenyl	o-therphenyl	m-therphenyl	p-therphenyl	benzo[g,h,i] fluoranthene	benzo[c] phenanthrene	benzo[a] anthracene	chrysene
0.00	0.15	0.37	0.03	0.08	0.00	0.00	0.00	0.00	0.00	0.00
0.00	0.13	0.32	0.04	0.11	0.00	0.00	0.00	0.00	0.00	0.00
0.00	0.24	0.50	0.11	0.27	0.20	0.13	0.00	0.00	0.00	0.19
0.26	0.00	0.06	0.02	0.36	0.89	0.44	0.07	0.00	0.00	0.77
0.06	0.01	0.35	0.09	0.21	0.45	0.32	0.01	0.00	0.00	0.52
0.40	0.00	0.06	0.02	0.28	0.81	0.43	0.06	0.00	0.00	0.65
0.92	0.00	0.00	0.00	0.13	0.32	0.18	0.20	0.04	0.00	0.60
0.41	0.00	0.00	0.00	0.20	0.70	0.40	0.15	0.15	0.04	0.97
0.66	0.00	0.00	0.00	0.13	0.57	0.29	0.25	0.07	0.04	0.82
1.06	0.00	0.00	0.00	0.05	0.25	0.03	0.10	0.00	0.00	0.25
1.01	0.00	0.00	0.00	0.03	0.18	0.06	0.07	0.00	0.00	0.19
0.03	0.00	0.00	0.00	0.00	0.00	0.00	0.03	0.00	0.00	0.10
0.00	0.00	0.00	0.00	0.00	0.00	0.00	0.00	0.00	0.00	0.00
0.40	0.00	0.00	0.00	0.30	0.94	0.48	0.15	0.00	0.00	0.75
0.20	0.08	0.28	0.22	0.26	0.53	0.29	0.07	0.00	0.00	0.98
0.09	0.00	0.00	0.00	0.05	0.03	0.00	0.00	0.00	0.00	0.09
0.05	0.00	0.00	0.00	0.16	0.00	0.00	0.00	0.00	0.00	0.14
1.17	0.00	0.00	0.00	0.09	0.10	0.04	0.13	0.00	0.00	0.33
1.03	0.00	0.00	0.00	0.08	0.05	0.03	0.12	0.01	0.00	0.23
0.00	0.00	0.00	0.00	0.00	0.00	0.00	0.00	0.00	0.00	0.00
0.00	0.00	0.00	0.00	0.00	0.00	0.00	0.00	0.00	0.00	0.00

Experimental data set II: $[C_6H_5I]_0$ = 50.6 ppm, p ~ 50 atm.

temperature	pressure	time	acetylene	diacetylene	benzene	phenylacetylene	phenyl iodide	triacetylene	naphthalene	biphenyl	biphenylene
1276.1	55.5	1.66	2.40	0.28	12.44	0.00	4.09	0.00	0.50	6.05	0.35
935.3	56.2	1.68	0.00	0.00	0.00	0.00	50.62	0.00	0.00	0.00	0.00
996.6	52.7	1.71	0.00	0.00	0.00	0.00	50.58	0.00	0.00	0.00	0.00
1178.2	56.9	1.80	0.89	0.00	4.69	0.00	31.85	0.00	0.05	1.69	0.00
1121.4	58.9	1.75	0.38	0.00	1.84	0.00	42.53	0.00	0.00	0.56	0.00
1201.4	51.4	1.86	0.94	0.00	6.40	0.00	26.75	0.00	0.10	2.47	0.09
1341.0	53.2	1.84	3.85	0.41	11.82	0.43	1.32	0.00	0.25	7.96	0.50
1177.7	43.5	1.99	1.08	0.00	4.59	0.00	32.07	0.00	0.09	1.71	0.07
1303.0	47.2	1.92	2.76	0.22	12.89	0.32	2.91	0.00	0.28	6.98	0.45
1018.9	52.3	1.69	0.00	0.00	0.23	0.00	50.81	0.00	0.00	0.05	0.00
1061.9	53.9	1.75	0.16	0.00	0.55	0.00	48.13	0.00	0.00	0.14	0.00
1300.3	53.1	1.88	3.16	0.21	13.31	0.39	3.25	0.00	0.37	6.62	0.48
1263.3	54.4	1.86	3.67	0.10	12.49	0.20	5.68	0.00	0.22	5.03	0.38
1169.9	46.6	1.86	2.69	0.00	4.03	0.08	30.30	0.00	0.04	1.02	0.05
1371.7	51.4	1.82	3.98	0.53	11.60	0.25	1.21	0.00	0.29	8.84	0.46
1498.7	55.4	1.63	15.90	8.03	8.05	0.31	0.48	2.15	0.30	3.48	0.04
1414.6	50.1	1.70	5.15	1.26	11.01	0.31	0.74	0.00	0.28	9.26	0.32
1448.9	53.6	1.68	9.96	3.83	10.68	0.37	1.35	0.69	0.34	6.98	0.10
1577.8	48.7	1.54	41.21	21.12	3.43	0.08	0.54	6.79	0.08	0.44	0.00
1695.4	54.9	1.43	62.87	20.57	0.39	0.00	0.29	12.08	0.00	0.00	0.00
1569.7	53.3	1.54	39.44	19.60	3.64	0.19	0.36	6.85	0.10	0.62	0.00
1607.3	44.9	1.46	47.15	24.85	2.20	0.12	0.38	9.29	0.06	0.24	0.00
1834.9	37.9	1.24	62.92	20.50	0.16	0.00	0.19	13.89	0.00	0.00	0.00
1720.6	47.4	1.26	63.03	21.71	0.49	0.00	0.56	14.13	0.00	0.00	0.00

acenaphthylene	o-iodobiphenyl	m-iodobiphenyl	p-iodobiphenyl	o-therphenyl	m-therphenyl	p-therphenyl	benzo[g,h,i] fluoranthene	benzo[c] phenanthrene	benzo[a] anthracene	chrysene
0.00	0.05	0.12	0.15	0.30	0.64	0.26	0.00	0.00	0.00	0.48
0.00	0.00	0.00	0.00	0.00	0.00	0.00	0.00	0.00	0.00	0.00
0.00	0.00	0.00	0.00	0.00	0.00	0.00	0.00	0.00	0.00	0.00
0.00	0.49	0.44	0.17	0.15	0.15	0.11	0.00	0.00	0.00	0.18
0.00	0.43	0.34	0.10	0.03	0.00	0.00	0.00	0.00	0.00	0.00
0.02	0.40	0.47	0.17	0.23	0.26	0.08	0.00	0.00	0.00	0.29
0.45	0.00	0.02	0.13	0.39	0.91	0.49	0.22	0.15	0.08	1.39
0.00	0.44	0.43	0.26	0.19	0.22	0.11	0.05	0.00	0.00	0.29
0.29	0.05	0.03	0.02	0.42	0.81	0.35	0.09	0.09	0.00	1.18
0.00	0.16	0.15	0.11	0.00	0.00	0.00	0.00	0.00	0.00	0.00
0.00	0.17	0.16	0.11	0.00	0.00	0.00	0.00	0.00	0.00	0.00
0.29	0.04	0.07	0.17	0.43	0.86	0.41	0.11	0.10	0.05	1.12
0.17	0.06	0.13	0.17	0.33	0.69	0.29	0.08	0.09	0.05	1.03
0.00	0.35	0.31	0.22	0.07	0.19	0.05	0.00	0.00	0.00	0.21
0.79	0.00	0.00	0.11	0.40	1.07	0.58	0.23	0.17	0.10	1.10
3.39	0.00	0.00	0.11	0.03	0.15	0.19	0.30	0.36	0.10	0.58
1.31	0.04	0.00	0.12	0.37	1.03	0.46	0.41	0.33	0.19	0.94
2.27	0.07	0.00	0.14	0.12	0.48	0.32	0.61	0.49	0.31	0.75
1.01	0.04	0.00	0.05	0.00	0.11	0.19	0.21	0.13	0.06	0.26
0.00	0.00	0.00	0.00	0.00	0.00	0.00	0.17	0.00	0.00	0.15
1.25	0.03	0.00	0.07	0.00	0.04	0.34	0.34	0.07	0.00	0.36
0.47	0.00	0.00	0.00	0.00	0.00	0.16	0.00	0.22	0.00	0.16
0.00	0.02	0.00	0.00	0.00	0.00	0.03	0.00	0.14	0.00	0.16
0.00	0.00	0.00	0.00	0.00	0.00	0.00	0.00	0.06	0.00	0.14

Experimental data set III: $[C_6H_5I]_0$ = 54.2 ppm, p ~ 25 atm.

temperature	pressure	time	acetylene	diacetylene	benzene	phenylacetylene	phenyl iodide	triacetylene	naphthalene	biphenyl	biphenylene
992.4	30.4	1.81	0.00	0.00	0.00	0.00	54.21	0.00	0.00	0.00	0.00
1022.7	29.3	1.76	0.00	0.00	0.19	0.00	53.39	0.00	0.00	0.00	0.00
947.9	27.8	1.85	0.00	0.00	0.00	0.00	53.25	0.00	0.00	0.00	0.00
1106.5	29.1	1.76	0.77	0.00	1.43	0.00	47.18	0.00	0.00	0.87	0.22
1216.7	29.1	2.15	2.31	0.00	8.77	0.09	14.40	0.00	0.26	5.37	0.31
1161.8	28.8	2.04	1.53	0.00	4.16	0.00	32.55	0.00	0.00	2.24	0.06
1182.1	26.4	1.71	1.28	0.00	5.56	0.00	27.88	0.00	0.11	3.56	0.13
1347.3	28.8	1.74	4.20	0.83	10.93	--	0.65	0.00	0.15	10.51	0.49
1287.4	28.3	1.86	2.08	0.20	12.12	0.11	3.36	0.00	0.15	8.31	0.55
1521.8	31.3	1.60	28.17	17.87	7.03	0.15	0.66	3.61	0.35	2.23	0.00
1425.2	28.6	1.78	10.42	3.75	11.30	0.16	0.29	0.18	0.31	8.82	0.16
1381.5	26.8	1.83	6.20	2.28	10.89	0.22	0.24	0.29	0.31	9.87	0.30
1502.5	25.3	1.68	21.20	14.00	9.16	0.00	0.14	1.95	0.38	3.91	0.00
1640.8	26.3	1.43	63.10	26.62	0.85	0.00	0.00	12.97	0.00	0.16	0.00
1664.6	30.2	1.34	67.54	23.80	0.29	0.00	0.00	13.98	0.00	0.00	0.00
1559.8	25.7	1.56	44.39	20.65	3.34	0.08	0.00	9.53	0.00	1.04	0.00
1732.3	23.7	1.35	66.88	22.25	0.00	0.00	0.00	14.62	0.00	0.00	0.00

acenaphthylene	o-iodobiphenyl	m-iodobiphenyl	p-iodobiphenyl	o-therphenyl	m-therphenyl	p-therphenyl	benzo[g,h,i] fluoranthene	benzo[c] phenanthrene	benzo[a] anthracene	chrysene
0.00	0.00	0.00	0.00	0.00	0.00	0.00	0.00	0.00	0.00	0.00
0.00	0.00	0.00	0.00	0.00	0.00	0.00	0.00	0.00	0.00	0.00
0.00	0.00	0.00	0.00	0.00	0.00	0.00	0.00	0.00	0.00	0.00
0.00	0.55	0.74	0.25	0.07	0.00	0.00	0.00	0.00	0.00	0.00
0.21	0.36	0.80	0.47	0.47	1.21	0.82	0.00	0.00	0.00	0.54
0.00	0.81	0.92	0.49	0.13	0.22	0.05	0.00	0.00	0.00	0.13
0.04	0.38	0.67	0.45	0.34	0.42	0.21	0.00	0.00	0.00	0.38
0.73	0.05	0.37	0.00	0.37	0.93	0.50	0.13	0.07	0.00	0.75
0.32	0.04	0.22	0.00	0.52	1.10	0.62	0.09	0.03	0.00	1.08
1.85	0.04	0.08	0.00	0.20	0.39	0.48	0.15	0.09	0.00	0.84
1.62	0.09	0.09	0.00	0.35	0.52	0.26	0.24	0.08	0.06	0.88
1.18	0.06	0.09	0.00	0.34	0.91	0.71	0.27	0.11	0.16	1.04
2.07	0.05	0.07	0.00	0.16	0.29	0.32	0.21	0.07	0.04	0.44
0.24	0.06	0.03	0.00	0.10	0.14	0.13	0.05	0.00	0.00	0.14
0.00	0.00	0.00	0.00	0.08	0.04	0.04	0.00	0.00	0.00	0.10
0.62	0.05	0.00	0.00	0.12	0.21	0.07	0.04	0.00	0.00	0.16
0.00	0.00	0.00	0.00	0.16	0.00	0.09	0.00	0.00	0.00	0.07

Experimental data set IV: $[C_6H_5I]_0$ = 95.6 ppm, p ~ 50 atm.

temperature	pressure	time	acetylene	diacetylene	benzene	phenylacetylene	phenyl iodide	triacetylene	naphthalene	biphenyl	biphenylene
961.8	55.5	1.66	0.00	0.00	0.00	0.00	95.60	0.00	0.00	0.00	0.00
968.0	56.2	1.68	0.00	0.00	0.00	0.00	95.28	0.00	0.00	0.00	0.00
1215.5	52.7	1.71	0.00	0.00	18.61	0.00	36.63	0.00	0.06	6.33	0.44
1049.9	56.9	1.80	0.00	0.00	0.71	0.00	96.07	0.00	0.00	0.21	0.00
1096.3	58.9	1.75	0.00	0.00	2.41	0.00	87.35	0.00	0.00	0.53	0.00
1168.5	51.4	1.86	0.00	0.00	7.98	0.16	67.36	0.00	0.00	2.21	0.09
1197.6	53.2	1.84	0.00	0.00	13.73	0.00	54.09	0.00	0.00	4.73	0.26
1464.3	43.5	1.99	9.08	4.01	17.45	0.20	0.85	1.89	0.51	10.55	0.14
1279.5	47.2	1.92	1.33	0.14	25.57	0.18	8.36	0.00	0.34	9.08	0.77
1367.2	52.3	1.69	3.11	0.78	23.47	0.16	1.53	0.25	0.37	12.86	0.79
1343.7	53.9	1.75	2.61	0.41	24.84	--	2.59	0.11	0.17	12.55	1.01
1348.1	53.1	1.88	2.62	0.53	24.85	0.53	2.10	0.18	0.30	12.69	0.88
1408.1	54.4	1.86	6.62	2.28	22.75	0.52	1.18	0.69	0.41	12.71	0.46
1581.2	46.6	1.86	63.71	23.74	6.14	0.00	0.54	12.16	0.08	0.53	0.00
1476.6	51.4	1.82	16.09	9.48	15.85	0.13	0.98	3.88	0.72	7.97	0.11
1604.0	55.4	1.63	76.20	26.20	2.36	0.00	0.53	13.93	0.06	0.36	0.00
1705.6	50.1	1.70	98.95	34.35	0.28	0.00	0.20	27.43	0.00	0.00	0.00
1602.8	53.6	1.68	77.95	30.22	2.43	0.00	0.33	16.64	0.00	0.33	0.00
1618.5	48.7	1.54	89.92	31.25	1.06	0.00	0.36	18.76	0.00	0.19	0.00
1769.8	54.9	1.43	105.22	37.62	0.22	0.00	0.00	29.52	0.00	0.00	0.00
1542.3	53.3	1.54	45.97	20.34	8.84	0.00	0.47	8.87	0.29	1.80	0.00

acenaphthylene	o-iodobiphenyl	m-iodobiphenyl	p-iodobiphenyl	o-therphenyl	m-therphenyl	p-therphenyl	benzo[g,h,i] fluoranthene	benzo[c] phenanthrene	benzo[a] anthracene	chrysene
0.00	0.00	0.00	0.00	0.00	0.00	0.00	0.00	0.00	0.00	0.00
0.00	0.00	0.00	0.00	0.00	0.00	0.00	0.00	0.00	0.00	0.00
0.11	0.46	0.46	0.25	0.34	0.29	0.09	0.17	0.00	0.00	1.12
0.00	0.14	0.11	0.04	0.00	0.00	0.00	0.16	0.00	0.00	0.00
0.26	0.42	0.26	0.09	0.00	0.00	0.00	0.12	0.00	0.00	0.00
0.00	0.72	0.42	0.23	0.11	0.01	0.02	0.11	0.00	0.00	0.15
0.05	0.84	0.69	0.35	0.26	0.18	0.07	0.26	0.00	0.00	0.66
3.71	0.01	0.03	0.10	0.11	0.17	0.13	0.70	0.56	0.41	1.28
0.31	0.07	0.12	0.13	0.44	0.48	0.32	0.24	0.06	0.14	1.59
1.25	0.02	0.04	0.09	0.41	0.93	0.60	0.57	0.22	0.31	2.13
0.81	0.03	0.05	0.06	0.45	0.88	0.60	0.45	0.15	0.33	2.22
0.96	0.02	0.03	0.08	0.41	1.00	0.54	0.45	0.15	0.37	2.22
1.90	0.00	0.02	0.06	0.24	0.65	0.41	0.52	0.26	0.33	1.59
1.15	0.10	0.01	0.07	0.04	0.13	0.02	0.54	0.51	0.20	1.46
4.38	0.14	0.00	0.09	0.12	0.21	0.19	0.69	0.73	0.56	1.60
0.63	0.04	0.00	0.05	0.03	0.25	0.07	0.99	0.32	0.00	0.78
0.00	0.00	0.06	0.05	0.07	0.08	0.06	0.30	0.27	0.11	0.85
0.70	0.03	0.00	0.03	0.05	0.11	0.05	0.85	0.24	0.10	0.79
0.33	0.00	0.02	0.02	0.03	0.12	0.02	0.88	0.07	0.08	0.79
0.00	0.00	0.00	0.00	0.00	0.00	0.00	0.35	0.00	0.06	0.24
2.50	0.09	0.03	0.07	0.11	0.09	0.17	0.84	0.54	0.39	1.34

Experimental data set V: $[C_6H_5I]_0$ = 58.1 ppm, $[C_2H_2]_0$ = 236.3 ppm, p ~ 50 atm.

temperature	pressure	time	methane	acetylene	diacetylene	acetone	benzene	toluene	phenylacetylene
1095.9	54.7	1.72	0.51	231.73	0.00	1.45	3.64	0.12	7.68
890.0	50.1	1.96	0.00	235.15	0.00	1.52	0.00	0.00	0.00
946.3	49.5	1.65	0.02	236.28	0.00	1.53	0.08	0.00	0.00
1134.8	48.5	1.91	0.41	217.93	0.00	1.18	6.05	0.13	14.80
1374.5	56.1	1.80	1.86	217.98	0.56	0.10	11.88	0.59	21.48
1232.8	47.0	1.90	0.70	209.82	0.07	0.95	9.38	0.24	21.78
1323.2	57.0	1.86	1.98	210.14	0.28	0.15	12.27	0.51	23.76
1491.3	50.3	1.56	1.94	222.87	9.48	0.08	9.96	0.04	10.88
1371.0	48.6	1.79	1.40	214.46	1.05	0.11	11.30	0.53	20.63
1615.8	50.9	1.45	0.72	233.14	37.21	0.08	1.78	0.00	0.00
1708.7	49.2	1.33	0.00	191.47	52.57	0.05	0.13	0.00	0.00
1776.8	43.9	1.33	0.00	164.30	52.08	0.04	0.07	0.00	0.00
887.0	54.5	1.73	0.00	237.07	0.00	--	0.00	0.00	0.00
871.5	48.1	1.77	0.03	236.18	0.00	--	0.05	0.00	0.00
1035.0	54.7	1.72	0.05	234.76	0.00	1.50	0.91	0.00	3.40
1152.0	53.2	1.93	0.28	213.59	0.00	1.36	5.64	0.00	14.48
1354.4	64.8	1.79	2.55	219.64	0.65	0.07	12.53	0.65	23.21
1233.0	52.7	2.04	0.97	210.59	0.08	0.75	10.72	0.20	22.84
1468.4	54.7	1.71	1.93	232.11	4.32	0.10	11.56	--	15.41
1538.7	46.8	1.62	1.63	239.54	21.46	0.06	6.78	0.00	4.85
1810.0	57.4	1.26	0.00	157.11	51.93	0.06	0.08	0.00	0.00
1624.1	56.7	1.31	0.18	219.70	39.17	0.02	0.37	0.00	0.00
1542.0	53.2	1.51	1.73	239.19	21.74	0.03	7.91	0.00	6.28

triacetylene	phenyl iodide	naphthalene	biphenyl	diphenylethyne	acenaphthylene	phenanthrene
0.34	38.27	0.28	0.42	0.57	0.11	0.29
0.00	57.76	0.00	0.00	0.00	0.00	0.00
0.00	57.57	0.00	0.00	0.00	0.00	0.00
0.31	27.05	0.25	0.62	1.05	0.06	0.73
1.71	0.41	0.25	3.61	1.48	0.36	1.42
0.66	13.84	0.13	1.22	1.90	0.13	1.25
1.63	0.70	0.12	2.87	1.75	0.24	1.36
1.29	0.37	0.45	2.88	0.26	1.52	0.86
2.07	0.27	0.18	4.02	1.03	0.42	1.14
17.04	0.18	0.00	0.11	0.00	0.30	0.15
40.95	0.19	0.00	0.00	0.00	0.00	0.00
47.85	0.00	0.00	0.00	0.00	0.00	0.00
0.00	58.07	0.00	0.00	0.00	0.00	0.00
0.00	58.06	0.00	0.00	0.00	0.00	0.00
0.00	55.49	0.00	0.27	0.13	0.00	0.00
0.00	22.55	0.00	0.79	1.72	0.00	0.44
2.61	0.49	0.36	3.60	1.72	0.36	1.50
1.26	6.55	0.16	1.58	1.90	0.00	1.13
0.57	0.10	0.39	3.53	0.53	1.17	0.90
8.41	0.11	0.34	0.97	0.07	1.45	0.26
48.32	0.00	0.00	0.00	0.00	0.00	0.00
28.87	0.00	0.00	0.00	0.00	0.00	0.00
7.20	0.11	0.51	0.37	0.06	1.20	0.36

Experimental data set VI: $[C_6H_5I]_0$ = 55.1 ppm, $[C_2H_2]_0$ = 511.3 ppm, p ~ 50 atm.

temperature	pressure	time	methane	acetylene	diacetylene	acetone	benzene	toluene	phenylacetylene
905.8	56.5	1.73	0.00	518.33	0.00	5.02	0.00	0.00	0.00
960.2	53.3	1.78	0.07	511.27	0.00	4.91	0.00	0.00	0.00
1064.0	54.3	1.67	0.10	503.37	0.00	5.00	0.72	0.00	4.00
1060.3	48.8	1.75	0.24	505.14	0.00	4.76	1.51	0.00	7.79
1212.7	50.5	2.02	2.21	478.76	0.12	4.19	8.74	0.39	32.79
1128.9	48.0	1.79	0.50	488.90	0.00	--	3.29	0.00	14.01
1437.4	57.2	1.75	4.26	466.16	0.95	0.22	10.27	0.50	26.24
1218.5	48.0	2.03	3.21	475.96	0.24	1.72	9.30	0.51	36.66
1330.3	52.6	1.86	4.17	462.52	0.54	0.33	9.86	0.87	34.41
1308.8	53.1	1.86	4.79	460.04	0.42	0.75	9.98	0.78	33.15
1140.7	47.7	1.75	0.67	473.89	0.05	5.40	4.46	0.00	18.46
1567.4	56.6	1.45	2.04	456.52	38.79	0.12	7.90	0.00	3.74
1478.9	51.1	1.55	3.49	474.24	8.46	0.14	9.90	0.13	13.65
941.1	53.2	1.64	0.00	506.18	0.00	4.76	0.21	0.00	0.57
1014.0	56.0	1.68	0.08	504.30	0.00	5.20	0.32	0.00	1.18
1642.2	53.9	1.39	0.50	430.52	65.05	--	0.87	0.00	0.35
1565.8	52.3	1.41	2.35	468.97	30.50	0.07	6.10	0.00	6.63
1402.3	45.9	1.42	4.06	467.03	3.28	0.10	10.60	0.74	20.97
1768.4	50.9	1.31	0.00	295.70	99.18	0.13	0.51	0.00	0.00
1639.8	47.3	1.36	0.28	426.78	71.16	0.07	0.97	0.00	0.00
1674.0	51.3	1.31	0.00	389.39	82.27	0.13	0.56	0.00	0.86
1720.2	52.6	1.29	0.00	341.09	92.24	0.12	0.24	0.00	0.61

triacetylene	phenyl iodide	naphthalene	biphenyl	diphenylethyne	acenaphthylene	phenanthrene
0.00	53.78	0.00	0.00	0.00	0.00	0.00
0.00	52.75	0.00	0.00	0.00	0.00	0.00
0.00	47.52	0.45	0.00	0.00	0.00	0.00
0.00	42.93	0.49	0.02	0.08	0.00	0.00
0.76	9.41	0.44	0.52	1.28	0.05	0.51
0.00	34.57	0.50	0.16	0.44	0.00	0.21
1.13	0.15	0.49	2.26	0.61	0.58	0.69
1.29	2.21	0.27	0.94	1.42	0.09	0.76
2.80	0.36	0.19	1.81	1.20	0.25	1.20
2.63	0.61	0.29	1.56	1.55	0.16	1.52
0.28	29.66	0.46	0.21	0.62	0.03	0.48
14.21	0.46	0.26	0.25	0.04	0.68	0.33
1.87	0.17	0.52	2.15	0.31	1.10	1.13
0.00	55.57	0.00	0.00	0.00	0.00	0.00
0.00	55.02	0.00	0.00	0.00	0.00	0.00
29.68	0.14	0.00	0.05	0.00	0.10	0.12
10.19	0.26	0.45	0.71	0.06	1.15	0.44
2.15	0.15	0.33	2.70	0.55	0.72	0.82
71.11	0.00	0.00	0.00	0.00	0.00	0.00
34.57	0.38	0.00	0.04	0.00	0.15	0.07
50.28	0.00	0.00	0.00	0.00	0.00	0.00
62.20	0.00	0.00	0.00	0.00	0.00	0.00

Experimental data set VII: $[C_6H_5I]_0$ = 52.9 ppm, $[C_2H_2]_0$ = 526.3 ppm, p ~ 25 atm.

temperature	pressure	time	methane	acetylene	diacetylene	acetone	benzene	toluene	phenylacetylene
883.6	27.3	1.78	0.00	526.18	0.00	--	0.00	0.00	0.00
943.9	27.4	1.81	0.07	526.28	0.00	5.32	0.00	0.00	0.00
1043.9	27.8	1.71	0.45	521.64	0.00	--	1.33	0.00	2.41
1095.3	28.1	1.74	0.98	511.51	0.00	4.95	2.59	0.00	9.08
1099.5	26.3	1.82	0.68	516.05	0.00	4.60	2.78	0.00	8.82
1158.6	27.9	1.85	0.74	500.72	0.06	4.09	4.98	0.06	19.35
1220.0	28.1	1.89	1.78	501.42	0.11	2.11	7.80	0.34	27.61
1291.2	28.2	1.93	3.59	494.69	0.27	0.67	9.44	0.70	33.70
1382.2	30.5	1.79	3.61	474.49	0.97	0.15	10.38	0.86	26.40
1337.1	25.9	1.75	3.82	476.61	0.64	0.20	10.24	0.93	29.82
1417.9	28.3	1.83	4.03	493.02	1.75	0.16	11.80	1.17	29.93
1421.9	26.9	1.76	3.92	488.98	2.19	0.13	10.67	0.89	25.03
1519.2	26.9	1.58	2.87	492.32	21.55	0.16	8.76	0.00	9.38
1038.7	29.4	1.77	0.00	516.07	0.00	4.91	0.00	0.00	0.00
1568.0	24.9	1.53	1.28	474.62	53.82	0.15	2.58	0.00	2.09
1804.1	26.6	1.33	0.00	292.00	91.61	0.05	0.07	0.00	0.00
1752.2	26.3	1.30	0.00	348.71	90.48	0.04	0.14	0.00	0.00
1664.7	26.9	1.46	0.63	458.67	72.52	0.10	0.91	0.00	0.32
1422.0	23.8	1.68	3.75	494.46	1.90	0.08	11.99	1.18	26.01
1524.7	29.1	1.50	3.41	492.20	19.86	0.20	8.35	0.00	8.80
1487.6	25.4	1.77	4.08	495.40	5.47	0.15	10.53	0.45	17.45
1610.4	27.9	1.38	0.90	474.62	62.78	0.15	1.81	0.00	0.42
1675.3	26.4	1.34	0.00	436.63	81.80	0.16	0.33	0.00	0.00

triacetylene	phenyl iodide	naphthalene	biphenyl	diphenylethyne	acenaphthylene	phenanthrene
0.00	52.86	0.00	0.00	0.00	0.00	0.00
0.00	53.37	0.00	0.00	0.00	0.00	0.00
0.00	50.24	0.36	0.03	0.00	0.00	0.11
0.00	41.26	0.36	0.28	0.28	0.00	0.10
0.00	37.70	0.38	0.37	0.29	0.00	0.21
0.47	26.25	0.41	0.41	1.10	0.00	0.25
1.35	9.12	0.21	0.83	1.63	0.06	1.00
2.90	0.95	0.19	1.74	1.38	0.14	1.08
3.65	0.23	0.23	3.10	1.14	0.37	1.48
4.23	0.38	0.15	3.07	1.43	0.30	1.54
5.24	1.00	0.31	3.30	0.80	0.40	1.02
4.57	0.14	0.09	3.32	0.68	0.57	1.16
5.81	0.53	0.40	1.20	0.11	1.29	0.58
0.00	50.04	0.00	0.00	0.00	0.00	0.00
21.05	0.08	0.08	0.28	0.00	0.63	0.34
76.54	0.00	0.00	0.00	0.00	0.00	0.00
68.33	0.00	0.00	0.00	0.00	0.00	0.00
33.45	0.00	0.00	0.23	0.00	0.17	0.02
5.51	2.19	0.16	4.42	1.28	0.71	1.63
4.80	0.12	0.50	1.10	0.10	1.35	0.69
1.84	0.11	0.27	3.17	0.62	1.06	1.62
27.55	0.04	0.04	0.13	0.00	0.36	0.11
41.66	0.00	0.00	0.00	0.00	0.00	0.00

$C_{12}H_8$ (biphenylene)
uB3LYP/6311+G(d,p) = -462.14241518 CCSD(T)/cc-pVDZ = -460.7210519
ZPVE = 0.157647

1	6	0.000000	0.694048	3.118938
2	6	0.000000	1.443263	1.913795
3	6	0.000000	0.710937	0.754478
4	6	0.000000	-0.710937	0.754478
5	6	0.000000	-1.443263	1.913795
6	6	0.000000	-0.694048	3.118938
7	1	0.000000	1.221005	4.066572
8	1	0.000000	2.526795	1.934277
9	1	0.000000	-2.526795	1.934277
10	1	0.000000	-1.221005	4.066572
11	6	0.000000	0.710937	-0.754478
12	6	0.000000	1.443263	-1.913795
13	6	0.000000	0.694048	-3.118938
14	6	0.000000	-0.694048	-3.118938
15	6	0.000000	-1.443263	-1.913795
16	6	0.000000	-0.710937	-0.754478
17	1	0.000000	2.526795	-1.934277
18	1	0.000000	1.221005	-4.066572
19	1	0.000000	-1.221005	-4.066572
20	1	0.000000	-2.526795	-1.934277

TS1
uB3LYP/6311+G(d,p) = -462.02138346 CCSD(T)/cc-pVDZ = -460.5962994
ZPVE = 0.152486 Imaginary Vibration = 482.02*i*

1	6	-3.016268	0.635618	-0.323358
2	6	-1.850640	1.319472	-0.591777
3	6	-0.640880	0.719214	-0.160416
4	6	-0.640841	-0.719194	0.160522
5	6	-1.850613	-1.319464	0.591792
6	6	-3.016247	-0.635662	0.323230
7	1	-3.968288	1.091370	-0.570540
8	1	-1.860156	2.309312	-1.032147
9	1	-1.860138	-2.309281	1.032214
10	1	-3.968263	-1.091467	0.570335
11	6	0.635791	1.117772	0.081088
12	6	1.822246	1.406223	0.571751
13	6	3.034366	0.631860	0.233575
14	6	3.034309	-0.631978	-0.233814
15	6	1.822082	-1.406290	-0.571658
16	6	0.635854	-1.117527	-0.080856
17	1	1.935395	2.203237	1.307823
18	1	3.985815	1.113195	0.433165
19	1	3.985712	-1.113345	-0.433546
20	1	1.934968	-2.203291	-1.307776

C_6H_4oct
uB3LYP/6311+G(d,p) = -462.02711048 CCSD(T)/cc-pVDZ = -460.6030743
ZPVE = 0.15346

1	6	-2.959467	0.598698	-0.404173
2	6	-1.809415	1.251894	-0.729365
3	6	-0.573417	0.735358	-0.201041
4	6	-0.573195	-0.735304	0.200755
5	6	-1.808981	-1.252032	0.729387
6	6	-2.959234	-0.599036	0.404482
7	1	-3.913372	1.005273	-0.720779
8	1	-1.820220	2.186221	-1.278219
9	1	-1.819483	-2.186342	1.278275
10	1	-3.912974	-1.005798	0.721350
11	6	0.578952	1.295979	0.137001
12	6	1.781571	1.390391	0.673153
13	6	2.963810	0.623803	0.263916
14	6	2.963986	-0.623513	-0.263507
15	6	1.782047	-1.390467	-0.673196
16	6	0.579183	-1.295758	-0.137648
17	1	1.907722	2.019684	1.555463
18	1	3.926929	1.072151	0.490887
19	1	3.927273	-1.071737	-0.490028
20	1	1.909082	-2.019520	-1.555543

TS2
uB3LYP/6311+G(d,p) = -462.00187391 CCSD(T)/cc-pVDZ = -460.5805575
ZPVE = 0.151961 Imaginary Vibration = 397.32*i*

1	6	2.006645	-1.315188	-0.393384
2	6	0.689337	-0.806032	-0.200451
3	6	0.522713	0.631770	0.078194
4	6	1.670777	1.421207	0.362632
5	6	2.915861	0.857581	0.238329
6	6	3.084946	-0.506127	-0.147735
7	1	2.133059	-2.352556	-0.679307
8	1	1.554666	2.467417	0.619314
9	1	3.796433	1.468107	0.403932
10	1	4.089715	-0.901842	-0.243092
11	6	-0.802300	0.978755	0.018313
12	6	-1.542605	-1.080174	0.594582
13	6	-0.526784	-1.465305	-0.226265
14	6	-1.968258	1.326393	-0.492725
15	6	-3.155075	0.502830	-0.203379
16	6	-2.946200	-0.738424	0.271512
17	1	-2.041177	2.103716	-1.252895
18	1	-4.146091	0.877411	-0.434494
19	1	-3.762848	-1.408058	0.519583
20	1	-1.318090	-1.097916	1.669219

BENZOHyl

uB3LYP/6311+G(d,p) = -462.04748396 CCSD(T)/cc-pVDZ = -460.6301156

ZPVE = 0.154793

1	6	2.130585	-1.284735	-0.201461
2	6	0.790716	-0.886595	-0.037618
3	6	0.474554	0.500589	0.160830
4	6	1.487778	1.460371	0.167889
5	6	2.804318	1.032768	0.012280
6	6	3.130567	-0.324877	-0.161609
7	1	2.357645	-2.332871	-0.360092
8	1	1.265008	2.512865	0.302244
9	1	3.603055	1.767026	0.021292
10	1	4.169082	-0.610774	-0.281091
11	6	-0.964412	0.581525	0.269480
12	6	-1.474033	-0.835060	0.434511
13	6	-0.377218	-1.733123	-0.109852
14	6	-1.973983	1.368093	-0.179988
15	6	-3.178039	0.542475	-0.319696
16	6	-2.898882	-0.751716	-0.035465
17	1	-1.894009	2.390627	-0.527641
18	1	-4.141234	0.925721	-0.632843
19	1	-3.597297	-1.577021	-0.029049
20	1	-1.473956	-1.093865	1.511362

TS3

uB3LYP/6311+G(d,p) = -462.02685084 CCSD(T)/cc-pVDZ = -460.6118569

ZPVE = 0.151556 Imaginary Vibration = 1071.89*i*

1	6	2.144092	-1.277891	-0.063324
2	6	0.818188	-0.875321	-0.016904
3	6	0.493413	0.514871	0.040046
4	6	1.496661	1.472880	0.057528
5	6	2.832861	1.047642	0.004825
6	6	3.155864	-0.305514	-0.055687
7	1	2.384545	-2.333738	-0.113437
8	1	1.263985	2.530663	0.112973
9	1	3.626204	1.787018	0.011947
10	1	4.195947	-0.607870	-0.098973
11	6	-0.962366	0.593569	0.080566
12	6	-1.437338	-0.819264	0.080782
13	6	-0.389278	-1.768147	-0.073306
14	6	-2.040894	1.394737	-0.040700
15	6	-3.259398	0.532041	-0.091439
16	6	-2.923883	-0.772784	-0.021750
17	1	-2.064711	2.472627	-0.139435
18	1	-4.263489	0.922707	-0.192242
19	1	-3.581251	-1.629078	-0.038983
20	1	-1.128766	-1.563254	1.054337

BENZO (cyclopenta[a]indene, benzopentalene)
uB3LYP/6311+G(d,p) = -462.15099539 CCSD(T)/cc-pVDZ = -460.7348812
ZPVE = 0.157159

1	6	3.118938	0.694048	0.000000
2	6	1.913795	1.443263	0.000000
3	6	0.754478	0.710937	0.000000
4	6	0.754478	-0.710937	0.000000
5	6	1.913795	-1.443263	0.000000
6	6	3.118938	-0.694048	0.000000
7	1	4.066572	1.221005	0.000000
8	1	1.934277	2.526795	0.000000
9	1	1.934277	-2.526795	0.000000
10	1	4.066572	-1.221005	0.000000
11	6	-0.754478	0.710937	0.000000
12	6	-1.913795	1.443263	0.000000
13	6	-3.118938	0.694048	0.000000
14	6	-3.118938	-0.694048	0.000000
15	6	-1.913795	-1.443263	0.000000
16	6	-0.754478	-0.710937	0.000000
17	1	-1.934277	2.526795	0.000000
18	1	-4.066572	1.221005	0.000000
19	1	-4.066572	-1.221005	0.000000
20	1	-1.934277	-2.526795	0.000000

APPENDIX B

CHEMICAL KINETIC MODEL FOR PHENYL PYROLYSIS AND PHENYL + ACETYLENE REACTIONS

Model includes the reaction mechanism in CHEMKIN format
Reaction rate expressed as $k=AT^{n}exp(-Ea/RT)$
Elementary reactions followed by corresponding reaction parameters A, n and Ea in cgs units (s, mol, cc, cal).

```
!
!UIC_phenyl-phenyl+acetylene_model
!
!A. Comandini, T. Malewicki, and K. Brezinsky, "Chemistry of PAHs Formation from Phenyl Radical
!Pyrolysis nd Phenyl + Acetylene Reaction"
!
!****************************************************************************
!
 !Reference sources can be found at the end of the file.
!
!****************************************************************************

ELEMENTS

 H  C  I  AR

END

SPECIES

AR

H       H2      I       HI      I2

C       CH      CH2     CH2*    CH3     CH4

C2H     C2H2    H2CC    C2H6    C2H5    C2H4    C2H3

C4      C4H2    C4H     nC4H3   iC4H3   iC4H5   nC4H5   C4H4    C4H6

C6H2    C6H     C6H3    c-C6H3  z-C6H4  o-C6H4  m-C6H4  p-C6H4  C6H5I   C6H5    C6H6

C8H2    C8H6    C6H5CHCH        C6H4C2H

C10H7-1         C10H7-2         C10H8   BICYCLO

o-C12H9I        m-C12H9I        p-C12H9I

C12H8           C12H10          o-C12H9         m-C12H9         p-C12H9         C6H5C6H3

BENZO           BIPHENH         C6H4oct         BENZOHyl        C6H4oct         BENZOH
C6H5CHC5H4

A2R5            A2R5J1          A2R5J3          A2R5J4          A2R5J5          A2R5YNE1
A2R5YNE3        A2R5YNE4        A2R5YNE5
```

A2R5YN1J2 A2R5YN4J5 A2R5YN5J4 A2R5YN3J4 A2R5YN4J3 A3R5J7
A3LR5JS A3R5J10 A3LR5

PHEN DPE PHENH A3J1 A3J2 A3J4 A3J9 A3R5

A3C2H-2 A3C2H-2JS A3C2H-1 A3C2H-1JP

o-TERPH m-TERPH p-TERPH

PYRENE TRIPH BBFLUOR BGHIF FLTHNJ7 FLTHN
CHRYSENJ1 CHRYSENJ4 CHRYSEN

!
!InChI identifiers
!InChI (IUPAC International Chemical Identifier) is a standard nomenclature for chemical species which !facilitates the identification of the species and the development of comprehensive databases of chemical !species and reactions (Stephen E. Stein, Stephen R. Heller, and Dmitrii Tchekhovskoi, *An Open Standard for* !*Chemical Structure Representation: The IUPAC Chemical Identifier*, in Proceedings of the 2003 International !Chemical Information Conference (Nimes), Infonortics, pp. 131-143.). More information is available on the !IUPAC website.
!
!AR: InChI=1S/H
!C: InChI=1S/C
!H: InChI=1S/H
!I: InChI=1S/I
!H2: InChI=1S/H2/h1H
!HI: InChI=1S/HI/h1H
!I2: InChI=1S/I2/c1-2
!CH: InChI=1S/CH/h1H
!CH2: InChI=1S/CH2/h1H2
!CH2*: InChI=1S/CH2/h1H2
!CH3: InChI=1S/CH3/h1H3
!CH4: InChI=1S/CH4/h1H4
!C2H: InChI=1S/C2H/c1-2/h1H
!H2CC: InChI=1S/C2H2/c1-2/h1H2
!C2H2: InChI=1S/C2H2/c1-2/h1-2H
!C2H3: InChI=1S/C2H3/c1-2/h1H,2H2
!C2H4: InChI=1S/C2H4/c1-2/h1-2H2
!C2H5: InChI=1S/C2H5/c1-2/h1H2,2H3
!C2H6: InChI=1S/C2H6/c1-2/h1-2H3
!C4: InChI=1S/C4/c1-3-4-2
!C4H: InChI=1S/C4H/c1-3-4-2/h1H
!C4H2: InChI=1S/C4H2/c1-3-4-2/h1-2H
!n-C4H3: InChI=1S/C4H3/c1-3-4-2/h1-3H
!i-C4H3: InChI=1S/C4H3/c1-3-4-2/h1H,2H2
!C4H4: InChI=1S/C4H4/c1-3-4-2/h1,4H,2H2
!n-C4H5: InChI=1S/C4H5/c1-3-4-2/h1,3-4H,2H2
!i-C4H5: InChI=1S/C4H5/c1-3-4-2/h3H,1-2H2
!C4H6: InChI=1S/C4H6/c1-3-4-2/h3-4H,1-2H2
!C6H: InChI=1S/C6H/c1-3-5-6-4-2/h1H
!C6H2: InChI=1S/C6H2/c1-3-5-6-4-2/h1-2H
!C6H3: InChI=1S/C6H3/c1-3-5-6-4-2/h1-3H
!c-C6H3: InChI=1S/C6H3/c1-2-4-6-5-3-1/h1-3H
!C8H2: InChI=1S/C8H2/c1-3-5-7-8-6-4-2/h1-2H
!z-C6H4: InChI=1S/C6H4/c1-3-5-6-4-2/h1-2,5-6H/b6-5-

!o-C6H4: InChI=1S/C6H4/c1-2-4-6-5-3-1/h1-4H
!m-C6H4: InChI=1S/C6H4/c1-2-4-6-5-3-1/h1-3,6H
!p-C6H4: InChI=1S/C6H4/c1-2-4-6-5-3-1/h1-2,5-6H
!C6H5: InChI=1S/C6H5/c1-2-4-6-5-3-1/h1-5H
!C6H6: InChI=1S/C6H6/c1-2-4-6-5-3-1/h1-6H
!C6H5I: InChI=1S/C6H5I/c7-6-4-2-1-3-5-6/h1-5H
!C6H4C2H: InChI=1S/C8H5/c1-2-8-6-4-3-5-7-8/h1,3-6H
!C6H5CHCH: InChI=1S/C8H7/c1-2-8-6-4-3-5-7-8/h1-7H
!C6H4CHCH2: InChI=1S/C8H7/c1-2-8-6-4-3-5-7-8/h2-6H,1H2
!C8H6: InChI=1S/C8H6/c1-2-8-6-4-3-5-7-8/h1,3-7H
!C10H7-1: InChI=1S/C10H7/c1-2-6-10-8-4-3-7-9(10)5-1/h1-7H
!C10H7-2: InChI=1S/C10H7/c1-2-6-10-8-4-3-7-9(10)5-1/h1-3,5-8H
!C10H8: InChI=1S/C10H8/c1-2-6-10-8-4-3-7-9(10)5-1/h1-8H
!C12H8: InChI=1S/C12H8/c1-2-6-10-9(5-1)11-7-3-4-8-12(10)11/h1-8H
!C12H10: InChI=1S/C12H10/c1-3-7-11(8-4-1)12-9-5-2-6-10-12/h1-10H
!o-C12H9: InChI=1S/C12H9/c1-3-7-11(8-4-1)12-9-5-2-6-10-12/h1-9H
!m-C12H9: InChI=1S/C12H9/c1-3-7-11(8-4-1)12-9-5-2-6-10-12/h1-5,7-10H
!p-C12H9: InChI=1S/C12H9/c1-3-7-11(8-4-1)12-9-5-2-6-10-12/h1,3-10H
!C6H5C6H3: InChI=1S/C12H8/c1-3-7-11(8-4-1)12-9-5-2-6-10-12/h1-5,7-9H
!o-C12H9I: InChI=1S/C12H9I/c13-12-9-5-4-8-11(12)10-6-2-1-3-7-10/h1-9H
!m-C12H9I: InChI=1S/C12H9I/c13-12-8-4-7-11(9-12)10-5-2-1-3-6-10/h1-9H
!p-C12H9I: InChI=1S/C12H9I/c13-12-8-6-11(7-9-12)10-4-2-1-3-5-10/h1-9H
!BENZO: InChI=1S/C12H8/c1-2-6-11-9(4-1)8-10-5-3-7-12(10)11/h1-8H
!BENZOH: InChI=1S/C12H9/c1-2-6-11-9(4-1)8-10-5-3-7-12(10)11/h1-8,10H
!BENZOHyl: InChI=1S/C12H8/c1-2-6-11-9(4-1)8-10-5-3-7-12(10)11/h1-7,10H
!BIPHENH: InChI=1S/C12H9/c1-2-6-10-9(5-1)11-7-3-4-8-12(10)11/h1-9H
!C6H5CHC5H4: InChI=1S/C12H10/c1-2-6-11(7-3-1)10-12-8-4-5-9-12/h1-10H
!C6H4oct: InChI=1S/C12H8/c1-2-4-8-12-10-6-5-9-11(12)7-3-1/h1-6,9-10H/b2-1-
!A2R5: InChI=1S/C12H8/c1-3-9-4-2-6-11-8-7-10(5-1)12(9)11/h1-8H
!A2R5J1: InChI=1S/C12H7/c1-3-9-4-2-6-11-8-7-10(5-1)12(9)11/h1-7H
!A2R5J3: InChI=1S/C12H7/c1-3-9-4-2-6-11-8-7-10(5-1)12(9)11/h1-5,7-8H
!A2R5J4: InChI=1S/C12H7/c1-3-9-4-2-6-11-8-7-10(5-1)12(9)11/h1,3-8H
!A2R5J5: InChI=1S/C12H7/c1-3-9-4-2-6-11-8-7-10(5-1)12(9)11/h1-3,5-8H
!BICYCLO: InChI=1S/C12H10/c1-2-4-12-10-7-5-9(6-8-10)11(12)3-1/h1-10H
!PHEN: InChI=1S/C14H10/c1-3-7-13-11(5-1)9-10-12-6-2-4-8-14(12)13/h1-10H
!DPE: InChI=1S/C14H10/c1-3-7-13(8-4-1)11-12-14-9-5-2-6-10-14/h1-10H
!A3J1: InChI=1S/C14H9/c1-3-7-13-11(5-1)9-10-12-6-2-4-8-14(12)13/h1-5,7-10H
!A3J2: InChI=1S/C14H9/c1-3-7-13-11(5-1)9-10-12-6-2-4-8-14(12)13/h1,3-10H
!A3J4: InChI=1S/C14H9/c1-3-7-13-11(5-1)9-10-12-6-2-4-8-14(12)13/h1-7,9-10H
!A3J9: InChI=1S/C14H9/c1-3-7-13-11(5-1)9-10-12-6-2-4-8-14(12)13/h1-9H
!PHENH: InChI=1S/C14H12/c1-3-7-13-11(5-1)9-10-12-6-2-4-8-14(12)13/h1-12H
!A2R5YN4J5: InChI=1S/C14H7/c1-2-10-8-12-5-3-4-11-6-7-13(9-10)14(11)12/h1,3-7,9H
!A2R5YN5J4: InChI=1S/C14H7/c1-2-10-6-7-12-9-8-11-4-3-5-13(10)14(11)12/h1,3-5,7-9H
!A2R5YN3J4: InChI=1S/C14H7/c1-2-10-6-7-11-4-3-5-12-8-9-13(10)14(11)12/h1,3-5,7-9H
!A2R5YN4J3: InChI=1S/C14H7/c1-2-10-8-12-5-3-4-11-6-7-13(9-10)14(11)12/h1,3-8H
!A2R5YN1J2: InChI=1S/C14H7/c1-2-10-9-12-7-3-5-11-6-4-8-13(10)14(11)12/h1,3-8H
!A2R5YNE1: InChI=1S/C14H8/c1-2-10-9-12-7-3-5-11-6-4-8-13(10)14(11)12/h1,3-9H
!A2R5YNE3: InChI=1S/C14H8/c1-2-10-6-7-11-4-3-5-12-8-9-13(10)14(11)12/h1,3-9H
!A2R5YNE4: InChI=1S/C14H8/c1-2-10-8-12-5-3-4-11-6-7-13(9-10)14(11)12/h1,3-9H
!A2R5YNE5: InChI=1S/C14H8/c1-2-10-6-7-12-9-8-11-4-3-5-13(10)14(11)12/h1,3-9H
!A3C2H-1: InChI=1S/C16H10/c1-2-12-7-5-9-16-14-8-4-3-6-13(14)10-11-15(12)16/h1,3-11H
!A3C2H-2: InChI=1S/C16H10/c1-2-12-7-10-16-14(11-12)9-8-13-5-3-4-6-15(13)16/h1,3-11H
!PYRENE: InChI=1S/C16H10/c1-3-11-7-9-13-5-2-6-14-10-8-12(4-1)15(11)16(13)14/h1-10H
!A3R5: InChI=1S/C16H10/c1-2-6-14-12(4-1)10-13-9-8-11-5-3-7-15(14)16(11)13/h1-10H
!A3LR5: InChI=1S/C16H10/c1-2-7-14-12(4-1)10-13-6-3-5-11-8-9-15(14)16(11)13/h1-10H
!A3R5J7: InChI=1S/C16H9/c1-2-6-14-12(4-1)10-13-9-8-11-5-3-7-15(14)16(11)13/h1-3,5-10H

!A3LR5JS: InChI=1S/C16H9/c1-2-7-14-12(4-1)10-13-6-3-5-11-8-9-15(14)16(11)13/h1-6,8-10H
!A3R5J10: InChI=1S/C16H9/c1-2-6-14-12(4-1)10-13-9-8-11-5-3-7-15(14)16(11)13/h1-5,7-10H
!A3C2H-2JS: InChI=1S/C16H9/c1-2-12-7-10-16-14(11-12)9-8-13-5-3-4-6-15(13)16/h1,3-10H
!A3C2H-1JP: InChI=1S/C16H9/c1-2-12-7-5-9-16-14-8-4-3-6-13(14)10-11-15(12)16/h1,3-6,8-11H
!FLTHN: InChI=1S/C16H10/c1-2-8-13-12(7-1)14-9-3-5-11-6-4-10-15(13)16(11)14/h1-10H
!FLTHNJ7: InChI=1S/C16H9/c1-2-8-13-12(7-1)14-9-3-5-11-6-4-10-15(13)16(11)14/h1-7,9-10H
!CHRYSENJ1: InChI=1S/C18H11/c1-3-7-15-13(5-1)9-11-18-16-8-4-2-6-14(16)10-12-17(15)18/h1-5,7-12H
!CHRYSENJ4: InChI=1S/C18H11/c1-3-7-15-13(5-1)9-11-18-16-8-4-2-6-14(16)10-12-17(15)18/h1-7,9-12H
!o-TERPH: InChI=1S/C18H14/c1-3-9-15(10-4-1)17-13-7-8-14-18(17)16-11-5-2-6-12-16/h1-14H
!m-TERPH: InChI=1S/C18H14/c1-3-8-15(9-4-1)17-12-7-13-18(14-17)16-10-5-2-6-11-16/h1-14H
!p-TERPH: InChI=1S/C18H14/c1-3-7-15(8-4-1)17-11-13-18(14-12-17)16-9-5-2-6-10-16/h1-14H
!TRIPH: InChI=1S/C18H12/c1-2-8-14-13(7-1)15-9-3-4-11-17(15)18-12-6-5-10-16(14)18/h1-12H
!BGHIF: InChI=1/C18H10/c1-3-11-7-9-13-10-8-12-4-2-6-15-14(5-1)16(11)18(13)17(12)15/h1-10H
!CHRYSEN: InChI=1S/C18H12/c1-3-7-15-13(5-1)9-11-18-16-8-4-2-6-14(16)10-12-17(15)18/h1-12H
!BBFLUOR:InChI=1S/C20H12/c1-2-7-14-13(6-1)12-19-16-9-4-3-8-15(16)18-11-5-10-17(14)20(18)19/h1-12H
!

! SPECIES FOR ACETONE DECOMPOSITION SUBMECHANISM

CH3COCH3 CH3CO CH3COCH2 CH2CO CO C6H5CH3

CH3CHCH C3H5 C5H7 c-C5H6 C3H4 ALLENE C3H6 C5H8 C3H3

!
!InChI identifiers
!
!CO: InChI=1S/CO/c1-2
!CH3COCH3: InChI=1S/C3H6O/c1-3(2)4/h1-2H3
!CH3CO: InChI=1S/C2H3O/c1-2-3/h1H3
!CH3COCH2: InChI=1S/C3H5O/c1-3(2)4/h1H2,2H3
!CH2CO: InChI=1S/C2H2O/c1-2-3/h1H2
!C6H5CH3: InChI=1S/C7H8/c1-7-5-3-2-4-6-7/h2-6H,1H3
!CH3CHCH: InChI=1S/C3H5/c1-3-2/h1,3H,2H3
!C3H5: InChI=1S/C3H5/c1-3-2/h3H,1-2H2
!C5H7: InChI=1S/C5H7/c1-3-5-4-2/h1,3-4H,2,5H2
!c-C5H6: InChI=1S/C5H6/c1-2-4-5-3-1/h1-4H,5H2
!C3H4: InChI=1S/C3H4/c1-3-2/h1H,2H3
!ALLENE: InChI=1S/C3H4/c1-3-2/h1-2H2
!C3H6: InChI=1S/C3H6/c1-3-2/h3H,1H2,2H3
!C5H8: InChI=1S/C5H8/c1-3-5-4-2/h3-4H,1-2,5H2
!C3H3: InChI=1S/C3H3/c1-3-2/h1H,2H2
!

END

REACTIONS

! IODO-COMPOUNDS

C6H5I => C6H5+I 1.374E+15 0.00 64406 !Michael kinf
C6H5+I => C6H5I 1.00E+13 0.00 0.00 !estimated
C6H5I = o-C6H4+HI 8.244E+13 0.00 64406 !0.06*rate of C6H5I = C6H5+I
C6H5I+H = C6H5+HI 8.73E+05 2.35 -37.3 !08GAO/MAR rate, n factor decreased within the exp. error

C6H5+HI = C6H6+I	3.00E+12	0.00	0	!estimated
C6H5I+C6H5 = C12H10+I	2.00E+12	0.00	11000	!09GIR/OLZ
C6H5+C6H5I = o-C12H9I+H	3.183E+11	0.00	4305	!99PAR/LIN As 2/6 of C6H5+C6H6 = c12h10+H
C6H5+C6H5I = m-C12H9I+H	3.183E+11	0.00	4305	!99PAR/LIN As 2/6 of C6H5+C6H6 = c12h10+H
C6H5+C6H5I = p-C12H9I+H	1.592E+11	0.00	4305	!99PAR/LIN As 1/6 of C6H5+C6H6 = c12h10+H
o-C12H9+I => o-C12H9I	1.00E+13	0.00	0	!estimated
m-C12H9+I => m-C12H9I	1.00E+13	0.00	0	!estimated
p-C12H9+I => p-C12H9I	1.00E+13	0.00	0	!estimated
o-C12H9I => o-C12H9+I	1.374E+15	0.00	64406	!P.W. as C6H5I => C6H5+I
m-C12H9I => m-C12H9+I	1.374E+15	0.00	64406	!P.W. as C6H5I => C6H5+I
p-C12H9I => p-C12H9+I	1.374E+15	0.00	64406	!P.W. as C6H5I => C6H5+I
H+I2 = HI+I	4.31E+14	0.00	431	!81BAU/DUX
I+I = I2	2.36E+14	0.00	-1498	!81BAU/DUX
I+H+AR = HI+AR	2.00E+21	-1.87	0	!81BAU/DUX
H+HI = H2+I	3.98E+13	0.00	0	!10TRA/KLI 09GIR/OLZ

! BIPHENYL and BENZENE

C6H5+C6H5 = C12H10	1.545E+12	0.036	-1702	!10TRA/KLI, 100atm/2
C6H5+C6H5 = o-C6H4+C6H6	8.52E-04	4.57	-5735	!10TRA/KLI, HP-LIMIT/2
C6H5+C6H5 = m-C6H4+C6H6	8.52E-04	4.57	-5735	!10TRA/KLI, HP-LIMIT/2
C6H5+C6H5 = p-C6H4+C6H6	4.26E-04	4.57	-5735	!10TRA/KLI, HP-LIMIT/2
o-C6H4 = m-C6H4	2.12E+14	0.00	73489.5	!99MOS/MAD
m-C6H4 = p-C6H4	2.83E+14	0.00	63045.7	!99MOS/MAD
p-C6H4 = z-C6H4	1.00E+13	0.00	17800	!99MOS/MAD, estimated P.W.
o-C6H4+C6H5 = o-C12H9	1.00E+13	0.00	3720	!estimated P.W.
m-C6H4+C6H5 => m-C12H9	1.00E+13	0.00	3720	!estimated P.W.
p-C6H4+C6H5 => p-C12H9	1.00E+13	0.00	3720	!estimated P.W.
m-C12H9 => m-C6H4+C6H5	2.223E+15	0.00	87232	!as reverse of o-C6H4+C6H5 = C12H9-1
p-C12H9 => p-C6H4+C6H5	2.223E+15	0.00	87232	!as reverse of o-C6H4+C6H5 = C12H9-1
o-C12H9+H2 = C12H10+H	5.707E+04	2.430	6273	!97MEB/LIN as C6H5+H2 = C6H6+H
m-C12H9+H2 = C12H10+H	5.707E+04	2.430	6273	!97MEB/LIN as C6H5+H2 = C6H6+H
p-C12H9+H2 = C12H10+H	5.707E+04	2.430	6273	!97MEB/LIN as C6H5+H2 = C6H6+H
o-C12H9+H = C12H10	4.27E+13	0.338	-158	!10TRA/KLI
m-C12H9+H = C12H10	1.25E+13	0.284	-155	!10TRA/KLI
p-C12H9+H = C12H10	2.78E+13	0.185	15.3	!10TRA/KLI
C6H6+C6H5 = C12H10+H	9.55E+11	0.00	4305	!99PAR/LIN
o-C12H9+H => C6H5C6H3+H2	2.000E+11	1.100	24500	!01MEB/LIN (JETSURF) as C6H5+H = o-C6H4+H2

C6H5C6H3+H2 => o-C12H9+H 5.707E+04 2.430 6273 !97MEB/LIN as C6H5+H2 = C6H6+H
o-C12H9 => C6H5C6H3+H 4.30E+12 0.62 77300 !C6H5 = o-C6H4+H HPlim
C6H5C6H3+H => o-C12H9 1.00E+14 0.00 3720 !estimated P.W.
C6H5+c-C6H3 = C6H5C6H3 1.00E+13 0.00 0 !estimated P.W.
C6H5+H(+M) = C6H6(+M) 1.00E+14 0.00 0 !97WAN/FRE
LOW / 6.6E+75 -16.3 7000 / !
TROE / 1.0 0.1 585 6113 / !
C6H6+H = C6H5+H2 4.00E+15 0.00 20776 !XU *2

! TERPHENYLS and 4-RING SPECIES (TRIPH)

C12H10+C6H5 = o-TERPH+H 6.367E+11 0.00 4305 !99PAR/LIN As 4/6 of C6H5+C6H6 = c12h10+H
C12H10+C6H5 = m-TERPH+H 6.367E+11 0.00 4305 !99PAR/LIN As 4/6 of C6H5+C6H6 = c12h10+H
C12H10+C6H5 = p-TERPH+H 3.183E+11 0.00 4305 !99PAR/LIN As 2/6 of C6H5+C6H6 = c12h10+H
o-C12H9+C6H5 => o-TERPH 1.00E+13 0.00 0 !estimated
m-C12H9+C6H5 => m-TERPH 1.00E+13 0.00 0 !estimated
p-C12H9+C6H5 => p-TERPH 1.00E+13 0.00 0 !estimated
o-TERPH => o-C12H9+C6H5 2.92E+15 0.00 109812 !as inverse of C6H5+C6H5=C12H10
m-TERPH => m-C12H9+C6H5 2.92E+15 0.00 109812 !as inverse of C6H5+C6H5=C12H10
p-TERPH => p-C12H9+C6H5 2.92E+15 0.00 109812 !as inverse of C6H5+C6H5=C12H1
o-TERPH = TRIPH+H2 1.50E+15 0.00 84700 !estimated, from 10ZHA/CAI
o-C12H9+o-C6H4 = TRIPH+H 1.00E+14 0.00 38000 !estimated, as BIPHENH=>C12H8+H
C12H8+o-C6H4 = TRIPH 4.96E+09 0.827 -1370 !as 10TRA/KLI for o-C6H4+o-C6H4 = C12H8, J Am Chem Soc 89:5, 1967

! ACENAPHTHYLENE/BENZOPENTALENE and BIPHENYLENE

o-C6H4+o-C6H4 = C12H8	4.96E+09	0.827	-1370	!10TRA/KLI
o-C12H9 => BIPHENH	5.00E+12	0.00	31056	!11SHU/KOS, P.W.
BIPHENH => o-C12H9	3.00E+13	0.00	19350	!11SHU/KOS, P.W.
BIPHENH => C12H8+H	5.00E+13	0.00	38223	!11SHU/KOS, P.W.
C12H8+H => BIPHENH	4.00E+14	0.00	5972	!11SHU/KOS, P.W.
BIPHENH => BENZOH	1.00E+13	0.00	31056	!11SHU/KOS, P.W.
BENZOH => BIPHENH	1.00E+13	0.00	46345	!11SHU/KOS, P.W.
BENZOH => BENZO+H	5.00E+13	0.00	41567	!11SHU/KOS, P.W.
BENZO+H => BENZOH	1.00E+14	0.00	1911	!11SHU/KOS, P.W.
BENZOH => A2R5+H	1.00E+13	0.00	44673	!11SHU/KOS, P.W.
C12H10 => C6H5CHC5H4	1.00E+14	0.00	109412	!11SHU/KOS, P.W.
C6H5CHC5H4 => C12H10	1.00E+13	0.00	76445	!11SHU/KOS, P.W.
C6H5CHC5H4 => BENZO+H2	5.00E+13	0.00	56617	!11SHU/KOS, P.W.
C6H5CHC5H4 => A2R5+H2	5.00E+13	0.00	60917	!11SHU/KOS, P.W.
C12H8 => C6H4oct	6.152E+14	0.00	77387.6	!P.W.
C6H4oct => C12H8	7.482E+12	0.00	4059.6	!P.W.
C6H4oct => BENZOHyl	1.205E+13	0.00	13712.9	!P.W.
BENZOHyl => C6H4oct	5.321E+13	0.00	31139.8	!P.W.
BENZOHyl => BENZO	1.941E+13	0.00	10615.0	!P.W.

BENZO => BENZOHyl	4.188E+13	0.00	75265.9	!P.W.
BENZO => C6H5C6H3	2.404E+14	0.00	85220.5	!03BLA/JON, calculated
C6H5C6H3 => BENZO	4.093E+12	0.00	45643.7	!03BLA/JON, calculated
! BENZO => A2R5	2.704E+14	0.00	87113.6	!03BLA/JON, calculated
BENZO => A2R5	4.699E+14	0.00	77831.2	!P.W.
C10H7-1+C2H2 = A2R5+H	1.87E+07	1.787	3262	!01RIC/MAZ HP-Limit
A2R5+H = A2R5J1+H2	3.23E+07	2.095	19800	!MIT
A2R5+H = A2R5J3+H2	3.23E+07	2.095	15842	!MIT
A2R5+H = A2R5J4+H2	3.23E+07	2.095	15842	!MIT
A2R5+H = A2R5J5+H2	3.23E+07	2.095	15842	!MIT
A2R5J1+H = A2R5	1.26E+20	-1.81	2900	!MIT
A2R5J3+H = A2R5	7.00E+19	-1.73	2790	!MIT
A2R5J4+H = A2R5	7.00E+19	-1.73	2790	!MIT
A2R5J5+H = A2R5	7.00E+19	-1.73	2790	!MIT

! PHENYLACETYLENE

C6H5+C2H2 = C8H6+H	1.00E+13	0.00	7648	!96HEC/HIP
C6H6+C2H = C8H6+H	1.00E+12	0.00	0	!MIT
C8H6+H = C6H4C2H+H2	4.845E+07	2.095	15842	!00RIC/HOW *1.5
C8H6 = C6H4C2H+H	5.00E+16	0.00	113394	!92HER/FRA
C6H5+C2H = C8H6	2.54E+17	-1.489	1541	!95ZAN/MCK
o-C6H4+C2H2 = C8H6	2.00E+13	0.00	20000	!00WAN/LAS

! DIPHENYLETHYNE

C8H6+C6H5 => DPE+H	1.00E+13	0.00	7648	!96HEC/HIP as C6H5+C2H2 = C8H6+H
DPE+H => C8H6+C6H5	4.00E+14	0.00	9691	!92HER/FRA as C8H6+H => C6H5+C2H2 *2 for multeplicity

! PHENANTHRENE

o-C12H9+C2H2 = PHEN+H	1.87E+07	1.787	3262	!01RIC/MAZ HP-Limit C10H7-1+C2H2
C8H6+C6H5 = PHEN+H	9.55E+11	0.00	4305	!99PAR/LIN as C6H5+C6H6 = c12H10+H
C6H4C2H+C6H6 = PHEN+H	9.55E+11	0.00	4305	!99PAR/LIN as C6H5+C6H6 = c12H10+H
PHEN+H = A3J1+H2	3.23E+07	2.095	15842	!97MEB/LIN (MIT) as reverse of C6H5+H2 = C6H6+H
PHEN+H = A3J2+H2	3.23E+07	2.095	15842	!97MEB/LIN (MIT) as reverse of C6H5+H2 = C6H6+H
PHEN+H = A3J4+H2	3.23E+07	2.095	15842	!97MEB/LIN (MIT) as reverse of C6H5+H2 = C6H6+H
PHEN+H = A3J9+H2	3.23E+07	2.095	15842	!97MEB/LIN (MIT) as reverse of C6H5+H2 = C6H6+H
A3J1+H = PHEN	2.02E+15	-0.30	330	!MIT
A3J2+H = PHEN	2.02E+15	-0.30	330	!MIT
A3J4+H = PHEN	2.02E+15	-0.30	330	!MIT
A3J9+H = PHEN	2.02E+15	-0.30	330	!MIT

A3J4+C2H2 = PYRENE+H	1.87E+07	1.787	3262	!01RIC/MAZ HP-Limit C10H7+C2H2
C12H10+C2H2 => PHENH	16.92182	2.6	42193	!05KIS/MEB
PHENH => PHEN+H2	4.73E+09	0.797	17176	!05KIS/MEB

! Ethynylacenaphthylene

A2R5J1+C2H2 = A2R5YNE1+H	1.51E+17	-0.72	20230	!MIT
A2R5J3+C2H2 = A2R5YNE3+H	1.51E+17	-0.72	20230	!MIT
A2R5J4+C2H2 = A2R5YNE4+H	1.51E+17	-0.72	20230	!MIT
A2R5J5+C2H2 = A2R5YNE5+H	4.43E-06	5.71	11070	!MIT

! FLUORANTHENE and Benzo[ghi]fluoranthene

A2R5YNE1+H = A2R5YN1J2+H2	3.23E+07	2.095	15842	!97MEB/LIN (MIT) as reverse of C6H5+H2 = C6H6+H
A2R5YN1J2+C2H2 = FLTHNJ7	1.87E+07	1.787	3262	!01RIC/MAZ HP-Limit C10H7-1+C2H2
FLTHNJ7+H = FLTHN	5.00E+13	0.00	0	!MIT
FLTHNJ7+C2H2 = BGHIF+H	1.87E+07	1.787	3262	!01RIC/MAZ HP-Limit C10H7-1+C2H2

! Benzo[b]fluoranthene

A3J1+C6H5 = BBFLUOR+H+H	5.00E+12	0.00	0	!MIT
A3J1+C6H6 = BBFLUOR+H2+H	4.00E+11	0.00	4000	!MIT
A3J9+C6H5 = BBFLUOR+H+H	5.00E+12	0.00	0	!MIT
A3J9+C6H6 = BBFLUOR+H2+H	4.00E+11	0.00	4000	!MIT

! ACEPHENANTHRYLENE

A3J1+C2H2 = A3R5+H	1.83E+13	0.295	14940	!MIT
A2R5YNE4+H = A2R5YN4J5+H2	3.23E+07	2.095	15842	!MIT
A2R5YN4J5+C2H2 = A3R5J7	1.87E+07	1.787	3262	!MIT
A3R5J7+H = A3R5	5.00E+13	0.00	0	!MIT
A2R5YNE5+H = A2R5YN5J4+H2	3.23E+07	2.095	15842	!MIT
A2R5YN5J4+C2H2 = A3R5J10	1.87E+07	1.787	3262	!MIT
A3R5J10+H = A3R5	5.00E+13	0.00	0	!MIT

! ACEANTHRYLENE

A2R5YNE3+H = A2R5YN3J4+H2	3.23E+07	2.095	15842	!MIT
A2R5YNE4+H = A2R5YN4J3+H2	3.23E+07	2.095	15842	!MIT
A2R5YN3J4+C2H2 = A3LR5JS	1.87E+07	1.787	3262	!MIT
A2R5YN4J3+C2H2 = A3LR5JS	1.87E+07	1.787	3262	!MIT
A3LR5JS+H = A3LR5	5.00E+13	0.00	0	!MIT

! CHRYSENE

A3J2+C2H2 = A3C2H-2+H	2.08E+15	-0.13	20860	!MIT
A3C2H-2+H = A3C2H-2JS+H2	3.23E+07	2.095	15842	!MIT
A3C2H-2JS+C2H2 = CHRYSENJ1	1.87E+07	1.787	3262	!01RIC/MAZ HP-Limit C10H7-1+C2H2
CHRYSENJ1+H = CHRYSEN	5.00E+13	0.00	0	!MIT
CHRYSEN+H = CHRYSENJ1+H2	3.23E+07	2.095	15842	!97MEB/LIN (MIT) as reverse of C6H5+H2 = C6H6+H

A3J1+C2H2 = A3C2H-1+H	4.63E-07	6.03	11850	!MIT
A3C2H-1+H = A3C2H-1JP+H2	3.23E+07	2.095	15842	!97MEB/LIN (MIT) as reverse of C6H5+H2 = C6H6+H
A3C2H-1JP+C2H2 = CHRYSENJ4	1.87E+07	1.787	3262	!01RIC/MAZ HP-Limit C10H7-1+C2H2
CHRYSEN+H = CHRYSENJ4+H2	3.23E+07	2.095	15842	!97MEB/LIN (MIT) as reverse of C6H5+H2 = C6H6+H
CHRYSENJ4+H = CHRYSEN	5.00E+13	0.00	0	!MIT

! NAPHTHALENE

o-C6H4+C6H6 => BICYCLO	1.1618E+04	2.526	5915.9	!11COM/BRE rate*2
BICYCLO => o-C6H4+C6H6	4.910E+16	0.00	66811	!11COM/BRE rate*2, calculated
BICYCLO = C10H8+C2H2	7.458E+14	0.0956	54780.1	!11COM/BRE
C6H4C2H+C2H2 = C10H7-1	1.87E+07	1.787	3262	!01RIC/MAZ HP-Limit C10H7+C2H2
C10H7-1+H2 = C10H8+H	5.707E+04	2.430	6273	!97MEB/LIN as C6H5+H2
C10H7-1+H(+M) = C10H8(+M)	1.000E+14	0.00	0.00	!97WAN/FRE as C6H5+H+M = C6H6+M
LOW / 6.600E+75 -16.300 7000.00 /				!
TROE / 1.0 0.1 584.9 6113. /				
H2/2.0/				
C10H7-2+H2 = C10H8+H	5.707E+04	2.430	6273	!97MEB/LIN as C6H5+H2
C10H7-2+H(+M) = C10H8(+M)	1.000E+14	0.00	0.00	!97WAN/FRE as C6H5+H+M = C6H6+M
LOW / 6.600E+75 -16.300 7000.00 /				!
TROE / 1.0 0.1 584.9 6113. /				
H2/2.0/				
C6H5+nC4H3 = C10H8	6.62E+35	-6.485	15420	!MIT
C6H5+nC4H3 = C10H7-2+H	2.43E+31	-4.541	36700	!MIT
C6H5+nC4H3 = C10H7-1+H	6.62E+35	-6.485	15420	!MIT

! PHENYL/BENZYNE DECOMPOSITION

C6H5(+AR) = o-C6H4+H(+AR)	4.30E+12	0.62	77300	!00WAN/LAS
LOW / 1.000E+84 -18.870 90100.00 /				!
TROE / 0.902 696 358 3856. /				
C6H5+H = o-C6H4+H2	2.000E+11	1.100	24500	!01MEB/LIN (JETSURF)
o-C6H4 = C4H2+C2H2	1.2E+18	-0.34	87776	!00WAN/LAS
o-C6H4 = c-C6H3+H	6.0E+15	0.00	98102	!07XU/FRA
c-C6H3 = C6H3	4.8E+10	0.00	53619	!07XU/FRA
C6H2+H = C6H3	1.10E+30	-4.92	10800	!97WAN/FRE 760 Torr
C6H2+M = C6H+H+M	5.0E+16	0.00	79435	!87FRE/WAR
C4H2+C2H = C6H2+H	3.00E+13	0.00	0	!00WAN/LAS
C4H+C2H2 = C6H2+H	3.00E+13	0.00	0	!00WAN/LAS
nC4H3+C2H = z-C6H4	1.00E+13	0.00	0	!estimated
z-C6H4+H = C6H3+H2	1.33E+06	2.53	9240	!JETSURF
nC4H3+C2H2 = z-C6H4+H	1.20E+17	-1.28	13700	!JETSURF 7600 Torr
nC4H3+C2H2 = C6H5	1.90E+63	-15.25	30600	!JETSURF 7600 Torr
nC4H3+C2H2 = o-C6H4+H	3.10E+49	-10.59	37700	!JETSURF 7600 Torr
nC4H5+C2H = C6H5+H	1.60E+13	0.00	0	!00POP/MIL

```
iC4H3+C2H3 = C6H5+H                 6.00E+12      0.00     0          !00POP/MIL
iC4H5+C2H = C6H5+H                  6.00E+12      0.00     0          !00POP/MIL
nC4H5+C2H2 = C6H6+H                 1.60E+18      -1.88    7400       !JETSURF 7600 Torr
nC4H5+C2H3 = C6H6+H2                1.84E-13      7.07     -3611      !89WES/DEA
C4H4+C2H = z-C6H4+H                 1.20E+13      0.00     0.         !estimated
C6H3+H = C4H2+C2H2                  2.80E+23      -2.55    10780      !JETSURF 760 Torr
C6H3+H = z-C6H4                     3.40E+43      -9.01    12120      !JETSURF 760 Torr
C6H3+H = C6H2+H2                    3.00E+13      0.00     0          !97WAN/FRE
C4H2+C2H = C6H3                     4.50E+37      -7.68    7100       !JETSURF
C6H2+C2H=C6H+C2H2                   2.00E+13      0.00     0          !87FRE/WAR
C6H2+C2H=C4H+C4H2                   1.00E+13      0.00     0          !87FRE/WAR
C6H+C2H2 = C8H2+H                   4.00E+13      0.00     0          !90KER/KIE
C4H2+C4H2 = C8H2+H+H                1.51E+14      0.00     56000      !02HID/HOK
C4H2+C4H2 = C8H2+H2                 1.51E+13      0.00     42700      !02HID/HOK
C4H2+C4H = C8H2+H                   4.00E+13      0.00     0          !90KER/KIE

! C0-C4 SUB-MECHANISM

H+H+M = H2+M                        1.78E+18      -1.00    0          !JETSURF
                      H2/0.0/ AR/0.63/
H+H+H2 = H2+H2                      9.000E+16     -0.600   0          !JETSURF
C4H = C4+H                          1.35E+14      0.00     116610     !80FRA/JUS
C2H2+M = C2H+H+M                    3.6E+16       0.00     106423     !80FRA/JUS
C2H+H2 = C2H2+H                     4.9E+05       2.50     560        !JETSURF
C4H2+H = C4H+H2                     2.00E+14      0.00     26000      !02HID/HOK
C2H2+C2H = C4H2+H                   9.6E+13       0.00     0.00       !97WAN/FRE
C4H+H(+M) => C4H2(+M)               1.0E+17       -1.00    0.00       !00WAN/LAS
                      LOW  / 2.6E+33  -4.8        1900  /             !
                      TROE / 0.646      132       1315     5566  /    !
C4H2 => C4H+H                       2.2E+14       0.00     116610     !80FRA/JUS
nC4H3+H = C4H2+H2                   3.00E+13      0.00     0          !JETSURF
iC4H3+H = C4H2+H2                   6.00E+13      0.00     0          !JETSURF
C2H2+C2H2 = C4H2+H2                 1.51E+13      0.00     42700      !90KER/KIE
C2H3+C2H = C2H2+C2H2                3.00E+13      0        0          !92MIL/MEL
C2H3+C2H = C4H4                     9.10E+45      -9.118   21130      !MIT
C4H2+H = nC4H3                      1.10E+42      -8.72    15300      !JETSURF 760 Torr
C4H2+H = iC4H3                      1.10E+30      -4.92    10800      !JETSURF 760 Torr
C2H2+C2H(+M) = nC4H3(+M)            8.300E+10     0.899    -363       !JETSURF
                      LOW   /1.240E+31   -4.718   1871.00  /
                      TROE  /1.0 100. 5613. 13387.         /
                      H2/2.0/ C2H2/2.5/ C2H4/2.5/
C2H2+C2H(+M) = iC4H3(+M)            8.300E+10     0.899    -363       !JETSURF
                      LOW   /1.240E+31   -4.718    1871.00 /
                      TROE   /1.0 100. 5613. 13387.        /
                      H2/2.0/ C2H2/2.5/ C2H4/2.5/
C2H3+H = C2H2+H2                    9.000E+13     0.00     0          !JETSURF
C2H3(+M) = C2H2+H(+M)               3.860E+08     1.620    37048      !JETSURF
                      LOW  /  2.565E+27   -3.400  35798.72  /
                      TROE/  1.9816  5383.7  4.2932 -0.0795 /
                      H2/2.0/ CH4/2.0/ C2H6/3.0/ AR/0.7/ C2H2/3.00/
C2H3+C2H2 = nC4H5                   8.10E+37      -8.09    13400      !JETSURF 7600 Torr
C2H3+C2H2 = iC4H5                   5.10E+53      -12.64   28800      !JETSURF 7600 Torr
C2H3+C2H2 = C4H4+H                  4.90E+16      -1.13    11800      !JETSURF 7600 Torr
C2H3+C2H3 = C4H6                    1.50E+42      -8.84    12483      !JETSURF 760 Torr
C2H3+C2H3 = iC4H5+H                 1.20E+22      -2.44    13654      !JETSURF 760 Torr
C2H3+C2H3 = nC4H5+H                 2.40E+20      -2.04    15361      !JETSURF 760 Torr
```

C2H3+C2H3 = C2H2+C2H4	9.600E+11	0.00	0	!JETSURF
nC4H5 = iC4H5	2.00E+60	-14.46	58600	!JETSURF 7600 Torr
nC4H5+H = iC4H5+H	3.10E+26	-3.35	17423	!JETSURF 760 Torr
nC4H5+H = C4H4+H2	1.50E+13	0.00	0	!97WAN/FRE
iC4H5+H = C4H4+H2	3.0E+13	0.00	0	!97WAN/FRE
nC4H3+H = C4H4	2.00E+47	-10.26	13070	!JETSURF 760 Torr
iC4H3+H = C4H4	3.40E+43	-9.01	12120	!JETSURF 760 Torr
C4H4+H = nC4H5	6.20E+45	-10.08	15800	!JETSURF 7600 Torr
C4H4+H = iC4H5	1.50E+48	-10.58	18800	!JETSURF 7600 Torr
C4H4+H = nC4H3+H2	6.65E+05	2.53	12240	!97WAN/FRE
C4H4+H = iC4H3+H2	3.33E+05	2.53	9240	!97WAN/FRE
nC4H3 = iC4H3	4.10E+43	-9.49	53000	!JETSURF 760 Torr
nC4H3+H = iC4H3+H	2.50E+20	-1.67	10800	!JETSURF 760 Torr
C2H2+C2H2 = iC4H3+H	1.13E+14	0.00	56000	!02HID/HOK
C4H4 = C2H2+C2H2	3.16E+13	0.00	77100	!02HID/HOK
C2H2(+M) = H2CC(+M)	8.000E+14	-0.520	50750	!JETSURF
	LOW / 2.450E+15 -0.640 49700.00 /			
	H2/2.0/ C2H2/2.5/ H2/2.0/ CH4/2.0/ C2H6/3.0/ C2H4/2.5/			
H2CC+H = C2H2+H	1.000E+14	0.00	0	!JETSURF
H2CC+C2H2(+M) = C4H4(+M)	3.500E+05	2.055	-2400	!JETSURF
	LOW /1.400E+60 -12.599 7417.00 /			
	TROE /0.980 56.0 580.0 4164.0 /			
	H2/2.0/ C2H2/3.00/			
C2H3+H = H2CC+H2	6.000E+13	0.000	0.00	!JETSURF
C2H4(+M) = H2+H2CC(+M)	8.000E+12	0.440	88770	!JETSURF
	LOW / 7.000E+50 -9.310 99860.00 /			
	TROE / 0.7345 180.0 1035.00 5417.0 /			
	H2/2.0/ AR/0.7/ CH4/2.0/ C2H6/3.0/			
nC4H3+H = C2H2+H2CC	6.30E+25	-3.34	10014	!JETSURF 760 Torr
iC4H3+H = C2H2+H2CC	2.80E+23	-2.55	10780	!JETSURF 760 Torr
CH2+CH2 = C2H2+H2	3.200E+13	0.00	0	!JETSURF
CH2+CH = C2H2+H	4.000E+13	0.000	0	!JETSURF
C2H4+M = C2H3+H+M	6.31E+18	0.00	108720	!02HID/OKU
C2H4+M = C2H2+H2+M	9.33E+16	0.00	77200	!02HID/OKU
C2H6+H = C2H5+H2	1.15E+08	1.900	7530	!JETSURF
C2H5+H = C2H4+H2	2.00E+12	0.00	0	!JETSURF
CH3+CH2 = C2H4+H	4.00E+13	0.00	0	!JETSURF
CH2*+AR = CH2+AR	9.000E+12	0.00	600	!JETSURF
CH2*+H = CH+H2	3.000E+13	0.00	0	!JETSURF
CH2*+H2 = CH3+H	7.000E+13	0.00	0	!JETSURF
CH3+CH2* = C2H4+H	1.200E+13	0.00	-570	!JETSURF
CH4+CH2* = CH3+CH3	1.600E+13	0.00	-570	!JETSURF
C2H4+CH2* = H2CC+CH4	5.000E+13	0.00	0	!JETSURF
CH3+H(+M) = CH4(+M)	1.270E+16	-0.630	383	!JETSURF
	LOW / 2.477E+33 -4.760 2440.00 /			
	TROE/ 0.7830 74.00 2941.00 6964.0 /			
	H2/2.0/ CH4/2.0/ C2H6/3.0/ AR/0.7/			
CH4+H = CH3+H2	6.600E+08	1.620	10840	!JETSURF
CH4+CH2 = CH3+CH3	2.460E+06	2.000	8270	!JETSURF
CH4+CH = C2H4+H	6.000E+13	0.000	0	!JETSURF
CH4+C2H = C2H2+CH3	1.810E+12	0.0	500	!JETSURF
C2H3+CH3 = C2H2+CH4	3.920E+11	0.000	0	!JETSURF
C2H4+CH3 = C2H3+CH4	2.270E+05	2.000	9200	!JETSURF
C2H6+CH3 = C2H5+CH4	6.14E+06	1.740	10450	!JETSURF
C4H6+CH3 = nC4H5+CH4	2.00E+14	0.0	22800	!JETSURF
C4H6+CH3 = iC4H5+CH4	1.00E+14	0.0	19800	!JETSURF

```
CH2+H(+M) = CH3(+M)                       2.500E+16     -0.800   0           !JETSURF
                          LOW  /  3.200E+27   -3.140   1230.00  /
                          TROE/  0.6800   78.00  1995.0  5590.0 /
                          H2/2.0/ CH4/2.0/ C2H6/3.0/ AR/0.7/
CH2+H2 = H+CH3                            5.000E+05     2.000    7230        !JETSURF
CH3+C = C2H2+H                            5.000E+13     0.000    0           !JETSURF
CH3+CH = C2H3+H                           3.000E+13     0.000    0           !JETSURF
CH3+CH3(+M) = C2H6(+M)                    2.120E+16     -0.970   620         !JETSURF
                          LOW  /  1.770E+50   -9.670   6220.00  /
                          TROE/  0.5325  151.0  1038.00  4970.0 /
                          H2/2.0/ CH4/2.0/ C2H6/3.0/ AR/0.7/
CH3+CH3 = H+C2H5                          4.990E+12     0.100    10600       !JETSURF
C2H4+H(+M) = C2H5(+M)                     1.367E+09     1.463    1355        !JETSURF
                          LOW  /  2.027E+39   -6.642   5769.00  /
                          TROE / -0.569  299.0  9147.0  -152.40 /
                          H2/2.0/ CH4/2.0/ C2H6/3.0/ AR/0.7/
C2H4+H = C2H3+H2                          5.070E+07     1.900    12950       !JETSURF
C2H4+C2H = C4H4+H                         1.20E+13      0.00     0.00        !JETSURF
CH+H2 = CH2+H                             1.107E+08     1.790    1670        !JETSURF
CH+H = C+H2                               1.100E+14     0.000    0           !JETSURF
CH2+CH2 = C2H2+H+H                        1.20E+14      0.00     795         !02HID/OKU
C4H6+H = C2H4+C2H3                        5.45E+30      -4.51    21877       !JETSURF

! ACETONE DECOMPOSITION SUBMECHANISM

CH3+HI = CH4+I                            3.00E+12      0.00     0           !estimated
CH3COCH3+C6H5 = C6H6+CH3COCH2  0.17                     4.2      234.65      !03CHO/LIN

! reaction from: S. Dooley, S.H. Won, M. Chaos, J. Heyne, Y. Ju, F.L. Dryer, K. Kumar, C.J. Sung, H. Wang,
! M.A. Oehlschlaeger, R.J. Santoro, T.A. Litzinger Combustion and Flame 157 (2010) 2333–2339.

CH3COCH3(+M) = CH3CO+CH3(+M)      7.108E+21     -1.57    8.468e+04
                   LOW / 7.0130e+89 -2.0380e+01 1.0715e+05 /
                   TROE / 8.6300e-01 1.0000e+10 4.1640e+02 3.2900E+09 / !troe fall-off reaction
CH3COCH3+H = CH3COCH2+H2          1.960E+06     2.43     5.160E+03    !rate *2
CH3COCH3+CH3 = CH3COCH2+CH4       3.960E+11     0.00     9.784E+03
CH3CO(+M) = CH3+CO(+M)            3.000E+12     0.00     1.672E+04
                   LOW / 1.2000e+15 0.0000e+00 1.2518e+04 / !lindemann fall-off reaction
CH3CO+H = CH2CO+H2                2.000E+13     0.00     0.000E+00
CH3CO+CH3 = CH2CO+CH4             5.000E+13     0.00     0.000E+00
CH3COCH2 = CH2CO+CH3              1.000e+14     0.00     3.100E+04
CH2+CO(+M) = CH2CO(+M)            8.100e+11     0.50     4.510E+03
                   LOW  /  2.690e+33   -5.110   7095.00/
                   TROE/  0.5907  275.00  1226.00  5185.00 /
                   H2/2.0/ CH4/2.0/ CO/1.5/ C2H6/3.0/ AR/0.7/
CH2CO+H = CH3+CO                  1.100e+13     0.00     3.400E+03
C6H5CH3(+M) = C6H5+CH3(+M)        1.95e+27      -3.16    1.07447E+05
                   LOW/1.00e+98 -22.966 1.2208e+05/
                   TROE/7.054562e-01  9.999989e+09  4.599180e+02  8.213938e+09/

! reaction from: Colket, M. B.; Seery, D. J.; Palmer, H.B. Combust. Flame 75:343–366 (1989).

C2H3+CH3COCH3 => C2H4+CH2CO+CH3       3.02E+12      0.00     6400
CH2CO+CH3 => C2H5+CO              2.00E+12      0.00     3000
C2H5+CO => CH2CO+CH3              2.19E+13      0.00     26700
CH3+C2H2 => CH3CHCH               6.16E+11      0.00     7700
```

CH3CHCH => CH3+C2H2	7.41E+12	0.00	33900
CH3CHCH => C3H5	1.41E+13	0.00	36000
C3H5 => CH3CHCH	1.26E+14	0.00	57400
C3H5+C2H2 => C5H7	1.00E+12	0.00	8000
C5H7 => C3H5+C2H2	1.29E+13	0.00	20100
C5H7 => c-C5H6+H	2.00E+10	0.00	5000
H+C3H4 => CH3CHCH	5.75E+12	0.00	3100
CH3CHCH => H+C3H4	3.31E+12	0.00	38200
H+ALLENE => C3H5	3.98E+12	0.00	2700
C3H5 => H+ALLENE	1.35E+13	0.00	60900
2C3H5 => C3H6+C3H4	5.00E+12	0.00	0
C3H6+C3H4 => 2C3H5	1.58E+13	0.00	30500
C3H5+C2H3 => C5H8	5.00E+12	0.00	0
C5H8 => C3H5+C2H3	4.17E+15	0.00	82500
C3H5+H => C3H6	3.98E+13	0.00	0
C3H6 => C3H5+H	6.46E+14	0.00	87000
CH2+C2H2 => C3H3+H	1.82E+12	0.00	0
C3H3+H => CH2+C2H2	2.29E+13	0.00	11500
2C3H3 => C6H6	5.00E+12	0.00	0

END

==

References

JETSURF - H. Wang, E. Dames, B. Sirjean, D. A. Sheen, R. Tangko, A. Violi, J. Y. W. Lai, F. N. Egolfopoulos, D. F. Davidson, R. K. Hanson,
C. T. Bowman, C. K. Law, W. Tsang, N. P. Cernansky, D. L. Miller, R. P. Lindstedt, A high-temperature chemical kinetic model of
n-alkane (up to n-dodecane), cyclohexane, and methyl-, ethyl-, n-propyl and n-butyl-cyclohexane oxidation at high temperatures, JetSurF version 2.0,
September 19, 2010 (http://melchior.usc.edu/JetSurF/JetSurF2.0).

MIT - MIT Atm Soot model - Richter, Granata, Green, Howard Proc. COmb. Inst. 30, 2005, 1397-1405 (http://web.mit.edu/anish/www/MITcomb.html).

71ASA/FUJ - Asaba, T.; Fujii, N. Proc. Int. Symp. Shock Tubes Waves 8, 1971, 1-12.

80FRA/JUS - Frank, P.; Just, T. Combust. Flame 1980, 38, 231–248.

81BAU/DUX - Baulch, D.L.; Duxbury, J.; Grant, S.J.; Montague, D.C. J. Phys. Chem. Ref. Data 10, 1981

87FRE/WAR - Frenklach, M.; Warnatz, J. Combust. Sci. Technol. 1987, 51, 265–283.

89FAH/STE - Fahr, A.; Stein, S.E. 22th symposium (international) on Combustion, The Combustion Institute, Pittsburgh, 1989, p.1023.

89WES/DEA - Westmoreland, P.R.; Dean, A.M.; Howard, J.B.; Longwell J.P. J.Phys.Chem. 1989, 93, 8171.

90KER/KIE - R. D. Kern, K. Xie, H. Chen, J. H. Kiefer Twenty-Third Symposium (International) on Combustion/The Combustion Institute, 1990/pp. 69-75.

92MIL/MEL - Combustion and Flame Volume 91, Issue 1, October 1992, Pages 21-39.

92WAN - Wang, H., Ph.D. Thesis, The Pennsylvania State University, University Park, PA, 1992.

92HER/FRA - Hertzler, J.; Frank, P. Ber. Bunsenges. Phys. Chem. 96, 1333 - 1338, 1992.

94COL/SEE - Colket, M. B.; Seery, D. J. Proc. Comb. Inst. 1994, 25, 883-891.

95ZAN/MCK - Zhang, H.Y., McKinnon, J.T., Combust. Sci. Technol. 107, 261-300, 1995.

96KNY/SLA - Knyazev, V.D.; Slagle, I.R. J.Phys.Chem. 1996, 100, 16899.

96HEC/HIP - Heckmann, E.; Hippler, H.; Troe, J. Proc. Combust. Inst. 26, 1996 , 543-550.

97WAN/FRE - Wang, H., and Frenklach, M., Combust. Flame 110:173–221 (1997).

97MAD/LIN - L. K. Madden, L. V. Moskaleva, S. Kristyan, and M. C. Lin, J. Phys. Chem. A 1997, 101, 6790-6797.

97MEB/LIN - Mebel, A.M.; Lin, M.C.; Yu, T.; Morokuma, K. J.Phys.Chem.A 1997, 101, 3189.

99PAR/LIN - J. Park, S. Burova, A. S. Rodgers, and M. C. Lin J. Phys. Chem. A 1999, 103, 9036-9041.

99MOS/MAD - L. V. Moskaleva, L. K. Madden and M. C. Lin, Phys. Chem. Chem. Phys., 1999, 1, 3967-3972

00RIC/HOW - Richter, H.; Benish, T. G.; Mazyar, O. A.; Green, W. H.; Howard, J. B. Proc. Combust. Inst. 28 (2000) 2609.
00POP/MIL - C. Pope, J.A. Miller, Proc. Combust. Inst. 28 (2000). 1519-1527.
00WAN/LAS - H. Wang, A. Laskin, N. W. Moriarty, M. Frenklach, Proc. Combust. Inst. 28 (2000) 1545.
01RIC/MAZ - Richter, H.; Mazyar, O. A.; Sumathi, R.; Green, W. H.; Howard, J. B.; Bozzelli, J. W. J. Phys. Chem. A 2001, 105, 1561.
01MEB/LIN - Mebel A.M., Lin M.C., Chakraborty D., Park J., Lin S.H. and Lee Y.T. J.Chem. Phys. 114, 19, 2001, 8421.
02HID/OKU - Y. Hidaka, Y. Henmi, T. Ohonishi, T. Okuno Combust. Flame 130:62–82 (2002).
03CHO/LIN - Y. M. Choi, J. Park, and M. C. Lin J. Phys. Chem. A 2003, 107, 7755-7761.
03BLA/JON - Blake, M. E.; Bartlett, K. L.; Jones, M. Jr. J. Am. Chem. Soc. 125, 2003, 6485-6490.
05KIS/MEB - V. V. Kislov, N. I. Islamova, A. M. Kolker, S. H. Lin, and A. M. Mebel, J. Chem. Theory Comput. 2005, 1, 908-924.
07XU/FRA - Xu, C.; Braun-Unkhoff, M.; Naumann, C.; Frank, P. Proc. Combust. Inst. 2007, 31, 231–239.
08GAO/MAR - Gao, Y.; Fessel, K.; McLeod, C.; Marshall, P. Chem. Phys. Lett. 2008, 451, 8–13.
09LIF/DUB - Lifshitz, A.; Tamburu, C.; Dubnikova, F. J. Phys. Chem. A 2009, 113, 10446.
09GIR/OLZ - Giri, B. R.; Bentz, T.; Hippler, H.; Olzmann, M. Z. Phys. Chem. 2009, 223, 539–549.
10TRA/KLI - Tranter, R. S.; Klippenstein, S. J.; Harding, L. B.; Giri, B. R.; Yang, X.; Kiefer, J. H. J. Phys. Chem. A 2010, 114, 8240.
10ZHA/CAI - Lidong Zhanga, Jianghuai Caia, Taichang Zhanga and Fei Qi, Combust. Flame 157, Issue 9, 1686-1697
11SHU/KOS - B. Shukla, K. Tsuchiya, M. Koshi, J. Phys. Chem. A, 2011, 115 (21), pp 5284–5293.
11COM/BRE - A. Comandini, K. Brezinsky, J. Phys. Chem. A, 2011, 115 (22), pp 5547–5559.
==

APPENDIX C

THERMODYNAMIC DATA IN NASA POLYNOMIAL FORMAT

```
THERMO
   298.000  1000.000  5000.000

! JetSurF Version 2.0
AR                120186AR  1               G  0300.00   5000.00  1000.00      1
 0.02500000E+02 0.00000000E+00 0.00000000E+00 0.00000000E+00 0.00000000E+00    2
-0.07453750E+04 0.04366000E+02 0.02500000E+02 0.00000000E+00 0.00000000E+00    3
 0.00000000E+00 0.00000000E+00-0.07453750E+04 0.04366000E+02                   4
H                 L 7/88H   1   00   00   00G   200.000  3500.000   1000.00    1
 2.50000001E+00-2.30842973E-11 1.61561948E-14-4.73515235E-18 4.98197357E-22    2
 2.54736599E+04-4.46682914E-01 2.50000000E+00 7.05332819E-13-1.99591964E-15    3
 2.30081632E-18-9.27732332E-22 2.54736599E+04-4.46682853E-01 6.19742800E+03    4
H2                TPIS78H   2   00   00   00G   200.000  3500.000   1000.00    1
 3.33727920E+00-4.94024731E-05 4.99456778E-07-1.79566394E-10 2.00255376E-14    2
-9.50158922E+02-3.20502331E+00 2.34433112E+00 7.98052075E-03-1.94781510E-05    3
 2.01572094E-08-7.37611761E-12-9.17935173E+02 6.83010238E-01 8.46810200E+03    4
C                 L11/88C   1   00   00   00G   200.000  3500.000  1000.000    1
 2.49266888E+00 4.79889284E-05-7.24335020E-08 3.74291029E-11-4.87277893E-15    2
 8.54512953E+04 4.80150373E+00 2.55423955E+00-3.21537724E-04 7.33792245E-07    3
-7.32234889E-10 2.66521446E-13 8.54438832E+04 4.53130848E+00 6.53589500E+03    4
CH                TPIS79C   1H   1   00   00G   200.000  3500.000  1000.000    1
 2.87846473E+00 9.70913681E-04 1.44445655E-07-1.30687849E-10 1.76079383E-14    2
 7.10124364E+04 5.48497999E+00 3.48981665E+00 3.23835541E-04-1.68899065E-06    3
 3.16217327E-09-1.40609067E-12 7.07972934E+04 2.08401108E+00 8.62500000E+03    4
CH2               L S/93C   1H   2   00   00G   200.000  3500.000  1000.000    1
 2.87410113E+00 3.65639292E-03-1.40894597E-06 2.60179549E-10-1.87727567E-14    2
 4.62636040E+04 6.17119324E+00 3.76267867E+00 9.68872143E-04 2.79489841E-06    3
-3.85091153E-09 1.68741719E-12 4.60040401E+04 1.56253185E+00 1.00274170E+04    4
CH2*              L S/93C   1H   2   00   00G   200.000  3500.000  1000.000    1
 2.29203842E+00 4.65588637E-03-2.01191947E-06 4.17906000E-10-3.39716365E-14    2
 5.09259997E+04 8.62650169E+00 4.19860411E+00-2.36661419E-03 8.23296220E-06    3
-6.68815981E-09 1.94314737E-12 5.04968163E+04-7.69118967E-01 9.93967200E+03    4
C2H               L 1/91C   2H   1   00   00G   200.000  3500.000  1000.000    1
 3.16780652E+00 4.75221902E-03-1.83787077E-06 3.04190252E-10-1.77232770E-14    2
 6.71210650E+04 6.63589475E+00 2.88965733E+00 1.34099611E-02-2.84769501E-05    3
 2.94791045E-08-1.09331511E-11 6.68393932E+04 6.22296438E+00 1.04544720E+04    4
CH3               L11/89C   1H   3   00   00G   200.000  3500.000  1000.000    1
 2.28571772E+00 7.23990037E-03-2.98714348E-06 5.95684644E-10-4.67154394E-14    2
 1.67755843E+04 8.48007179E+00 3.67359040E+00 2.01095175E-03 5.73021856E-06    3
-6.87117425E-09 2.54385734E-12 1.64449988E+04 1.60456433E+00 1.03663400E+04    4
CH4               L 8/88C   1H   4   00   00G   200.000  3500.000  1000.000    1
 7.48514950E-02 1.33909467E-02-5.73285809E-06 1.22292535E-09-1.01815230E-13    2
-9.46834459E+03 1.84373180E+01 5.14987613E+00-1.36709788E-02 4.91800599E-05    3
-4.84743026E-08 1.66693956E-11-1.02466476E+04-4.64130376E+00 1.00161980E+04    4
C2H2              L 1/91C   2H   2   00   00G   200.000  3500.000  1000.000    1
 4.14756964E+00 5.96166664E-03-2.37294852E-06 4.67412171E-10-3.61235213E-14    2
 2.59359992E+04-1.23028121E+00 8.08681094E-01 2.33615629E-02-3.55171815E-05    3
 2.80152437E-08-8.50072974E-12 2.64289807E+04 1.39397051E+01 1.00058390E+04    4
H2CC              L12/89H   2C   2    0    0G   200.000  6000.000  1000.000    1
 0.42780340E+01 0.47562804E-02-0.16301009E-05 0.25462806E-09-0.14886379E-13    2
 0.48316688E+05 0.64023701E+00 0.32815483E+01 0.69764791E-02-0.23855244E-05    3
```

```
-0.12104432E-08 0.98189545E-12 0.48621794E+05 0.59203910E+01 0.49887266E+05    4
C2H3              L 2/92C   2H   3   00   00G   200.000  3500.000  1000.000    1
 3.01672400E+00 1.03302292E-02-4.68082349E-06 1.01763288E-09-8.62607041E-14    2
 3.46128739E+04 7.78732378E+00 3.21246645E+00 1.51479162E-03 2.59209412E-05    3
-3.57657847E-08 1.47150873E-11 3.48598468E+04 8.51054025E+00 1.05750490E+04    4
C2H4              L 1/91C   2H   4   00   00G   200.000  3500.000  1000.000    1
 2.03611116E+00 1.46454151E-02-6.71077915E-06 1.47222923E-09-1.25706061E-13    2
 4.93988614E+03 1.03053693E+01 3.95920148E+00-7.57052247E-03 5.70990292E-05    3
-6.91588753E-08 2.69884373E-11 5.08977593E+03 4.09733096E+00 1.05186890E+04    4
C2H5              L12/92C   2H   5   00   00G   200.000  3500.000  1000.000    1
 1.95465642E+00 1.73972722E-02-7.98206668E-06 1.75217689E-09-1.49641576E-13    2
 1.28575200E+04 1.34624343E+01 4.30646568E+00-4.18658892E-03 4.97142807E-05    3
-5.99126606E-08 2.30509004E-11 1.28416265E+04 4.70720924E+00 1.21852440E+04    4
C2H6              L 8/88C   2H   6   00   00G   200.000  3500.000  1000.000    1
 1.07188150E+00 2.16852677E-02-1.00256067E-05 2.21412001E-09-1.90002890E-13    2
-1.14263932E+04 1.51156107E+01 4.29142492E+00-5.50154270E-03 5.99438288E-05    3
-7.08466285E-08 2.68685771E-11-1.15222055E+04 2.66682316E+00 1.18915940E+04    4
C4H              P 1/93C   4H   1    0    0G   300.000  3000.000   1000.00    1
 0.77697593E+01 0.49829976E-02-0.17628546E-05 0.28144284E-09-0.16689869E-13    2
 0.94345900E+05-0.14165274E+02 0.13186295E+01 0.38582956E-01-0.71385623E-04    3
 0.65356359E-07-0.22617666E-10 0.95456106E+05 0.15567583E+02                   4
C4H2              D11/99C   4H   2    0    0G   300.000  3000.000   1000.00    1
 0.91576328E+01 0.55430518E-02-0.13591604E-05 0.18780075E-10 0.23189536E-13    2
 0.52588039E+05-0.23711460E+02 0.10543978E+01 0.41626960E-01-0.65871784E-04    3
 0.53257075E-07-0.16683162E-10 0.54185211E+05 0.14866591E+02                   4
nC4H3             USC/07C   4H   3O   0    0G   300.000  5000.000   1000.00    1
 0.78045716E+01 0.10712364E-01-0.41939124E-05 0.70446277E-09-0.36271326E-13    2
 0.62987805E+05-0.14129741E+02 0.81667686E+00 0.38716201E-01-0.48045651E-04    3
 0.32066808E-07-0.85628215E-11 0.64455754E+05 0.19740503E+02                   4
iC4H3             USC/07C   4H   3O   0    0G   300.000  5000.000   1000.00    1
 0.76538548E+01 0.11204055E-01-0.46401342E-05 0.86786639E-09-0.57430562E-13    2
 0.57954363E+05-0.11756476E+02 0.37221482E+01 0.25957543E-01-0.26356343E-04    3
 0.15508920E-07-0.38040565E-11 0.58837121E+05 0.75637245E+01                   4
C4H4              USC/07C   4H   4O   0    0G   300.000  5000.000   1000.00    1
 0.72539601E+01 0.13914094E-01-0.52932214E-05 0.83480450E-09-0.35197882E-13    2
 0.31766016E+05-0.12629521E+02 0.58857048E+00 0.36546685E-01-0.34106968E-04    3
 0.16652619E-07-0.30064623E-11 0.33359492E+05 0.20657881E+02                   4
nC4H5             USC/07C   4H   5O   0    0G   300.000  5000.000   1000.00    1
 0.74087291E+01 0.17752748E-01-0.75601506E-05 0.14203795E-08-0.91100182E-13    2
 0.40438762E+05-0.13150027E+02 0.22611290E+00 0.36742371E-01-0.22120474E-04    3
 0.14390138E-08 0.26435809E-11 0.42428410E+05 0.24066401E+02                   4
iC4H5             USC/07C   4H   5O   0    0G   300.000  5000.000   1000.00    1
 0.69646029E+01 0.18274333E-01-0.78133735E-05 0.15292154E-08-0.10920493E-12    2
 0.34725098E+05-0.10649321E+02 0.11308105E+00 0.40950615E-01-0.35413581E-04    3
 0.15530969E-07-0.23355122E-11 0.36383371E+05 0.23692457E+02                   4
C4H6              H6W/94C   4H   6    0    0G   300.000  3000.000   1000.00    1
 0.88673134E+01 0.14918670E-01-0.31548716E-05-0.41841330E-09 0.15761258E-12    2
 0.91338516E+04-0.23328171E+02 0.11284465E+00 0.34369022E-01-0.11107392E-04    3
-0.92106660E-08 0.62065179E-11 0.11802270E+05 0.23089996E+02                   4
C6H              P 1/93C   6H   1    0    0G   300.000  3000.000   1000.00    1
 0.12370055E+02 0.52177699E-02-0.16885009E-05 0.25807149E-09-0.15472851E-13    2
 0.12158739E+06-0.34952797E+02-0.25630299E+00 0.63793827E-01-0.11440118E-03    3
 0.10136744E-06-0.34361855E-10 0.12408855E+06 0.24930750E+02                   4
C6H2              D11/99C   6H   2    0    0G   300.000  3000.000   1000.00    1
 0.12893918E+02 0.79145068E-02-0.24027240E-05 0.24340149E-09 0.31383246E-14    2
 0.79832406E+05-0.40771996E+02 0.45099974E+00 0.67475192E-01-0.11809925E-03    3
```

```
 0.10367632E-06-0.34851039E-10 0.82173062E+05 0.17704124E+02                   4
C6H3              H6W/94C   6H   3    0    0G   300.000  3000.000   1000.00    1
 0.58188343E+01 0.27933408E-01-0.17825427E-04 0.53702536E-08-0.61707627E-12    2
 0.85188250E+05-0.92147827E+00 0.11790619E+01 0.55547360E-01-0.73076168E-04    3
 0.52076736E-07-0.15046964E-10 0.85647312E+05 0.19179199E+02                   4
z-C6H4            D11/99C   6H   4    0    0G   300.000  3000.000   1000.00    1
 0.11186811E+02 0.17122138E-01-0.73898623E-05 0.14678845E-08-0.10733922E-12    2
 0.60743207E+05-0.29537384E+02 0.20895090E+01 0.53276263E-01-0.63299172E-04    3
 0.40811642E-07-0.10598600E-10 0.62662203E+05 0.14613283E+02                   4
C6H6              D11/99C   6H   6    0    0G   300.000  3000.000   1000.00    1
 0.91381245E+01 0.23854433E-01-0.88127726E-05 0.12099021E-08-0.18221503E-13    2
 0.52043462E+04-0.29115665E+02-0.48437734E+01 0.58427613E-01-0.29485855E-04    3
-0.69390440E-08 0.82125253E-11 0.91817773E+04 0.43889832E+02                   4
C8H6              H6W/94C   8H   6    0    0G   300.000  3000.000              1
 0.24090759E+02 0.78232400E-03 0.11453964E-04-0.61620504E-08 0.93346685E-12    2
 0.27429445E+05-0.10499631E+03-0.52645016E+01 0.84511042E-01-0.76597848E-04    3
 0.33216978E-07-0.47673063E-11 0.35566242E+05 0.46378815E+02                   4

! Burcat's Thermodynamic Database
I                 J 6/82I   1    0    0    0G   200.000  6000.000 1000.        1
 2.61667712E+00-2.66010320E-04 1.86060150E-07-3.81927472E-11 2.52036053E-15    2
 1.20582790E+04 6.87896653E+00 2.50041683E+00-4.48046831E-06 1.69962536E-08    3
-2.67708030E-11 1.48927452E-14 1.20947990E+04 7.49816581E+00 1.28402035E+04    4
HI                j 9/61H  1.I  1.   0.   0.G   200.000  6000.000 1000.        1
 2.97348457E+00 1.43564535E-03-5.02266380E-07 8.15769578E-11-4.90179013E-15    2
 2.25405142E+03 7.52526168E+00 3.55499590E+00-3.48919962E-04 2.02666229E-07    3
 1.78572096E-09-1.21092442E-12 2.14501374E+03 4.67388039E+00 3.19417500E+03    4
I2 gas            tpis89I  2.   0.   0.   0.G   200.000  6000.000 1000.        1
 4.56588102E+00-3.42229361E-04 4.84410977E-07-1.42632157E-10 1.14951099E-14    2
 6.16023838E+03 5.41958286E+00 3.87234634E+00 3.64265414E-03-7.95349191E-06    3
 7.82149773E-09-2.80608071E-12 6.24644830E+03 8.49410267E+00 7.50675626E+03    4
C4  singlet       T05/09C  4.   0.   0.   0.G   200.000  6000.000 1000.        1
 7.40814694E+00 3.01895448E-03-1.14910268E-06 1.92636047E-10-1.18334627E-14    2
 1.24380520E+05-1.40637637E+01 3.68331740E+00 1.73134716E-02-2.61612090E-05    3
 2.24303657E-08-7.80714433E-12 1.25295090E+05 4.41423439E+00 1.26972309E+05    4
C8H2 linear       T11/07C  8.H  2.   0.   0.G   200.000  6000.000 1000.        1
 1.63586996E+01 1.08592595E-02-3.91654796E-06 6.34107033E-10-3.80413156E-14    2
 1.02366984E+05-5.56746562E+01-3.26701608E-01 9.43328676E-02-1.72876384E-04    3
 1.56816538E-07-5.40488426E-11 1.05392079E+05 2.20322120E+01 1.08244503E+05    4
c-C6H3 Radical Cy A02/05C  6.H  3.   0.   0.G   200.000  6000.000 1000.        1
 1.07791236E+01 1.29752918E-02-4.74348788E-06 7.75171464E-10-4.68121821E-14    2
 8.28078760E+04-3.23817342E+01 8.25343066E-01 2.54304386E-02 2.14951562E-05    3
-5.23692607E-08 2.43576096E-11 8.61930921E+04 2.24157823E+01 8.76673882E+04    4
C6H5I Iodobenzen  T 7/10C  6.H  5.I  1.   0.G   200.000  6000.000 1000.        1
 1.33736645E+01 1.87627447E-02-6.84193191E-06 1.11591315E-09-6.72888556E-14    2
 1.33030078E+04-4.44152368E+01 1.93178979E+00 2.79645387E-02 4.02135174E-05    3
-7.91975312E-08 3.54307869E-11 1.74375817E+04 1.97895442E+01 1.94719833E+04    4
o-C12H9           g 8/00C 12.H  9.   0.   0.G   200.000  6000.000 1000.        1
 2.25692222E+01 3.45619984E-02-1.27020877E-05 2.08111819E-09-1.25849407E-13    2
 4.05907457E+04-9.57787051E+01 4.07668089E-01 5.42794698E-02 7.12515775E-05    3
-1.44404112E-07 6.48497982E-11 4.85351870E+04 2.81980814E+01 5.14438013E+04    4
TRIPH             T11/05C 18.H 12.   0.   0.G   200.000  6000.000 1000.        1
 3.23692778E+01 5.05001645E-02-1.84004568E-05 3.00025561E-09-1.80901476E-13    2
 1.76447014E+04-1.54285580E+02-1.97977711E+00 8.49435086E-02 9.96440464E-05    3
-2.10795604E-07 9.54761656E-11 2.97414679E+04 3.68747093E+01 3.34355242E+04    4
o-C6H4            A02/05C  6.H  4.   0.   0.G   200.000  6000.000 1000.        1
```

```
 1.05707063E+01 1.56860613E-02-5.68267148E-06 9.22956737E-10-5.54966417E-14    2
 5.04976657E+04-3.32563927E+01 7.21604591E-01 2.47976151E-02 3.16372209E-05    3
-6.53230986E-08 2.96082142E-11 5.39797980E+04 2.16733825E+01 5.54615216E+04    4
m-C6H4            A02/05C  6.H  4.   0.   0.G   200.000  6000.000 1000.        1
 1.10822567E+01 1.52050006E-02-5.50413279E-06 8.93543569E-10-5.37122075E-14    2
 5.78788327E+04-3.59993464E+01 1.90321135E-01 2.91815358E-02 2.38253207E-05    3
-5.98452144E-08 2.82709926E-11 6.15257646E+04 2.37632933E+01 6.29851140E+04    4
p-C6H4            A02/05C  6.H  4.   0.   0.G   200.000  6000.000 1000.        1
 1.18961684E+01 1.43787478E-02-5.18375433E-06 8.39304747E-10-5.03613102E-14    2
 6.37981144E+04-4.05006008E+01-5.78996617E-01 3.95315415E-02-1.83312631E-06    3
-3.45973149E-08 1.93580017E-11 6.75574889E+04 2.58067944E+01 6.90664874E+04    4
C6H5              T07/10C  6.H  5.   0.   0.G   200.000  6000.000 1000.        1
 1.09540673E+01 1.82072569E-02-6.63331157E-06 1.08125690E-09-6.51736617E-14    2
 3.51098413E+04-3.64320659E+01 4.91024498E-01 1.72669813E-02 7.02556406E-05    3
-1.13389805E-07 4.89202543E-11 3.92340510E+04 2.42505364E+01 4.05676342E+04    4

! MIT Atm Soot (Richter, Granata, Green, Howard Proc. COmb. Inst. 30, 2005, 1397-1405)
C6H4C2H   HR 6/99 BLYP00C   8H   5    0    0G   300.000  5000.000 1403.000      1
 1.88370382E+01 1.52445522E-02-5.22469596E-06 8.12518874E-10-4.72045178E-14    2
 5.96821996E+04-7.49107592E+01-1.49929738E+00 7.01891496E-02-6.29429910E-05    3
 2.85073827E-08-5.11137313E-12 6.59494823E+04 3.15838359E+01                   4
C6H5CHCH  HR 4/99 BLYP  C   8H   7    0    0G   300.000  5000.000 1389.000      1
 1.98379960E+01 1.97278283E-02-6.91751721E-06 1.09198104E-09-6.40922808E-14    2
 3.91003225E+04-8.25068718E+01-4.32680301E+00 8.65370210E-02-8.07602858E-05    3
 3.89465367E-08-7.48186804E-12 4.66230204E+04 4.38812546E+01                   4
C10H8     HR11/99BLYP00C  10H   8    0    0G   300.000  5000.000 1401.000      1
 2.34025312E+01 2.42434427E-02-8.36282016E-06 1.30620111E-09-7.61153748E-14    2
 6.51911936E+03-1.07434728E+02-8.83645988E+00 1.09300567E-01-9.55200914E-05    3
 4.21647669E-08-7.39851710E-12 1.66533366E+04 6.21064766E+01                   4
C10H7-1   TB 1/99 BLYP00C  10H   7    0    0G   300.000  5000.000 1401.000      1
 2.32134837E+01 2.19245132E-02-7.57801031E-06 1.18526564E-09-6.91369406E-14    2
 3.75456274E+04-1.03911378E+02-7.74269427E+00 1.04220941E-01-9.25076899E-05    3
 4.12403544E-08-7.28199643E-12 4.72057155E+04 5.86484815E+01                   4
C10H7-2   TB 1/99 BLYP00C  10H   7    0    0G   300.000  5000.000 1401.000      1
 2.32356550E+01 2.19168575E-02-7.57777612E-06 1.18547456E-09-6.91588767E-14    2
 3.76662306E+04-1.04074200E+02-7.71898395E+00 1.04275854E-01-9.26741654E-05    3
 4.13767346E-08-7.31737931E-12 4.73225871E+04 5.84596982E+01                   4
C12H8     HR 4/99 BLYP00C  12H   8    0    0G   300.000  5000.000 1401.000      1
 2.75844041E+01 2.58939856E-02-8.95813505E-06 1.40202452E-09-8.18183535E-14    2
 3.71546148E+04-1.29116717E+02-9.78321241E+00 1.25214234E-01-1.11372820E-04    3
 4.96439934E-08-8.75662028E-12 4.88101806E+04 6.71068024E+01                   4
A2R5      HR11/99BLYP00C  12H   8    0    0G   300.000  5000.000 1403.000      1
 2.76084357E+01 2.58970568E-02-8.96396991E-06 1.40340023E-09-8.19162718E-14    2
 1.76013063E+04-1.29907331E+02-1.03455978E+01 1.27178065E-01-1.13761164E-04    3
 5.08965892E-08-8.99713706E-12 2.93924490E+04 6.92405711E+01                   4
A2R5J1    TB 1/99 BLYP  C  12H   7    0    0G   300.000  5000.000 1402.000      1
 2.72278172E+01 2.37367077E-02-8.23307891E-06 1.29080949E-09-7.54211310E-14    2
 5.07348517E+04-1.26018952E+02-9.08815670E+00 1.20984551E-01-1.09212390E-04    3
 4.91391820E-08-8.72000920E-12 6.19816965E+04 6.44119214E+01                   4
A2R5J3    TB 1/99 BLYP  C  12H   7    0    0G   300.000  5000.000 1402.000      1
 2.95753866E+01 2.14830939E-02-7.41615728E-06 1.16054865E-09-6.77674004E-14    2
 4.75148199E+04-1.40035567E+02-1.00212736E+01 1.23858020E-01-1.08541906E-04    3
 4.63139645E-08-7.72705443E-12 5.99924259E+04 6.86456422E+01                   4
A2R5J4    TB 1/99 BLYP  C  12H   7    0    0G   300.000  5000.000 1402.000      1
 2.73864003E+01 2.35907344E-02-8.18015231E-06 1.28227389E-09-7.49128449E-14    2
 4.86973348E+04-1.26836980E+02-9.11350427E+00 1.21783503E-01-1.10617562E-04    3
```

```
 5.00287584E-08-8.91366253E-12 5.99556335E+04 6.43973708E+01                   4
A2R5J5    TB 1/99 BLYP  C  12H   7    0    0G   300.000  5000.000 1402.000      1
 2.73127115E+01 2.36607767E-02-8.20602003E-06 1.28649401E-09-7.51660931E-14    2
 4.89445491E+04-1.26433916E+02-9.18225753E+00 1.21652543E-01-1.10229668E-04    3
 4.97449695E-08-8.84730241E-12 6.02194179E+04 6.48400542E+01                   4
A2R5YNE1   HR 7/99 BLYP C  14H   8    0    0G   300.000  5000.000 1402.000      1
 3.21119732E+01 2.71033090E-02-9.36641900E-06 1.46485221E-09-8.54407854E-14    2
 4.12237735E+04-1.50347391E+02-7.94248081E+00 1.35252778E-01-1.22773168E-04    3
 5.57488358E-08-9.98622256E-12 5.35583225E+04 5.94025060E+01                   4
A2R5YNE3   HR 7/99 BLYP C  14H   8    0    0G   300.000  5000.000 1402.000      1
 3.22753161E+01 2.69761865E-02-9.32481150E-06 1.45856542E-09-8.50823247E-14    2
 4.22413139E+04-1.50406092E+02-7.68051241E+00 1.35299173E-01-1.23464227E-04    3
 5.63670416E-08-1.01469540E-11 5.45113980E+04 5.86879351E+01                   4
A2R5YNE4   HR 7/99 BLYP C  14H   8    0    0G   300.000  5000.000 1401.000      1
 3.23047034E+01 2.69617198E-02-9.32221063E-06 1.45841344E-09-8.50839096E-14    2
 4.26767312E+04-1.50798504E+02-7.99432137E+00 1.36928258E-01-1.26084103E-04    3
 5.80711675E-08-1.05356870E-11 5.49966516E+04 5.98652621E+01                   4
A2R5YNE5   HR 7/99 BLYP C  14H   8    0    0G   300.000  5000.000 1402.000      1
 3.21612525E+01 2.70662867E-02-9.35425400E-06 1.46297989E-09-8.53316967E-14    2
 4.22611911E+04-1.50529220E+02-7.89238679E+00 1.35676852E-01-1.23792033E-04    3
 5.65006962E-08-1.01667537E-11 5.45561956E+04 5.90637239E+01                   4
A2R5YN1J2  HR 7/99 BLYP C  14H   7    0    0G   300.000  5000.000 1400.000      1
 3.18826308E+01 2.48270613E-02-8.59898020E-06 1.34696470E-09-7.86553246E-14    2
 7.46950504E+04-1.48000717E+02-7.22261674E+00 1.31395484E-01-1.21449249E-04    3
 5.58755730E-08-1.01085404E-11 8.66450722E+04 5.64412655E+01                   4
A2R5YN3J4  HR 11/99BLYP C  14H   7    0    0G   300.000  5000.000 1403.000      1
 3.20556827E+01 2.46638522E-02-8.53744993E-06 1.33668652E-09-7.80255741E-14    2
 7.38766433E+04-1.48236755E+02-6.40177627E+00 1.29670640E-01-1.19833893E-04    3
 5.51057999E-08-9.95836756E-12 8.55974978E+04 5.27271055E+01                   4
A2R5YN4J3  HR 11/99BLYP C  14H   7    0    0G   300.000  5000.000 1402.000      1
 3.20292021E+01 2.46955395E-02-8.55137550E-06 1.33924806E-09-7.81927998E-14    2
 7.41627859E+04-1.48567777E+02-6.80724534E+00 1.30160012E-01-1.19646053E-04    3
 5.46843524E-08-9.82662943E-12 8.60464782E+04 5.45642178E+01                   4
A2R5YN4J5  HR 11/99BLYP C  14H   7    0    0G   300.000  5000.000 1403.000      1
 3.20221044E+01 2.46903037E-02-8.54681341E-06 1.33822804E-09-7.81202921E-14    2
 7.45108809E+04-1.48012549E+02-6.55646892E+00 1.29404033E-01-1.18784303E-04    3
 5.42365974E-08-9.73841861E-12 8.63194759E+04 5.37863099E+01                   4
A2R5YN5J4  HR 7/99 BLYP C  14H   7    0    0G   300.000  5000.000 1404.000      1
 3.20640677E+01 2.46700966E-02-8.54302844E-06 1.33795145E-09-7.81163664E-14    2
 7.37678190E+04-1.48575286E+02-6.58001201E+00 1.29178493E-01-1.18016707E-04    3
 5.35722667E-08-9.56225179E-12 8.56189900E+04 5.36752525E+01                   4
A3R5J7    HR 11/99 BLYP C  16H   9    0    0G   300.000  5000.000 1402.000     1
 3.65198841E+01 3.12053139E-02-1.08300483E-05 1.69870300E-09-9.92854587E-14    2
 5.19613121E+04-1.77370872E+02-1.22352016E+01 1.61692639E-01-1.46124302E-04    3
 6.56704260E-08-1.16286724E-11 6.70531193E+04 7.82881978E+01                   4
A3R5J10   HR 11/99 BLYP C  16H   9    0    0G   300.000  5000.000 1401.000     1
 3.66422872E+01 3.10853394E-02-1.07862682E-05 1.69170990E-09-9.88746344E-14    2
 5.14040913E+04-1.78135777E+02-1.21897707E+01 1.61189097E-01-1.44965037E-04    3
 6.47870002E-08-1.14113841E-11 6.65676994E+04 7.81180690E+01                   4
A3LR5JS    MM300-THERM  C  16H   9    0    0G   300.000  5000.000 1394.000     1
 3.51937788E+01 3.24891140E-02-1.13089072E-05 1.77729051E-09-1.04019562E-13    2
 5.48035190E+04-1.67315319E+02-8.50245255E+00 1.42965250E-01-1.19412269E-04    3
 5.02477747E-08-8.45566931E-12 6.90225761E+04 6.41914316E+01                   4
A3LR5      HR04/00 BLYP C  16H  10    0    0G   300.000  5000.000 1400.000     1
 3.68457135E+01 3.34150918E-02-1.15801847E-05 1.81464809E-09-1.05993871E-13    2
 1.99631829E+04-1.80251762E+02-1.31351173E+01 1.65787508E-01-1.47428990E-04    3
```

```
 6.54689019E-08-1.14931149E-11 3.55827405E+04 8.23449607E+01                   4
BIPHENH   HR 4/99 BLYP00C  12H   9    0    0G   300.000  5000.000 1402.000      1
 2.87663424E+01 2.73722766E-02-9.45354931E-06 1.47784724E-09-8.61724077E-14    2
 4.70722218E+04-1.34442577E+02-1.03237782E+01 1.32036012E-01-1.18286026E-04    3
 5.31769275E-08-9.45503080E-12 5.91991673E+04 7.05721752E+01                   4
C12H10     HR11/99BLYP00C  12H  10    0    0G   300.000  5000.000 1394.000      1
 2.86695178E+01 3.02015016E-02-1.05655370E-05 1.66543513E-09-9.76572185E-14    2
 7.60422537E+03-1.34434827E+02-1.08038552E+01 1.35543795E-01-1.21268985E-04    3
 5.53819438E-08-1.00979145E-11 2.00556981E+04 7.30009993E+01                   4
PHEN       HR11/99BLYP00C  14H  10    0    0G   300.000  5000.000 1402.000      1
 3.25629928E+01 3.18642789E-02-1.10210129E-05 1.72454013E-09-1.00623319E-13    2
 8.20029214E+03-1.57226303E+02-1.19404574E+01 1.49110249E-01-1.30758245E-04    3
 5.75914058E-08-1.00591474E-11 2.21810569E+04 7.68295519E+01                   4
A3J1      HR 6/99BLYP00C  14H   9    0    0G   300.000  5000.000 1401.000      1
 3.22842997E+01 2.96288141E-02-1.02664407E-05 1.60846116E-09-9.39327423E-14    2
 3.93429658E+04-1.53865589E+02-1.09040715E+01 1.44543895E-01-1.28948698E-04    3
 5.76183034E-08-1.01854264E-11 5.28076539E+04 7.28898322E+01                   4
A3J2      HR 6/99 BLYP C  14H   9    0    0G   300.000  5000.000 1403.000      1
 3.24061829E+01 2.94901003E-02-1.02110654E-05 1.59905455E-09-9.33548206E-14    2
 3.94950191E+04-1.54635510E+02-1.03837170E+01 1.41986852E-01-1.24578102E-04    3
 5.46229132E-08-9.47662806E-12 5.29307683E+04 7.04410467E+01                   4
A3J4      HR 6/99BLYP00C  14H   9    0    0G   300.000  5000.000 1401.000      1
 3.24592632E+01 2.94561329E-02-1.02023235E-05 1.59803996E-09-9.33111464E-14    2
 3.82894894E+04-1.54957971E+02-1.09120537E+01 1.44627958E-01-1.28798224E-04    3
 5.73715648E-08-1.01060264E-11 5.18219254E+04 7.28191713E+01                   4
A3J9      HR 6/99 BLYP C  14H   9    0    0G   300.000  5000.000 1401.000      1
 3.23091706E+01 2.95756612E-02-1.02418755E-05 1.60404506E-09-9.36541706E-14    2
 3.93266179E+04-1.54092471E+02-1.08338659E+01 1.43759844E-01-1.27400954E-04    3
 5.65119210E-08-9.92057090E-12 5.28246534E+04 7.26189092E+01                   4
A3C2H-1   HR 6/99 BLYP C  16H  10    0    0G   300.000  5000.000 1401.000      1
 3.73588865E+01 3.27870345E-02-1.13180045E-05 1.76874124E-09-1.03111666E-13    2
 3.34456064E+04-1.78293824E+02-9.27377401E+00 1.57876205E-01-1.41734955E-04    3
 6.39142152E-08-1.14013129E-11 4.79003559E+04 6.62159504E+01                   4
A3C2H-1JP  HR BLYP-THERMC  16H   9    0    0G   300.000  5000.000 1397.000      1
 3.70857649E+01 3.04702886E-02-1.05239953E-05 1.64574966E-09-9.60012998E-14    2
 6.46707148E+04-1.75357378E+02-7.64228357E+00 1.48096120E-01-1.30459803E-04    3
 5.75544684E-08-1.00616675E-11 7.87427736E+04 5.99568969E+01                   4
A3C2H-2   HR 7/99 BLYP C  16H  10    0    0G   300.000  5000.000 1401.000      1
 3.72598081E+01 3.29424978E-02-1.13861351E-05 1.78078654E-09-1.03866988E-13    2
 3.32307992E+04-1.77354975E+02-9.00521419E+00 1.57177024E-01-1.41194806E-04    3
 6.38147186E-08-1.14169607E-11 4.75751775E+04 6.52082588E+01                   4
A3C2H-2JS  HR BLYP-THERMC  16H   9    0    0G   300.000  5000.000 1398.000      1
 3.67812640E+01 3.10152926E-02-1.07699767E-05 1.68976783E-09-9.87789667E-14    2
 6.37587690E+04-1.73313834E+02-7.59050661E+00 1.48490072E-01-1.31806093E-04    3
 5.88251124E-08-1.04170126E-11 7.76876714E+04 5.99259097E+01                   4
A3R5      HR 4/99 BLYP  C  16H  10    0    0G   300.000  5000.000 1402.000      1
 3.67462285E+01 3.34932026E-02-1.16049002E-05 1.81821016E-09-1.06187329E-13    2
 2.08682892E+04-1.79724343E+02-1.30559449E+01 1.65231504E-01-1.46521443E-04    3
 6.48635058E-08-1.13498164E-11 3.64369485E+04 8.19714754E+01                   4
PYRENE     HR11/99 BLYP C  16H  10    0    0G   300.000  5000.000 1401.000      1
 3.65839677E+01 3.36764102E-02-1.16783938E-05 1.83077466E-09-1.06963777E-13    2
 9.29809483E+03-1.81272070E+02-1.29758980E+01 1.63790064E-01-1.43851166E-04    3
 6.31057915E-08-1.09568047E-11 2.48866399E+04 7.94950474E+01                   4
CHRYSENJ1   MM300-THERM C  18H  11    0    0G   300.000  5000.000 1395.000      1
 3.94271918E+01 3.92828136E-02-1.36947073E-05 2.15400475E-09-1.26125737E-13    2
 4.43864722E+04-1.91848271E+02-9.12122835E+00 1.60307896E-01-1.30504730E-04    3
```

```
 5.38950856E-08-8.95299337E-12 6.03944025E+04 6.60377334E+01                   4
CHRYSENJ4   MM300-THERM C  18H  11    0    0G   300.000  5000.000 1395.000      1
 3.94271918E+01 3.92828136E-02-1.36947073E-05 2.15400475E-09-1.26125737E-13    2
 4.43864722E+04-1.91848271E+02-9.12122835E+00 1.60307896E-01-1.30504730E-04    3
 5.38950856E-08-8.95299337E-12 6.03944025E+04 6.60377334E+01                   4
CHRYSEN     CJP MM300   C  18H  12    0    0G   300.000  5000.000 1396.000      1
 4.02767814E+01 4.07664763E-02-1.41327835E-05 2.21487630E-09-1.29371528E-13    2
 1.36797665E+04-1.98070319E+02-1.06837095E+01 1.69184362E-01-1.39372979E-04    3
 5.81858481E-08-9.74318604E-12 3.03145297E+04 7.20877574E+01                   4
FLTHNJ7     HR 7/99 BLYP C  16H   9    0    0G   300.000  5000.000 1401.000     1
 3.63148950E+01 3.14318646E-02-1.09199042E-05 1.71395677E-09-1.00223601E-13    2
 4.83383327E+04-1.76380800E+02-1.22209030E+01 1.60459694E-01-1.43780999E-04    3
 6.41350151E-08-1.12883975E-11 6.34501455E+04 7.84391373E+01                   4
FLTHN       HR 4/99 BLYP  C  16H  10    0    0G   300.000  5000.000 1401.000    1
 3.65828989E+01 3.36775448E-02-1.16788087E-05 1.83083981E-09-1.06967522E-13    2
 1.72680575E+04-1.79821482E+02-1.30869351E+01 1.64239769E-01-1.44492135E-04    3
 6.34903784E-08-1.10395110E-11 3.28765164E+04 8.14697326E+01                   4
BGHIF       10/07/93 MM395C  18H  10    0    0G   300.000  5000.000 1392.000    1
 3.89402846E+01 3.75036664E-02-1.33632064E-05 2.14509430E-09-1.27219014E-13    2
 2.83699011E+04-1.91759886E+02-1.16928756E+01 1.67865779E-01-1.44270086E-04    3
 6.26787591E-08-1.09009059E-11 4.46898283E+04 7.57989908E+01                   4
BBFLUOR     CJP MM300   C  20H  12    0    0G   300.000  5000.000 1396.000      1
 4.43530126E+01 4.25497219E-02-1.47832424E-05 2.32027261E-09-1.35670659E-13    2
 2.06334287E+04-2.20678121E+02-1.21872196E+01 1.86403342E-01-1.56436955E-04    3
 6.61852991E-08-1.11867885E-11 3.89302853E+04 7.85360438E+01                   4

! Estimated P.W.
o-C12H9I                C  12H   9I   1     G   200.000  6000.000 1000.00       1
 0.24643894E+02 0.35544564E-01-0.12920983E-04 0.21050735E-08-0.12691161E-12    2
 0.23119372E+05-0.10275618E+03 0.14695996E+01 0.62628007E-01 0.44874455E-04    3
-0.10203895E-06 0.42312529E-10 0.31034918E+05 0.25449825E+02                   4
m-C12H9I                C  12H   9I   1     G   200.000  6000.000 1000.00       1
 0.24578051E+02 0.35604135E-01-0.12942920E-04 0.21087022E-08-0.12713353E-12    2
 0.21411232E+05-0.10274886E+03 0.14381733E+01 0.62612809E-01 0.44870325E-04    3
-0.10198430E-06 0.42283826E-10 0.29316749E+05 0.25275382E+02                   4
p-C12H9I                C  12H   9I   1     G   200.000  6000.000 1000.00       1
 0.24538955E+02 0.35647590E-01-0.12960758E-04 0.21118431E-08-0.12733320E-12    2
 0.21409114E+05-0.10252608E+03 0.14119425E+01 0.62609621E-01 0.44915226E-04    3
-0.10201817E-06 0.42291675E-10 0.29311818E+05 0.25434893E+02                   4
DPE                     C  14H  10          G   200.000  6000.000 1000.00       1
 0.25425461E+02 0.40303195E-01-0.14661438E-04 0.23898144E-08-0.14413009E-12    2
 0.34275447E+05-0.10842533E+03-0.85541767E+00 0.75342219E-01 0.37906758E-04    3
-0.10274014E-06 0.43659480E-10 0.43035847E+05 0.35885841E+02                   4
BENZO                   C  12H   8          G   200.000  6000.000 1000.00       1
 0.21693066E+02 0.32964679E-01-0.12025652E-04 0.19639620E-08-0.11860776E-12    2
 0.38273211E+05-0.94072694E+02-0.18952793E+01 0.65010411E-01 0.33367222E-04    3
-0.90605602E-07 0.38600695E-10 0.46106262E+05 0.35304347E+02                   4
C6H5C6H3                C  12H   8          G   200.000  6000.000 1000.00       1
 0.21834240E+02 0.32817030E-01-0.11966625E-04 0.19537358E-08-0.11796545E-12    2
 0.57854999E+05-0.94186618E+02-0.21008708E-01 0.60759237E-01 0.35338246E-04    3
-0.89061632E-07 0.37505573E-10 0.65199988E+05 0.26122019E+02                   4
BICYCLO                 C  12H  10          G   200.000  6000.000 1000.00       1
 0.22254488E+02 0.37643162E-01-0.13667443E-04 0.22246959E-08-0.13403330E-12    2
 0.32117245E+05-0.99857186E+02-0.38085817E+01 0.73943066E-01 0.33811263E-04    3
-0.97380150E-07 0.41755272E-10 0.40727478E+05 0.42870152E+02                   4
o-TERPH                 C  18H  14          G   200.000  6000.000 1000.00       1
```

```
 0.33297406E+02 0.54875869E-01-0.19956343E-04 0.32517896E-08-0.19605477E-12    2
 0.22130067E+05-0.15494507E+03-0.50678468E+00 0.87105849E-01 0.86178861E-04    3
-0.17049180E-06 0.68986537E-10 0.34040244E+05 0.33887307E+02                   4
m-TERPH                C  18H  14          G   200.000  6000.000 1000.00      1
 0.33247445E+02 0.54924357E-01-0.19975048E-04 0.32549825E-08-0.19625439E-12    2
 0.20384334E+05-0.15453354E+03-0.57179147E+00 0.87428769E-01 0.85427137E-04    3
-0.16978568E-06 0.68757044E-10 0.32286809E+05 0.34317865E+02                   4
p-TERPH                C  18H  14          G   200.000  6000.000 1000.00      1
 0.33227265E+02 0.54949329E-01-0.19985956E-04 0.32569825E-08-0.19638519E-12    2
 0.20295647E+05-0.15433427E+03-0.64797155E+00 0.87859710E-01 0.84534319E-04    3
-0.16901376E-06 0.68518943E-10 0.32200223E+05 0.34741802E+02                   4
BENZOHyl               C  12H   8          G   200.000  6000.000 1000.00      1
 0.22329921E+02 0.32464872E-01-0.11860251E-04 0.19386509E-08-0.11714541E-12    2
 0.71799829E+05-0.97326366E+02-0.18394670E+01 0.65759690E-01 0.33271619E-04    3
-0.91531995E-07 0.39096199E-10 0.79802843E+05 0.35122642E+02                   4
C6H4oct                C  12H   8          G   200.000  6000.000 1000.00      1
 0.22258902E+02 0.32508123E-01-0.11874998E-04 0.19413826E-08-0.11734107E-12    2
 0.77457998E+05-0.94706235E+02-0.84547124E+00 0.71818526E-01 0.88200312E-05    3
-0.64962392E-07 0.29885375E-10 0.84734227E+05 0.30035780E+02                   4
BENZOH                 C  12H   9          G   200.000  6000.000 1000.00      1
 0.24654472E+02 0.31111906E-01-0.11550007E-04 0.19083460E-08-0.11618184E-12    2
 0.43329829E+05-0.10950280E+03-0.21429115E+01 0.67246072E-01 0.40831798E-04    3
-0.10406823E-06 0.44141803E-10 0.52242075E+05 0.37542932E+02                   4
C6H5CHC5H4             C  12H  10          G   200.000  6000.000 1000.00      1
 0.24625803E+02 0.33500872E-01-0.12333638E-04 0.20264977E-08-0.12289634E-12    2
 0.28004028E+05-0.10781289E+03-0.29541656E+00 0.60178758E-01 0.57160022E-04    3
-0.11730960E-06 0.47962877E-10 0.36638622E+05 0.30669341E+02                   4
m-C12H9                C  12H   9          G   200.000  6000.000 1000.00      1
 0.21986992E+02 0.35279510E-01-0.12832818E-04 0.20913912E-08-0.12610805E-12    2
 0.43003230E+05-0.93392213E+02-0.28427623E+00 0.57934910E-01 0.52828593E-04    3
-0.10811256E-06 0.44032297E-10 0.50778968E+05 0.30661200E+02                   4
p-C12H9                C  12H   9          G   200.000  6000.000 1000.00      1
 0.22045218E+02 0.35229926E-01-0.12815783E-04 0.20887523E-08-0.12595575E-12    2
 0.43261735E+05-0.93705289E+02-0.36709458E+00 0.58991362E-01 0.50373785E-04    3
-0.10592544E-06 0.43349546E-10 0.51038588E+05 0.30893116E+02                   4
PHENH                  C  14H  12          G   200.000  6000.000 1000.00      1
 0.26719757E+02 0.43996436E-01-0.16084604E-04 0.26303590E-08-0.15899272E-12    2
 0.45330018E+05-0.12159388E+03-0.13819074E+01 0.74515415E-01 0.60968444E-04    3
-0.13062602E-06 0.53627021E-10 0.55044735E+05 0.34452321E+02                   4

! SPECIES FOR ACETONE DECOMPOSITION SUBMECHANISM
! S. Dooley, S.H. Won, M. Chaos, J. Heyne, Y. Ju, F.L. Dryer, K. Kumar, C.J. Sung, H. Wang,
! M.A. Oehlschlaeger, R.J. Santoro, T.A. Litzinger Combustion and Flame 157 (2010) 2333–2339.
CH3COCH3   8/30/ 4 thermC   3H   6O   1    0g   300.000  5000.000 1382.000      1
 9.62674379e+00 1.45519245e-02-4.97749457e-06 7.72794591e-10-4.48367165e-14    2
-3.11862263e+04-2.61613449e+01 1.24527408e+00 2.99760255e-02-1.40026661e-05    3
 2.16453512e-09 1.27637295e-13-2.78348727e+04 2.03682615e+01                   4
CH3CO           t 9/92C   2H   3O   1    0g   200.000  6000.0    1000.0       1
 0.59447731e+01 0.78667205e-02-0.28865882e-05 0.47270875e-09-0.28599861e-13    2
-0.37873075e+04-0.50136751e+01 0.41634257e+01-0.23261610e-03 0.34267820e-04    3
-0.44105227e-07 0.17275612e-10-0.26574529e+04 0.73468280e+01-0.12027167e+04    4
CH3COCH2   8/30/ 4 thermC   3H   5O   1    0g   300.000  5000.000 1388.000      1
 1.08892477e+01 1.11540675e-02-3.85516785e-06 6.02834048e-10-3.51533449e-14    2
-1.00741464e+04-3.18043322e+01 1.22337251e+00 3.24546742e-02-2.13542518e-05    3
 6.96777735e-09-8.99160299e-13-6.59419324e+03 2.05537233e+01                   4
CH2CO           l 5/90C   2H   2O   1   00g   200.000  3500.000  1000.000    1
```

```
 4.51129732e+00 9.00359745e-03-4.16939635e-06 9.23345882e-10-7.94838201e-14    2
-7.55105311e+03 6.32247205e-01 2.13583630e+00 1.81188721e-02-1.73947474e-05    3
 9.34397568e-09-2.01457615e-12-7.04291804e+03 1.22156480e+01 1.17977430e+04    4
CO              121286C   1O   1          g  0300.00   5000.00  1000.00      1
 0.03025078e+02 0.01442689e-01-0.05630828e-05 0.01018581e-08-0.06910952e-13    2
-0.01426835e+06 0.06108218e+02 0.03262452e+02 0.01511941e-01-0.03881755e-04    3
 0.05581944e-07-0.02474951e-10-0.01431054e+06 0.04848897e+02                   4
C6H5CH3          l 6/87C   7H   8    0    0g   200.000  6000.000 1000.        1
 0.12940034e+02 0.26691287e-01-0.96838505e-05 0.15738629e-08-0.94663601e-13    2
-0.69764908e+03-0.46728785e+02 0.16152663e+01 0.21099438e-01 0.85366018e-04    3
-0.13261066e-06 0.55956604e-10 0.40756300e+04 0.20282210e+02 0.60135835e+04    4

! Burcat's Thermodynamic Database
CH3CHCH          A12/04C  3.H  5.   0.   0.G   200.000  6000.000 1000.        1
 6.05091412E+00 1.34052084E-02-4.73450586E-06 7.55380897E-10-4.48421084E-14    2
 2.90860210E+04-6.73692060E+00 3.33277282E+00 1.06102499E-02 2.17559727E-05    3
-3.47145235E-08 1.44476835E-11 3.03404530E+04 9.78922358E+00 3.19361425E+04    4
C3H3 PROPARGYL    T 6/09C   3H   3    0    0G   200.000  6000.000 1000.        1
 7.14221719E+00 7.61902211E-03-2.67460030E-06 4.24914904E-10-2.51475443E-14    2
 3.72008859E+04-1.25848690E+01 1.35110873E+00 3.27411291E-02-4.73827407E-05    3
 3.76310220E-08-1.18541128E-11 3.83979206E+04 1.52058598E+01 3.99061400E+04    4
C3H6 propylene    g 2/00C  3.H  6.   0.   0.G   200.000  6000.000 1000.        1
 6.03870234E+00 1.62963931E-02-5.82130800E-06 9.35936829E-10-5.58603143E-14    2
-7.41715057E+02-8.43825992E+00 3.83464468E+00 3.29078952E-03 5.05228001E-05    3
-6.66251176E-08 2.63707473E-11 7.88717123E+02 7.53408013E+00 2.40543339E+03    4
ALLENE           L 8/89C   3H   4    0    0G   200.000  6000.000 1000.        1
 0.63168722E+01 0.11133728E-01-0.39629378E-05 0.63564238E-09-0.37875540E-13    2
 0.20117495E+05-0.10995766E+02 0.26130445E+01 0.12122575E-01 0.18539880E-04    3
-0.34525149E-07 0.15335079E-10 0.21541567E+05 0.10226139E+02 0.22962267E+05    4
C5H8  CycloPente  T11/10C  5.H  8.   0.   0.G   200.000  6000.000 1000.        1
 8.91460073E+00 2.49544912E-02-8.95888089E-06 1.44576296E-09-8.65296298E-14    2
-6.43700968E+02-2.68476506E+01 3.36332222E+00-4.00403786E-03 1.26080496E-04    3
-1.65877230E-07 6.67068939E-11 2.84577994E+03 1.20140385E+01 4.48818944E+03    4
C3H4 PROPYNE      T 2/90H   4C   3    0    0G   200.000  6000.000 1000.        1
 0.60252400E+01 0.11336542E-01-0.40223391E-05 0.64376063E-09-0.38299635E-13    2
 0.19620942E+05-0.86043785E+01 0.26803869E+01 0.15799651E-01 0.25070596E-05    3
-0.13657623E-07 0.66154285E-11 0.20802374E+05 0.98769351E+01 0.22302059E+05    4
c-C5H6           T 1/90C   5H   6    0    0G   200.000  6000.000 1000.        1
 0.99757848E+01 0.18905543E-01-0.68411461E-05 0.11099340E-08-0.66680236E-13    2
 0.11081693E+05-0.32209454E+02 0.86108957E+00 0.14804031E-01 0.72108895E-04    3
-0.11338055E-06 0.48689972E-10 0.14801755E+05 0.21353453E+02 0.16152485E+05    4
C5H7 Cy-1en-1-yl  A 9/04C  5.H  7.   0.   0.G   200.000  6000.000 1000.        1
 9.74013709E+00 2.15079576E-02-7.71169114E-06 1.24352828E-09-7.43887470E-14    2
 1.56355223E+04-2.89664925E+01 2.31203194E+00 7.01023600E-03 9.35725543E-05    3
-1.33744658E-07 5.55553794E-11 1.91721662E+04 1.72892593E+01 2.07617132E+04    4
C3H5 SYMMETRIC    T 9/96C   3H   5    0    0G   200.000  6000.000 1000.        1
 0.70094568D+01 0.13106629D-01-0.46533442D-05 0.74514323D-09-0.44350051D-13    2
 0.16412909D+05-0.13946114D+02 0.14698036D+01 0.19034365D-01 0.14480425D-04    3
-0.35468652D-07 0.16647594D-10 0.18325831D+05 0.16724114D+02 0.19675772D+05    4

ENDOFDATA
```

APPENDIX D

Included for each optimized stationary structures reported Chapter 7:

- Cartesian Coordinates (Ǻngströms);
- uB3LYP/6-311+G(d,p) electronic energies (hartrees);
- uCCSD(T)/cc-pVDZ electronic energies (hartrees);
- zero-point vibrational energies ZPVE (hartrees);
- imaginary vibrational frequencies (cm^{-1}) (only for saddle points).

benzene (C_6H_6)
uB3LYP/6311+G(d,p) = -232.3112456 uCCSD(T)/cc-pVDZ = -231.5806796
ZPVE = 0.100142

1	6	-1.394361	0.028850	0.000000
2	6	-0.672211	1.221976	0.000000
3	6	0.722155	1.193070	0.000000
4	6	1.394450	-0.028853	0.000000
5	6	0.672180	-1.221917	0.000000
6	6	-0.722188	-1.193128	0.000000
7	1	-2.478599	0.051288	0.000001
8	1	-1.195012	2.172009	0.000001
9	1	1.283736	2.120776	0.000000
10	1	1.194906	-2.172058	-0.000001
11	1	-1.283839	-2.120723	0.000000
12	1	2.478661	-0.051289	-0.000001

singlet o-benzyne ($C_6H_4^s$)
uB3LYP/6311+G(d,p) = -230.9726840 uCCSD(T)/cc-pVDZ = -230.2593904
ZPVE = 0.074883

1	6	1.170104	0.491488	0.000000
2	6	0.000000	1.269077	0.000000
3	6	-1.289206	0.695776	0.000000
4	6	-1.201746	-0.683828	0.000000
5	6	-0.165049	-1.372534	0.000000
6	6	1.140814	-0.919196	0.000000
7	1	2.133449	0.991446	0.000000
8	1	0.087848	2.350868	0.000000
9	1	-2.191661	1.293016	0.000000
10	1	2.040865	-1.520029	0.000000

triplet o-benzyne ($C_6H_4^t$)
uB3LYP/6311+G(d,p) = -230.9220022 uCCSD(T)/cc-pVDZ = -230.2077155
ZPVE = 0.074066

1	6	1.175138	0.550417	0.000000
2	6	0.000000	1.297480	0.000000
3	6	-1.249551	0.656116	0.000000
4	6	-1.284797	-0.719846	0.000000
5	6	-0.106738	-1.467893	0.000000
6	6	1.124486	-0.853237	0.000000
7	1	2.137334	1.050571	0.000000
8	1	0.044583	2.380858	0.000000
9	1	-2.169981	1.232892	0.000000
10	1	2.036834	-1.442545	0.000000

acetylene
uB3LYP/6311+G(d,p) = -77.3566458 uCCSD(T)/cc-pVDZ = -77.1088354
ZPVE = 0.027032

1	6	0.000000	0.000000	0.599658
2	6	0.000000	0.000000	-0.599658
3	1	0.000000	0.000000	1.662781
4	1	0.000000	0.000000	-1.662781

TS1

uB3LYP/6311+G(d,p) = -463.2634968 uCCSD(T)/cc-pVDZ = -461.8304529

ZPVE = 0.176272 Imaginary Vibration = 335.32*i*

1	6	1.759756	1.433016	-0.000015
2	6	0.625799	0.642306	-0.000031
3	6	0.625767	-0.642095	-0.000011
4	6	1.759662	-1.432891	0.000002
5	6	2.963323	-0.699697	0.000012
6	6	2.963369	0.699743	0.000003
7	1	1.765064	2.518033	-0.000020
8	1	1.764894	-2.517908	0.000004
9	1	3.909101	-1.232349	0.000027
10	1	3.909184	1.232331	0.000013
11	6	-1.619104	-1.356759	0.000031
12	6	-1.619615	1.356707	-0.000017
13	6	-1.882902	-0.684586	-1.223952
14	6	-1.883136	0.684380	-1.223976
15	6	-1.882890	-0.684525	1.223988
16	6	-1.883123	0.684444	1.223963
17	1	-1.539731	-2.437993	0.000054
18	1	-1.957123	-1.248917	2.145934
19	1	-1.957547	1.248851	2.145888
20	1	-1.540557	2.437963	-0.000070
21	1	-1.957585	1.248746	-2.145924
22	1	-1.957136	-1.249014	-2.145880

singlet benzobicyclo-[2,2,2]octatriene ($S1^s$)

uB3LYP/6311+G(d,p) = -463.3571048 uCCSD(T)/cc-pVDZ = -461.9395410

ZPVE = 0.180692

1	6	1.536741	1.403385	-0.000152
2	6	0.343688	0.700801	-0.000052
3	6	0.343687	-0.700801	-0.000029
4	6	1.536739	-1.403385	-0.000107
5	6	2.748029	-0.695071	-0.000211
6	6	2.748030	0.695069	-0.000233
7	1	1.538737	2.488719	-0.000167
8	1	1.538734	-2.488719	-0.000086
9	1	3.687347	-1.236724	-0.000273
10	1	3.687349	1.236721	-0.000312
11	6	-1.077631	-1.279170	0.000108
12	6	-1.077632	1.279171	0.000066
13	6	-1.759099	-0.664942	-1.231753
14	6	-1.759098	0.664903	-1.231775
15	6	-1.758874	-0.664902	1.232073
16	6	-1.758875	0.664941	1.232052
17	1	-1.087113	-2.367886	0.000130
18	1	-2.167872	-1.291630	2.014051
19	1	-2.167861	1.291693	2.014017
20	1	-1.087117	2.367888	0.000046
21	1	-2.168218	1.291630	-2.013690
22	1	-2.168223	-1.291694	-2.013646

TS2

uB3LYP/6311+G(d,p) = -463.2836931 uCCSD(T)/cc-pVDZ = -461.8511331

ZPVE = 0.175188 Imaginary Vibration = 585.31*i*

1	6	1.546494	1.400613	-0.075858
2	6	0.336898	0.706117	-0.233555
3	6	0.336836	-0.706261	-0.233791
4	6	1.546389	-1.400794	-0.076204
5	6	2.736866	-0.701920	0.053870
6	6	2.736891	0.701853	0.054066
7	1	1.544922	2.485894	-0.066642
8	1	1.545098	-2.486078	-0.067471
9	1	3.672041	-1.240637	0.158025
10	1	3.672120	1.240495	0.158131
11	6	-0.967390	-1.337528	-0.326362
12	6	-0.967298	1.337930	-0.325752
13	6	-1.963084	-0.684964	-1.102321
14	6	-1.963113	0.685917	-1.101946
15	6	-1.633335	-0.622565	1.612099
16	6	-1.632808	0.621524	1.612547
17	1	-1.000089	-2.419959	-0.244652
18	1	-1.781041	-1.553105	2.117803
19	1	-1.779037	1.552244	2.118277
20	1	-0.998912	2.420440	-0.242940
21	1	-2.777583	1.254401	-1.535350
22	1	-2.777600	-1.253219	-1.535936

naphthalene

uB3LYP/6311+G(d,p) = -385.9888875 uCCSD(T)/cc-pVDZ = -384.7923752

ZPVE = 0.146920

1	6	2.430302	-0.707684	0.000008
2	6	1.243637	-1.400817	-0.000014
3	6	-0.000004	-0.715377	-0.000005
4	6	0.000007	0.715388	-0.000013
5	6	1.243655	1.400820	-0.000005
6	6	2.430313	0.707663	0.000016
7	1	-1.242069	-2.485458	-0.000028
8	1	3.372621	-1.242770	0.000008
9	1	1.242046	-2.485460	-0.000017
10	6	-1.243650	-1.400812	0.000003
11	6	-1.243643	1.400813	-0.000014
12	1	1.242090	2.485473	0.000015
13	1	3.372640	1.242744	0.000024
14	6	-2.430306	0.707678	0.000001
15	6	-2.430312	-0.707672	0.000017
16	1	-1.242061	2.485455	-0.000020
17	1	-3.372626	1.242768	0.000034
18	1	-3.372638	-1.242754	0.000021

TS3

uB3LYP/6311+G(d,p) = -463.2214998 uCCSD(T)/cc-pVDZ = -461.7704917

ZPVE = 0.169352 Imaginary Vibration = 1454.46*i*

1	6	-4.091647	0.000308	-0.007244
2	6	-3.397643	-1.209621	-0.029166
3	6	-1.999737	-1.214615	-0.038730
4	6	-1.332348	0.000238	-0.024808
5	6	-1.999462	1.215160	-0.004461
6	6	-3.397368	1.210218	0.004948
7	1	-5.175927	0.000338	-0.000700
8	1	-3.941091	-2.148453	-0.039858
9	1	-1.451815	-2.150550	-0.057791
10	1	-1.451321	2.151131	0.002953
11	1	-3.940602	2.149101	0.020776
12	1	-0.053003	0.000051	-0.018843
13	6	4.131888	0.001116	-0.061806
14	6	3.451159	-0.017897	1.154098
15	6	2.050929	-0.018595	1.185497
16	6	1.338809	-0.000081	-0.007576
17	6	2.046291	0.018579	-1.202153
18	6	3.420045	0.019842	-1.272246
19	1	5.216522	0.001538	-0.079295
20	1	4.008071	-0.032314	2.084595
21	1	1.522807	-0.033465	2.134356
22	1	3.940862	0.034715	-2.224314

phenyl (C_6H_5)

uB3LYP/6311+G(d,p) = -231.6223286 uCCSD(T)/cc-pVDZ = -230.8955608

ZPVE = 0.086973

1	6	0.000006	1.322454	0.000000
2	6	1.212392	0.631605	0.000000
3	6	1.224456	-0.771219	0.000000
4	6	-0.000012	-1.395602	-0.000001
5	6	-1.224459	-0.771211	0.000000
6	6	-1.212385	0.631619	0.000000
7	1	0.000011	2.406517	-0.000001
8	1	2.150979	1.176070	0.000005
9	1	2.158301	-1.322285	-0.000003
10	1	-2.158314	-1.322264	0.000004
11	1	-2.150967	1.176090	-0.000003

TS4

uB3LYP/6311+G(d,p) = -463.2285989 uCCSD(T)/cc-pVDZ = -461.7841341

ZPVE = 0.174560 Imaginary Vibration = 238.97*i*

1	6	3.282132	-0.856341	0.017441
2	6	1.961647	-1.242700	0.079836
3	6	0.905459	-0.343507	0.061845
4	6	1.177763	1.011980	-0.024123
5	6	2.510608	1.441844	-0.088711
6	6	3.555033	0.518649	-0.067985
7	1	4.088158	-1.583479	0.033643
8	1	0.364111	1.731863	-0.040746
9	1	2.729030	2.502444	-0.155485
10	1	4.584212	0.857749	-0.117895
11	6	-3.084911	0.904936	-0.138465
12	6	-1.248381	-1.193611	0.154674
13	6	-2.656338	0.522590	1.138016
14	6	-1.766966	-0.531017	1.290738
15	6	-2.631538	0.209255	-1.264934
16	6	-1.741523	-0.845505	-1.123877
17	1	-3.782729	1.726701	-0.252805
18	1	-2.987413	0.487824	-2.250693
19	1	-1.396410	-1.390744	-1.994524
20	1	-0.702813	-2.121360	0.280822
21	1	-1.441865	-0.833983	2.279180
22	1	-3.032196	1.043537	2.011765

S2

uB3LYP/6311+G(d,p) = -463.2743733 uCCSD(T)/cc-pVDZ = -461.8345613

ZPVE = 0.176376

1	6	-3.420025	0.506685	-0.004176
2	6	-2.371436	1.428797	-0.010445
3	6	-1.044969	1.002295	-0.006827
4	6	-0.729521	-0.368500	0.003248
5	6	-1.810895	-1.220702	0.008906
6	6	-3.139397	-0.866125	0.005829
7	1	-4.450175	0.846837	-0.007028
8	1	-2.590746	2.490567	-0.018239
9	1	-3.935965	-1.601920	0.010822
10	6	0.722344	-0.866792	0.007309
11	6	1.452395	-0.464115	-1.250467
12	6	2.648577	0.190556	-1.225888
13	6	3.277192	0.541066	-0.004860
14	6	2.648949	0.211112	1.222068
15	6	1.452801	-0.443087	1.257925
16	1	0.642179	-1.968078	0.016564
17	1	0.983721	-0.721549	-2.194128
18	1	3.130717	0.452419	-2.162440
19	1	3.131319	0.488690	2.153962
20	1	0.984394	-0.684678	2.205906
21	1	4.226397	1.062188	-0.009398
22	1	-0.237930	1.728382	-0.011763

TS5

uB3LYP/6311+G(d,p) = -463.2041816 uCCSD(T)/cc-pVDZ = -461.7614322

ZPVE = 0.170345 Imaginary Vibration = 2213.96*i*

1	6	3.457823	0.137534	0.000035
2	6	2.705303	1.319489	0.000017
3	6	1.305382	1.297701	-0.000026
4	6	0.711334	0.041372	-0.000044
5	6	1.458634	-1.109038	-0.000038
6	6	2.845776	-1.125089	-0.000004
7	1	4.541441	0.200949	0.000069
8	1	3.224702	2.271757	0.000035
9	1	3.433388	-2.035182	-0.000012
10	6	-0.689556	-0.589187	-0.000048
11	6	-1.470756	-0.441566	1.260577
12	6	-2.703715	0.136472	1.232883
13	6	-3.331929	0.477412	0.000060
14	6	-2.703795	0.136517	-1.232813
15	6	-1.470838	-0.441521	-1.260624
16	1	0.195004	-1.752744	-0.000030
17	1	-1.006248	-0.739964	2.193605
18	1	-3.238581	0.306196	2.162243
19	1	-3.238720	0.306279	-2.162133
20	1	-1.006395	-0.739880	-2.193697
21	1	-4.318228	0.924075	0.000097
22	1	0.731662	2.217937	-0.000031

TS6

uB3LYP/6311+G(d,p) = -463.2701145 uCCSD(T)/cc-pVDZ = -461.8298113

ZPVE = 0.176177 Imaginary Vibration = 46.42*i*

1	6	-3.459264	-0.101423	-0.408314
2	6	-2.734133	-1.284727	-0.210476
3	6	-1.416047	-1.146082	0.147105
4	6	-0.718752	0.030023	0.328202
5	6	-1.476448	1.196524	0.121038
6	6	-2.822653	1.127248	-0.240236
7	1	-4.505073	-0.146535	-0.692700
8	1	-3.199661	-2.256201	-0.336894
9	1	-1.012069	2.169434	0.234416
10	1	-3.377261	2.045793	-0.395891
11	6	0.757170	0.043830	0.779527
12	6	1.459053	-1.240667	0.416366
13	6	2.649594	-1.267791	-0.246192
14	6	3.306256	-0.075830	-0.639373
15	6	2.716449	1.173663	-0.328693
16	6	1.525543	1.260356	0.330089
17	1	0.698571	0.084276	1.885459
18	1	0.971350	-2.164878	0.705742
19	1	3.104561	-2.224707	-0.481312
20	1	3.228197	2.085694	-0.619265
21	1	1.121198	2.235331	0.575360
22	1	4.249577	-0.118957	-1.169167

S3

uB3LYP/6311+G(d,p) = -463.2734901 uCCSD(T)/cc-pVDZ = -461.8334300

ZPVE = 0.176311

1	6	-3.385961	0.617827	-0.003689
2	6	-2.320634	1.532169	-0.007910
3	6	-1.054640	1.003790	-0.004715
4	6	-0.717997	-0.334048	0.002255
5	6	-1.806558	-1.221796	0.006302
6	6	-3.120925	-0.750317	0.003355
7	1	-4.408668	0.979629	-0.005907
8	1	-2.501089	2.601671	-0.013403
9	1	-1.615692	-2.291433	0.011839
10	1	-3.942064	-1.458246	0.006629
11	6	0.734056	-0.827908	0.005280
12	6	1.464695	-0.423380	-1.251526
13	6	2.664240	0.224344	-1.225263
14	6	3.295391	0.566915	-0.003795
15	6	2.664439	0.239929	1.222040
16	6	1.464939	-0.407459	1.256696
17	1	0.658780	-1.930675	0.012290
18	1	0.992005	-0.670031	-2.196094
19	1	3.145520	0.489557	-2.161262
20	1	3.145849	0.517032	2.154517
21	1	0.992401	-0.642115	2.204394
22	1	4.246691	1.084217	-0.007184

TS7

uB3LYP/6311+G(d,p) = -463.2275844 uCCSD(T)/cc-pVDZ = -461.7848104

ZPVE = 0.169477 Imaginary Vibration = 957.41*i*

1	6	3.587354	-0.029272	-0.106659
2	6	2.862326	1.130071	-0.374879
3	6	1.470388	1.144671	-0.279264
4	6	0.755661	-0.007045	0.099305
5	6	1.541292	-1.119442	0.338701
6	6	2.906591	-1.200424	0.262013
7	1	4.669211	-0.033420	-0.184400
8	1	3.382872	2.033765	-0.670669
9	1	0.929471	2.053236	-0.519756
10	1	3.444319	-2.117462	0.476656
11	6	-0.737184	-0.039123	0.196545
12	6	-1.490730	1.156339	0.345236
13	6	-2.868930	1.147734	0.204128
14	6	-3.539657	-0.027045	-0.148272
15	6	-2.807503	-1.193215	-0.388286
16	6	-1.429099	-1.197152	-0.252718
17	1	-0.717538	-0.442880	1.932565
18	1	-0.987446	2.068783	0.641309
19	1	-3.429117	2.061774	0.366987
20	1	-3.317603	-2.097464	-0.701406
21	1	-0.859300	-2.095514	-0.459075
22	1	-4.617929	-0.027407	-0.257314

biphenyl radical ($C_{12}H_9$)
uB3LYP/6311+G(d,p) = -462.7347045 uCCSD(T)/cc-pVDZ = -461.2971722
ZPVE = 0.167665

1	6	0.743147	0.001272	-0.003329
2	6	1.447344	-1.178599	0.280311
3	6	2.838456	-1.197055	0.281686
4	6	3.556592	-0.035740	-0.001805
5	6	2.869279	1.141764	-0.291488
6	6	1.476895	1.159948	-0.294590
7	6	-0.739402	0.002448	0.000387
8	6	-1.485318	-1.123158	-0.303040
9	6	-2.851739	-1.226637	-0.341535
10	6	-3.580530	-0.069908	-0.026127
11	6	-2.899767	1.102357	0.302790
12	6	-1.506907	1.142256	0.319302
13	1	0.892592	-2.081129	0.511073
14	1	3.363123	-2.118466	0.508866
15	1	4.640579	-0.049292	-0.000611
16	1	3.417815	2.047441	-0.525407
17	1	0.958486	2.077159	-0.548944
18	1	-3.354185	-2.151481	-0.603204
19	1	-4.664894	-0.093196	-0.035816
20	1	-3.459652	1.995012	0.557685
21	1	-1.002156	2.060274	0.600993

TS8
uB3LYP/6311+G(d,p) = -463.2391818 uCCSD(T)/cc-pVDZ = -461.7984383
ZPVE = 0.174782 Imaginary Vibration = 626.87*i*

1	6	2.549115	0.804676	-0.878930
2	6	1.640946	1.457459	-0.021360
3	6	0.759648	0.705916	0.918290
4	6	1.079551	-0.804181	0.991218
5	6	2.111817	-1.339902	0.233468
6	6	2.777638	-0.548258	-0.794803
7	1	3.084159	1.393684	-1.616634
8	1	1.483436	2.526370	-0.115784
9	1	0.769673	1.165340	1.916173
10	1	2.383679	-2.382413	0.355034
11	1	3.482522	-1.030457	-1.461052
12	6	-2.995382	-0.650924	-0.527695
13	6	-2.934732	0.731458	-0.318914
14	6	-1.770612	1.345231	0.157588
15	6	-0.673724	0.524633	0.404405
16	6	-0.755213	-0.830854	0.188900
17	6	-1.889489	-1.475298	-0.262977
18	1	-3.912511	-1.093255	-0.904025
19	1	-3.810224	1.336266	-0.528799
20	1	-1.740323	2.417236	0.326970
21	1	0.805344	-1.305455	1.914608
22	1	-1.943118	-2.547052	-0.421619

S4

uB3LYP/6311+G(d,p) = -463.2617268 uCCSD(T)/cc-pVDZ = -461.8284323

ZPVE = 0.175701

1	6	-2.721349	-0.680411	-0.741007
2	6	-2.721326	0.680419	-0.741039
3	6	-1.792396	1.448074	0.063247
4	6	-0.761115	0.793361	0.902826
5	6	-0.761125	-0.793335	0.902841
6	6	-1.792439	-1.448057	0.063314
7	1	-3.434381	-1.218835	-1.355489
8	1	-3.434340	1.218837	-1.355548
9	1	-1.802034	2.530637	0.002560
10	1	-1.802119	-2.530623	0.002687
11	6	0.677720	-0.692782	0.347750
12	6	0.677740	0.692784	0.347771
13	6	1.775216	1.436714	-0.053134
14	6	2.893603	0.700247	-0.471172
15	6	2.893582	-0.700283	-0.471196
16	6	1.775172	-1.436730	-0.053184
17	1	1.790082	2.521372	-0.055371
18	1	3.782651	1.224844	-0.804348
19	1	3.782616	-1.224894	-0.804387
20	1	1.790010	-2.521389	-0.055446
21	1	-0.766104	1.203254	1.921610
22	1	-0.766085	-1.203206	1.921636

TS9

uB3LYP/6311+G(d,p) = -463.9227171 uCCSD(T)/cc-pVDZ = -462.4683910

ZPVE = 0.187356 Imaginary Vibration = 330.13*i*

1	6	-3.447927	0.650636	-0.000873
2	6	-2.355240	1.520033	-0.000887
3	6	-1.051817	1.010385	-0.000050
4	6	-0.892725	-0.360570	0.000771
5	6	-1.947913	-1.250614	0.000805
6	6	-3.248840	-0.729601	-0.000028
7	1	-4.455823	1.050273	-0.001518
8	1	-2.515250	2.593558	-0.001540
9	1	-0.195131	1.676358	-0.000036
10	1	-1.790350	-2.325374	0.001451
11	1	-4.100130	-1.402977	-0.000016
12	6	1.184447	-1.182806	0.001705
13	6	1.714772	-0.687667	-1.217443
14	6	2.618166	0.363730	-1.212157
15	6	3.067927	0.905517	-0.001597
16	6	2.618557	0.367199	1.210661
17	6	1.715164	-0.684180	1.219256
18	1	0.679711	-2.141522	0.003169
19	1	1.381289	-1.116116	-2.155546
20	1	2.993148	0.756870	-2.150887
21	1	3.779265	1.723472	-0.002883
22	1	2.993852	0.763025	2.148137
23	1	1.381991	-1.109945	2.158690

S5
uB3LYP/6311+G(d,p) = -463.9627045 uCCSD(T)/cc-pVDZ = -462.5197559
ZPVE = 0.189369

1	6	-3.376307	0.590159	-0.003393
2	6	-2.312299	1.493145	-0.006658
3	6	-0.999554	1.029419	-0.003774
4	6	-0.727981	-0.343428	0.002411
5	6	-1.799384	-1.239106	0.005635
6	6	-3.116428	-0.777918	0.002761
7	1	-4.398524	0.951564	-0.005620
8	1	-2.506425	2.560194	-0.011454
9	1	-0.175681	1.735065	-0.006312
10	1	-1.604094	-2.307089	0.010459
11	1	-3.936241	-1.487921	0.005365
12	6	0.722685	-0.848516	0.005164
13	6	1.458142	-0.449044	-1.250580
14	6	2.657811	0.199442	-1.225361
15	6	3.288578	0.543730	-0.003779
16	6	2.658559	0.213812	1.222150
17	6	1.458904	-0.434307	1.255654
18	1	0.643782	-1.950873	0.011712
19	1	0.988158	-0.699854	-2.195556
20	1	3.140715	0.461669	-2.161462
21	1	3.142019	0.486985	2.154823
22	1	0.989493	-0.674056	2.203787
23	1	4.240439	1.059992	-0.007119

TS10
uB3LYP/6311+G(d,p) = -463.8052339 uCCSD(T)/cc-pVDZ = -462.3713759
ZPVE = 0.182237 Imaginary Vibration = 1342.92*i*

1	6	2.791939	0.795499	-0.000136
2	6	2.840460	-0.593661	-0.000137
3	6	1.657906	-1.350864	-0.000038
4	6	0.431672	-0.698407	0.000099
5	6	0.415974	0.685908	0.000141
6	6	1.550455	1.460421	-0.000030
7	1	3.710755	1.372323	-0.000214
8	1	3.799445	-1.099541	-0.000224
9	1	1.704530	-2.435861	-0.000068
10	1	-1.117552	2.329119	-0.000565
11	1	1.508794	2.545512	-0.000087
12	6	-1.793208	0.541795	-1.268892
13	6	-1.664127	-0.784293	-1.236325
14	6	-0.962058	-1.341837	0.000155
15	6	-1.663817	-0.783976	1.236545
16	6	-1.792911	0.542084	1.268966
17	6	-1.419635	1.283666	-0.000298
18	1	-2.191286	1.094281	-2.110229
19	1	-1.962954	-1.437285	-2.046969
20	1	-0.909135	-2.429737	0.000282
21	1	-2.190119	1.095110	2.110351
22	1	-2.746197	1.864936	-0.000083
23	1	-1.962177	-1.436857	2.047501

TS11

uB3LYP/6311+G(d,p) = -463.8850513 uCCSD(T)/cc-pVDZ = -462.4501814
ZPVE = 0.188272 Imaginary Vibration = 545.97*i*

1	6	2.736812	0.676630	0.149754
2	6	2.678416	-0.725650	0.038531
3	6	1.459481	-1.350432	-0.278545
4	6	0.325279	-0.610100	-0.539937
5	6	0.385972	0.841984	-0.565810
6	6	1.638115	1.446150	-0.164525
7	1	3.667676	1.153894	0.436875
8	1	3.558213	-1.325341	0.240620
9	1	1.392646	-2.434303	-0.243972
10	1	-0.083222	1.335692	-1.412261
11	1	1.718103	2.528435	-0.172522
12	6	-2.221935	0.863724	-0.594853
13	6	-2.132279	-0.399031	-1.036067
14	6	-1.078838	-1.235170	-0.343092
15	6	-1.223140	-1.059805	1.169115
16	6	-1.263481	0.217837	1.575253
17	6	-1.291089	1.224376	0.498535
18	1	-2.875829	1.607807	-1.036519
19	1	-2.722286	-0.801420	-1.850334
20	1	-1.089221	-2.282194	-0.645070
21	1	-1.231195	0.519859	2.615390
22	1	-1.245288	2.269747	0.786994
23	1	-1.169486	-1.915252	1.830655

S6

uB3LYP/6311+G(d,p) = -463.9010630 uCCSD(T)/cc-pVDZ = -462.4753942
ZPVE = 0.189606

1	6	-2.698200	-0.684629	0.066135
2	6	-2.707030	0.727938	-0.083380
3	6	-1.478167	1.431272	-0.166724
4	6	-0.299909	0.751209	-0.284581
5	6	-0.288562	-0.737162	-0.532972
6	6	-1.544887	-1.406212	-0.056094
7	1	-3.627430	-1.192209	0.304878
8	1	-3.639534	1.273808	-0.006306
9	1	-1.473058	2.510116	-0.037935
10	1	-0.255686	-0.894583	-1.628139
11	1	-1.545022	-2.484607	0.068138
12	6	1.108983	-1.275336	-0.005699
13	6	2.119986	-0.620092	-0.939329
14	6	2.090404	0.711791	-0.920442
15	6	1.084609	1.295461	0.064655
16	6	1.307567	0.631132	1.430428
17	6	1.313839	-0.701632	1.388976
18	1	1.146811	-2.364132	-0.034827
19	1	2.755307	-1.212587	-1.586895
20	1	2.697309	1.353035	-1.547886
21	1	1.376204	1.227470	2.331904
22	1	1.413428	-1.342147	2.256417
23	1	1.099862	2.383398	0.114806

TS12
uB3LYP/6311+G(d,p) = -463.8515292 uCCSD(T)/cc-pVDZ = -462.4235904
ZPVE = 0.182567 Imaginary Vibration = 847.93*i*

1	6	-2.742810	-0.673571	0.068004
2	6	-2.734181	0.718602	-0.023434
3	6	-1.519121	1.419297	-0.084093
4	6	-0.329887	0.716146	-0.105720
5	6	-0.337875	-0.700333	-0.153880
6	6	-1.547136	-1.389533	0.038565
7	1	-3.684200	-1.202486	0.164942
8	1	-3.669363	1.266741	-0.005303
9	1	-1.516912	2.504632	-0.075028
10	1	-0.402754	-0.971281	-1.971056
11	1	-1.550562	-2.472535	0.101145
12	6	1.087677	-1.272023	0.007872
13	6	1.910437	-0.645621	-1.123901
14	6	1.907063	0.684329	-1.114586
15	6	1.086224	1.287780	0.029586
16	6	1.610767	0.661580	1.332456
17	6	1.607811	-0.668483	1.320740
18	1	2.405557	-1.264771	-1.860374
19	1	2.389539	1.315435	-1.849609
20	1	1.919287	1.280913	2.164932
21	1	1.920732	-1.301762	2.140977
22	1	1.094981	2.376446	0.042231
23	1	1.099888	-2.360349	-0.002513

TS13
uB3LYP/6311+G(d,p) = -463.9157838 uCCSD(T)/cc-pVDZ = -462.4662997
ZPVE = 0.182621 Imaginary Vibration = 935.96*i*

1	6	3.560414	0.061724	-0.139410
2	6	2.795000	1.170441	-0.492230
3	6	1.406356	1.131488	-0.374940
4	6	0.758454	-0.014157	0.103027
5	6	1.540466	-1.122330	0.455841
6	6	2.926180	-1.086836	0.333939
7	1	4.640245	0.091122	-0.231061
8	1	3.276146	2.066461	-0.868415
9	1	0.820582	1.991251	-0.678991
10	1	1.057614	-2.008565	0.852229
11	1	3.512798	-1.952967	0.619556
12	6	-0.736571	-0.062296	0.189198
13	6	-1.484039	1.106958	0.497586
14	6	-2.862428	1.127351	0.358930
15	6	-3.540017	0.015207	-0.149018
16	6	-2.815561	-1.110039	-0.550215
17	6	-1.436130	-1.141332	-0.417188
18	1	-0.768757	-0.699820	1.863033
19	1	-0.968239	1.966760	0.908849
20	1	-3.416985	2.014240	0.644933
21	1	-3.331193	-1.957224	-0.988833
22	1	-0.876624	-2.004268	-0.758604
23	1	-4.618325	0.035932	-0.255818

biphenyl ($C_{12}H_{10}$)
uB3LYP/6311+G(d,p) = -463.4227458 uCCSD(T)/cc-pVDZ = -461.9865358
ZPVE = 0.180811

1	6	0.742812	0.000000	0.000000
2	6	1.463796	-1.126966	0.422100
3	6	2.856239	-1.127298	0.422350
4	6	3.559085	0.000000	0.000000
5	6	2.856239	1.127298	-0.422350
6	6	1.463796	1.126966	-0.422100
7	6	-0.742812	0.000000	0.000000
8	6	-1.463796	-1.126966	-0.422100
9	6	-2.856239	-1.127298	-0.422350
10	6	-3.559085	0.000000	0.000000
11	6	-2.856239	1.127298	0.422350
12	6	-1.463796	1.126965	0.422100
13	1	0.928265	-2.000847	0.775657
14	1	3.392845	-2.006525	0.761529
15	1	4.643187	0.000000	0.000000
16	1	3.392844	2.006525	-0.761530
17	1	0.928264	2.000847	-0.775657
18	1	-0.928265	-2.000847	-0.775657
19	1	-3.392845	-2.006525	-0.761529
20	1	-4.643187	0.000000	0.000000
21	1	-3.392844	2.006525	0.761530
22	1	-0.928264	2.000847	0.775657

TS14^t
uB3LYP/6311+G(d,p) = -463.2350710 uCCSD(T)/cc-pVDZ = -461.7878057
ZPVE = 0.174318 Imaginary Vibration = 315.23*i*

1	6	3.411408	0.592485	-0.123442
2	6	2.339292	1.486005	-0.163183
3	6	1.026716	1.014069	-0.047382
4	6	0.838472	-0.344753	0.104507
5	6	1.872808	-1.258139	0.147065
6	6	3.183028	-0.774572	0.031192
7	1	4.426391	0.963088	-0.212999
8	1	2.522085	2.549055	-0.283528
9	1	0.186739	1.700529	-0.075445
10	1	1.692566	-2.322652	0.266369
11	1	4.018701	-1.466486	0.062057
12	6	-1.273005	-1.110337	0.251795
13	6	-1.802768	-0.343582	1.322217
14	6	-2.673635	0.714356	1.069099
15	6	-3.037316	0.926561	-0.246326
16	6	-2.634541	0.163880	-1.324649
17	6	-1.763785	-0.891988	-1.062435
18	1	-0.793750	-2.054899	0.477724
19	1	-1.498372	-0.562569	2.339803
20	1	-3.057690	1.324498	1.879292
21	1	-2.987151	0.356830	-2.331842
22	1	-1.429557	-1.531312	-1.872175

TS14[s]

uB3LYP/6311+G(d,p) = -463.2233067 uCCSD(T)/cc-pVDZ = -461.7856833

ZPVE = 0.175676 Imaginary Vibration = 524.26*i*

1	6	-3.104695	0.636072	-0.084020
2	6	-2.016549	1.517657	-0.114844
3	6	-0.718264	1.039257	-0.055913
4	6	-0.491710	-0.342557	0.018743
5	6	-1.577128	-1.227695	0.048037
6	6	-2.879518	-0.734634	0.000968
7	1	-4.116986	1.020822	-0.121586
8	1	-2.186391	2.586650	-0.173487
9	1	0.122738	1.722221	-0.055598
10	1	-1.405799	-2.297262	0.104327
11	1	-3.713933	-1.426045	0.027340
12	6	1.019266	-1.038302	-0.610616
13	6	1.899022	-0.194172	-1.363083
14	6	2.831613	0.545482	-0.667493
15	6	2.719408	0.817032	0.732451
16	6	1.778983	0.112267	1.445913
17	6	1.019459	-0.949031	0.832139
18	1	0.677591	-1.946165	-1.092076
19	1	1.888759	-0.264177	-2.446992
20	1	3.686770	0.937274	-1.216736
21	1	1.531166	0.367283	2.475121
22	1	0.636751	-1.788860	1.405999

S7[t]

uB3LYP/6311+G(d,p) = -463.2760604 uCCSD(T)/cc-pVDZ = -461.8421796

ZPVE = 0.176780

1	6	-3.325419	0.558755	-0.007288
2	6	-2.273947	1.476132	-0.015890
3	6	-0.954942	1.030344	-0.009663
4	6	-0.665243	-0.338602	0.005293
5	6	-1.724228	-1.248938	0.013706
6	6	-3.047285	-0.805716	0.007487
7	1	-4.352398	0.906303	-0.012117
8	1	-2.482511	2.540344	-0.027479
9	1	-0.141234	1.747668	-0.016406
10	1	-1.514481	-2.314119	0.025235
11	1	-3.857429	-1.526632	0.014227
12	6	0.791960	-0.825278	0.011406
13	6	1.516090	-0.427203	-1.256310
14	6	2.707122	0.248167	-1.245340
15	6	3.271215	0.579719	-0.008934
16	6	2.708570	0.281590	1.236611
17	6	1.517544	-0.393148	1.267060
18	1	0.727629	-1.927897	0.026381
19	1	1.048410	-0.697308	-2.197585
20	1	3.194966	0.518124	-2.176458
21	1	3.197475	0.576463	2.159576
22	1	1.050953	-0.637882	2.215796

S7[s]
uB3LYP/6311+G(d,p) = -463.2683087 uCCSD(T)/cc-pVDZ = -461.8353688
ZPVE = 0.177339

1	6	3.276293	0.610551	-0.015528
2	6	2.198613	1.497014	-0.026122
3	6	0.893042	1.014455	-0.012322
4	6	0.647410	-0.362799	0.012371
5	6	1.730172	-1.244108	0.022902
6	6	3.039260	-0.761084	0.008983
7	1	4.292402	0.988140	-0.026259
8	1	2.375063	2.566630	-0.045172
9	1	0.060338	1.709577	-0.020837
10	1	1.553367	-2.314872	0.041969
11	1	3.869986	-1.457876	0.017425
12	6	-0.795275	-0.891911	0.024865
13	6	-1.541000	-0.487849	1.256237
14	6	-2.668121	0.269096	1.198084
15	6	-3.076564	0.893388	-0.027879
16	6	-2.662650	0.204815	-1.217020
17	6	-1.535515	-0.554309	-1.229666
18	1	-0.707764	-1.991860	0.054583
19	1	-1.091592	-0.755301	2.209700
20	1	-3.156980	0.558859	2.125505
21	1	-3.146981	0.445111	-2.160811
22	1	-1.081824	-0.871967	-2.165529

TS15[t]
uB3LYP/6311+G(d,p) = --463.1934985 uCCSD(T)/cc-pVDZ = -461.7610426
ZPVE = 0.171264 Imaginary Vibration = 1571.12*i*

1	6	3.023921	0.686732	0.000219
2	6	1.874216	1.492249	-0.000010
3	6	0.645558	0.869952	-0.000418
4	6	0.468589	-0.511984	-0.000535
5	6	1.629558	-1.293709	-0.000261
6	6	2.894535	-0.698227	0.000078
7	1	4.006658	1.146284	0.000516
8	1	1.961359	2.573604	0.000109
9	1	-0.762785	1.547580	0.000241
10	1	1.543680	-2.376473	-0.000336
11	1	3.779555	-1.324726	0.000247
12	6	-0.932938	-1.164082	-0.000562
13	6	-1.689920	-0.718574	1.248651
14	6	-2.195787	0.523406	1.248714
15	6	-1.974438	1.257362	0.000683
16	6	-2.196496	0.524371	-1.247717
17	6	-1.690607	-0.717579	-1.248953
18	1	-0.798349	-2.246846	-0.000880
19	1	-1.756649	-1.384970	2.101923
20	1	-2.675891	0.973798	2.110798
21	1	-2.677000	0.975472	-2.109209
22	1	-1.757717	-1.383229	-2.102747

TS15^{s}

uB3LYP/6311+G(d,p) = -463.2179256 uCCSD(T)/cc-pVDZ = -461.7951498

ZPVE = 0.173446 Imaginary Vibration = 1268.93*i*

1	6	2.896252	0.714712	-0.000223
2	6	1.711108	1.467238	-0.000401
3	6	0.503187	0.795600	-0.000266
4	6	0.419178	-0.587542	0.000096
5	6	1.598069	-1.329284	0.000259
6	6	2.835607	-0.673615	0.000056
7	1	3.855265	1.221221	-0.000291
8	1	1.750983	2.551623	-0.000584
9	1	-0.513959	1.704091	-0.000540
10	1	1.558557	-2.414138	0.000533
11	1	3.749829	-1.256425	0.000136
12	6	-0.991008	-1.247001	0.000537
13	6	-1.691070	-0.725817	1.238386
14	6	-2.022645	0.569410	1.225708
15	6	-1.728024	1.359998	-0.000675
16	6	-2.022501	0.567833	-1.226241
17	6	-1.691526	-0.727585	-1.237617
18	1	-0.887628	-2.331786	0.002391
19	1	-1.780336	-1.366093	2.109982
20	1	-2.425243	1.079692	2.095338
21	1	-2.425336	1.077109	-2.096353
22	1	-1.781899	-1.368982	-2.108321

triplet benzobicyclo-[2,2,2]octatriene (S1^{t})

uB3LYP/6311+G(d,p) = -463.2351411 uCCSD(T)/cc-pVDZ = -461.8092956

ZPVE = 0.174798

1	6	-1.516547	-1.443733	-0.000145
2	6	-0.302555	-0.756686	-0.000046
3	6	-0.302555	0.756686	-0.000022
4	6	-1.516547	1.443733	-0.000101
5	6	-2.708335	0.746797	-0.000204
6	6	-2.708335	-0.746797	-0.000226
7	1	-1.521432	-2.529848	-0.000160
8	1	-1.521432	2.529848	-0.000082
9	1	-3.655945	1.270316	-0.000269
10	1	-3.655945	-1.270316	-0.000307
11	6	1.112192	1.301082	0.000108
12	6	1.112192	-1.301082	0.000065
13	6	1.710792	0.672455	-1.249866
14	6	1.710792	-0.672414	-1.249889
15	6	1.710562	0.672414	1.250171
16	6	1.710563	-0.672456	1.250149
17	1	1.148422	2.389316	0.000129
18	1	1.995952	1.282007	2.099511
19	1	1.995952	-1.282076	2.099468
20	1	1.148422	-2.389316	0.000050
21	1	1.996345	-1.282006	-2.099173
22	1	1.996345	1.282076	-2.099131

TS16^{t}

uB3LYP/6311+G(d,p) = -463.2011287 uCCSD(T)/cc-pVDZ = -461.7725585

ZPVE = 0.175343 Imaginary Vibration = 577.02*i*

1	6	-2.740660	-0.640485	0.186175
2	6	-2.647735	0.748643	-0.005943
3	6	-1.413102	1.325680	-0.355847
4	6	-0.296876	0.545380	-0.571959
5	6	-0.397386	-0.902551	-0.513000
6	6	-1.659066	-1.454061	-0.082930
7	1	-3.682345	-1.077842	0.499836
8	1	-3.512053	1.381066	0.160047
9	1	-1.320612	2.407861	-0.381681
10	1	0.086103	-1.469564	-1.301963
11	1	-1.760641	-2.532486	-0.027129
12	6	1.286893	-1.182069	0.581158
13	6	2.232191	-0.978926	-0.510283
14	6	2.164738	0.256992	-1.038641
15	6	1.121130	1.154779	-0.403607
16	6	1.249200	1.081354	1.122131
17	6	1.262979	-0.169246	1.622461
18	1	2.873908	-1.769273	-0.885343
19	1	2.772221	0.595572	-1.870238
20	1	1.209523	1.982281	1.723227
21	1	1.205882	-0.409944	2.677553
22	1	1.154178	2.179397	-0.772598

TS16^{s}

uB3LYP/6311+G(d,p) = -463.1959405 uCCSD(T)/cc-pVDZ = -461.7836673

ZPVE = 0.175282 Imaginary Vibration = 268.13*i*

1	6	-2.727742	-0.638018	0.172306
2	6	-2.617171	0.770927	-0.008785
3	6	-1.402278	1.334690	-0.342088
4	6	-0.269611	0.537297	-0.562299
5	6	-0.347983	-0.913420	-0.441566
6	6	-1.651976	-1.443285	-0.039509
7	1	-3.684074	-1.066138	0.451382
8	1	-3.486099	1.401483	0.141372
9	1	-1.307569	2.414132	-0.409578
10	1	0.048931	-1.469422	-1.285881
11	1	-1.749307	-2.520405	0.039382
12	6	1.097273	-1.204857	0.573651
13	6	2.192862	-1.029589	-0.440726
14	6	2.161100	0.177626	-1.023605
15	6	1.127782	1.147283	-0.457199
16	6	1.260901	1.150580	1.072155
17	6	1.276089	-0.096936	1.559707
18	1	2.834546	-1.845648	-0.760325
19	1	2.745443	0.458061	-1.892926
20	1	1.322486	2.069382	1.645899
21	1	1.502665	-0.339934	2.593842
22	1	1.177496	2.144695	-0.895431

S8^t
uB3LYP/6311+G(d,p) = -463.2222630 uCCSD(T)/cc-pVDZ = -461.8017128
ZPVE = 0.176319

1	6	-2.697114	-0.659512	0.064719
2	6	-2.676301	0.752951	-0.083603
3	6	-1.434138	1.433072	-0.162129
4	6	-0.268497	0.733606	-0.283953
5	6	-0.292696	-0.770030	-0.546103
6	6	-1.561810	-1.408781	-0.058328
7	1	-3.636846	-1.145954	0.306146
8	1	-3.597465	1.317672	-0.006648
9	1	-1.408884	2.510973	-0.025681
10	1	-0.271066	-0.916407	-1.641865
11	1	-1.581401	-2.485354	0.071106
12	6	1.082890	-1.251246	-0.024171
13	6	2.118587	-0.690541	-0.950664
14	6	2.129298	0.645285	-0.911488
15	6	1.130819	1.239017	0.081720
16	6	1.336936	0.550593	1.442779
17	6	1.306100	-0.785127	1.381632
18	1	2.726179	-1.302837	-1.607518
19	1	2.753282	1.279919	-1.530394
20	1	1.420202	1.132693	2.353537
21	1	1.379912	-1.451828	2.232318
22	1	1.171645	2.325397	0.146540

S8^s
uB3LYP/6311+G(d,p) = -463.1857549 uCCSD(T)/cc-pVDZ = -462.3128374*
ZPVE = 0.175852

1	6	-2.691654	-0.645613	0.011489
2	6	-2.651424	0.769731	-0.064124
3	6	-1.429685	1.472037	-0.050878
4	6	-0.257519	0.751761	-0.081261
5	6	-0.300154	-0.706771	-0.535392
6	6	-1.552881	-1.394729	-0.126128
7	1	-3.643679	-1.130232	0.198757
8	1	-3.582025	1.324658	-0.018454
9	1	-1.428599	2.541792	0.142219
10	1	-0.440142	-0.602879	-1.639025
11	1	-1.561055	-2.475942	-0.033705
12	6	1.085707	-1.247017	-0.285924
13	6	2.054012	-0.451174	-1.099746
14	6	2.086389	0.857202	-0.827429
15	6	1.136617	1.203092	0.310800
16	6	1.393361	0.237303	1.484962
17	6	1.349091	-1.071365	1.175931
18	1	2.702901	-0.921641	-1.833675
19	1	2.720617	1.597595	-1.306374
20	1	1.425790	0.635048	2.493199
21	1	1.318498	-1.866082	1.913694
22	1	1.156538	2.250941	0.609565

* energy value corrected based on the CCSD(T) energy for TS16s and the difference between the B3LYP energies for S8s and TS16s

TS17^{s}

uB3LYP/6311+G(d,p) = -463.1703475 uCCSD(T)/cc-pVDZ = -461.7558490
ZPVE = 0.173084 Imaginary Vibration = 1102.10*i*

1	6	-2.711587	-0.679207	0.019881
2	6	-2.699131	0.724559	-0.000948
3	6	-1.493237	1.445704	-0.034791
4	6	-0.305435	0.745565	-0.100907
5	6	-0.300436	-0.682378	-0.371374
6	6	-1.533670	-1.390347	-0.126921
7	1	-3.652968	-1.204958	0.128757
8	1	-3.637167	1.263405	0.078609
9	1	-1.505589	2.520394	0.121558
10	1	-0.120705	-1.193223	-1.434712
11	1	-1.526039	-2.475010	-0.179177
12	6	1.118309	-1.249201	-0.314261
13	6	1.993914	-0.373293	-1.168956
14	6	1.977428	0.929648	-0.881769
15	6	1.079599	1.213300	0.321836
16	6	1.492836	0.236965	1.457914
17	6	1.513680	-1.064658	1.151319
18	1	2.615805	-0.800819	-1.950397
19	1	2.516941	1.717007	-1.399336
20	1	1.707169	0.647552	2.438295
21	1	1.725265	-1.868591	1.847069
22	1	1.083668	2.254293	0.643189

TS18^{t}

uB3LYP/6311+G(d,p) = -463.1704743 uCCSD(T)/cc-pVDZ = -461.747545
ZPVE = 0.169142 Imaginary Vibration = 828.52*i*

1	6	-2.743096	-0.655395	0.067995
2	6	-2.708496	0.736169	-0.022334
3	6	-1.481631	1.416246	-0.082664
4	6	-0.304946	0.692995	-0.108892
5	6	-0.342603	-0.730562	-0.157363
6	6	-1.562792	-1.397098	0.038981
7	1	-3.694677	-1.165587	0.165220
8	1	-3.633555	1.301109	-0.003115
9	1	-1.460563	2.501465	-0.070357
10	1	-0.406473	-0.998014	-1.992325
11	1	-1.583574	-2.478786	0.103861
12	6	1.073842	-1.247161	0.005417
13	6	1.911856	-0.716414	-1.128463
14	6	1.940138	0.617385	-1.115044
15	6	1.126947	1.234381	0.033032
16	6	1.639649	0.593380	1.338893
17	6	1.607213	-0.740400	1.323585
18	1	2.379914	-1.355355	-1.866588
19	1	2.432869	1.240556	-1.851324
20	1	1.966120	1.204460	2.171795
21	1	1.904347	-1.393426	2.134778
22	1	1.159098	2.322424	0.049201

S9

uB3LYP/6311+G(d,p) = -462.6758062 uCCSD(T)/cc-pVDZ = -461.2605325

ZPVE = 0.167350

1	6	-1.500755	1.399409	-0.000121
2	6	-0.319914	0.677186	-0.000060
3	6	-0.348763	-0.731063	0.000067
4	6	-1.553405	-1.412956	0.000130
5	6	-2.749277	-0.678825	0.000066
6	6	-2.723698	0.711006	-0.000057
7	1	-1.484569	2.484720	-0.000217
8	1	-1.572282	-2.497014	0.000225
9	1	-3.698955	-1.201954	0.000114
10	1	-3.653243	1.269159	-0.000105
11	6	1.066434	-1.254612	0.000111
12	6	1.117640	1.225973	-0.000114
13	6	1.761353	-0.735699	1.235388
14	6	1.789331	0.597957	1.235660
15	6	1.761346	-0.735923	-1.235263
16	6	1.789324	0.597733	-1.235777
17	1	2.150143	-1.381989	-2.012465
18	1	2.210384	1.216568	-2.018871
19	1	1.150284	2.314097	-0.000212
20	1	2.210397	1.216934	2.018639
21	1	2.150154	-1.381625	2.012705

TS19

uB3LYP/6311+G(d,p) = -462.6002423 uCCSD(T)/cc-pVDZ = -461.1644730

ZPVE = 0.161448 Imaginary Vibration = 388.85*i*

1	6	1.660791	1.308091	0.367002
2	6	0.396403	0.797393	0.032941
3	6	0.287187	-0.543109	-0.413191
4	6	1.423480	-1.345940	-0.504118
5	6	2.673919	-0.815286	-0.195726
6	6	2.789974	0.509145	0.241910
7	1	1.751546	2.334366	0.707880
8	1	1.328853	-2.377884	-0.823234
9	1	3.559902	-1.433085	-0.289058
10	1	3.766190	0.913377	0.485077
11	6	-1.106121	-0.990941	-0.547470
12	6	-0.840404	1.544681	0.125365
13	6	-2.008414	-0.078249	-1.200064
14	6	-1.883526	1.225847	-0.781689
15	6	-1.674626	-1.365232	0.858159
16	6	-1.732207	-0.393567	1.718440
17	1	-1.970592	-2.398517	1.039255
18	1	-1.962277	-0.199933	2.752214
19	1	-0.824578	2.518384	0.602435
20	1	-2.653428	1.957433	-1.002369
21	1	-2.914353	-0.431137	-1.681561

naphthyl vinyl
uB3LYP/6311+G(d,p) = -462.7174082 uCCSD(T)/cc-pVDZ = -461.2792450
ZPVE = 0.165536

1	6	-2.939321	-0.612987	-0.038915
2	6	-2.390923	0.645722	-0.037114
3	6	-0.983595	0.833559	-0.005010
4	6	-0.123372	-0.313492	0.036897
5	6	-0.729080	-1.599524	0.017236
6	6	-2.095988	-1.746321	-0.015828
7	1	-1.077955	2.992397	-0.054733
8	1	-4.015515	-0.741186	-0.064515
9	1	-3.029425	1.522695	-0.064284
10	6	-0.416570	2.132996	-0.023229
11	6	1.297469	-0.112129	0.076776
12	1	-0.107134	-2.485471	0.013407
13	1	-2.530757	-2.739479	-0.030558
14	6	1.797417	1.178701	0.057711
15	6	0.946946	2.299441	0.001059
16	1	2.870650	1.322453	0.106270
17	1	1.376773	3.294743	-0.009191
18	6	2.227112	-1.258752	0.156110
19	6	3.472876	-1.282405	-0.264087
20	1	1.843122	-2.170708	0.623293
21	1	4.292410	-1.984293	-0.289322

TS20
uB3LYP/6311+G(d,p) = -462.5985294 uCCSD(T)/cc-pVDZ = -461.1603227
ZPVE = 0.161964 Imaginary Vibration = 580.29*i*

1	6	-1.534335	1.391521	0.045522
2	6	-0.324530	0.713389	-0.178843
3	6	-0.337181	-0.702184	-0.296352
4	6	-1.545751	-1.406764	-0.196706
5	6	-2.731176	-0.713075	-0.007599
6	6	-2.724674	0.685625	0.117547
7	1	-1.530494	2.471899	0.150334
8	1	-1.543306	-2.487832	-0.276038
9	1	-3.669100	-1.253707	0.050565
10	1	-3.657736	1.215499	0.272787
11	6	0.982342	-1.258580	-0.408268
12	6	0.974862	1.350664	-0.256102
13	6	1.641947	-0.867659	1.507495
14	6	1.674894	0.359635	1.700609
15	6	1.972921	-0.623369	-1.176120
16	6	1.983670	0.749657	-1.049940
17	1	2.777991	-1.169265	-1.654855
18	1	2.807995	1.344148	-1.428820
19	1	1.015535	2.422510	-0.087670
20	1	1.825401	1.243381	2.279820
21	1	1.775785	-1.859791	1.886422

naphthyl radical ($C_{10}H_7$)
uB3LYP/6311+G(d,p) = -385.2998382 uCCSD(T)/cc-pVDZ = -384.1021807
ZPVE = 0.133909

1	6	-2.395048	0.729102	0.000020
2	6	-1.190809	1.391913	0.000194
3	6	0.035414	0.677305	0.000123
4	6	-0.014562	-0.762063	-0.000137
5	6	-1.273656	-1.417043	-0.000312
6	6	-2.436891	-0.685465	-0.000235
7	1	1.330709	2.407304	0.000490
8	1	-3.322165	1.290817	0.000077
9	1	-1.161882	2.476632	0.000387
10	6	1.301950	1.323032	0.000297
11	6	1.226944	-1.408640	-0.000195
12	1	-1.297762	-2.500281	-0.000506
13	1	-3.395175	-1.191963	-0.000370
14	6	2.447129	-0.820808	-0.000034
15	6	2.473844	0.604562	0.000223
16	1	3.370065	-1.389842	-0.000093
17	1	3.430311	1.115973	0.000358

TS21^t
uB3LYP/6311+G(d,p) = -463.2058661 uCCSD(T)/cc-pVDZ = -461.7604222
ZPVE = 0.171877 Imaginary Vibration = 2388.53*i*

1	6	-3.537931	-0.038814	-0.086115
2	6	-2.864766	1.151961	0.202373
3	6	-1.479596	1.180646	0.278288
4	6	-0.708178	0.016496	0.059775
5	6	-1.405279	-1.174370	-0.235571
6	6	-2.794981	-1.197729	-0.304291
7	1	-4.620036	-0.059687	-0.139761
8	1	-3.426706	2.062689	0.379315
9	1	-0.988293	2.113333	0.530459
10	1	-0.856590	-2.084464	-0.444606
11	1	-3.299457	-2.128119	-0.542232
12	6	0.753557	0.052533	0.153949
13	6	1.524211	1.244967	-0.194189
14	6	2.878254	1.243697	-0.320374
15	6	3.574392	0.004187	-0.130989
16	6	2.990986	-1.182494	0.129582
17	6	1.570645	-1.223387	0.325541
18	1	1.189831	-0.405724	1.278525
19	1	0.975515	2.154223	-0.409381
20	1	3.408045	2.147434	-0.596276
21	1	3.556383	-2.105598	0.208072
22	1	1.053428	-2.160241	0.468021

TS21^{s}
uB3LYP/6311+G(d,p) = -463.2386327 uCCSD(T)/cc-pVDZ = -461.7984884
ZPVE = 0.173782 Imaginary Vibration = 1021.06*i*

1	6	-3.526962	-0.053171	-0.089309
2	6	-2.882643	1.073723	0.420279
3	6	-1.493388	1.110560	0.494963
4	6	-0.728646	0.018516	0.064278
5	6	-1.384087	-1.108261	-0.446929
6	6	-2.774537	-1.142227	-0.524415
7	1	-4.608923	-0.080830	-0.148336
8	1	-3.462400	1.922622	0.764142
9	1	-0.998328	1.986196	0.900271
10	1	-0.805234	-1.951453	-0.806147
11	1	-3.268440	-2.017077	-0.931432
12	6	0.760845	0.067078	0.114726
13	6	1.497746	1.177012	-0.392188
14	6	2.865891	1.082722	-0.567634
15	6	3.690183	-0.015915	-0.155416
16	6	2.959485	-1.072888	0.410543
17	6	1.548419	-1.103179	0.501923
18	1	1.177687	-0.135733	1.326199
19	1	0.944066	2.058232	-0.702737
20	1	3.345715	1.924337	-1.067609
21	1	3.479318	-1.932880	0.831184
22	1	1.002700	-1.977244	0.849538

TS22^{t}
uB3LYP/6311+G(d,p) = -463.2272925 uCCSD(T)/cc-pVDZ = -461.7849236
ZPVE = 0.169560 Imaginary Vibration = 881.87*i*

1	6	3.498410	0.061744	-0.132454
2	6	2.733277	1.165798	-0.500026
3	6	1.344245	1.126446	-0.387783
4	6	0.695948	-0.014473	0.100918
5	6	1.477547	-1.117919	0.468721
6	6	2.863674	-1.082258	0.350945
7	1	4.578508	0.091269	-0.220472
8	1	3.214783	2.058195	-0.884163
9	1	0.758786	1.982027	-0.704219
10	1	0.994395	-1.999981	0.873912
11	1	3.450063	-1.944619	0.648069
12	6	-0.799669	-0.062231	0.181701
13	6	-1.540790	1.109962	0.498647
14	6	-2.925810	1.143979	0.357887
15	6	-3.530818	0.017173	-0.156720
16	6	-2.877077	-1.121119	-0.575355
17	6	-1.491255	-1.143569	-0.431731
18	1	-0.840843	-0.715668	1.875486
19	1	-1.022189	1.965804	0.916092
20	1	-3.490282	2.024519	0.643762
21	1	-3.401454	-1.959225	-1.020793
22	1	-0.927857	-2.003500	-0.776173

S10^t
uB3LYP/6311+G(d,p) = -463.2844057 uCCSD(T)/cc-pVDZ = -461.8412484
ZPVE = 0.176399

1	6	0.699302	0.034941	-0.013748
2	6	1.461380	1.208020	0.182418
3	6	2.848943	1.178917	0.189534
4	6	3.534582	-0.024064	0.008823
5	6	2.805823	-1.196868	-0.172345
6	6	1.414314	-1.169876	-0.179162
7	6	-0.768365	0.054566	-0.028313
8	6	-1.488337	1.227573	-0.200533
9	6	-2.894764	1.273767	-0.178699
10	6	-3.565326	0.059076	0.039159
11	6	-3.014454	-1.143887	0.201650
12	6	-1.504134	-1.261963	0.136731
13	1	0.962501	2.152780	0.357767
14	1	3.400871	2.098722	0.349124
15	1	4.618199	-0.045325	0.017326
16	1	3.321465	-2.140795	-0.311167
17	1	0.881424	-2.099715	-0.331031
18	1	-0.959955	2.158336	-0.372970
19	1	-3.422172	2.207871	-0.324768
20	1	-3.591379	-2.048909	0.361084
21	1	-1.247336	-1.941915	-0.693613
22	1	-1.137391	-1.782260	1.035161

S10^s
uB3LYP/6311+G(d,p) = -463.2924532 uCCSD(T)/cc-pVDZ = -461.863113
ZPVE = 0.177478

1	6	0.692897	-0.031647	-0.004883
2	6	1.434541	-1.139088	0.442506
3	6	2.825478	-1.117436	0.447349
4	6	3.514558	0.013006	0.009904
5	6	2.794884	1.124534	-0.424845
6	6	1.403086	1.106443	-0.424169
7	6	-0.786096	-0.066730	-0.034055
8	6	-1.466995	-1.202783	-0.330497
9	6	-2.908764	-1.073554	-0.610745
10	6	-3.491688	-0.084766	0.063801
11	6	-2.959034	0.969800	0.663725
12	6	-1.543720	1.262432	0.208510
13	1	0.913141	-2.013528	0.813597
14	1	3.372777	-1.982638	0.804931
15	1	4.598344	0.030671	0.016521
16	1	3.318081	2.011194	-0.765456
17	1	0.866750	1.981530	-0.771410
18	1	-0.940631	-2.122664	-0.559027
19	1	-3.340076	-1.589711	-1.462750
20	1	-3.339966	1.415790	1.576679
21	1	-1.044826	1.824733	1.002365
22	1	-1.458469	1.883357	-0.695052

TS23^t

uB3LYP/6311+G(d,p) = -463.2310184 uCCSD(T)/cc-pVDZ = -461.788515
ZPVE = 0.169247 Imaginary Vibration = 751.93*i*

1	6	0.697397	0.012679	-0.017647
2	6	1.426170	1.122791	0.435106
3	6	2.818380	1.112522	0.434892
4	6	3.512541	-0.008425	-0.017453
5	6	2.801887	-1.119461	-0.468688
6	6	1.409717	-1.109236	-0.467550
7	6	-0.786007	0.024841	-0.019589
8	6	-1.494596	1.164427	-0.416818
9	6	-2.896286	1.178563	-0.442183
10	6	-3.536562	0.014933	-0.078177
11	6	-2.924459	-1.139615	0.323562
12	6	-1.511753	-1.113202	0.413998
13	1	0.897278	1.989883	0.814158
14	1	3.361504	1.977819	0.798327
15	1	4.596555	-0.016508	-0.017409
16	1	3.332006	-1.993495	-0.830379
17	1	0.869602	-1.970382	-0.844737
18	1	-0.951798	2.043702	-0.746603
19	1	-3.435597	2.063156	-0.761259
20	1	-3.475631	-2.030423	0.602149
21	1	-0.981392	-2.034749	0.624423
22	1	-1.311099	-0.873908	2.284616

p-$C_{12}H_9$

uB3LYP/6311+G(d,p) = -462.7332169 uCCSD(T)/cc-pVDZ = -461.2971975
ZPVE = 0.167681

1	6	-0.680201	0.000000	0.000000
2	6	-1.400673	-1.120822	-0.438347
3	6	-2.793219	-1.121312	-0.438029
4	6	-3.495968	0.000000	0.000000
5	6	-2.793220	1.121312	0.438029
6	6	-1.400673	1.120822	0.438347
7	6	0.806472	0.000000	0.000000
8	6	1.520854	-1.128221	0.432833
9	6	2.921340	-1.140063	0.437084
10	6	3.551548	0.000000	0.000000
11	6	2.921341	1.140063	-0.437084
12	6	1.520854	1.128221	-0.432833
13	1	-0.865113	-1.989386	-0.804911
14	1	-3.329734	-1.995741	-0.789416
15	1	-4.580031	0.000000	0.000000
16	1	-3.329735	1.995741	0.789416
17	1	-0.865114	1.989387	0.804911
18	1	0.982342	-1.998082	0.793509
19	1	3.467154	-2.011029	0.782375
20	1	3.467155	2.011029	-0.782374
21	1	0.982343	1.998083	-0.793509

TS24^s

uB3LYP/6311+G(d,p) = -463.2491756 uCCSD(T)/cc-pVDZ = -461.8096372

ZPVE = 0.174155 Imaginary Vibration = 975.96*i*

1	6	0.737012	0.002489	0.016305
2	6	1.448793	1.149692	-0.366727
3	6	2.840360	1.152074	-0.387447
4	6	3.550869	0.007898	-0.027427
5	6	2.857266	-1.139361	0.353663
6	6	1.465288	-1.142161	0.375013
7	6	-0.744101	0.006819	0.033301
8	6	-1.489822	1.116843	0.448053
9	6	-2.888126	1.156215	0.357198
10	6	-3.712537	0.096984	-0.081603
11	6	-2.961220	-1.063330	-0.406293
12	6	-1.481202	-1.118876	-0.391821
13	1	0.907474	2.036875	-0.674527
14	1	3.370373	2.046448	-0.695066
15	1	4.634643	0.010302	-0.043960
16	1	3.400294	-2.031627	0.644313
17	1	0.940964	-2.034073	0.699937
18	1	-0.954601	1.982601	0.829755
19	1	-3.357624	2.104257	0.618141
20	1	-3.445569	-1.982875	-0.730979
21	1	-0.981671	-2.004547	-0.773692
22	1	-2.249762	-1.479078	0.592801

S11^s

uB3LYP/6311+G(d,p) = -463.2771421 uCCSD(T)/cc-pVDZ = -461.8394264

ZPVE = 0.175846

1	6	-0.741368	-0.015096	-0.010398
2	6	-1.446191	1.135714	0.372503
3	6	-2.838500	1.149400	0.384090
4	6	-3.554598	0.013489	0.010176
5	6	-2.867294	-1.135885	-0.376325
6	6	-1.475034	-1.148787	-0.388995
7	6	0.744152	-0.040473	-0.008796
8	6	1.485808	1.119737	-0.434853
9	6	2.857806	1.235875	-0.300797
10	6	3.680125	0.107264	-0.084781
11	6	2.937375	-1.117468	0.325179
12	6	1.457407	-1.107795	0.445447
13	1	-0.902873	2.019326	0.688601
14	1	-3.364077	2.046241	0.692362
15	1	-4.638520	0.025013	0.017066
16	1	-3.415493	-2.020893	-0.679462
17	1	-0.948808	-2.038005	-0.717430
18	1	0.918144	1.942297	-0.865770
19	1	3.317378	2.199149	-0.511620
20	1	3.239115	-1.903930	-0.390130
21	1	0.952586	-1.943854	0.922513
22	1	3.404414	-1.501184	1.249173

TS25^{s}
uB3LYP/6311+G(d,p) = -463.2737393 uCCSD(T)/cc-pVDZ = -461.8380283
ZPVE = 0.174631 Imaginary Vibration = 653.41*i*

1	6	-0.743229	-0.011564	-0.002403
2	6	-1.451741	1.129835	0.400162
3	6	-2.843993	1.138873	0.406594
4	6	-3.554986	0.009385	0.004364
5	6	-2.863003	-1.129863	-0.403235
6	6	-1.470733	-1.140054	-0.406643
7	6	0.741803	-0.026858	0.006389
8	6	1.483783	1.120757	-0.429643
9	6	2.855430	1.165425	-0.406918
10	6	3.702472	0.094452	0.064133
11	6	2.906940	-1.081887	0.406415
12	6	1.455765	-1.111242	0.443771
13	1	-0.910906	2.007753	0.735316
14	1	-3.373614	2.027141	0.732118
15	1	-4.638946	0.017858	0.006300
16	1	-3.407439	-2.009422	-0.728066
17	1	-0.941255	-2.022367	-0.748139
18	1	0.924081	1.977177	-0.796783
19	1	3.339243	2.086795	-0.722380
20	1	3.423965	-1.909332	0.890283
21	1	0.946788	-1.985978	0.836162
22	1	3.327031	-1.133179	-0.702722

TS26
uB3LYP/6311+G(d,p) = -463.2357468 uCCSD(T)/cc-pVDZ = -461.787458
ZPVE = 0.174380 Imaginary Vibration = 300.15*i*

1	6	-3.446465	0.475745	-0.371634
2	6	-3.159101	-0.859145	-0.084925
3	6	-1.855158	-1.238039	0.259055
4	6	-0.889657	-0.253134	0.306172
5	6	-1.132677	1.075161	0.026817
6	6	-2.439862	1.440899	-0.317791
7	1	-4.456804	0.764399	-0.638880
8	1	-3.944278	-1.607074	-0.129826
9	1	-1.624118	-2.276684	0.475098
10	1	-0.341205	1.816049	0.071047
11	1	-2.668220	2.477733	-0.543365
12	6	2.541575	-0.639337	-1.267651
13	6	3.066382	0.567952	-0.772714
14	6	2.717943	1.006100	0.513029
15	6	1.843993	0.277391	1.305776
16	6	1.226690	-0.904609	0.801166
17	6	1.688618	-1.325973	-0.446404
18	1	2.818217	-1.004935	-2.250541
19	1	3.751786	1.147788	-1.381251
20	1	3.154545	1.920023	0.900583
21	1	0.737707	-1.588626	1.484224
22	1	1.598687	0.613254	2.307540

S12

uB3LYP/6311+G(d,p) = -463.2784453 uCCSD(T)/cc-pVDZ = -461.8432983
ZPVE = 0.176693

1	6	-3.362091	0.599875	0.026408
2	6	-2.289850	1.491023	0.084702
3	6	-0.981591	1.016465	0.047347
4	6	-0.725778	-0.355021	-0.049929
5	6	-1.803487	-1.239858	-0.108604
6	6	-3.115772	-0.767284	-0.070325
7	1	-4.380769	0.969919	0.055598
8	1	-2.473851	2.557199	0.159020
9	1	-0.151189	1.712757	0.092605
10	1	-1.617795	-2.306522	-0.186847
11	1	-3.942371	-1.467680	-0.117229
12	6	0.717820	-0.878638	-0.083417
13	6	1.493900	-0.390448	-1.249594
14	6	2.670750	0.266933	-1.266741
15	6	3.303123	0.546812	-0.021881
16	6	2.672843	0.130837	1.181560
17	6	1.480753	-0.530315	1.190684
18	1	0.639957	-1.977551	-0.143117
19	1	3.134964	0.578980	-2.197503
20	1	4.250195	1.072002	0.004045
21	1	3.158611	0.350489	2.127037
22	1	1.018534	-0.831868	2.125137

TS27

uB3LYP/6311+G(d,p) = -463.1153625 uCCSD(T)/cc-pVDZ = -461.6879948
ZPVE = 0.169354 Imaginary Vibration = 1380.09*i*

1	6	2.749697	0.830328	-0.079286
2	6	2.832077	-0.553347	0.019430
3	6	1.668098	-1.335382	0.092411
4	6	0.427762	-0.712355	0.060068
5	6	0.376023	0.670023	-0.035861
6	6	1.492789	1.465915	-0.106393
7	1	3.654084	1.426658	-0.136150
8	1	3.802669	-1.035804	0.041516
9	1	1.740091	-2.415662	0.174260
10	1	-1.176934	2.287491	-0.070356
11	1	1.426966	2.547160	-0.180076
12	6	-1.847911	0.413930	-1.228817
13	6	-1.697460	-0.906640	-1.124785
14	6	-0.950002	-1.388001	0.124527
15	6	-1.638812	-0.733247	1.291820
16	6	-1.821742	0.572752	1.313879
17	6	-1.469355	1.240210	-0.015028
18	1	-2.252673	0.908273	-2.102376
19	1	-2.001906	-1.611944	-1.887789
20	1	-0.886015	-2.473291	0.191313
21	1	-2.222085	1.156953	2.131864
22	1	-2.811180	1.825048	-0.034004

S13
uB3LYP/6311+G(d,p) = -462.6674807 uCCSD(T)/cc-pVDZ = -461.2536856
ZPVE = 0.167858

1	6	-1.479728	-1.411736	-0.102057
2	6	-0.302190	-0.689518	-0.022886
3	6	-0.334285	0.710389	0.069054
4	6	-1.540204	1.388268	0.088699
5	6	-2.736298	0.657339	0.010978
6	6	-2.706211	-0.728427	-0.083460
7	1	-1.459657	-2.494344	-0.174717
8	1	-1.565197	2.470534	0.163347
9	1	-3.686454	1.179277	0.026471
10	1	-3.633247	-1.287650	-0.141663
11	6	1.076017	1.322772	0.132558
12	6	1.129216	-1.241737	-0.029091
13	6	1.799808	0.794065	-1.122121
14	6	1.821853	-0.533381	-1.203761
15	6	1.731020	0.609726	1.295177
16	6	1.785825	-0.703633	1.277094
17	1	1.067816	2.408769	0.207753
18	1	2.185489	-1.371307	2.027677
19	1	1.163786	-2.328557	-0.094244
20	1	2.246443	-1.099040	-2.022976
21	1	2.212076	1.477559	-1.852754

TS28
uB3LYP/6311+G(d,p) = -463.1966935 uCCSD(T)/cc-pVDZ = -461.7688569
ZPVE = 0.175558 Imaginary Vibration = 551.09*i*

1	6	-2.709100	-0.697412	0.076733
2	6	-2.668304	0.709276	0.103424
3	6	-1.455707	1.377712	-0.143608
4	6	-0.312579	0.681219	-0.470607
5	6	-0.346937	-0.767234	-0.624672
6	6	-1.597878	-1.419651	-0.299046
7	1	-3.635692	-1.211746	0.308085
8	1	-3.556443	1.275653	0.357794
9	1	-1.403007	2.453238	-0.000830
10	1	0.130356	-1.172901	-1.512957
11	1	-1.663674	-2.497138	-0.410635
12	6	2.243641	-0.761649	-0.606014
13	6	2.163402	0.534157	-0.938593
14	6	1.082110	1.307205	-0.202451
15	6	1.218252	0.956155	1.256140
16	6	1.246641	-0.322754	1.615303
17	6	1.292384	-1.225666	0.435018
18	1	2.901031	-1.464329	-1.106277
19	1	2.773873	1.011218	-1.695095
20	1	1.091775	2.377663	-0.406709
21	1	1.176619	-0.706691	2.625143
22	1	1.249608	-2.293116	0.631708

S14
uB3LYP/6311+G(d,p) = -463.2115697 uCCSD(T)/cc-pVDZ = -461.7922795
ZPVE = 0.176868

1	6	-2.676104	-0.697951	0.002675
2	6	-2.697640	0.719379	-0.047365
3	6	-1.472921	1.439766	-0.063198
4	6	-0.288828	0.781946	-0.212950
5	6	-0.254235	-0.689161	-0.557864
6	6	-1.512860	-1.399145	-0.151634
7	1	-3.603141	-1.230126	0.190561
8	1	-3.635612	1.250622	0.058554
9	1	-1.481457	2.505330	0.147521
10	1	-0.195490	-0.774857	-1.659538
11	1	-1.504794	-2.483536	-0.104880
12	6	1.133662	-1.248668	-0.031222
13	6	2.158043	-0.528088	-0.902178
14	6	2.124022	0.800821	-0.806835
15	6	1.088479	1.323703	0.190415
16	6	1.296328	0.549887	1.470947
17	6	1.306510	-0.767591	1.423504
18	1	1.182504	-2.334380	-0.119651
19	1	2.798338	-1.075099	-1.583922
20	1	2.740655	1.481970	-1.379938
21	1	1.094952	2.406461	0.310366
22	1	1.377302	-1.455770	2.255158

APPENDIX E

Included for each optimized stationary structures reported Chapter 8:

- Cartesian Coordinates (Ångströms);
- uB3LYP/6-311+G(d,p) electronic energies (hartrees);
- zero-point vibrational energies ZPVE (hartrees);
- imaginary vibrational frequencies (cm^{-1}) (only for saddle points).

o-benzyne (o-C_6H_4)
uB3LYP/6311+G(d,p) = -230.9726840 ZPVE = 0.074883

1	6	1.170104	0.491488	0.000000
2	6	0.000000	1.269077	0.000000
3	6	-1.289206	0.695776	0.000000
4	6	-1.201746	-0.683828	0.000000
5	6	-0.165049	-1.372534	0.000000
6	6	1.140814	-0.919196	0.000000
7	1	2.133449	0.991446	0.000000
8	1	0.087848	2.350868	0.000000
9	1	-2.191661	1.293016	0.000000
10	1	2.040865	-1.520029	0.000000

cyclopentadiene (c-C_5H_6)
uB3LYP/6311+G(d,p) = -194.1562362 ZPVE = 0.092109

1	6	0.000041	-1.216095	0.000373
2	1	0.000069	-1.877974	-0.876444
3	1	0.000057	-1.877191	0.877805
4	6	1.179387	-0.281634	-0.000370
5	1	2.210570	-0.607605	-0.000569
6	6	0.734102	0.990260	0.000119
7	1	1.347656	1.882210	0.000229
8	6	-1.179368	-0.281712	-0.000392
9	1	-2.210530	-0.607752	-0.000606
10	6	-0.734168	0.990212	0.000154
11	1	-1.347780	1.882122	0.000283

TS1
uB3LYP/6311+G(d,p) = -425.1273851 ZPVE = 0.168586
Imaginary Vibration = 113.7947*i*

1	6	1.917325	1.476620	-0.015911
2	6	0.706525	0.798572	0.056698
3	6	0.618685	-0.461495	0.083521
4	6	1.633162	-1.395061	0.029026
5	6	2.896244	-0.776506	-0.059809
6	6	3.032886	0.620113	-0.082524
7	1	2.033837	2.554754	-0.030099
8	1	1.521449	-2.472748	0.054590
9	1	3.784425	-1.398323	-0.112249
10	1	4.026803	1.050851	-0.157143
11	6	-1.799912	-1.145122	0.376722
12	6	-2.253307	1.147516	0.190695
13	6	-2.086548	-0.839665	-0.923678
14	6	-2.346512	0.573872	-1.038155
15	6	-2.058763	0.073071	1.221866
16	1	-1.628375	-2.134784	0.777110
17	1	-2.398572	2.192780	0.425066
18	1	-2.536477	1.092813	-1.968330
19	1	-2.068596	-1.533918	-1.753817
20	1	-3.002885	-0.074072	1.770797
21	1	-1.290317	0.291165	1.963364

S1 (benzonorbornadiene)
uB3LYP/6311+G(d,p) = -425.2506890 ZPVE = 0.175623

1	6	-1.395107	-1.413582	-0.001847
2	6	-0.217803	-0.703308	0.135228
3	6	-0.217825	0.703416	0.135588
4	6	-1.395227	1.413594	-0.001378
5	6	-2.595636	0.695511	-0.140712
6	6	-2.595587	-0.695588	-0.140930
7	1	-1.403302	-2.498745	0.001478
8	1	-1.403587	2.498752	0.002256
9	1	-3.531790	1.232503	-0.246901
10	1	-3.531714	-1.232596	-0.247273
11	6	1.247000	1.132427	0.293503
12	6	1.247060	-1.132322	0.293005
13	6	1.970395	0.667936	-0.983456
14	6	1.970745	-0.667350	-0.983460
15	6	1.717332	-0.000486	1.259045
16	1	1.414784	2.164421	0.597540
17	1	1.413816	-2.164497	0.597041
18	1	2.323638	-1.329252	-1.763129
19	1	2.323445	1.330588	-1.762429
20	1	2.797188	-0.001070	1.420399
21	1	1.185435	-0.001595	2.213505

TS2
uB3LYP/6311+G(d,p) = -425.1473867 ZPVE = 0.167786
Imaginary Vibration = 462.5661*i*

1	6	1.402150	-1.427015	-0.030210
2	6	0.215935	-0.722651	-0.374337
3	6	0.215957	0.722730	-0.374239
4	6	1.402195	1.427019	-0.030033
5	6	2.531244	0.714437	0.282238
6	6	2.531222	-0.714506	0.282151
7	1	1.411197	-2.511875	-0.023513
8	1	1.411274	2.511878	-0.023209
9	1	3.448420	1.236270	0.532617
10	1	3.448380	-1.236398	0.532472
11	6	-1.081576	1.167211	-0.656771
12	6	-1.081611	-1.167064	-0.656897
13	6	-1.997360	0.614433	1.433829
14	6	-1.997322	-0.614699	1.433737
15	6	-1.834889	0.000102	-1.231262
16	1	-1.357848	2.200550	-0.826599
17	1	-1.357904	-2.200379	-0.826840
18	1	-2.139432	-1.612018	1.782247
19	1	-2.139828	1.611715	1.782321
20	1	-2.911625	0.000116	-1.078337
21	1	-1.648313	0.000147	-2.320395

S2

uB3LYP/6311+G(d,p) = -347.8159451 ZPVE = 0.138472

1	6	0.000003	-1.006681	1.440420
2	6	-0.000033	0.253909	0.740939
3	6	-0.000033	0.253909	-0.740939
4	6	0.000003	-1.006681	-1.440420
5	6	0.000027	-2.160485	-0.725277
6	6	0.000027	-2.160485	0.725277
7	1	-0.000008	-1.021672	2.525026
8	1	-0.000008	-1.021672	-2.525026
9	1	0.000035	-3.116004	-1.238356
10	1	0.000035	-3.116004	1.238356
11	6	-0.000085	1.540426	-1.185353
12	6	-0.000085	1.540426	1.185353
13	6	0.000116	2.458818	0.000000
14	1	-0.000091	1.872801	-2.214498
15	1	-0.000091	1.872801	2.214498
16	1	0.875268	3.125240	0.000000
17	1	-0.874772	3.125574	0.000000

acetylene

uB3LYP/6311+G(d,p) = -77.3566458 ZPVE = 0.027032

1	6	0.000000	0.000000	0.599658
2	6	0.000000	0.000000	-0.599658
3	1	0.000000	0.000000	1.662781
4	1	0.000000	0.000000	-1.662781

TS3

uB3LYP/6311+G(d,p) = -425.1172570 ZPVE = 0.168763

Imaginary Vibration = 299.0606*i*

1	6	-2.876140	-0.899499	0.029347
2	6	-1.533525	-1.286335	0.015593
3	6	-0.598950	-0.391411	0.015510
4	6	-0.744772	0.985972	-0.077834
5	6	-2.080780	1.406796	-0.079643
6	6	-3.129635	0.477944	-0.021492
7	1	-3.700962	-1.605953	0.042178
8	1	0.067722	1.699582	-0.131939
9	1	-2.301890	2.467602	-0.134912
10	1	-4.155541	0.834598	-0.044839
11	6	2.756087	0.824399	0.338345
12	6	1.277609	-1.026818	0.279831
13	6	2.646572	0.390775	-0.945602
14	6	1.812936	-0.778748	-0.986187
15	6	1.990786	-0.091872	1.245881
16	1	3.282806	1.708635	0.672017
17	1	0.968183	-2.008632	0.596916
18	1	1.595011	-1.357275	-1.873866
19	1	3.106573	0.848899	-1.811520
20	1	2.683323	-0.686529	1.859114
21	1	1.333647	0.431859	1.944363

S3
uB3LYP/6311+G(d,p) = -425.1586038 ZPVE = 0.170071

1	6	1.496643	-1.187822	0.364517
2	6	0.462842	-0.291479	0.206498
3	6	0.857158	1.004724	-0.176512
4	6	2.200757	1.317749	-0.376475
5	6	3.194504	0.353657	-0.199333
6	6	2.837719	-0.946074	0.185539
7	1	2.476036	2.324885	-0.669072
8	1	4.238529	0.604917	-0.353699
9	1	3.589840	-1.713195	0.334126
10	6	-3.004364	0.026278	-0.781348
11	6	-0.998531	-0.671886	0.401010
12	6	-2.953850	0.698172	0.432183
13	6	-1.819246	0.354122	1.151936
14	6	-1.792347	-0.851659	-0.943976
15	1	-3.785713	0.119964	-1.524086
16	1	-1.006969	-1.618932	0.952702
17	1	-1.545573	0.730043	2.128907
18	1	-3.705927	1.398972	0.775504
19	1	-2.058965	-1.900846	-1.114642
20	1	0.095901	1.767889	-0.309141
21	1	-1.184861	-0.548394	-1.804833

TS4
uB3LYP/6311+G(d,p) = -425.1553581 ZPVE = 0.170051
Imaginary Vibration = 40.7761*i*

1	6	-1.321187	-1.130953	0.385939
2	6	-0.470365	-0.048424	0.275035
3	6	-1.097668	1.140572	-0.132090
4	6	-2.468699	1.181404	-0.400623
5	6	-3.259891	0.043189	-0.271184
6	6	-2.669007	-1.162548	0.139299
7	1	-2.919154	2.117122	-0.712176
8	1	-4.323174	0.082318	-0.482411
9	1	-3.258326	-2.066031	0.252691
10	6	3.177730	0.568391	-0.163811
11	6	1.014779	-0.190882	0.599576
12	6	2.986185	-0.725304	-0.626521
13	6	1.734714	-1.203232	-0.268249
14	6	1.921950	1.073062	0.498881
15	1	4.061800	1.172858	-0.317317
16	1	1.057254	-0.553544	1.637445
17	1	1.321043	-2.171928	-0.512944
18	1	3.715051	-1.286892	-1.198853
19	1	2.102189	1.530918	1.476509
20	1	-0.516136	2.049650	-0.236125
21	1	1.468208	1.853877	-0.124341

S4
uB3LYP/6311+G(d,p) = -425.1592693 ZPVE = 0.170008

1	6	1.472945	-1.195228	0.405829
2	6	0.457527	-0.235951	0.259614
3	6	0.869332	1.016259	-0.160923
4	6	2.161344	1.391339	-0.440937
5	6	3.152423	0.408610	-0.296114
6	6	2.802136	-0.873810	0.126609
7	1	2.415222	2.396122	-0.761293
8	1	4.188142	0.651167	-0.509583
9	1	3.571366	-1.628542	0.246264
10	6	-3.064085	-0.188162	-0.713290
11	6	-1.002816	-0.504760	0.516869
12	6	-2.956262	0.832437	0.216274
13	6	-1.760075	0.743344	0.919761
14	6	-1.804727	-1.011590	-0.733277
15	1	-1.091034	-1.256963	1.314638
16	1	-1.438874	1.397175	1.718903
17	1	-3.704432	1.599933	0.374974
18	1	-1.232826	-0.818867	-1.651158
19	1	-3.901701	-0.350290	-1.379253
20	1	1.218280	-2.194815	0.746879
21	1	-1.990592	-2.089839	-0.702854

TS5
uB3LYP/6311+G(d,p) = -425.159234 ZPVE = 0.169936
Imaginary Vibration = 47.7803*i*

1	6	1.472817	-1.222582	0.365325
2	6	0.449675	-0.264779	0.300625
3	6	0.822611	1.013577	-0.080456
4	6	2.101105	1.410889	-0.397003
5	6	3.104457	0.432027	-0.335484
6	6	2.785636	-0.872235	0.045543
7	1	2.335949	2.430289	-0.684257
8	1	4.128369	0.693795	-0.581426
9	1	3.567849	-1.621262	0.099156
10	6	-3.006511	-0.191989	-0.736293
11	6	-1.005945	-0.512704	0.592694
12	6	-2.867262	0.902629	0.094281
13	6	-1.707861	0.803787	0.862110
14	6	-1.822276	-1.111644	-0.606876
15	1	-1.106333	-1.179821	1.460699
16	1	-1.401978	1.485477	1.643281
17	1	-3.567281	1.727907	0.145593
18	1	-1.219093	-1.101722	-1.524021
19	1	-3.827939	-0.362953	-1.420365
20	1	1.242350	-2.239257	0.671230
21	1	-2.110570	-2.154313	-0.436690

S5
uB3LYP/6311+G(d,p) = -425.2387408 ZPVE = 0.174478

1	6	1.480200	-1.450157	-0.018342
2	6	0.385128	-0.676652	0.332185
3	6	0.435239	0.715970	0.346807
4	6	1.581202	1.421026	0.018361
5	6	2.697109	0.648952	-0.339793
6	6	2.647566	-0.749727	-0.359178
7	1	1.635967	2.504295	0.030651
8	1	3.623904	1.144693	-0.608048
9	1	3.537530	-1.302141	-0.640964
10	6	-2.582838	0.133870	-0.861908
11	6	-1.066901	-0.741466	0.793881
12	6	-2.005530	1.208100	-0.320544
13	6	-1.030733	0.852561	0.771753
14	6	-2.145149	-1.170233	-0.230813
15	1	-3.292671	0.167305	-1.681765
16	1	-1.208691	-1.191932	1.778177
17	1	-1.208335	1.375646	1.716310
18	1	-2.183192	2.229846	-0.637058
19	1	-2.987996	-1.676743	0.253880
20	1	-1.749212	-1.869620	-0.975997
21	1	1.460937	-2.534828	-0.029643

TS6
uB3LYP/6311+G(d,p) = -425.1609018 ZPVE = 0.168882
Imaginary Vibration = 62.9075*i*

1	6	1.414041	-1.410410	0.170248
2	6	0.300985	-0.681050	-0.204983
3	6	0.382334	0.723963	-0.289314
4	6	1.628193	1.347904	-0.141429
5	6	2.765314	0.595486	0.182543
6	6	2.658203	-0.773078	0.368217
7	1	1.349469	-2.492030	0.235868
8	1	1.707431	2.421409	-0.280981
9	1	3.726357	1.087421	0.282147
10	1	3.533169	-1.365093	0.610575
11	6	-0.842014	1.477879	-0.454328
12	6	-2.091644	1.226598	0.276850
13	6	-2.645112	-0.097003	0.597732
14	6	-2.182798	-1.261972	-0.007244
15	6	-0.962587	-1.374724	-0.636548
16	1	-0.737006	2.501942	-0.803989
17	1	-2.904195	1.823172	-0.170792
18	1	-1.938234	1.751305	1.247732
19	1	-3.572804	-0.104349	1.158560
20	1	-2.888476	-2.089126	-0.091905
21	1	-0.825195	-2.176205	-1.357672

S6
uB3LYP/6311+G(d,p) = -425.2453858 ZPVE = 0.173652

1	6	1.572908	1.330702	0.359888
2	6	0.277176	0.729111	0.160078
3	6	0.242034	-0.717077	-0.060102
4	6	1.488703	-1.371744	-0.386282
5	6	2.682621	-0.735254	-0.253540
6	6	2.725717	0.632981	0.168761
7	1	1.608210	2.384859	0.615037
8	1	1.451804	-2.419461	-0.666351
9	1	3.608670	-1.263334	-0.450681
10	1	3.685287	1.120684	0.299185
11	6	-0.896417	-1.477170	0.083605
12	6	-2.132529	-0.968931	0.746667
13	6	-2.689729	-0.038541	-0.289483
14	6	-2.102173	1.169371	-0.516133
15	6	-0.822548	1.561648	-0.043083
16	1	-0.881821	-2.504209	-0.270215
17	1	-1.894752	-0.422127	1.667576
18	1	-2.823288	-1.778416	0.983657
19	1	-3.578327	-0.328729	-0.841004
20	1	-2.634968	1.891524	-1.130249
21	1	-0.615396	2.628639	-0.029201

TS7
uB3LYP/6311+G(d,p) = -425.2443451 ZPVE = 0.173088
Imaginary Vibration = 285.9807*i*

1	6	1.595906	1.311574	0.342969
2	6	0.296957	0.739465	0.166412
3	6	0.218408	-0.684650	-0.065442
4	6	1.428492	-1.385208	-0.365928
5	6	2.652040	-0.785341	-0.232201
6	6	2.736683	0.575576	0.164556
7	1	1.661648	2.369248	0.576933
8	1	1.361412	-2.435174	-0.632139
9	1	3.558582	-1.351548	-0.413457
10	1	3.708621	1.039464	0.290051
11	6	-0.983882	-1.400642	0.023099
12	6	-2.136370	-0.933165	0.827143
13	6	-2.593835	-0.087043	-0.309083
14	6	-2.057733	1.178887	-0.510123
15	6	-0.810023	1.594305	-0.054028
16	1	-1.037441	-2.386984	-0.427006
17	1	-1.855769	-0.352331	1.709020
18	1	-2.832276	-1.728131	1.088993
19	1	-3.420058	-0.435343	-0.919480
20	1	-2.635607	1.881095	-1.105652
21	1	-0.588961	2.657152	-0.091508

S7
uB3LYP/6311+G(d,p) = -425.2652381 ZPVE = 0.1748950

1	6	1.666457	1.298670	0.193507
2	6	0.366819	0.794010	0.037568
3	6	0.188334	-0.596004	-0.149316
4	6	1.311243	-1.422120	-0.230902
5	6	2.596618	-0.905938	-0.077903
6	6	2.773964	0.459405	0.146670
7	1	1.801875	2.365836	0.338810
8	1	1.174772	-2.486030	-0.397888
9	1	3.454389	-1.567309	-0.126875
10	1	3.770512	0.867326	0.272741
11	6	-1.179435	-1.163874	-0.260770
12	6	-0.784038	1.691860	-0.036329
13	6	-2.360468	-0.184563	-0.343587
14	6	-2.031002	1.253071	-0.275804
15	6	-2.158708	-1.048315	0.883378
16	1	-1.254162	-2.071933	-0.849807
17	1	-0.589400	2.757217	0.037864
18	1	-2.838476	1.962629	-0.426707
19	1	-3.189684	-0.456547	-0.987970
20	1	-1.825594	-0.553677	1.787841
21	1	-2.842942	-1.874722	1.032922

TS8
uB3LYP/6311+G(d,p) = -425.1091123 ZPVE = 0.167255
Imaginary Vibration = 706.1172*i*

1	6	0.803026	0.996553	-0.017110
2	6	0.613162	-0.366111	0.178753
3	6	1.564831	-1.250523	0.166922
4	6	2.906701	-0.924803	0.016732
5	6	3.173117	0.437467	-0.187449
6	6	2.137021	1.380946	-0.203204
7	1	0.000792	1.725667	0.001827
8	1	3.711539	-1.652546	0.027009
9	1	4.196449	0.764764	-0.344597
10	1	2.370282	2.429824	-0.354482
11	6	-2.750088	0.862087	0.339470
12	6	-1.846047	-1.004238	-0.768582
13	6	-1.967145	0.198443	1.203670
14	6	-1.312422	-0.944962	0.520054
15	6	-2.733502	0.179522	-1.005996
16	1	-3.320591	1.757367	0.549607
17	1	-1.623411	-1.760349	-1.508196
18	1	-0.974808	-1.815096	1.062160
19	1	-1.784792	0.463152	2.236911
20	1	-3.739559	-0.134837	-1.320023
21	1	-2.367827	0.835764	-1.809776

S8
uB3LYP/6311+G(d,p) = -425.1369414 ZPVE = 0.169183

1	6	0.840960	0.991366	-0.073209
2	6	0.484263	-0.358105	0.107582
3	6	1.540681	-1.237186	0.160179
4	6	2.877607	-0.931288	0.061292
5	6	3.198802	0.421157	-0.115751
6	6	2.177248	1.371098	-0.181625
7	1	3.651604	-1.689104	0.114584
8	1	4.237156	0.723615	-0.201509
9	1	2.425674	2.417704	-0.317949
10	6	-2.996150	0.219071	-0.813963
11	6	-0.978411	-0.800868	0.214712
12	6	-2.882465	0.545644	0.659194
13	6	-1.799893	-0.001404	1.213324
14	6	-1.770292	-0.609583	-1.053866
15	1	-3.037614	1.125236	-1.439362
16	1	-0.956931	-1.861034	0.509179
17	1	-1.509029	0.090198	2.253063
18	1	-3.613347	1.149159	1.184889
19	1	-1.481285	-1.027794	-2.008716
20	1	-3.926334	-0.327595	-1.040208
21	1	0.056005	1.740209	-0.121178

TS9
uB3LYP/6311+G(d,p) = -425.1346531 ZPVE = 0.169067
Imaginary Vibration = 36.0261*i*

1	6	-1.211361	1.194172	0.145054
2	6	-0.469750	0.014239	0.329189
3	6	-1.180027	-1.149544	0.157039
4	6	-2.508359	-1.270032	-0.172519
5	6	-3.221432	-0.075246	-0.345209
6	6	-2.565909	1.145818	-0.185776
7	1	-2.990317	-2.233475	-0.298899
8	1	-4.273790	-0.105191	-0.607098
9	1	-3.113060	2.071543	-0.324844
10	6	3.034244	0.634637	-0.556712
11	6	1.012903	0.025333	0.741786
12	6	2.871822	-0.863613	-0.431301
13	6	1.787072	-1.193200	0.268463
14	6	1.844555	1.151045	0.194201
15	1	3.055795	0.963163	-1.608439
16	1	1.007151	0.055169	1.846318
17	1	1.459488	-2.202223	0.486145
18	1	3.567748	-1.568536	-0.870644
19	1	1.657519	2.199251	0.384021
20	1	3.986967	0.983026	-0.126561
21	1	-0.720054	2.155624	0.254713

TS10
uB3LYP/6311+G(d,p) = -425.1336149 ZPVE = 0.168962
Imaginary Vibration = 56.4806*i*

1	6	1.200545	1.186204	0.107026
2	6	0.467388	0.008052	0.333618
3	6	1.194036	-1.156786	0.202551
4	6	2.522051	-1.273767	-0.124913
5	6	3.222342	-0.078901	-0.346375
6	6	2.554873	1.139223	-0.228384
7	1	3.014402	-2.236357	-0.211524
8	1	4.274236	-0.107807	-0.609949
9	1	3.091442	2.065250	-0.402238
10	6	-3.004118	-0.747590	-0.531242
11	6	-1.010277	0.002565	0.742009
12	6	-2.913685	0.759511	-0.453242
13	6	-1.841470	1.165898	0.226656
14	6	-1.788936	-1.181368	0.229031
15	1	-3.011502	-1.107493	-1.572703
16	1	-1.013882	0.015178	1.847625
17	1	-1.592090	2.201282	0.422681
18	1	-3.651600	1.416287	-0.899128
19	1	-1.493657	-2.209206	0.388178
20	1	-3.941178	-1.124367	-0.089938
21	1	0.707339	2.148982	0.186596

S9
uB3LYP/6311+G(d,p) = -425.1365086 ZPVE = 0.169064

1	6	1.516578	-1.225605	0.240741
2	6	0.464094	-0.296665	0.175676
3	6	0.849589	1.002328	-0.081308
4	6	2.129553	1.459536	-0.269551
5	6	3.156181	0.503876	-0.207867
6	6	2.841345	-0.829799	0.047377
7	1	2.349640	2.504779	-0.458373
8	1	4.187127	0.808020	-0.354593
9	1	3.632565	-1.569059	0.102464
10	6	-2.973810	0.121169	-0.883388
11	6	-0.993877	-0.719410	0.357524
12	6	-2.888442	0.700672	0.511484
13	6	-1.825493	0.251730	1.178783
14	6	-1.773704	-0.774976	-0.931585
15	1	-2.955101	0.906622	-1.656384
16	1	-0.970456	-1.707552	0.845738
17	1	-1.550766	0.530814	2.188935
18	1	-3.617334	1.401740	0.901085
19	1	-1.458473	-1.341815	-1.797554
20	1	-3.917174	-0.423542	-1.048512
21	1	1.287879	-2.267140	0.449878

TS11
uB3LYP/6311+G(d,p) = -425.1060279 ZPVE = 0.170321
Imaginary Vibration = 359.7289*i*

1	6	-1.456885	-1.284472	0.172524
2	6	-0.315769	-0.477254	-0.174358
3	6	-0.377520	0.913034	-0.431288
4	6	-1.687118	1.469986	-0.284313
5	6	-2.812027	0.686401	-0.145595
6	6	-2.695419	-0.710445	0.104907
7	1	-1.813518	2.547575	-0.368334
8	1	-3.805022	1.126308	-0.197246
9	1	-3.588246	-1.304289	0.268206
10	6	2.113263	0.852353	0.878402
11	6	1.081501	-1.137251	-0.078877
12	6	2.715497	0.482713	-0.456983
13	6	2.176727	-0.631062	-0.957128
14	6	0.992267	-0.158141	1.026033
15	1	1.802976	1.892416	0.949855
16	1	1.011135	-2.202177	0.125841
17	1	2.436575	-1.097497	-1.898297
18	1	3.489170	1.073758	-0.930347
19	1	0.570183	-0.401156	1.991081
20	1	2.829960	0.660973	1.698225
21	1	-1.340325	-2.331089	0.441079

TS12
uB3LYP/6311+G(d,p) = -347.7866913 ZPVE = 0.135605
Imaginary Vibration = 1205.3426*i*

1	6	0.991120	1.425116	0.006155
2	6	-0.248380	0.728173	-0.029144
3	6	-0.240598	-0.715839	-0.029551
4	6	0.986506	-1.425013	-0.003712
5	6	2.162973	-0.716638	0.004517
6	6	2.161831	0.708724	0.013144
7	1	1.005578	2.509697	0.018297
8	1	0.991976	-2.509919	-0.002831
9	1	3.111371	-1.242065	0.008366
10	1	3.112093	1.231528	0.027981
11	6	-1.576915	-1.163283	-0.046599
12	6	-1.577251	1.185524	-0.027495
13	6	-2.430655	0.055786	-0.015118
14	1	-1.953667	-2.171877	-0.129873
15	1	-1.906101	2.213732	0.001684
16	1	-3.495807	0.045697	-0.203239
17	1	-2.237233	-0.572092	1.046435

indene
uB3LYP/6311+G(d,p) = -347.8510448 ZPVE = 0.139899

1	6	0.998397	1.414150	0.000121
2	6	-0.212031	0.721164	-0.000042
3	6	-0.229496	-0.688823	0.000032
4	6	0.955994	-1.408805	-0.000063
5	6	2.169733	-0.712232	-0.000110
6	6	2.188411	0.684507	0.000046
7	1	1.018547	2.498770	0.000309
8	1	0.950501	-2.494143	-0.000198
9	1	3.104630	-1.261402	-0.000303
10	1	3.138819	1.206715	0.000135
11	6	-1.666598	-1.155018	0.000195
12	6	-1.599440	1.194980	-0.000133
13	6	-2.438369	0.143070	-0.000154
14	1	-1.902168	-1.769422	-0.877951
15	1	-1.888545	2.238580	-0.000080
16	1	-3.519390	0.191409	-0.000284
17	1	-1.902007	-1.768465	0.879017

TS13
uB3LYP/6311+G(d,p) = -425.1743778 ZPVE = 0.1695170
Imaginary Vibration = 394.9013*i*

1	6	-1.327312	-1.384368	-0.302408
2	6	-0.180409	-0.637225	-0.106800
3	6	-0.256735	0.750697	0.135620
4	6	-1.507309	1.367941	0.214083
5	6	-2.666055	0.608219	0.026553
6	6	-2.581100	-0.756043	-0.239333
7	1	-1.262283	-2.453500	-0.478805
8	1	-1.578666	2.434534	0.400595
9	1	-3.636967	1.087641	0.084419
10	1	-3.484383	-1.338446	-0.381377
11	6	1.034142	1.431839	0.219871
12	6	1.251596	-1.132267	0.015197
13	6	2.073760	0.993672	-0.686426
14	6	2.157255	-0.337170	-0.911101
15	6	1.693249	-0.765245	1.427454
16	1	1.070875	2.433096	0.637212
17	1	1.319095	-2.213060	-0.163771
18	1	2.844895	-0.808796	-1.600882
19	1	2.746102	1.716354	-1.136735
20	1	2.747498	-0.594294	1.617952
21	1	1.087347	-1.103828	2.265131

cyclopentadienyl radical (c-C_5H_5)

uB3LYP/6311+G(d,p) = -193.5157530 ZPVE = 0.077508

1	6	0.000067	1.187041	-0.000086
2	1	0.000121	2.269816	0.000344
3	6	-1.169496	0.353448	-0.000015
4	1	-2.191453	0.701699	0.000078
5	6	-0.740919	-0.947228	0.000014
6	1	-1.359401	-1.834302	0.000008
7	6	1.169532	0.353334	-0.000016
8	1	2.191526	0.701475	0.000076
9	6	0.740816	-0.947303	0.000017
10	1	1.359208	-1.834441	0.000011

S10

uB3LYP/6311+G(d,p) = -424.5726037 ZPVE = 0.160186

1	6	-1.466548	-1.246527	0.019212
2	6	-0.428848	-0.342635	0.009836
3	6	-0.814188	1.011435	-0.011152
4	6	-2.159494	1.370536	-0.020649
5	6	-3.161486	0.396968	-0.009793
6	6	-2.811747	-0.958922	0.010751
7	1	-2.431426	2.419951	-0.036637
8	1	-4.207308	0.685224	-0.017200
9	1	-3.569784	-1.734279	0.019453
10	6	2.947774	0.381728	0.723057
11	6	1.034164	-0.760850	0.019793
12	6	2.945911	0.343401	-0.747053
13	6	1.842454	-0.297467	-1.174030
14	6	1.845379	-0.235857	1.185633
15	1	3.725393	0.835675	1.324217
16	1	1.061829	-1.859781	0.048256
17	1	1.548550	-0.487418	-2.197137
18	1	3.721892	0.765475	-1.373029
19	1	1.554243	-0.372048	2.218069
20	1	-0.043622	1.776337	-0.019619

TS15
uB3LYP/6311+G(d,p) = -424.5698758 ZPVE = 0.160047
Imaginary Vibration = 39.0584*i*

1	6	-1.143971	-1.154682	0.170480
2	6	-0.415076	0.009020	0.298683
3	6	-1.153842	1.190441	0.107725
4	6	-2.516129	1.146776	-0.191621
5	6	-3.185672	-0.070269	-0.310183
6	6	-2.479743	-1.267617	-0.124891
7	1	-0.657541	2.151246	0.188323
8	1	-3.057369	2.074720	-0.337692
9	1	-4.243917	-0.096263	-0.547077
10	1	-2.973111	-2.229298	-0.214337
11	6	2.993451	0.680147	-0.457230
12	6	1.064317	0.003876	0.666746
13	6	2.951344	-0.787625	-0.457929
14	6	1.837704	-1.199245	0.173838
15	6	1.902291	1.159670	0.167706
16	1	3.789740	1.271864	-0.890765
17	1	1.125282	0.005895	1.769368
18	1	1.514527	-2.218066	0.334591
19	1	3.706039	-1.423614	-0.902487
20	1	1.668305	2.200555	0.340122

S11
uB3LYP/6311+G(d,p) = -424.5716575 ZPVE = 0.160100

1	6	-1.441213	-1.210162	0.300951
2	6	-0.413934	-0.259571	0.173075
3	6	-0.835390	1.016957	-0.140270
4	6	-2.129227	1.430261	-0.331955
5	6	-3.130580	0.454810	-0.202689
6	6	-2.778655	-0.855956	0.113121
7	1	-1.184563	-2.234759	0.555084
8	1	-2.377487	2.458331	-0.572468
9	1	-4.171230	0.726081	-0.344898
10	1	-3.550054	-1.610220	0.219807
11	6	2.971208	0.695274	0.415458
12	6	1.049049	-0.630083	0.346308
13	6	2.935488	0.001941	-0.880230
14	6	1.826803	-0.756430	-0.949290
15	6	1.883465	0.357739	1.131270
16	1	3.757800	1.369770	0.728879
17	1	1.088513	-1.601903	0.861806
18	1	1.507044	-1.379094	-1.773423
19	1	3.691469	0.098398	-1.649186
20	1	1.616419	0.704726	2.119910

TS16
uB3LYP/6311+G(d,p) = -424.5182175 ZPVE = 0.1545290
Imaginary Vibration = 2110.8815*i*

1	6	1.025617	-1.056774	0.000858
2	6	0.479231	0.206025	-0.000354
3	6	1.296429	1.331730	-0.001315
4	6	2.677413	1.101339	-0.001012
5	6	3.207553	-0.194955	0.000240
6	6	2.380808	-1.330374	0.001284
7	1	3.358400	1.945234	-0.001726
8	1	4.284781	-0.326845	0.000431
9	1	2.793777	-2.331381	0.002284
10	6	-3.149685	0.043844	-0.733231
11	6	-0.983777	-0.127750	0.000202
12	6	-3.149688	0.045870	0.733140
13	6	-1.870701	-0.032691	1.178683
14	6	-1.870694	-0.035941	-1.178550
15	1	-4.038297	0.091998	-1.348786
16	1	-0.464333	-1.404986	0.001583
17	1	-1.524759	-0.052960	2.201835
18	1	-4.038302	0.095730	1.348556
19	1	-1.524734	-0.058930	-2.201637
20	1	0.898438	2.340194	-0.002211

S12
uB3LYP/6311+G(d,p) = -424.6397278 ZPVE = 0.1603800

1	6	1.155552	-1.209807	0.000018
2	6	0.419819	-0.000079	-0.000066
3	6	1.155308	1.209790	-0.000378
4	6	2.541949	1.207257	-0.000288
5	6	3.245619	0.000185	0.000202
6	6	2.542206	-1.207012	0.000364
7	1	3.080863	2.148059	-0.000596
8	1	4.329578	0.000299	0.000376
9	1	3.081296	-2.147713	0.000797
10	6	-3.178625	0.734373	0.000471
11	6	-1.020639	-0.000207	0.000044
12	6	-3.178129	-0.734737	-0.000312
13	6	-1.883064	-1.166528	-0.000405
14	6	-1.884001	1.166794	0.000273
15	1	-4.063942	1.355375	0.000917
16	1	-1.557128	-2.195282	-0.000650
17	1	-4.063015	-1.356371	-0.000398
18	1	-1.558239	2.195597	0.000819
19	1	0.627061	2.154510	-0.001004
20	1	0.627559	-2.154652	0.000207

TS17
uB3LYP/6311+G(d,p) = -424.5548952 ZPVE = 0.158965
Imaginary Vibration = 473.2356*i*

1	6	-1.469724	-1.336692	0.202219
2	6	-0.388373	-0.472984	0.369816
3	6	-0.551681	0.884692	0.160229
4	6	-1.747821	1.462570	-0.216059
5	6	-2.835416	0.591196	-0.390422
6	6	-2.696071	-0.783876	-0.181178
7	1	-1.375453	-2.405783	0.366103
8	1	-1.862457	2.529606	-0.373696
9	1	-3.798821	0.992215	-0.689334
10	1	-3.555221	-1.431336	-0.317946
11	6	2.489600	1.019021	-0.114801
12	6	1.066231	-0.678463	0.730211
13	6	2.699639	-0.185031	-0.883884
14	6	1.902627	-1.182943	-0.424113
15	6	1.500116	0.793158	0.827831
16	1	3.007668	1.955042	-0.275275
17	1	1.231862	-1.253679	1.649655
18	1	1.821071	-2.182019	-0.830188
19	1	3.388502	-0.265855	-1.715671
20	1	1.328079	1.397918	1.707247

S13
uB3LYP/6311+G(d,p) = -424.5964737 ZPVE = 0.1607800

1	6	1.499472	1.436940	-0.004630
2	6	0.380629	0.695631	0.338369
3	6	0.380750	-0.695744	0.338535
4	6	1.499658	-1.436856	-0.004458
5	6	2.641725	-0.699921	-0.352781
6	6	2.641638	0.700138	-0.352855
7	1	1.514921	2.521436	-0.007257
8	1	1.515262	-2.521351	-0.006993
9	1	3.550275	-1.224359	-0.628535
10	1	3.550129	1.224662	-0.628642
11	6	-2.092579	-1.153816	-0.281993
12	6	-1.087798	0.797611	0.776972
13	6	-2.617932	0.000123	-0.853433
14	6	-2.092914	1.153790	-0.281199
15	6	-1.087688	-0.797911	0.776876
16	1	-2.339331	-2.167036	-0.570633
17	1	-1.250781	1.293365	1.739103
18	1	-2.339038	2.167138	-0.569965
19	1	-3.339941	0.000307	-1.662185
20	1	-1.251258	-1.294076	1.738685

TS18
uB3LYP/6311+G(d,p) = -424.5352877 ZPVE = 0.159379
Imaginary Vibration = 442.5924*i*

1	6	-1.406508	-1.348409	0.069728
2	6	-0.245805	-0.588748	0.157015
3	6	-0.332584	0.792170	0.069111
4	6	-1.520502	1.469257	-0.080059
5	6	-2.693508	0.696841	-0.190262
6	6	-2.632878	-0.692186	-0.114281
7	1	-1.371811	-2.431058	0.149317
8	1	-1.571533	2.552363	-0.122812
9	1	-3.649671	1.190448	-0.331379
10	1	-3.544326	-1.274428	-0.192802
11	6	1.864249	1.087745	0.365495
12	6	1.215409	-1.099615	0.371325
13	6	2.256735	0.501452	-0.933152
14	6	1.935385	-0.804049	-0.926353
15	6	1.685500	0.030954	1.263696
16	1	2.043879	2.118328	0.641391
17	1	1.260710	-2.120237	0.747851
18	1	2.012581	-1.501566	-1.748895
19	1	2.662594	1.067473	-1.760591
20	1	1.404617	0.126196	2.304339

S14
uB3LYP/6311+G(d,p) = -424.5752343 ZPVE = 0.161613

1	6	1.366094	1.415608	-0.017993
2	6	0.187381	0.704894	0.119500
3	6	0.187521	-0.704962	0.119552
4	6	1.366340	-1.415506	-0.017883
5	6	2.563480	-0.696028	-0.168306
6	6	2.563356	0.696316	-0.168367
7	1	1.375207	2.500494	-0.007601
8	1	1.375612	-2.500393	-0.007552
9	1	3.499513	-1.231765	-0.281659
10	1	3.499302	1.232204	-0.281722
11	6	-1.276861	-1.135632	0.338836
12	6	-1.277026	1.135403	0.339231
13	6	-2.060879	-0.667603	-0.899897
14	6	-2.061428	0.667777	-0.899377
15	6	-1.649776	-0.000296	1.290928
16	1	-1.429269	-2.163983	0.659410
17	1	-1.429447	2.163625	0.660214
18	1	-2.460451	1.330841	-1.655105
19	1	-2.459493	-1.330401	-1.656076
20	1	-1.420184	-0.000447	2.352752

TS19
uB3LYP/6311+G(d,p) = -424.5361208 ZPVE = 0.158479
Imaginary Vibration = -503.8089*i*

1	6	1.306091	-1.416557	-0.171403
2	6	0.184543	-0.625380	-0.341095
3	6	0.256971	0.775285	-0.194812
4	6	1.457991	1.391684	0.128515
5	6	2.597288	0.591971	0.285054
6	6	2.524981	-0.792171	0.134007
7	1	1.254804	-2.495501	-0.274562
8	1	1.521829	2.468148	0.246751
9	1	3.548506	1.055402	0.522166
10	1	3.420052	-1.392370	0.253434
11	6	-1.093687	1.317433	-0.457708
12	6	-1.273601	-0.964313	-0.571264
13	6	-2.098557	0.342806	1.299901
14	6	-1.959310	-0.881194	0.833991
15	6	-1.805767	0.335550	-1.146915
16	1	-1.322509	2.375326	-0.465955
17	1	-1.482357	-1.891252	-1.102902
18	1	-2.222345	-1.795743	1.360877
19	1	-2.489312	0.783692	2.205995
20	1	-2.810327	0.441607	-1.535433

S15
uB3LYP/6311+G(d,p) = -424.5745150 ZPVE = 0.158758

1	6	0.924872	-1.450746	-0.356260
2	6	0.132790	-0.313629	-0.331137
3	6	0.676526	0.932878	0.037213
4	6	2.022941	1.042647	0.380871
5	6	2.817253	-0.105610	0.357238
6	6	2.276012	-1.340083	-0.006674
7	1	0.516195	-2.414955	-0.640826
8	1	2.448441	1.999961	0.662242
9	1	3.866055	-0.038998	0.624460
10	1	2.907834	-2.221057	-0.019113
11	6	-0.389336	1.936812	-0.031403
12	6	-1.339079	-0.123496	-0.667660
13	6	-3.217705	-0.661271	0.924289
14	6	-2.270943	-1.040139	0.105409
15	6	-1.537717	1.356513	-0.417756
16	1	-0.255026	2.985942	0.200702
17	1	-1.486969	-0.334228	-1.738586
18	1	-2.111145	-2.111775	-0.061365
19	1	-3.966157	-1.114663	1.556087
20	1	-2.492907	1.846524	-0.548378

TS20

uB3LYP/6311+G(d,p) = -424.5709461 ZPVE = 0.15849

Imaginary Vibration = 123.6993*i*

1	6	0.809893	-1.416016	-0.475058
2	6	0.065886	-0.251535	-0.376812
3	6	0.658639	0.945057	0.070087
4	6	2.008382	0.978605	0.416391
5	6	2.755866	-0.196796	0.316615
6	6	2.164278	-1.382769	-0.122636
7	1	0.355998	-2.343008	-0.809310
8	1	2.471972	1.897640	0.758811
9	1	3.806410	-0.189839	0.585345
10	1	2.758843	-2.287021	-0.189137
11	6	-0.368868	1.991321	0.076836
12	6	-1.394728	0.014498	-0.710754
13	6	-2.569200	-1.077568	1.246068
14	6	-2.413888	-0.906839	-0.041288
15	6	-1.537359	1.483702	-0.348169
16	1	-0.196938	3.015166	0.384810
17	1	-1.528163	-0.087228	-1.796190
18	1	-3.072631	-1.461347	-0.719471
19	1	-3.193370	-1.649064	1.915611
20	1	-2.475525	2.014738	-0.438160

TS21

uB3LYP/6311+G(d,p) = -424.5726099 ZPVE = 0.158328

Imaginary Vibration = 114.8198*i*

1	6	-0.876519	-1.473517	0.311903
2	6	-0.138294	-0.301402	0.264751
3	6	-0.757803	0.925696	-0.043434
4	6	-2.125863	0.981025	-0.304125
5	6	-2.865874	-0.202763	-0.259090
6	6	-2.250016	-1.418271	0.044034
7	1	-0.408284	-2.422293	0.554437
8	1	-2.609787	1.923012	-0.538940
9	1	-3.930790	-0.178458	-0.462116
10	1	-2.840435	-2.327073	0.074394
11	6	0.267881	1.973842	-0.021497
12	6	1.336542	-0.057988	0.522715
13	6	3.580884	-0.745305	-0.413717
14	6	2.288405	-0.913030	-0.313838
15	6	1.459941	1.436447	0.285883
16	1	0.077525	3.019331	-0.229758
17	1	1.551176	-0.265844	1.581393
18	1	1.821090	-1.735804	-0.865870
19	1	4.419741	-1.199565	-0.917878
20	1	2.404048	1.958279	0.362840

S16
uB3LYP/6311+G(d,p) = -424.5740598 ZPVE = 0.15875

1	6	0.697523	-1.381472	-0.518711
2	6	0.010690	-0.188612	-0.353219
3	6	0.676078	0.964498	0.107137
4	6	2.037044	0.925502	0.406861
5	6	2.724185	-0.278548	0.242510
6	6	2.063079	-1.420590	-0.214593
7	1	0.190481	-2.272676	-0.871485
8	1	2.554898	1.811028	0.759535
9	1	3.782835	-0.328681	0.472123
10	1	2.613172	-2.347227	-0.334129
11	6	-0.296090	2.059368	0.175024
12	6	-1.441131	0.155562	-0.620329
13	6	-2.262632	-1.680626	0.914430
14	6	-2.484896	-0.684568	0.096965
15	6	-1.501371	1.623101	-0.227114
16	1	-0.062199	3.065024	0.501808
17	1	-1.644752	0.075331	-1.699890
18	1	-3.521910	-0.393934	-0.111545
19	1	-2.835863	-2.377013	1.507103
20	1	-2.411541	2.206465	-0.277283

TS22
uB3LYP/6311+G(d,p) = -424.5718073 ZPVE = 0.158296
Imaginary Vibration = 123.5812*i*

1	6	-0.576027	-1.438567	0.360081
2	6	-0.006746	-0.178602	0.266019
3	6	-0.794259	0.941427	-0.065683
4	6	-2.161202	0.802383	-0.300651
5	6	-2.731142	-0.468658	-0.205898
6	6	-1.947908	-1.578089	0.118758
7	1	0.027384	-2.305314	0.606555
8	1	-2.772282	1.662228	-0.553711
9	1	-3.792409	-0.596974	-0.387957
10	1	-2.406644	-2.558332	0.184034
11	6	0.075032	2.121373	-0.099656
12	6	1.425981	0.279102	0.490878
13	6	2.675023	-1.740998	-0.388843
14	6	2.505981	-0.447439	-0.308632
15	6	1.334959	1.764255	0.198652
16	1	-0.263958	3.123794	-0.329710
17	1	1.669782	0.151385	1.556587
18	1	3.206655	0.201475	-0.846495
19	1	3.341625	-2.439508	-0.870656
20	1	2.191688	2.424123	0.251202

S17
uB3LYP/6311+G(d,p) = -424.5770523 ZPVE = 0.158964

1	6	0.664973	-1.486696	-0.294142
2	6	0.068194	-0.236858	-0.242199
3	6	0.830543	0.915136	0.034691
4	6	2.204238	0.818120	0.251508
5	6	2.803377	-0.441977	0.193747
6	6	2.044081	-1.583060	-0.074762
7	1	0.077537	-2.375716	-0.497945
8	1	2.798749	1.700742	0.461850
9	1	3.870614	-0.536967	0.360743
10	1	2.527777	-2.552648	-0.112631
11	6	-0.071740	2.070868	0.033693
12	6	-1.383307	0.165598	-0.447249
13	6	-3.378460	-1.248241	0.139981
14	6	-2.343094	-0.533159	0.498481
15	6	-1.326609	1.668228	-0.231430
16	1	0.242274	3.091156	0.216317
17	1	-1.696622	-0.050471	-1.475826
18	1	-2.117873	-0.405252	1.563355
19	1	-4.170590	-1.815166	0.605218
20	1	-2.205035	2.296573	-0.294995

TS23
uB3LYP/6311+G(d,p) = -424.5571198 ZPVE = 0.1580920
Imaginary Vibration = 592.4253*i*

1	6	1.156126	-1.428385	-0.295046
2	6	0.174253	-0.454300	-0.366485
3	6	0.473008	0.897064	-0.065089
4	6	1.772041	1.261723	0.308577
5	6	2.755586	0.276099	0.372807
6	6	2.455381	-1.056167	0.074097
7	1	0.932306	-2.464790	-0.526394
8	1	2.011259	2.293774	0.541311
9	1	3.767016	0.544713	0.657086
10	1	3.235606	-1.807067	0.126550
11	6	-0.723428	1.694781	-0.230129
12	6	-1.296849	-0.572258	-0.707088
13	6	-2.763647	-0.192473	0.995002
14	6	-2.123882	-1.182958	0.404069
15	6	-1.785294	0.882397	-0.573560
16	1	-0.772134	2.766167	-0.083721
17	1	-1.465494	-1.016242	-1.695534
18	1	-2.124429	-2.240587	0.667368
19	1	-3.437354	-0.057175	1.832426
20	1	-2.706550	1.228068	-1.022014

S18
uB3LYP/6311+G(d,p) = -424.5954009 ZPVE = 0.1605140

1	6	-1.261813	-1.429344	0.221768
2	6	-0.204935	-0.541692	0.300053
3	6	-0.412179	0.857973	0.087352
4	6	-1.710379	1.326862	-0.225336
5	6	-2.757771	0.420177	-0.301715
6	6	-2.545586	-0.948121	-0.078574
7	1	-1.106751	-2.490370	0.389793
8	1	-1.882702	2.384280	-0.394735
9	1	-3.756864	0.772634	-0.534049
10	1	-3.379545	-1.637956	-0.138840
11	6	0.796025	1.569203	0.238257
12	6	1.253471	-0.803115	0.576431
13	6	2.706289	0.086530	-0.675427
14	6	2.138207	-1.121858	-0.630663
15	6	1.925482	0.631519	0.530476
16	1	0.905852	2.639939	0.119115
17	1	1.436189	-1.405668	1.471122
18	1	2.247306	-2.021103	-1.226173
19	1	3.432742	0.552861	-1.331024
20	1	2.542909	0.916582	1.389056

TS24
uB3LYP/6311+G(d,p) = -424.5434498 ZPVE = 0.1577470
Imaginary Vibration = 631.1078*i*

1	6	0.907589	-1.274983	-0.669755
2	6	-0.100451	-0.357284	-0.250162
3	6	0.318509	0.960448	0.156688
4	6	1.651812	1.217730	0.459475
5	6	2.604338	0.224463	0.221200
6	6	2.230497	-0.993959	-0.382396
7	1	0.627521	-2.213766	-1.134944
8	1	1.958623	2.195752	0.815889
9	1	3.648831	0.413706	0.440447
10	1	2.998723	-1.715247	-0.639161
11	6	-0.819261	1.857173	0.045364
12	6	-1.582630	-0.254433	-0.700613
13	6	-1.115510	-1.370804	1.175625
14	6	-2.157010	-1.117488	0.404919
15	6	-1.885724	1.212459	-0.472625
16	1	-0.794532	2.903696	0.324857
17	1	-1.785047	-0.591261	-1.724148
18	1	-3.206461	-1.370789	0.543612
19	1	-0.900128	-1.888293	2.103026
20	1	-2.860488	1.646267	-0.655895

S19

uB3LYP/6311+G(d,p) = -424.5641235 ZPVE = 0.1594200

1	6	0.924727	-1.305766	-0.640788
2	6	-0.167741	-0.473959	-0.057860
3	6	0.258490	0.943865	0.222092
4	6	1.593107	1.250238	0.455063
5	6	2.574281	0.295334	0.181459
6	6	2.222072	-0.944676	-0.443643
7	1	0.668125	-2.251208	-1.107564
8	1	1.881529	2.256721	0.743761
9	1	3.620125	0.531666	0.337891
10	1	3.019268	-1.596959	-0.785293
11	6	-0.854440	1.815513	-0.017018
12	6	-1.628247	-0.328978	-0.684700
13	6	-0.915735	-1.205271	1.094295
14	6	-2.117613	-1.129729	0.521727
15	6	-1.900692	1.149276	-0.574020
16	1	-0.835464	2.881358	0.181252
17	1	-1.801094	-0.759604	-1.676390
18	1	-3.111270	-1.443067	0.819970
19	1	-0.532746	-1.616043	2.021474
20	1	-2.837732	1.602049	-0.874744

TS25

uB3LYP/6311+G(d,p) = -424.5241854 ZPVE = 0.157669

Imaginary Vibration = 499.7315*i*

1	6	1.116376	-1.395100	-0.530782
2	6	-0.001335	-0.609871	-0.458222
3	6	0.054382	0.775670	-0.021475
4	6	1.337245	1.344624	0.248000
5	6	2.456316	0.528163	0.189830
6	6	2.363213	-0.817839	-0.202404
7	1	1.055513	-2.436500	-0.828129
8	1	1.430831	2.396560	0.494555
9	1	3.432597	0.943900	0.414957
10	1	3.264191	-1.416317	-0.271966
11	6	-1.127235	1.424209	-0.655562
12	6	-1.493776	-0.859816	-0.482734
13	6	-0.949960	0.027037	1.691879
14	6	-1.723309	-0.837798	1.078476
15	6	-2.009233	0.473118	-1.002257
16	1	-1.238632	2.493742	-0.775697
17	1	-1.862202	-1.762265	-0.966490
18	1	-2.473045	-1.483417	1.527048
19	1	-0.754733	0.329632	2.709442
20	1	-2.990626	0.620271	-1.432225

S20
uB3LYP/6311+G(d,p) = -424.5491997 ZPVE = 0.159822

1	6	-1.109408	1.535513	-0.000380
2	6	0.023710	0.798619	-0.000300
3	6	0.052491	-0.726993	0.000008
4	6	-1.299618	-1.354401	0.000108
5	6	-2.419609	-0.563984	0.000065
6	6	-2.361642	0.852856	-0.000197
7	1	-1.076719	2.619979	-0.000511
8	1	-1.385362	-2.436220	0.000290
9	1	-3.396928	-1.036582	0.000195
10	1	-3.281907	1.423917	-0.000301
11	6	0.973597	-0.890274	-1.245160
12	6	1.528915	0.999757	-0.000148
13	6	0.973186	-0.889573	1.245640
14	6	1.832268	0.133040	1.246000
15	6	1.832758	0.132295	-1.245741
16	1	0.897269	-1.706164	-1.951343
17	1	1.929465	2.011119	-0.000447
18	1	2.628395	0.334565	1.949933
19	1	0.896651	-1.705119	1.952194
20	1	2.629247	0.333378	-1.949390

TS26
uB3LYP/6311+G(d,p) = -424.5482226 ZPVE = 0.1585810
Imaginary Vibration = 521.2864*i*

1	6	-0.726387	-1.195587	0.598440
2	6	0.112672	-0.049273	0.615087
3	6	-0.291237	1.170604	0.074507
4	6	-1.622180	1.362966	-0.315859
5	6	-2.503065	0.271684	-0.236531
6	6	-2.083062	-0.975041	0.207831
7	1	-0.518211	-2.040584	1.247702
8	1	-1.958621	2.311270	-0.719868
9	1	-3.537557	0.405126	-0.534898
10	1	-2.793951	-1.791555	0.266414
11	6	0.919610	1.967042	-0.179613
12	6	1.610116	-0.164841	0.541177
13	6	0.699512	-2.030232	-0.730527
14	6	1.781696	-1.331075	-0.440105
15	6	2.011841	1.212475	0.044992
16	1	0.917222	2.989150	-0.537857
17	1	2.111687	-0.399977	1.490458
18	1	2.765176	-1.547286	-0.855574
19	1	0.517020	-2.889232	-1.363606
20	1	3.040152	1.530749	-0.069170

S21
uB3LYP/6311+G(d,p) = -424.5790018 ZPVE = 0.1607950

1	6	0.422300	1.212061	0.161337
2	6	-0.139318	-0.022711	0.386114
3	6	0.474229	-1.242940	0.140891
4	6	1.862726	-1.224572	-0.039720
5	6	2.508024	0.022452	-0.067071
6	6	1.807299	1.242563	-0.027092
7	1	-0.896701	2.886739	0.723443
8	1	2.429798	-2.128860	-0.231855
9	1	3.582028	0.047657	-0.217660
10	1	2.341311	2.170120	-0.204387
11	6	-0.632068	-2.176345	-0.157960
12	6	-1.622630	-0.085010	0.332556
13	6	-0.724311	2.186248	-0.111083
14	6	-1.917291	1.252805	-0.309893
15	6	-1.817054	-1.517239	-0.164351
16	1	-0.507963	-3.227618	-0.389590
17	1	-2.058118	-0.079749	1.354629
18	1	-2.907205	1.610747	-0.567610
19	1	-0.531829	2.811909	-0.990624
20	1	-2.782756	-1.974821	-0.338720

TS27
uB3LYP/6311+G(d,p) = -424.5457458 ZPVE = 0.155334
Imaginary Vibration = 637.3948*i*

1	6	0.791923	-1.426566	-0.578366
2	6	0.107732	-0.222484	-0.461140
3	6	0.749607	0.923473	0.081774
4	6	2.072881	0.850670	0.507799
5	6	2.755040	-0.364762	0.383852
6	6	2.124776	-1.488733	-0.156098
7	1	0.304686	-2.306730	-0.984371
8	1	2.574569	1.720629	0.918363
9	1	3.787440	-0.434863	0.707805
10	1	2.673393	-2.419446	-0.245872
11	6	-0.205110	2.027876	0.036998
12	6	-1.275718	0.156295	-0.777780
13	6	-3.332922	-1.301230	0.599639
14	6	-2.316821	-0.634146	0.833785
15	6	-1.376186	1.581546	-0.506738
16	1	-0.000755	3.036782	0.370748
17	1	-1.848861	-0.334290	-1.551481
18	1	-1.675002	-0.253260	1.605161
19	1	-4.120230	-1.791130	0.073451
20	1	-2.266445	2.170675	-0.676153

S22 (indenyl radical)
uB3LYP/6311+G(d,p) = -347.2163579 ZPVE = 0.127134

1	6	0.938986	1.415601	0.000019
2	6	-0.258111	0.714150	-0.000021
3	6	-0.258064	-0.714179	-0.000031
4	6	0.939342	-1.415538	0.000009
5	6	2.146886	-0.696306	0.000037
6	6	2.146770	0.696409	0.000040
7	1	0.950922	2.500539	0.000040
8	1	0.950836	-2.500478	-0.000013
9	1	3.089011	-1.232574	0.000054
10	1	3.088700	1.233005	0.000067
11	6	-1.645529	-1.141019	-0.000157
12	6	-1.646120	1.140828	-0.000001
13	6	-2.458406	-0.000046	0.000064
14	1	-1.987957	-2.167325	-0.000158
15	1	-1.986936	2.167603	0.000081
16	1	-3.539099	-0.000169	0.000171

TS28
uB3LYP/6311+G(d,p) = -424.5592033 ZPVE = 0.1584610
Imaginary Vibration = 745.3387*i*

1	6	1.427247	1.437610	-0.088255
2	6	0.312869	0.686430	0.268868
3	6	0.376707	-0.695342	0.360158
4	6	1.540970	-1.398383	0.074037
5	6	2.665516	-0.650889	-0.294093
6	6	2.609196	0.744028	-0.373968
7	1	1.392284	2.520733	-0.138690
8	1	1.591294	-2.479459	0.145475
9	1	3.598519	-1.158471	-0.512892
10	1	3.498887	1.295923	-0.656746
11	6	-1.980290	-1.216779	-0.336682
12	6	-1.076604	1.093370	0.691653
13	6	-2.543501	-0.086719	-0.849928
14	6	-2.208269	1.115441	-0.157607
15	6	-1.021246	-1.036828	0.772717
16	1	-2.197290	-2.207336	-0.728974
17	1	-1.099796	1.800597	1.523297
18	1	-2.927653	1.927881	-0.099893
19	1	-3.269101	-0.111079	-1.655344
20	1	-1.202711	-1.540416	1.722368

S23
uB3LYP/6311+G(d,p) = -424.6529665 ZPVE = 0.1620140

1	6	-1.537023	-1.376394	-0.000019
2	6	-0.294679	-0.715919	-0.000106
3	6	-0.294677	0.715806	0.000004
4	6	-1.536858	1.376433	0.000056
5	6	-2.749736	0.695865	0.000047
6	6	-2.749795	-0.695712	0.000065
7	1	-1.539296	-2.461138	-0.000046
8	1	-1.539046	2.461170	0.000088
9	1	-3.682162	1.248562	0.000106
10	1	-3.682274	-1.248320	0.000095
11	6	0.883828	1.568785	-0.000065
12	6	2.221842	1.257920	-0.000108
13	6	2.854723	-0.000148	0.000133
14	6	2.221674	-1.257916	0.000047
15	6	0.883569	-1.568703	-0.000149
16	1	0.650984	2.629367	-0.000196
17	1	2.892510	2.113598	-0.000164
18	1	3.939038	-0.000233	0.000574
19	1	2.892130	-2.113771	0.000334
20	1	0.650909	-2.629343	-0.000222

TS29
uB3LYP/6311+G(d,p) = -424.5733434 ZPVE = 0.1594890
Imaginary Vibration = 437.2373*i*

1	6	-1.345057	-1.403521	-0.291207
2	6	-0.179393	-0.637173	-0.071203
3	6	-0.312061	0.765431	0.140858
4	6	-1.614403	1.304379	0.274521
5	6	-2.739382	0.516724	0.142350
6	6	-2.604084	-0.847196	-0.169528
7	1	-1.241335	-2.461681	-0.508381
8	1	-1.716336	2.369358	0.456392
9	1	-3.725589	0.953711	0.250799
10	1	-3.484520	-1.465089	-0.304339
11	6	0.811300	1.642825	-0.025268
12	6	1.091302	-1.326848	-0.042549
13	6	2.059948	1.218674	-0.362013
14	6	2.543341	-0.125734	-0.237288
15	6	2.194248	-1.031785	0.835619
16	1	0.595708	2.705770	-0.071171
17	1	1.103472	-2.297986	-0.538685
18	1	3.404060	-0.392687	-0.849928
19	1	2.757372	1.933372	-0.790158
20	1	2.872614	-1.799438	1.189712

S24
uB3LYP/6311+G(d,p) = -424.5834768 ZPVE = 0.1607160

1	6	-1.337149	-1.407288	-0.200428
2	6	-0.181558	-0.628113	-0.118140
3	6	-0.298152	0.773209	0.037531
4	6	-1.576862	1.336173	0.160183
5	6	-2.719646	0.544844	0.114644
6	6	-2.600324	-0.831506	-0.077863
7	1	-1.244568	-2.479421	-0.342130
8	1	-1.668147	2.411448	0.277225
9	1	-3.698686	0.999181	0.216347
10	1	-3.485900	-1.455164	-0.125340
11	6	0.886836	1.626961	-0.043400
12	6	1.166459	-1.251888	-0.188537
13	6	2.125230	1.151665	-0.267821
14	6	2.411498	-0.298011	-0.295171
15	6	2.124671	-1.091912	0.911727
16	1	0.724277	2.699366	0.002023
17	1	1.234397	-2.167518	-0.773113
18	1	3.215320	-0.632343	-0.947335
19	1	2.951688	1.835687	-0.432230
20	1	1.965607	-0.756033	1.928207

TS30
uB3LYP/6311+G(d,p) = -424.5576745 ZPVE = 0.1582330
Imaginary Vibration = 736.0906*i*

1	6	1.340210	-1.399379	-0.259304
2	6	0.216855	-0.577129	-0.321965
3	6	0.347907	0.816656	-0.066306
4	6	1.608182	1.344204	0.261299
5	6	2.713926	0.506229	0.340410
6	6	2.584598	-0.860907	0.075808
7	1	1.249397	-2.459262	-0.472746
8	1	1.714761	2.407918	0.446215
9	1	3.684790	0.915981	0.595802
10	1	3.455417	-1.505268	0.121007
11	6	-0.855808	1.564733	-0.330767
12	6	-2.081519	0.870161	-0.375205
13	6	-2.604569	-0.020268	0.723620
14	6	-2.049515	-1.214870	0.566174
15	6	-1.166714	-1.017581	-0.624708
16	1	-0.776750	2.565018	-0.747526
17	1	-2.856035	1.330056	-0.993842
18	1	-3.299453	0.321982	1.487183
19	1	-2.123002	-2.103717	1.185763
20	1	-1.370453	-1.543793	-1.556185

S15 → S25+H
uB3LYP/6311+G(d,p) = -424.5051083 ZPVE = 0.1506130
Imaginary Vibration = 649.0956*i*

1	6	0.763228	-1.459270	-0.374834
2	6	0.093585	-0.248720	-0.313831
3	6	0.761135	0.930660	0.065442
4	6	2.118686	0.901386	0.380202
5	6	2.794049	-0.319048	0.318097
6	6	2.125290	-1.487080	-0.053178
7	1	0.245866	-2.368446	-0.659801
8	1	2.641832	1.806232	0.670037
9	1	3.849526	-0.361412	0.562884
10	1	2.665673	-2.426101	-0.091565
11	6	-0.201916	2.035967	0.048299
12	6	-1.359003	0.096047	-0.631564
13	6	-3.217721	-1.034845	0.899372
14	6	-2.362323	-0.677764	0.116514
15	6	-1.410746	1.587250	-0.323413
16	1	0.040430	3.060362	0.302129
17	1	-1.536435	-0.053253	-1.705624
18	1	-2.251710	-2.291733	-0.966034
19	1	-3.960236	-1.476670	1.518930
20	1	-2.320523	2.163520	-0.417586

S16 → S25+H
uB3LYP/6311+G(d,p) = -424.5054864 ZPVE = 0.1505050
Imaginary Vibration = 637.2107*i*

1	6	-0.716826	-1.436373	0.445492
2	6	-0.073556	-0.217094	0.317703
3	6	-0.770370	0.931917	-0.099163
4	6	-2.133442	0.862951	-0.382968
5	6	-2.783096	-0.365966	-0.251677
6	6	-2.084364	-1.504465	0.155532
7	1	-0.175511	-2.323877	0.754718
8	1	-2.680456	1.743485	-0.702074
9	1	-3.842417	-0.438937	-0.471309
10	1	-2.605752	-2.450605	0.246122
11	6	0.174209	2.052198	-0.153202
12	6	1.375818	0.165806	0.593806
13	6	2.926870	-1.460384	-0.832864
14	6	2.365025	-0.657441	-0.118424
15	6	1.397731	1.641222	0.214264
16	1	-0.090312	3.059503	-0.449502
17	1	1.572675	0.080305	1.672202
18	1	3.919073	0.135281	0.762674
19	1	3.535246	-2.114154	-1.409740
20	1	2.299457	2.234773	0.265906

S17 → S25+H
uB3LYP/6311+G(d,p) = -424.5051954 ZPVE = 0.1503580
Imaginary Vibration = 648.2965*i*

1	6	0.672626	-1.478898	-0.351649
2	6	0.072720	-0.232845	-0.283056
3	6	0.815773	0.914505	0.050204
4	6	2.181853	0.816279	0.309557
5	6	2.787596	-0.439701	0.238546
6	6	2.043193	-1.575969	-0.085725
7	1	0.095302	-2.363884	-0.596412
8	1	2.764210	1.694570	0.566147
9	1	3.848411	-0.535795	0.441461
10	1	2.531208	-2.543020	-0.129094
11	6	-0.091790	2.065243	0.063525
12	6	-1.367988	0.181373	-0.553086
13	6	-3.339496	-1.292572	0.450599
14	6	-2.396727	-0.585126	0.164548
15	6	-1.337456	1.672257	-0.246413
16	1	0.210247	3.078215	0.298044
17	1	-1.575230	0.054750	-1.626855
18	1	-1.765648	-0.062056	1.962054
19	1	-4.129608	-1.882782	0.847870
20	1	-2.220717	2.292730	-0.305516

S25
uB3LYP/6311+G(d,p) = -424.0075013 ZPVE = 0.1491820

1	6	-0.691014	-1.461174	0.396794
2	6	-0.049671	-0.237573	0.306054
3	6	-0.746791	0.921329	-0.081511
4	6	-2.109087	0.858447	-0.370724
5	6	-2.757244	-0.374604	-0.275358
6	6	-2.057738	-1.523069	0.101390
7	1	-0.148493	-2.356090	0.681740
8	1	-2.656483	1.746518	-0.667605
9	1	-3.815816	-0.442986	-0.500061
10	1	-2.577751	-2.472308	0.163041
11	6	0.197028	2.043185	-0.105101
12	6	1.400998	0.136494	0.590717
13	6	3.227763	-1.309936	-0.700673
14	6	2.398369	-0.657057	-0.125034
15	6	1.420616	1.622547	0.251731
16	1	-0.067756	3.057717	-0.375579
17	1	1.589816	0.024155	1.669713
18	1	3.955869	-1.885535	-1.217787
19	1	2.321257	2.216998	0.316830

S21 → S26+H
uB3LYP/6311+G(d,p) = -424.5214654 ZPVE = 0.1528950
Imaginary Vibration = 644.0408*i*

1	6	0.496588	1.194467	0.176010
2	6	-0.156466	-0.007162	0.457190
3	6	0.351576	-1.263550	0.181007
4	6	1.732739	-1.358308	-0.047394
5	6	2.475499	-0.165224	-0.130619
6	6	1.880837	1.101191	-0.102025
7	1	0.648767	2.064178	1.921775
8	1	2.216132	-2.306783	-0.253413
9	1	3.539683	-0.232278	-0.329882
10	1	2.470460	1.980738	-0.333729
11	6	-0.824734	-2.096880	-0.150816
12	6	-1.630495	0.070657	0.335427
13	6	-0.589673	2.101438	-0.289063
14	6	-1.773689	1.448719	-0.307403
15	6	-1.940846	-1.329893	-0.184873
16	1	-0.788838	-3.153206	-0.388319
17	1	-2.113333	0.143314	1.327508
18	1	-2.722517	1.892533	-0.581588
19	1	-0.438504	3.129789	-0.593128
20	1	-2.939868	-1.691014	-0.393873

S26
uB3LYP/6311+G(d,p) = -424.0222839 ZPVE = 0.1515720

1	6	0.432135	1.226328	0.164703
2	6	-0.147048	0.000036	0.445343
3	6	0.431987	-1.226255	0.164553
4	6	1.819954	-1.234597	-0.032842
5	6	2.492496	-0.000084	-0.064183
6	6	1.820102	1.234389	-0.033069
7	1	2.365788	-2.148294	-0.240932
8	1	2.365951	2.148131	-0.241014
9	6	-0.700153	-2.111246	-0.188531
10	6	-1.622965	0.000100	0.344218
11	6	-0.700068	2.111359	-0.188330
12	6	-1.856212	1.402992	-0.214186
13	6	-1.856396	-1.403013	-0.213886
14	1	-0.612138	-3.160779	-0.442756
15	1	-2.833744	1.815689	-0.429591
16	1	-0.612027	3.160991	-0.442158
17	1	-2.834078	-1.815653	-0.428717
18	1	3.565375	-0.000216	-0.224632
19	1	-2.088123	0.000075	1.347061

S23 → S27+H
uB3LYP/6311+G(d,p) = -424.5046929 ZPVE = 0.1502190
Imaginary Vibration = 30.1138*i*

1	6	-1.539318	1.382596	-0.122630
2	6	-0.309846	0.720765	-0.263345
3	6	-0.245948	-0.697400	-0.105642
4	6	-1.455661	-1.372791	0.169505
5	6	-2.658117	-0.701720	0.318505
6	6	-2.703050	0.688094	0.169355
7	1	-1.567744	2.458306	-0.258987
8	1	-1.432695	-2.452278	0.276624
9	1	-3.562798	-1.256321	0.540227
10	1	-3.644000	1.218008	0.265670
11	6	0.946719	-1.550953	-0.250638
12	6	2.256568	-1.287307	-0.013485
13	6	2.677341	0.031458	0.461295
14	6	2.020573	1.031377	-0.096765
15	6	0.911912	1.433958	-0.682566
16	1	0.706013	-2.579382	-0.509831
17	1	2.977863	-2.096016	-0.105163
18	1	3.375405	0.138023	1.286102
19	1	2.863417	4.349604	2.501007
20	1	0.877493	2.151588	-1.497177

S27
uB3LYP/6311+G(d,p) = -424.0025421 ZPVE = 0.1502030

1	6	1.599753	-1.332614	0.028456
2	6	0.321925	-0.779804	-0.147371
3	6	0.157768	0.639014	-0.151427
4	6	1.321000	1.425033	0.004398
5	6	2.572823	0.862123	0.190317
6	6	2.716126	-0.528925	0.200753
7	1	1.703847	-2.412224	0.015456
8	1	1.221314	2.505367	-0.012064
9	1	3.439272	1.501121	0.317324
10	1	3.695473	-0.976666	0.326759
11	6	-1.097615	1.384100	-0.353610
12	6	-2.378308	1.058268	-0.045242
13	6	-2.688817	-0.222863	0.590372
14	6	-1.974662	-1.232313	0.128235
15	6	-0.853374	-1.621636	-0.442238
16	1	-0.939700	2.390125	-0.735408
17	1	-3.159272	1.798105	-0.204635
18	1	-0.784912	-2.426419	-1.168496
19	1	-3.355752	-0.281700	1.445207

VITA

EDUCATION

University of Illinois at Chicago, Chicago, USA

Ph.D. Candidate Mechanical Engineering, GPA: 4.00/4.00, August 2007 – Q4 2011
Advisor: Prof. K. Brezinsky
M.S. Mechanical Engineering, GPA: 4.00/4.00, August 2005
Advisor: Prof. K. Brezinsky

Italian State Exam, qualifying to practice as mechanical engineer, Mark: 100/100, February 2006

Politecnico di Milano, Milan, Italy

LAUREA in Ingegneria Meccanica (equivalent to a Master of Science in Mechanical Engineering), Final degree mark: 100/100 summa cum laude, October 2005
Advisor: Prof. G. Ferrari

WORK EXPERIENCE

University of Illinois at Chicago, Chicago, USA

Research Assistant at the High Pressure Shock Tube Laboratory, March 2007 – present

Universität Karlsruhe, Karlsruhe, Germany

Research Assistant at the Molecular Physical Chemistry Group, summer 2008

ENI S.p.A., Gas & Power Division, Milan, Italy

International Negotiator, March 2006 – March 2007

University of Illinois at Chicago, Chicago, USA

Teaching Assistant; course: "Experimental Methods in Mechanical Engineering", January 2004 – May 2004

University of Illinois at Chicago, Chicago, USA

Research Assistant at the High Pressure Shock Tube Laboratory, August 2003 – August 2005

AREAS OF SPECIALIZATION

<u>Experimental techniques</u>

- Shock Tube: development and execution of chemical kinetic studies of complex hydrocarbon fuel molecules and PAHs formation chemistry for jet fuel applications; operation and maintenance of the high pressure shock tube equipment and the ultra-high vacuum technology; development of new experimental solutions to address specific experimental challenges related to recovery and measurement of PAH compounds.
- Analytical Techniques: gas chromatography and mass spectrometry for measurement of stable products; time-of-flight mass spectrometry for time resolved species profiles.

Combustion modeling and simulation

- CHEMKIN: chemical kinetic modeling of high pressure experimental gas phase chemistry.
- Gaussian/GaussView: computational chemistry methods for the study of reaction pathways and reaction rate constants relevant to the development of chemical kinetic models.

PUBLICATIONS

R. Sivaramakrishnan, A. Comandini, R. S. Tranter, K. Brezinsky, S.G. Davis, H. Wang: "Combustion of CO/H2 Mixtures at High Pressure", Proceedings of the Combustion Institute 31, Issue 1, 429-437, 2007

S. Gudiyella, T. Malewicki, A. Comandini, K. Brezinsky: "High Pressure Study of m-Xylene Oxidation", Combustion and Flames 158, Issue 4, 687-704, 2011

A. Comandini, K. Brezinsky: "Theoretical Study of the Formation of Naphthalene from the Radical/π-Bond Addition between Single-Ring Aromatic Hydrocarbons", Journal of Physical Chemistry A 115, Issue 22, 5547-5559, 2011

A. Comandini, K. Brezinsky: "Formation of PAH's in the Pyrolytic Reactions of the Phenyl Radical with Acetylene", 7th US National Technical Meeting of the Combustion Institute, 2011

A. Comandini, T. Malewicki, K. Brezinsky: "Online and Offline Experimental Techniques for PAHs Recovery and Measurement", journal article submitted for publication

A. Comandini, T. Malewicki, K. Brezinsky: "Chemistry of PAHs Formation from Phenyl Radical Pyrolysis and Phenyl + Acetylene Reaction", journal article submitted for publication

A. Comandini, K. Brezinsky: "Radical/π-Bond Addition between o-Benzyne and Cyclic C5 Hydrocarbons", journal article submitted for publication

S. H. Dürrstein, A. Comandini, T. Bentz, K. Brezinsky, M. Olzmann: “Iodobenzene pyrolysis and the phenyl + acetylene reaction – collaborative shock-tube studies and kinetic modeling”, journal article, in preparation

PRESENTATIONS

A. Comandini, K. Brezinsky: “Aromatic Radicals-Acetylene Particulate Matter Chemistry”, CNRS, Orleans, France, May 2008

A. Comandini, K. Brezinsky: “Aromatic Radicals-Acetylene Particulate Matter Chemistry”, Universität Karlsruhe, Karlsruhe, Germany, July 2008

A. Comandini, K. Brezinsky: “Aromatic Radicals-Acetylene Particulate Matter Chemistry”, SERDP Soot Science Team Meeting, Washington D.C., December 1, 2010

A. Comandini, K. Brezinsky: “Formation of PAH’s in the Pyrolytic Reactions of the Phenyl Radical with Acetylene”, 7th US National Technical Meeting of the Combustion Institute, Georgia Institute of Technology, Atlanta, GA, March 20-23, 2011

A. Comandini, K. Brezinsky: “Formation of Fused-Ring Aromatic Compounds from the Pyrolytic Reactions of the Phenyl Radical with Acetylene”, The 7th International Conference on Chemical Kinetics, MIT, Cambridge, MA, July 10-14, 2011